Non-coding RNAs in ovarian cancer

Jaynish Shailesh Shah

This thesis is submitted in fulfilment of the requirement for the degree of Doctor of Philosophy, Faculty of Medicine, University of Sydney

Functional Genomics Laboratory
Hormones and Cancer Group
Kolling Institute of Medical Research
Northern Clinical School
Royal North Shore Hospital
Faculty of Medicine
University of Sydney

September, 2017

Declaration

This is to certify that to the best of my knowledge, the content of this thesis is my own work. This thesis has not been submitted for any degree or other purposes.

I certify that the intellectual content of this thesis is the product of my own work and that all the assistance received in preparing this thesis and sources have been acknowledged.

Parts of the work presented within this thesis have been published in the following peer reviewed articles, the patent, oral and poster presentations.

Chapter 4 has been in published in *Plos One* (Publication #1 below). Some parts of the Materials & methods as well as complete Results and Discussion sections of that chapter is identical to the published work, but has been re-formatted in the thesis. Figures are identical to the publications where they were drafted in American English.

Publications

1. **Shah JS**, Soon PS, Marsh DJ. Comparison of Methodologies to Detect Low Levels of Hemolysis in Serum for Accurate Assessment of Serum microRNAs, *PloS One* (2016): doi: `http://dx.doi.org/10.1371/journal.pone.0153200`

2. Marsh DJ, **Shah JS**, Cole AJ. Histones and their modifications in ovarian cancer – drivers of disease and therapeutic targets. *Frontiers in Oncology* (2014): doi: `http://doi.org/10.3389/fonc.2014.00144`

Patent

- **Shah JS**, Marsh DJ, Gard G, Soon PS. Selection methods for the treatment of cancer (Australian Provisional patent #2015904120)

Oral Presentations

- **Shah JS**, Soon PS and Marsh DJ (2015) Investigating the complexity of p53 pathways in ovarian cancer: are non-coding RNAs the key?, *SydneyVital Translational Cancer Research Symposium*, Sydney, Australia

- **Shah JS**, Gard G, Soon P and Marsh DJ (2014). Going macro from micro – harnessing the power of serum microRNAs to predict surgical outcome for women with ovarian cancer. *New Horizons 2014*, Sydney, Australia

- **Shah JS** (2014). Treasure hunting in the 'junk DNA' to improve clinical management of ovarian cancer. *3 Minute Thesis competition*, University of Sydney, Sydney, Australia

Poster Presentations

- **Shah JS**, Gard GB, Soon PS, Marsh DJ (2015). Harnessing the power of serum microRNAs to predict surgical outcome for women with ovarian cancer. *Australasian Genomic Technologies Association*, Hunter Valley, Australia.
- **Shah JS**, Gard GB, Soon PS, Marsh DJ (2015). Harnessing the power of serum microRNAs to predict surgical outcome for women with ovarian cancer. *The Lowy Cancer Symposium: Drug Discovery to Personalised Medicine*. Sydney, Australia.
- **Shah JS**, Cole AJ, Dickson KA, Soon P and Marsh DJ (2014). Investigating the role of long non-coding RNAs in cisplatin resistance in ovarian cancer. *BioinfoSummer 2014*. Melbourne, Australia.
- **Shah JS**, Cole AJ, Dickson KA, Soon P and Marsh DJ (2014). Investigating the role of long non-coding RNAs in cisplatin resistance in ovarian cancer. *Sydney Cancer Conference*. Sydney, Australia.
- **Shah JS**, Cole AJ, Dickson KA, Soon P and Marsh DJ (2014). Investigating the role of long non-coding RNAs in cisplatin resistance in ovarian cancer. *Joint Australia Japan RNA meeting*. Sydney, Australia.
- **Shah JS**, Cole AJ, Dickson KA, Soon P and Marsh DJ (2014). Investigating the role of long non-coding RNAs in cisplatin resistance in ovarian cancer. *Cell Symposia: Regulatory RNAs*. Berkeley, United States of America.
- **Shah J**, Kurdyukov S, Dickson K, Soon P, Marsh D (2014). Investigating the role of long non-coding RNAs in cisplatin resistance in ovarian cancer. *Australian Society for Medical Research NSW 2014 Meeting*. Sydney, Australia.
- **Shah J**, Kurdyukov S, Dickson K, Soon P, Marsh D (2014). Investigating the role of long non-coding RNAs in cisplatin resistance in ovarian cancer. *EMBL Australia PhD course*. Canberra, Australia.

Jaynish Shailesh Shah
June, 2017

Acknowledgements

Undertaking a PhD would not have been possible without the help and advice from many people, whom I would like to express my gratitude. First and foremost, I would like to thank my primary supervisor Professor Deborah Marsh, who has encouraged me to pursue my passion, nourished my career and being supportive in difficult times. I would like to thank my associate supervisor Dr. Patsy Soon, who supervised me over Skype for last two years and provided much needed clinical insights.

I would like to acknowledge the members of the Functional Genomics Laboratory and Hormones and Cancer group for being helpful over the duration of the PhD, especially Mrs. Kristie Dickson, the walking wikipedia, for teaching me various laboratory techniques. I would like to thank Dr. Sergey Kurdyukov for training me on RT-qPCR, which has been a crux to my project. I would also like to thank Dr. Gregory Gard and Dr. Susan Valmadre for providing serum samples for this study as well as Ms. Kathleen Phillips, Mr. Graham Wilkins and Mrs. Ussha Pillai for managing the samples. I would also like to thank Dr. Giles Best and Mr. Lyndsay Peters for teaching me flow cytometry as well as Professor Jean Yang for the help with machine learning. My sincere thanks goes to Dr. Nenad Bartonicek and Mr. James Torpy for their immense help with the analysis of RNA-sequencing data.

Besides pursuing a PhD at the Kolling Institute, I had a wonderful opportunity for personal growth by becoming involved with the Postgraduate Research Students' Society (PReSS). I would like to thank Dr. Rosemary Rabindran for being a wonderful co-leader, Ms. Burcu Karlsson and Dr. Carolyn Scott for the support.

I would also like to acknowledge the financial support provided by the Australian Postgraduate Award, the Northern Clinical School Top-Up, The Postgraduate Research Support Scheme, the Ovarian Cancer Research Foundation and SydneyVital Translational Cancer Research.

I would like to thank Mr. Alexander Cole for being a wonderful friend over the years and a fierce table-tennis competitor, who is statistically not better than me at this game (N=5; $P = 0.064$). I would like to acknowledge and appreciate support of my friends to help me get through the PhD: (in no particular order) Aaron, Elvia, Justin, Mehul, Sneha, Jag, Harriet, Sofia, Amy, Harveen, Umang and Shipra.

Last but not least, I would like to thank my brother, Shreejay, for being supportive and awesome, and my parents for their love and continued support.

To my grandmother

Abstract

Ovarian cancer (OC) is the most lethal form of gynaecological cancer, with high-grade serous ovarian carcinoma (HGSOC) being the most common and the deadliest subtype. Non-coding RNAs are a recently discovered species of RNAs that do not code for proteins, yet play a crucial role in both normal physiology and disease. The overall goal of this thesis was to apply the power of non-coding RNAs to OC with the following aims: (1) to identify novel small non-coding RNAs present in serum that could separate patients with HGSOC from healthy women as well as predict their surgical outcome, (2) to assess the role of long non-coding RNAs (lncRNAs) in promoting cisplatin resistance in cell line models of OC, and (3) to study the effects of mutant-p53 on mRNAs and lncRNAs using a small compound known as APR-246 as well as investigating the drug's mechanisms of action.

Firstly, the lethality of OC could partially be attributed to the lack of specific symptoms, leading this disease to be termed the 'silent killer', as well as low incidence rate of 9.4 cases per 100,000 individuals, both requiring a highly accurate test for population screening that remains an ongoing challenge. Measuring the levels of small non-coding RNAs, known as microRNAs, in serum, experiments described in this thesis aimed to identify novel microRNAs that could separate patients with HGSOC from healthy women as well as predict their surgical outcome, one of the most important factors influencing overall patient survival. Because serum microRNAs can be affected by pre-analytical factors such as haemolysis, the sensitivity of four methodologies to detect low levels of haemolysis was first determined. This work is published in *Plos One*. The work described in this thesis identified a novel serum microRNA, miR-375, that could improve the accuracy of CA-125, a routinely used biomarker in diagnosing OC, in separating patients with HGSOC from healthy women. Next, serum microRNA miR-34a-5p was found to predict the surgical outcome of patients with HGSOC. In fact, miR-34a-5p was found to be superior to CA-125 for this purpose. Although the standard therapy for treating OC consists of surgical removal of the tumour followed by chemotherapy containing platinum/taxane agents, this regimen may be too aggressive for a subset of patients who might benefit from neoadjuvant chemotherapy, i.e. chemotherapy followed by the surgery. A pre-operative expectation of the the surgical outcome could help surgeons decide on optimal timing for surgery. Both miR-375 and miR-34a-5p were also unaffected by haemolysis.

Secondly, although OC is initially sensitive to chemotherapy, most patients develop resistance within two years, resulting in recurrent disease that is difficult to treat. To identify novel lncRNAs that could promote drug resistance, expression of ninety lncRNAs was

profiled in cell line models of cisplatin resistance. Five lncRNAs were found to have the potential to promote cisplatin resistance *in vitro*, and lncRNA Urothelial Cancer Associated 1 (UCA1) was selected for further investigations. Despite its role in promoting cisplatin resistance in bladder cancer, UCA1 was not found to promote cisplatin resistance in cell line models of OC.

Lastly, the tumour suppressor *TP53* plays a central role in the biology of cancer and it is almost universally mutated in HGSOC. Recent evidence suggests that p53, the protein encoded by *TP53*, can significantly influence the expression of both small and long non-coding RNAs. Experiments described in this thesis aimed to investigate the effect of mutant-p53 on protein-coding and non-coding RNAs by using a small compound known as APR-246 which has been reported to restore wild-type p53 activities in multiple cancers by stabilising the structure of mutant-p53. Despite currently undergoing a phase Ib/II clinical trial for potential treatment of recurrent HGSOC, the ability of APR-246 to restore wild-type p53 activities in HGSOC has not been tested. A global transcriptomic analysis conducted in this thesis discovered that p53-responsive mRNAs and lncRNAs were not robustly induced following APR-246 treatment in two cell line models of HGSOC, but indicated that APR-246 could function by inducing high levels of reactive oxidative species (ROS).

Overall, data presented in this thesis demonstrated the utility of small non-coding RNAs in identifying patients with HGSOC from healthy women as well as predicting their surgical outcome. This thesis also implicated that lncRNAs, in general, could have a role in promoting cisplatin resistance in OC as well as suggested that APR-246 could, based on evidence obtained from the expression of p53-responsive mRNAs and lncRNAs, act independently of mutant-p53. Together, this research raises novel ways for clinical management of patients with HGSOC and addresses the challenge of drug resistance using non-coding RNAs, as well as questions the assumed mechanisms of action of the 'p53-activating' drug APR-246.

Table of Contents

List of Tables

List of Figures

Abbreviations

E.coli *Escherichia coli*

ACTB β-actin

AIC Akaike information criterion

ANOVA Analysis of variance

ARE antioxidant responsive element

AS AllStars

AS-488 AllStars Negative Control siRNA labelled with Alexa Fluor 488

AS-UNL unlabelled AllStars Negative Control siRNA

ASO antisense oligonucleotides

ATM ataxia telangiectasia mutated

AUC area under curve

BAX BCL2 Associated X

BBC3 BCL2 Binding Component 3

BH Benjamini–Hochberg

BRCA1 breast cancer type 1 susceptibility gene

BSO Buthionine sulphoximine

CA-125 Cancer Antigen 125

CDKN1A Cyclin Dependent Kinase Inhibitor 1A

CEBP cAMP response-element binding protein

ceRNA competing endogenous RNA

circRNA circular RNA

CLL chronic lymphocytic leukaemia

CRISPR Clustered regularly interspaced short palindromic repeats

CT Computed Tomography

CV cross validation

DE differentially expressed

DGCR8 DiGeorge syndrome critical region 8

DHFR dihydrofolate reductase

DLDA diagonal linear discriminatory analysis

DMSO dimethyl sulfoxide

DRC dose response curve

EDTA ethylenediaminetetraacetic acid

EEC ectrodactyly ectodermal dysplasia-cleft

EMT epithelial-mesenchymal transition

EOC epithelial ovarian cancer

ERα oestrogen receptor alpha

ES enrichment score

EZH2 Enhancer of zeste homolog 2

FBS fetal bovine serum

FC fold-change

FDA Food and Drug Administration

FDR false discovery rate

FPKM Fragments Per Kilobase of transcript per Million mapped reads

GADD45A Growth Arrest And DNA Damage Inducible Alpha

GAPDH Glyceraldehyde-3-Phosphate Dehydrogenase

GCLC Glutamate-Cysteine Ligase Catalytic Subunit

GCLM Glutamate-Cysteine Ligase Modifier Subunit

GDF15 Growth/differentiation factor 15

GOF gain-of-function

GOG Gynaecologic Oncology Group

GSEA Gene Set Enrichment Analysis

GSH glutathione

HCC hepatocellular carcinoma

HE4 human epididymis protein 4

HGSOC high-grade serous ovarian carcinoma

HMBS Hydroxymethylbilane Synthase

hnRNP-K heterogeneous nuclear ribonucleoprotein K

HOTAIR HOX transcript anti-sense RNA

HR homologous recombination

HULC Highly Upregulated in Liver Cancer

KEAP1 Kelch-like ECH-associated protein 1

LB Luria broth

LES leading edge subset

lincRNA long intervening RNA

LNA locked nucleic acid

lncRNA long non-coding RNA

LR logistic regression

LSD1 lysine-specific demethylase 1

Malat1 Metastasis Associated Lung Adenocarcinoma Transcript 1

MCC Matthews correlation coefficient

MDM2 Mouse double minute 2 homologue

MEG3 maternally expressed gene 3

miRISC microRNA-induced silencing complex

ML machine learning

MOPS 3 (N-Morpholino) propanesulfonic acid

MQ methylene quinuclidinone

NAC N-acetyl cysteine

NACT neoadjuvant chemotherapy

NCCN National Comprehensive Cancer Network

ncRNA non-coding RNA

NEAT1 nuclear enriched abundant transcript 1

NPV negative predictive value

NRF2 nuclear factor erythroid 2-related factor 2

NSCLC non-small cell lung cancer

NTC no template control

OC ovarian cancer

ORF open reading frame

OS overall survival

PARP poly ADP ribose polymerase

PARPi PARP inhibitors

PBS phosphate buffered saline

PCA3 prostate cancer antigen 3

PFS progression-free survival

PI3K phosphoinositide-3-kinase

PID protein interactions database

piRNA PIWI-interacting RNA

PMAIP1 Phorbol-12-Myristate-13-Acetate-Induced Protein 1

Pol II RNA polymerase II

PPV positive predictive value

PRC2 Polycomb repressive complex 2

pre-miRNA precursor microRNA

pri-miRNA primary microRNA

Provean Protein Variation Effect Analyzer

PSA prostate-specific antigen

PTEN phosphatase and tensin homolog

PTENP1 PTEN pseudogene 1

RBC red blood cells

RIN RNA Integrity Number

RNA-seq RNA sequencing

ROC receiver operator characteristic

ROCA Risk of Ovarian Cancer Algorithm

ROMA Risk of Malignancy Algorithm

ROS reactive oxidative species

RQ relative quantification

RRM2B ribonucleotide reductase regulatory TP53 inducible subunit M2B

rRNA ribosomal RNA

RT reverse transcription

RT-qPCR real-time quantitative PCR

SDS sodium dodecyl sulfate

SEM standard error of mean

SI Survival Index

SLC7A11 solute carrier family 7 member 11

SNHG snoRNA host gene

snoRNA small nucleolar RNA

SRPK1 SR Protein Kinase 1

STIC serous tubal intraepithelial carcinomas

SVM support vector machine

TAE Tris-acetate-EDTA

TCGA The Cancer Genome Atlas

TP53I3 TP53-Induced Gene 3

TRBP transactivation-responsive RNA-binding protein

TUCP transcripts of unknown coding potential

UCA1 Urothelial Cancer Associated 1

UKCTOCS UK Collaborative Trial of Ovarian Cancer Screening

UTR untranslated region

wt wild-type

XIST X-inactive specific transcript

Chapter 1

Literature Review

1.1 Ovarian cancer

1.1.1 Management of ovarian cancer

1.1.1.1 Epidemiology

Ovarian cancer (OC) is the seventh most common form of cancer and the eighth most frequent cause of death from cancer in women worldwide, which translates to roughly 239,000 new cases worldwide and 152,000 deaths from the disease annually (Ferlay et al. 2015). The age-standardised incidence rate in developed countries has been estimated to be 9.4 per 100,000 population (Soerjomataram et al. 2012). The life time risk of being diagnosed with and succumbing to OC in the United States is approximately 1 in 70, and 1 in 95, respectively (Clarke-Pearson 2009; Romero and Bast 2012). Similar to the US, 1 in 106 women under the age of 85 will succumb to OC in Australia (AIHW 2017). Although the 5-year survival rate for patients with OC has risen from 32% in 1982-1987 to 44.4% in 2009-2013, it remains significantly lower than other cancers such as breast cancer (72% in 1982-1987 to 90.2% in 2009-2013) (AIHW 2017). Thus, there is an urgent need to gain a deeper understanding of the disease and translate it into the clinical management of patients.

1.1.1.2 Risk factors

Early menarche, late menopause and nulliparity have been linked to an increased risk of developing OC (Hamajima et al. 2012). These factors increase the number of ovulatory cycles, implicating the role of hormones in the pathogenesis of this disease. In support of this so-called incessant ovulation hypothesis, factors that decrease the number of ovulatory cycles such as multiple pregnancies and prolonged lactation have been linked to reducing the risk of developing OC (AIHW 2017; Hunn and Rodriguez 2012). Tubal ligation, unilateral or bilateral oophorectomy (removal of the ovary), salpingectomy (removal of the fallopian tube) and hysterectomy (removal of the uterus) have also been found effective in reducing the risk (Bassuk and Manson 2015; Moorman et al. 2013; Wentzensen et al. 2016).

Germline mutations in breast cancer type 1 susceptibility gene (*BRCA1*) or *BRCA2* are observed in 14.1% of OC patients and 44% of the families that have germline mutations in *BRCA1/2* did not have reported family history of breast or ovarian cancer. (Alsop et al. 2012). BRCA1/2 play a role in the DNA repair pathway by homologous recombination (HR). Other genes encoding proteins involved in this pathway such as *RAD51C*, *RAD51D*, *BRIP1*, *BARD1*, *PALB2*, *CHEK2*, *MRE11A*, *RAD50* and *ATM* are also altered in OC (Matulonis et al. 2016). The defectiveness in HR is currently being investigated to efficiently target a subset of OC patients (subsection 1.1.1.8) (Bowtell et al. 2015; Matulonis et al. 2016; Romero and Bast 2012)). In addition, inherited disorders such as Lynch syndrome, characterised by mutations in the DNA mismatch genes *MLH1*, *MSH2*, *MSH6* and *PMS2*, increase risk of developing OC as well as multiple other cancers (Crispens 2012; Engel et al. 2012). It is becoming increasingly clear that OC is a collection of histologically and molecularly distinct diseases, with the ovary as the primary site of anatomical location. Evidence supporting this theory and molecular signatures is presented in subsection 1.1.2.1.

1.1.1.3 Diagnosis

OC is termed the "silent killer" due to nonspecific symptoms. Over 90% of women diagnosed with OC experience symptoms such as constipation, diarrhoea, nausea, vomiting, abdominal bloating or pain, which are nonspecific and can also occur as symptoms of ageing, menopause, weight gain and other benign conditions of the gastrointestinal tract (Bankhead et al. 2008; Goff et al. 2000; Jayson et al. 2014). The disease is often detected when these symptoms have remained unresolved, become frequent or severe, requiring a detailed examination. Unfortunately, OC has frequently already reached an advanced stage (stage III or IV) upon diagnosis. Diagnostic procedures involve transvaginal ultrasonogra-

phy and measurement of the serum protein Cancer Antigen 125 (CA-125) (Cannistra 2004; Goff et al. 2000; Matulonis et al. 2016).

CA-125, first characterised in 1981 (Bast Jr. et al. 1981), is the only biomarker that is widely used for routine management of OC (Felder et al. 2014; Matulonis et al. 2016). This membrane glycoprotein is expressed by epithelial cells of the bronchus, endometrium, ovary and cornea (Davies et al. 2007; Hattrup and Gendler 2008; Rustin et al. 2004). Due to its expression in multiple tissues, a rise in CA-125 levels above the "normal" level cut-off of 35 U/ml is not limited to OC but can be affected by pregnancy, menstruation, infection, uterine fibroids and other factors such as the patient's race, previous or current history of other cancers, whether she has had a hysterectomy, smokes regularly and consumes caffeine (Medeiros et al. 2009; Pauler et al. 2001; Verheijen et al. 1999). Therefore, CA-125 itself is not adequate to diagnose OC and is used in combination with modalities such as ultrasonography which can readily detect the presence of cysts surrounded by solid tissue mass of the carcinoma (Felder et al. 2014; Jayson et al. 2014; Matulonis et al. 2016). Nevertheless, CA-125 remains a robust biomarker to monitor disease recurrence (Burg, Lammes, and Verweij 1992, 1993; Felder et al. 2014).

1.1.1.4 Screening

Based on the low prevalence of OC, epidemiologists have estimated a minimum sensitivity of 0.75 and specificity of 0.996* of a test to be effective in population-wide screening (Clarke-Pearson 2009; Hennessy, Coleman, and Markman 2009). This is a significant hurdle to overcome. Although the baseline levels of CA-125 are variable amongst healthy women, they tend to remain relatively stable over time in a given woman, unless offset by conditions such as OC (Skates, Pauler, and Jacobs 2001; Skates et al. 1995). An algorithm named Risk of Ovarian Cancer Algorithm (ROCA) based on this concept and incorporating age-standardised risk was put forward to classify risk of having OC into three categories: low, intermediate and high (Menon et al. 2005). Recently, a large prospective randomised clinical trial, the UK Collaborative Trial of Ovarian Cancer Screening (UKCTOCS), on 202,638 post-menopausal women was conducted to test the effect of no screening, transvaginal ultrasonography and transvaginal ultrasonography + CA-125 on the diagnosis of OC. Although both of the screening methods detected OC at an earlier stage compared to no screening (Jacobs et al. 2016), no overall differences in the percentage of women diagnosed with OC and mortality reduction were observed

*Values of the diagnostic statistics such as sensitivity, specificity, accuracy and area under curve (AUC) are presented in proportions instead of percentages.

amongst the three groups (Jacobs et al. 2016). A reduction in mortality over the long-term (7-14 years) with ROCA was observed, but further follow-up of these women is required to validate this finding (Jacobs et al. 2016).

Besides CA-125, multiple meta-analyses have found human epididymis protein 4 (HE4) to be a superior marker compared to CA-125 in detecting OC in suspected cases, and a combination of both biomarkers was superior to either biomarker alone (Hu et al. 2016, 21 studies, N = 4,544; Chen et al. 2016, 8 studies, N = 1,832; Ferrarow et al. 2013, 16 studies, N = 3,858). This could be due to a lack of correlation in HE4 and CA-125 levels, suggesting that both biomarkers work independently (Chudecka-Głaz 2015). Risk of Malignancy Algorithm (ROMA) encompassing menopausal status and levels of HE4 and CA-125 is approved by the Food and Drug Administration (FDA) to assess the risk of epithelial ovarian cancer (EOC) in women with a pelvic mass (ROMA® 2011).

An FDA-approved multivariate Index Assay commercially sold as the 'OVA1' test (Vermillion 2009), comprising CA-125, transthyretin (prealbumin), apolipoprotein A1, beta 2 microglobulin, and transferrin, can also be helpful with pre-operative assessment of OC (Rai et al. 2002; Ueland et al. 2011; Zhang et al. 2004). An improvement of the OVA1 test called 'Overa' was made available in 2015. ROMA was found to be more specific than OVA1 in identifying malignancy in women with an adnexal mass (a lump in tissue of the adnexa of uterus) while no statistically significant difference was observed in the sensitivities of these tests (Grenache et al. 2015). The lower specificity of OVA1 could increase the referral to a gynaecological oncologist for further examination (Li 2012). OVA1 was more expensive than ROMA (~USD 600 versus ~USD 100) according data available in 2012[†] (Li 2012), suggesting that ROMA could be an economic option. Despite recent improvements, ROMA and OVA1 lack the sensitivities and specificities to be used as a population screening test, and they must be combined with a physical examination and imaging modalities to be clinically useful.

1.1.1.5 Role of surgery in the management of OC patients

Surgical resection of the tumour followed by chemotherapy is the standard primary treatment for newly diagnosed cases of OC. Systematic examination of the peritoneal cavity upon surgery to determine the spread of the tumour, including to the omentum, diaphragm, pelvic and para-aortic lymph nodes, as well as histology of the tumour, dictate tumour staging and grading. Adjuvant chemotherapy consists of six cycles of agents containing platin (cisplatin, carboplatin or oxaliplatin) and taxane (paclitaxel or docetaxel),

[†]It was not possible to update the quote without a physician's referral.

with carboplatin/paclitaxel being the most common combination (Coleman, Ramirez, and Gershenson 2017; Matulonis et al. 2016).

The goal of cytoreductive surgery is to remove the maximum amount of tumour mass and palliate symptoms for as long as possible (Fader and Rose 2007; Matulonis et al. 2016). Women with OC generally undergo total abdominal hysterectomy and bilateral salpingo-oophorectomy with omentectomy and comprehensive surgical staging. Cytoreductive surgery can be extensive, often requiring bowel resection, splenectomy, partial hepatic or pancreatic resection and diaphragm stripping (Fader and Rose 2007; Martín-Cameàn et al. 2016; Romanidis et al. 2014; Zapardiel et al. 2011). The extent of resectability depends on the health of the patient, tumour location and extent of disease, as well as expertise of the surgeon and the medical centre (Martín-Cameàn et al. 2016). Surgery performed by gynaecological oncologists usually have better outcomes for patients in terms of overall survival (OS) compared to non-gynaecological oncologists (Matulonis et al. 2016).

Griffiths 1975 first conclusively demonstrated the inverse relationship between the size of residual disease and patient survival, which has been subsequently confirmed by multiple independent studies (reviewed in Fader and Rose 2007). A meta-analysis of 6,885 OC patients compiled from 81 cohorts of advanced OC treated by debulking surgery followed by platinum-based drugs conducted by Bristow et al. 2002 led them to postulate that the median survival period increases by 5.5% for each 10% increase in maximal cytoreduction[‡]. Based on these studies, resecting tumours to a certain size was considered 'optimal'. The definition of 'optimal' has changed over time, ranging from <2 cm, <1 cm and 'no macroscopic' residual disease (0 mm, also called R0 resection). Optimal cytoreduction is currently defined as <1 cm of residual disease at the conclusion of the surgery (Matulonis et al. 2016; Nick et al. 2015). However, the R0 resection offers the longest OS period compared to any residual disease. For example, a retrospective pooled analysis of 7 Gynaecologic Oncology Group (GOG) protocols performed by Winter et al. 2008 on women with Stage IV EOC reported the median OS of R0 resected patients to be 64 months compared to 30 months for patients with 0.1-5 cm of residual disease. A meta-analysis from 3 European AGO-OVAR prospective random trials confirmed the benefits of R0 resection over >1 mm residual tumour (du Bois et al. 2009; N =3,126). Consequently, an increasing number of studies have been defining 'optimal' cytoreduction as R0 resection, and guidelines from reputed sources such as the National Comprehensive Cancer Network (NCCN) encourage

[‡]maximal cytoreduction effort was graded from 0-100%, with >2 cm residual tumour as 0% and <0.5 cm as 100%.

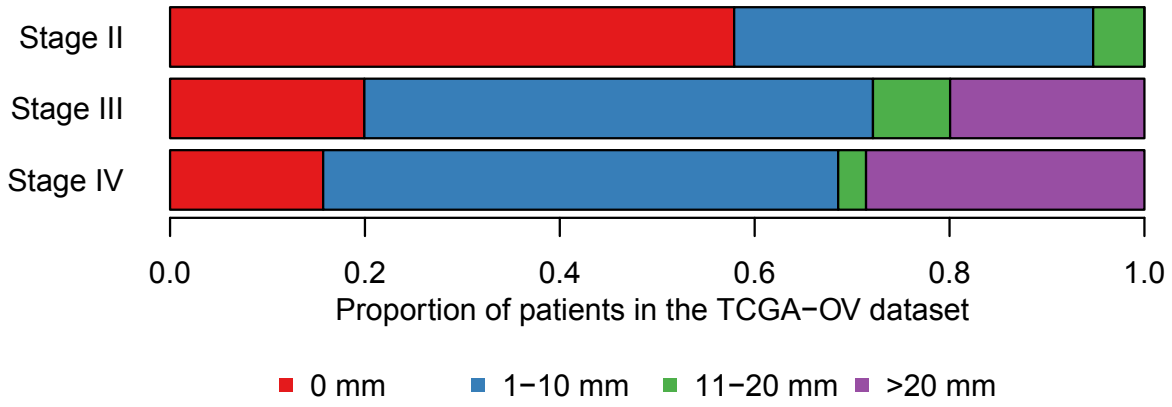

Figure 1.1: Size of the residual tumour reported in the TCGA-OV dataset
Size of the residual tumour reported in the TCGA-OV dataset (Bell et al. 2011) has been colour-coded. '0 mm' refers to 'no macroscopic' residual tumour, equivalent to the R0 status.

surgeons to be aggressive and achieve optimal cytoreduction whenever this is feasible (Chang et al. 2013; Horowitz et al. 2015; Jayson et al. 2014; NCCN 2017; Nick et al. 2015).

Despite the benefits, the R0 status is achieved in only 20 - 25% of the patients (Figure 1.1)(Bell et al. 2011; du Bois et al. 2009; Eisenhauer et al. 2008). Importantly, considering the aggressiveness of the surgery and significant subsequent morbidity, the overall benefits of the surgery in patients with >1 cm residual tumour are limited or none (Bristow 2006; Bristow et al. 2007). In fact, it may be better to avoid surgery and rely purely on chemotherapy in cases with extensive disease (Bowtell et al. 2015). Neoadjuvant chemotherapy (NACT), in which a patient receives 3 rounds of chemotherapy to 'shrink' tumours prior to the surgery followed by 3 additional cycles of adjuvant chemotherapy, remains an option for patients with advanced OC, although the efficiency of this approach remains a highly debatable topic (Kehoe et al. 2015; Trimbos et al. 2003). Two initial studies comparing NACT with standard therapy reported lower morbidity in patients receiving NACT while the OS remained unchanged (Morice et al. 2003, N = 85; Schwartz et al. 1999, N = 265). Larger randomised studies have supported this finding (Vergote et al. 2010, N = 632; Kehoe et al. 2015, N = 552). The current NCCN guidelines recommend NACT if maximal cytoreduction is unlikely to be achieved following pre-surgical assessment of a patient with or without minimally invasive surgical approaches. Criticisms of NACT include increased theoretical odds of developing drug resistance by exposing a greater number of tumour cells to chemotherapy, lost opportunities to cytoreduce where tumours could have been optimally cytoreduced but NACT was prescribed instead, and lack of solid long-term

survival data compared to standard therapy (Coleman, Ramirez, and Gershenson 2017; Coleman et al. 2013).

The decision whether to use standard therapy versus NACT has the potential to make a significant impact on the therapeutic route for OC patients. On one hand, it remains important to identify the patients that are likely to achieve the R0 resection because of the benefits in OS and PFS associated with it. On the other hand, NACT may well be suitable for a subset of patients that are unlikely to achieve the R0 resection due to age, health status or extent of the disease, and reduce their morbidity even though no significant benefit in terms of OS has been found to date. In fact, the 'Ovarian Cancer Action' meeting held in 2015 recommended the integration of tools to predict the surgical outcome as one of the seven priorities that will improve outcomes for women with advanced OC (Bowtell et al. 2015).

1.1.1.6 Prediction of surgical outcome in women with OC

1.1.1.6.1 Computed tomography Computed Tomography (CT) is the most common imaging modality for pre-operative assessment of OC (Ibeanu and Bristow 2010; Nick et al. 2015). The definition of optimal cytoreduction as <1 cm of residual disease is only used in recent studies aimed at predicting surgical outcome. By using the presence of diffuse peritoneal thickening and large volumes of ascites out of a total of 17 parameters, Dowdy et al. 2004 could predict the suboptimal cytoreduction outcome with a positive predictive value (PPV) of 0.68 and sensitivity of 0.52. Similarly, Bristow et al. 2000 devised a predictive model using 13 radiographic criteria and GOG performance status that could predict suboptimal cytoreduction with an accuracy of 0.93; however, this model did not reach the same level of accuracy in an independent study (Axtell et al. 2007). Two subsequent multicentre studies conducted in the UK reported conflicting results. Using CT pre-surgically, Borley et al. 2015 discovered that presence of the disease at certain sites (lung metastasis, pleural effusion, deposits on large-bowel mesentery and infrarenal para-aortic nodes) was associated with suboptimal cytoreduction. In contrast, Mackintosh et al. 2014 concluded that CT could not reliably predict the surgical outcome in multicentre studies, possibly due to variability in radiologists' skills in addition to differences in institutional policies and surgical skills.

1.1.1.6.2 CA-125 Circulatory protein CA-125 has been extensively tested for its ability to predict surgical outcome. However, these studies have generated conflicting results on (1) whether CA-125 is a predictive marker of surgical outcome, and (2) identifying

a reliable cut-off value for prediction (Arits et al. 2008; Barlow et al. 2006; Gemer et al. 2005; Memarzadeh et al. 2003; Rossi et al. 2004; Vorgias et al. 2009). These studies have defined optimal cytoreduction as <1 cm residual disease. Because of the recent advances and positive attitudes towards aggressive surgical procedures, optimal cytoreduction (<1 cm) was achieved in roughly 85% (24/28) of the patients with CA-125 levels exceeding 5000 U/ml, ten-times higher than the proposed cut-off of 500 U/ml (Chi et al. 2009). Thus, CA-125 levels seem to reflect the disease burden and need for aggressive surgery instead of predicting the surgical outcome (Ibeanu and Bristow 2010; Nick et al. 2015).

1.1.1.6.3 HE4 Circulatory protein HE4 used in the ROMA algorithm has been found to be superior to CA-125 in predicting surgical outcome from the primary (Angioli et al. 2013), N = 57, Shen and Li 2016, N = 83; Yang et al. 2013, N = 260; Tang et al. 2015; N = 90) as well as secondary surgery since the first relapse (Braicu et al. 2014, N = 73). Interestingly, the presence of ascites (Braicu et al. 2014) or the volume of ascites (>500 ml; Angioli et al. 2013) appears to improve the predictive power of HE4. Thus, HE4 has the potential to be a useful biomarker to predict surgical outcome, and should be tested vigorously in multicentre randomised studies.

1.1.1.6.4 Laparoscopy A series of studies conducted by Fagotti and colleagues have reported as a viable tool to predict surgical outcome with an accuracy of 0.773 - 1 (Fagotti et al. 2005, 2006, 2008, 2014). Laparoscopy is currently being investigated in the prospective randomised control SCORPION trial (NCT01461850 2013).

1.1.1.6.5 The Anderson Algorithm Researchers at the MD Anderson Cancer centre have proposed an algorithmic approach (The Anderson Algorithm) to manage patients with advanced OC as a part of the Cancer Moon Shot Program. This prospective trial consists of laparoscopy for pre-operative assessment of the disease, consensus guidelines on the choice of standard therapy versus NACT, involvement of multidisciplinary surgical teams to perform aggressive surgeries and the opinion of two surgeons, with the option of consultation with a third surgeon if required, to increase rates of the R0 resection and anticipated subsequent increase in progression-free survival (PFS) and OS (Nick et al. 2015). In a recent review, the author reported the rate of achieving R0 resection increased from 20% to 84% since adoption of the algorithm (Nick et al. 2015). While promising, an agreement on the likely surgical outcome with two to three surgeons may be difficult to achieve in smaller centres, and a dedicated publication on this approach outside of a review paper, awaits.

1.1.1.6.6 Gene expression of the tissues The use of gene signatures to predict surgical outcome has been limited. Bonome et al. 2008 reported a lack of gene signatures that could cluster high-grade OC samples according to the surgical outcome (N = 185). In contrast, Berchuck et al. 2004 reported the classification accuracy of ~0.75 based on a 32-gene signature, suggesting that optimally and suboptimally cytoreduced tumours could be genetically different. Similarly, a study validating performance of gene signatures in two publicly available datasets estimated the accuracy of prediction to be 0.56 - 0.73 (Abdallah et al. 2015). Finally, by analysing the The Cancer Genome Atlas (TCGA) dataset, Tucker et al. 2014 found *FABP4* and *ADH1B* to be differentially expressed in optimally (R0 resection) versus suboptimally (>0mm) cytoreduced samples, and a PPV of 0.86 was reported by using the 75th percentile (top 25%) in *FABP4* expression as the cut-off.

1.1.1.6.7 Machine learning/artificial intelligence As a novel approach, Enshaei, Robson, and Edmondson 2015 applied a machine learning algorithm known as artificial neural networks to predict the surgical outcome based on clinical data including age, stage, grade, histological type, and pre-operative CA-125 levels. The accuracy of the model was 0.77 in this single centre study, which is comparable to the accuracy prediction of CA-125 alone. Since the value of CA-125 in predicting surgical outcome is controversial, the significance of this model remains unclear.

1.1.1.6.8 Lymphocyte to monocyte ratio Eo et al. 2016 reported pre-operative ratio of lymphocyte to monocyte higher than as being 3.75 as being predictive of suboptimal cytoreduction (N = 154). However, the area under the receiver operator characteristic curve was found to be 0.593, which is marginally higher than the result obtained by chance, indicating that this approach is not suitable for reliable prediction.

1.1.1.7 Recurrence

Over 80% of the patients with advanced OC (Stage III or IV) are likely to experience disease recurrence (Herzog and Pothuri 2006). Recurrent disease is rarely cured, and the treatment options are largely focused on palliative care and a balance of efficacy versus toxicity of additional treatments (Matulonis et al. 2016). The choice of therapy also remains empirical after considering factors such as complications from the primary therapy, treatment history, observed and expected toxicity and performance status (Coleman, Ramirez, and Gershenson 2017). Most patients will undergo chemotherapy using a variety of agents instead of secondary surgery, which is only offered in limited cases where the

complete resection of the tumour mass is highly likely to be achieved such as the presence of isolated tumours (Jayson et al. 2014).

Recurrence could be detected in several ways. The symptoms could resemble the initial diagnosis or patients could experience new symptoms such as lymphoedema, shortness of breath or bloating (Herzog and Pothuri 2006). The disease could remain asymptomatic and be detected only by radiological or physical examinations. A rise in CA-125 levels after surgery, especially a doubling of the initial post-operative levels, is useful in monitoring the disease (Diaz-Padilla et al. 2012; Pignata et al. 2011; Verheijen et al. 2012). Resuming treatments purely based on CA-125 levels without any symptoms is not recommended. Rustin et al. 2010 evaluated the effect of resuming treatment immediately after observing a doubling in CA-125 levels without radiological evidence of recurrent disease versus delayed treatment upon confirmation of recurrence. As expected, women treated purely based on a doubling in CA-125 levels received chemotherapy roughly 5 months earlier than the 'delayed' group. However, no overall improvement in survival was observed, and the women receiving chemotherapy earlier had adverse effects on the quality of life (Rustin et al. 2010).

1.1.1.8 Drug resistance

OC is initially sensitive to chemotherapy. Approximately 70% of patients with OC will respond to the carboplatin/paclitaxel first-line chemotherapy; however, most will develop resistance to the therapy within first two years of the treatment, resulting in a 5-year survival rate of ~25% for patients with advanced OC (Agarwal and Kaye 2003; Hennessy, Coleman, and Markman 2009; Romero and Bast 2012). Recurrent OC is classified into 3 categories: platinum-refractory, -resistant or -sensitive, depending on the progression-free interval since the last chemotherapy.

Progression of the disease while receiving the last cycle of chemotherapy or within 4 weeks of the last platinum dose classifies a tumour as platinum-refractory (Romero and Bast 2012). These tumours are difficult to treat as they are already resistant to almost all available agents. The choice of treatment depends on the womans' wishes and comorbidity (Coleman, Ramirez, and Gershenson 2017).

Recurrence within the first 6 months since the last platinum therapy is termed platinum-resistant OC. A response rate of 10-30% using multiple agents has been observed (Mould 2012; Romero and Bast 2012). Considering the response to a platinum-based agent is no better than other agents (Coleman, Ramirez, and Gershenson 2017), current recommendation for treating platinum-resistant OC is nonplatin agents, such as the anti-angiogenic

bevacizumab with weekly paclitaxel (Pujade-Lauraine et al. 2014), pegylated liposomal doxorubicin or topotecan (Poveda et al. 2015), until such a time as the disease is stable, or when the toxicity outweighs the benefits (Coleman, Ramirez, and Gershenson 2017; Matulonis et al. 2016).

Patients with platinum-sensitive OC, where the recurrence is observed after 6-12 months since the last platinum treatment, are good candidates for chemotherapy containing platinum alone or in combinations with other drugs (Matulonis et al. 2016; Mould 2012; Romero and Bast 2012). A response rate of up to 50% is observed when treating with the carboplatin/paclitaxel combination (Parmar et al. 2003; Pujade-Lauraine et al. 2010). Currently, only a combination of gemcitabine and carboplatin is approved in the US for treatment of relapsed platinum-sensitive OC (Coleman, Ramirez, and Gershenson 2017; Pfisterer et al. 2006).

Recently, PARP inhibitors (PARPi), utilising the concept of synthetic lethality (subsection 1.1.2.2), have been found promising for the treatment of recurrent OC with defects in the HR pathway. The PARPi Olaparib was approved by the FDA in 2014 for use in patients carrying *BRCA1/2* mutations who developed recurrent disease (Kroeger and Drapkin 2017). Lynparza (Olaparib) was approved on the Pharmaceutical Benefits Scheme in Australia in February, 2017 (Sibthorpe 2017). In December 2016, a second PARPi called Rucaparib gained FDA approval for the treatment of tumours harbouring *BRCA1/2* mutations that have been treated with two or more chemotherapies (FDA 2016). A third PARPi called Niraparib also gained FDA approval in March 2017 as a maintenance therapy for EOC that has shown complete or partial response to platinum-based therapy (FDA 2017). Unlike Olaparib and Rucaparib, mutations in *BRCA1/2* genes is *not* a pre-requisite for Niraparib.

1.1.2 Biology of high-grade serous ovarian carcinoma

High-grade serous ovarian carcinoma (HGSOC) is the most common (~75%) and aggressive form of EOC with little improvement in the survival of affected women for decades (Bell et al. 2011; Bowtell et al. 2015; Kroeger and Drapkin 2017; Vaughan et al. 2011). Urgent measures are required to tackle this disease; therefore, the rest of the thesis will focus on HGSOC.

1.1.2.1 Histological subtypes

Approximately 90% of OC were thought to originate from the surface epithelium or surface epithelial inclusion cysts of the ovary (Chen et al. 2003; Feeley and Wells 2001; Romero and

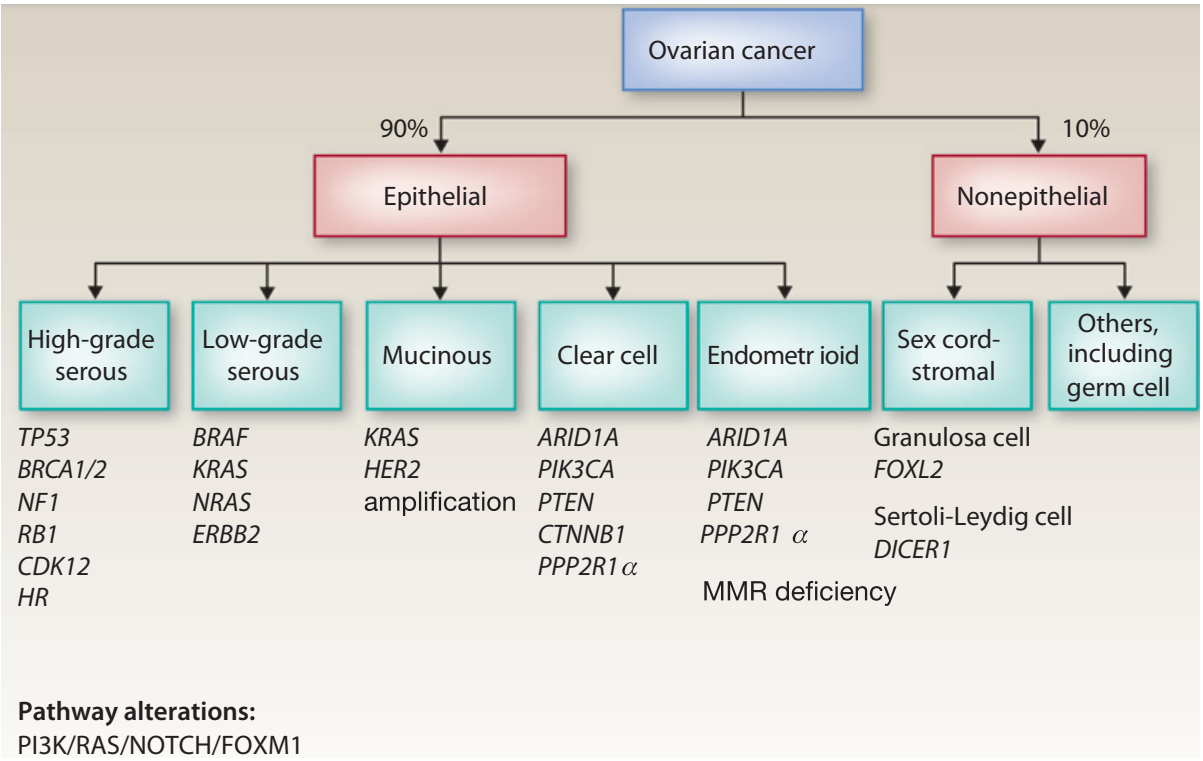

Figure 1.2: Ovarian cancer subtypes and their mutation spectrum
'HR': deficiency in homologous recombination due to aberrations in *CHK2*, *BARD1*, *BRIP1*, *PALB2*, *RAD50*, *RAD51C*, *ATM*, *ATR*, *EMSY*. 'MMR': mismatch repair (Adapted from Banerjee and Kaye 2013).

Bast 2012); however, new evidence support the fallopian origin of EOC (discussed shortly). EOC is classified into four major subtypes — serous, endometrioid, mucinous and clear cell — based on their similarity to the epithelium of the fallopian tube, endometrium, mucin-secreting endocervical glands and glycogen-filled vaginal rests, respectively (Figure 1.2) (Chen et al. 2003; Lalwani et al. 2011).

Additionally, OC can also be classified based on the degree of differentiation (tumour grade). Type I are indolent low-grade tumours that tend to be diagnosed at early stages (I or II). Low-grade serous, low-grade endometrioid, clear cell and mucinous carcinomas are Type I tumours (Lalwani et al. 2011). In contrast, Type II tend to be high-grade, highly aggressive and usually diagnosed at an advanced stage. Type II tumours include HGSOC, high-grade endometrioid, malignant mixed mesodermal tumours and undifferentiated carcinomas (Lalwani et al. 2011). Type I tumours are already resistant to conventional chemotheraphy whereas Type II tumours tend to respond well initially. In addition, Type I tumours tend to have frequent mutations in *BRAF*, *KRAS*, *PTEN*, *PI3KCA* and *ARID1A*, which are found to be mutated in <1% of Type II tumours (Figure 1.2) (Jones et al. 2010;

Wiegand et al. 2010). Notably, *TP53*, which is almost universally mutated in HGSOC, is rarely mutated in Type I tumours (Romero and Bast 2012). According to the 'dualistic model', Type I and II tumours represent two main pathways of carcinogenesis where Type I tumours are thought to arise from borderline tumours and in a stepwise manner while Type II tumours develop de novo (Hennessy, Coleman, and Markman 2009; Kurman and Shih 2011; Shih and Kurman 2004). Recent molecular and histological evidence suggest that a subset of EOC may undergo Type I to Type II conversion upon acquiring mutations in *TP53* or *PI3KCA* (Wu et al. 2013a).

There is now a substantial body of evidence supporting the idea that HGSOC, in fact, originates from the fallopian tube secretory epithelial cells. Briefly, analyses on women facing a genetic predisposition to OC (*BRCA1/2* mutations) discovered serous tubal intraepithelial carcinomas (STIC) in the fallopian tube that closely resemble HGSOC present at the ovary (Piek et al. 2001, 2003). Moreover, STICs were found in the fallopian tube in 50-60% of cases of sporadic OC, and the carcinomas were almost always detected in the fimbria (Colgan et al. 2001; Finch et al. 2006; Kindelberger et al. 2007; Medeiros et al. 2006). Subsequently, STICs were found to harbour identical *TP53* mutations to the concomitant HGSOC, suggesting that STICs were a precursor to HGSOC (Lee et al. 2007). Powered by the tools that genetically modify key genes only in the epithelial cells of the fallopian tube, genetically engineered mouse models provided mechanistic evidence supporting the pathogenesis of HGSOC: transformation of the fallopian tube epithelia, presence of STICs and their dissemination to the ovary in 56% to 100% of the mice, depending on the model (Perets et al. 2013; Sherman-Baust et al. 2014).

1.1.2.2 Genomic landscape of HGSOC

Studies conducted by Australian Ovarian Cancer Study Group (Tothill et al. 2008) and TCGA (Bell et al. 2011) have been instrumental in elucidating the genomic landscape of HGSOC. The TCGA study demonstrated four subtypes of HGSOC: immunoreactive, differentiated, proliferative and mesenchymal (Bell et al. 2011). The *TP53* gene was found to be mutated in almost all cases. Other significantly mutated genes include *BRCA1/2* (~22% cases), *CSMD3*, *NF1*, *CDK12*, *FAT3*, *GABRA6* and *RB1*. While HGSOC was not found to harbour a large number of mutations, the HGSOC genome showed extensive somatic copy number alterations, probably due to mutations in *TP53* and *BRCA1/2* (Bell et al. 2011). Pathway analyses identified RB1, PI3K/Ras, NOTCH, HR and FOXM1 as prominent pathways operating in the disease.

The HR pathway was found to be defective in ~50% of the TCGA cases (Bell et al. 2011). *BRCA1/2* genes were mutated in roughly 22% (including both germline and somatic cases), and a further 11% of the cases had inactivation in one or both genes due to DNA hypermethylation. Besides *BRCA1/2*, other genes in the HR pathway such as *EMSY*, *PTEN*, *RAD51C*, *ATM* and *ATR* were found to be deregulated in HGSOC. Synthetic lethality by inhibiting poly ADP ribose polymerase (PARP), a key protein in the HR pathway, remains an appealing strategy in cases where HR is defective (subsection 1.1.1.8) (Bell et al. 2011). Rapid advances like these attest to the value of large-scale genomic studies in enhancing cancer treatment.

1.1.2.3 Role of *TP53* in HGSOC

TP53 is the most mutated gene in human cancers (Muller and Vousden 2013; Oren and Rotter 2010; Strano et al. 2007b). Roughly 50% of all cancers have loss or mutations in *TP53* (Muller, Vousden, and Norman 2011). In its simplest manner, p53 is activated upon a wide range of stressors, such as DNA damage, nutrient deprivation, telomere erosion, hypoxia, ribosomal stress and/or oncogene activation, which then executes appropriate responses such as DNA repair, apoptosis, cell cycle arrest, cell survival, DNA repair and senescence to resolve the assault (Bieging and Attardi 2012; Vousden and Lane 2007; Vousden and Prives 2009). The overall action of functional p53 is preservation of integrity of the genome, explaining its moniker as the 'guardian of the genome' (Lane 1992).

The majority of the *TP53* mutations lie in the DNA binding domain, suggesting that deregulation of transcriptional activities is pivotal to the function of mutant-p53 (Strano et al. 2007a; Weisz, Oren, and Rotter 2007). The mutations in the amino acid residues that directly contact DNA (e.g. R273 and R248) are classified as the 'contact' mutations whereas those affecting the protein structure (e.g. R175 and H179) are known as 'conformational' mutations. Several 'hotspot' residues R273, R248Q, R175 and G245 tend to be altered in malignancies at a higher frequency than other amino acids (Walerych, Lisek, and Del Sal 2015).

Mutations in most tumour suppressors result in a loss of protein expression due to creation of early nonsense mutations and/or frame-shifts. Loss of wild-type (wt) tumour suppressor functions can ultimately culminate in cancer (Bieging and Attardi 2012; Muller, Vousden, and Norman 2011; Walerych, Lisek, and Del Sal 2015). In contrast, missense mutations are the most common type of mutations seen in *TP53*, which often result in higher expression levels of the mutant-p53 than its wt counterpart (Oren and Rotter 2010). p53 is a tetramer consisting of a dimer of dimers (Weinberg et al. 2004). Heterodimer of wt-

p53/mutant-p53 was found to have impaired ability of binding to p53-response elements on DNA, inhibiting the functions of wt-p53 due to a dominant-negative effect (Goh, Coffill, and Lane 2010). Mutant-p53 retains the ability to bind to the DNA, but the binding sites of mutant-p53 were found to be significantly different than the p53-response element (Thukral et al. 1995). Furthermore, a number of conformational and contact mutant-p53 were also shown to bind to p63 and p73, proteins that are additional members of the p53 family. Similar to inactivation of wt-p53 by mutant-p53 by dominant-negative effects, mutant-p53 associated with p63 was found to be present at sites on DNA that are not normally recognised by p63 (Martynova et al. 2012).

Moreover, mutant-p53 was found to interact with transcription factors and proteins that do not influence transcription directly, enhancing or preventing their activities, depending on the mutant-p53 and interacting partners (Muller and Vousden 2013). These pieces of evidence led investigators to propose that effects of mutations in p53 extend beyond a mere loss of wild-type p53 activities but play an active role in promoting carcinogenesis, and *some* mutations in p53 such as R273H and R175H may offer novel properties that greatly enhance carcinogenesis, known as the gain-of-function (GOF) hypothesis (Muller and Vousden 2013; Oren and Rotter 2010; Strano et al. 2007a). Consistent with this hypothesis, mouse models harbouring mutant-p53 were found to have more aggressive and metastatic tumours than p53-wild-type or p53-null mice (Doyle et al. 2010; Lang et al. 2004; Morton et al. 2010; Olive et al. 2004). Furthermore, patients with Li–Fraumeni syndrome harbouring germline *TP53* missense mutations developed tumours 9-15 years earlier than those with mutations that resulted in a loss of p53 expression (Bougeard et al. 2008; Zerdoumi et al. 2013).

The *TP53* gene is mutated in nearly 100% of cases of HGSOC (Bell et al. 2011). Mutations in *TP53* seem to be a necessary early event in the pathogenesis of HGSOC; however, it is not sufficient for development of this neoplasia (Bowtell 2010). Patients with Li-Fraumeni syndrome harbouring germline *TP53* mutations have higher frequencies of the "p53 signature"[§] in the distal fallopian tube, but they are not at an increased risk of developing HGSOC (Xian et al. 2010). In contrast, the frequency of the p53 signature is similar in women with or without *BRCA1/2* germline mutations (Lee et al. 2007). Furthermore, the p53 signature in patients with germline *BRCA1/2* were found to have a functional second copy of the allele, reiterating that the p53 signature alone is benign, even

[§]The p53 signature is a benign lesion in non-ciliated epithelium of the fallopian tube characterised by overexpression of the nuclear immunostaining of p53, partly due to mutations, in at least 12 consecutive cells. Despite the increased p53 staining, the cells are not highly proliferative (increased Ki67 staining in <10% of $p53^+$ cells; Lee et al. 2007). The p53 signature is not associated with elevated risk of developing OC (Crum et al. 2013).

in this high-risk population (Norquist et al. 2010). STICs from these patients, on the other hand, not only acquired mutations in *TP53* but also inactivated the second functional copy of *BRCA1/2* (Norquist et al. 2010). In short, precursor STICs developed on the mutant-p53 background only after a complete loss of *BRCA1/2* (Bowtell 2010).

1.1.2.4 Mutant-p53 as a therapeutic target

Given its central role in the biology of cancer, it is not surprising that mutant-p53 is an appealing therapeutic target (Table 1.1). Since mutant-p53 with missense mutations retains its full-length polypeptide that is highly expressed in a cell, reactivating wt-p53 activities from mutant-p53 is an intensive area of research. The following discussion is restricted to an agent known as APR-246/PRIMA-1^{MET} because it is currently undergoing FDA Ib/II trials for platinum-sensitive recurrent HGSOC with mutated p53 to test its efficacy with carboplatin (NCT02098343 2014).

A small molecule known as PRIMA-1 (p53 reactivation and induction of massive apoptosis 1) has been found to bind to mutant-p53 and activate wt-p53 activities. Briefly, p53-null Saos-2 cells were transfected with p53-R273H expression vector or control, and a library of small molecules was screened to identify compounds that inhibited cell growth (Bykov et al. 2002). Subsequently, a methylated form of the drug known as APR-246 (PRIMA-1^{MET}) was found to be much more potent than PRIMA-1 (Bykov et al. 2005b). APR-246 induced expression of canonical p53 target genes such as Cyclin Dependent Kinase Inhibitor 1A (*CDKN1A*)/*p21* (Liu et al. 2015; Zandi et al. 2011), Growth Arrest And DNA Damage Inducible Alpha (*GADD45A*) (Liu et al. 2015), BCL2 Associated X (*BAX*) (Bykov et al. 2005b; Izetti et al. 2014; Zandi et al. 2011), BCL2 Binding Component 3 (*BBC3*)/*PUMA* (Bykov et al. 2005b; Liu et al. 2015) and Mouse double minute 2 homologue (*MDM2*) (Izetti et al. 2014; Zandi et al. 2011) in a range of cancer cell lines harbouring mutant-p53, their xenografts, and, in selected cases, patient-derived xenografts transplanted into immunoincompetent mice.

Mechanistic insights as to why APR-246 is effective in diverse cell lines harbouring a wide range of missense mutations was provided by a seminal study by Lambert et al. 2009. APR-246 dissolved in phosphate buffered saline (PBS) *in vitro* spontaneously gave rise to its active agent methylene quinuclidinone (MQ); however, this process was significantly accelerated *in vivo*, possibly due to reactions with other molecules carrying thiol groups. MQ was found to be a Michael acceptor which reacts with nucleophiles such as thiol groups of the cysteine residues. Using mass spectrometry, up to 10 MQ molecules were found to be attached to the mutant-p53. Although it remains unclear precisely where MQ binds to the

	Mechanism	References
Degradation of mutant-p53		
HDAC inhibitors SAHA and NaB	Destablisation of mutant-p53 followed by proteasome degradation	Li, Marchenko, and Moll 2011; Yan et al. 2013
Dietary glucose restriction	autophagy-mediated degradation	Rodriguez et al. 2012
Inhibiting interactions with other proteins/pathways		
RETRA	Inhibiting p73/mutant-p53 interactions, liberating p73 for tumour suppression	Kravchenko et al. 2008
Statins	Inhibiting mutant-p53/cholesterol-meadited change in tumour architecture	Freed-Pastor et al. 2012; Singh and Singh 2013
Integrin inhibitors	Interfering with signalling pathways between RTK and integrin recycling	Desgrosellier and Cheresh 2010; Muller and Vousden 2014
Conversion to wild-type p53		
PRIMA-1/PRIMA-1^{MET}/APR-246	Michael acceptor. Stablisation of unfolded mutant-p53	Bykov et al. 2002, 2005b
NSC319726	Restoring wt-p53 folding from p53-R175H by increasing bioavailability of zinc ion required for correct folding.	Yu et al. 2012
STIMA-1	Stablisation of unfolded mutant-p53. similar to CP-31398	Zache et al. 2008b
SCH529074	Conversion to wild-type p53	Demma et al. 2010
CP-31398	Stablisation of unfolded mutant-p53	Foster et al. 1999
MIRA-1	Conversion to wild-type p53	Bykov et al. 2005c
PK7088	Stablisation of unfolded p53-Y220C	Liu et al. 2013b
PhiKan083	Stablisation of unfolded p53-Y220C	Boeckler et al. 2008

Table 1.1: Strategies targeting mutant-p53 for cancer therapies
Data for this table was supplied by Muller and Vousden 2014.

mutant-p53, the p53 core domain contains 10 cysteine residues, of which Cys182, Cys229, Cys242, and Cys277 are surface accessible and could be the primary targets. Interestingly, MQ preferred the unfolded protein state at 37 °C in p53-null H1299 cells expressing p53-R175H compared to the correctly folded structure at 32 °C, which also explained its specificity towards mutant-p53. Thus, by modifying mutant-p53, APR-246 is thought to restore the original wt-p53 structure. Since the p53 protein family also comprises p63 and p73 (Khoury and Bourdon 2010), it is theoretically possible that APR-246 also affects functions of these proteins. Unlike p53, p63 and p73 are rarely mutated in cancers (Irwin and Kaelin 2001; Melino, De Laurenzi, and Vousden 2002). However, certain mis-sence mutations in wt-p63 are common in the developmental syndrome ectrodactyly ectodermal

dysplasia-cleft (EEC), in which APR-246 treatment partially restored expression of p63 target genes as well as rescued keratinocyte differentiation (Shen et al. 2013).

Additionally, APR-246 is found to be synergistic with anti-cancer agents including cisplatin (Bykov et al. 2005a; Fransson et al. 2016; Izetti et al. 2014; Liu et al. 2015; Mohell et al. 2015), carboplatin (Fransson et al. 2016), doxorubicin (Fransson et al. 2016; Mohell et al. 2015; Saha et al. 2013), 5-fluorouracil (Bykov et al. 2005a; Liu et al. 2015), adriamycin (Bykov et al. 2005a), camptothecin (Bykov et al. 2005a), epirubicin (Liu et al. 2015), gemcitabine (Izetti et al. 2014; Mohell et al. 2015), erlotinib (Izetti et al. 2014) and olaparib (Deben et al. 2016) in multiple cancers. Many of these drugs elevate the expression of mutant-p53, potentiating even greater wt-p53 activities upon dual drug treatment (Bykov et al. 2016). Furthermore, MQ could also induce oxidative stress by depleting glutathione (GSH) and inhibiting thioredoxin reductase 1 (Bykov et al. 2016; Lambert et al. 2009). Cisplatin, carboplatin, doxorubicin, epirubicin and 5-fluorouracil generate extremely high levels of reactive oxidative species (ROS) (Conklin 2004a; Gorrini, Harris, and Mak 2013), indicating that oxidative stress could be a significant factor contributing to the observed synergy.

As mentioned above, APR-246 is currently undergoing clinical trials for treatment for OC (NCT02098343 2014). To the knowledge of the candidate, there are only three published studies investigating effects of APR-246 in OC. The first study conducted by Mohell et al. 2015 showed that APR-246 was synergistic with cisplatin, carboplatin and doxorubicin, and restored sensitivities of these drugs in the resistant cell lines harbouring mutant-p53. With the exception of OVCAR-3, cell lines used in this study (IGROV-1 and 3 cell lines derived from A2780) are not representative of OC, ranking as 'unlikely' HGSOC or 'hyper-mutated' according to an analysis by Domcke et al. 2013. Additionally, APR-246 was found to be synergistic with cisplatin in primary OC cells derived from five patients; however, one patient carried missense mutation Y220C, one harboured wt-p53 while the majority (3/5) had frameshift or nonsense mutations that might be expected to result in low to absent levels of mutant p53 protein. Synergy between APR-246 and cisplatin in the absence of missense mutations suggests additional mechanisms of action by APR-246. The effect of APR-246 was found to be at least additive with cisplatin in mice bearing xenografts of cisplatin-resistant A2780-CP20 cells, derived from A2780 cells by gradually increasing doses of cisplatin *in vitro*, carrying the *TP53* mutation V172F. Immunohistological analysis showed activation of the effector caspase-3 in mice treated with the dual drug combination, but typical wt-p53-response genes such as *CDKN1A* were not examined (Mohell et al. 2015). An extension of this work on cells obtained from

ascites of 10 platinum-resistant OC patients, of which 8 had HGSOC and 7 carried missense mutations in p53, reported strong synergy between APR-246 and cisplatin in the patients harbouring missense *TP53* mutations and at least an additive effect in patients harbouring wt-p53 or nonsense mutations (Fransson et al. 2016). An induction in wt-p53-like activities upon APR-246 was assumed, but not tested (Fransson et al. 2016). It is important to note that a number of authors of these two studies were employed by Aprea AB, the company undertaking clinical trials for APR-246, including the senior author Klas G. Wiman who is a co-founder of Aprea. Finally, an independent study showed that APR-246 induces apoptosis by accumulating ROS, irrespective of the p53 status of nine EOC cell lines (Yoshikawa et al. 2016). The authors tested this by using the ROS scavenger N-acetyl cysteine (NAC) to rescue cells from APR-246 treatment. Again, the typical downstream gene targets of p53 were not examined.

The exact mechanisms of how APR-246 operates in OC remain unclear despite its efficacy in restoring drug sensitivities in platinum-resistant OC cell lines and a limited number of primary cells. In particular, it has not been convincingly shown that APR-246 induces expression of canonical p53 genes in OC from mutant-p53, which was the predominant rationale for its current clinical trial titled 'p53 Suppressor Activation in Recurrent High Grade Serous Ovarian Cancer' (NCT02098343 2014). This thesis tests this, and whether wt-p53 is observed in mutant-p53 cell lines upon APR-246 treatment. APR-246 will also be used to identify the effect of mutant-p53 on non-coding RNAs (subsection 1.2.3).

1.2 Non-coding RNAs — a revolution

The haploid human genome is approximately 3 billion nucleotides in length. However, the information to code for all proteins represents merely 2% of the DNA; the rest was previously considered as 'junk'. Intriguingly, the number of protein coding genes do not correlate to organismal complexity, whereas the proportion of the 'junk' DNA increases with complexity, while being tissue-specific in its expression (Barry 2014; Derrien et al. 2012). One of the earliest study systematically investigating the mouse transcriptome (the FANTOM Consortium) discovered that roughly 47% (15,815/33,409) of the cloned 'transcriptional units' did not code for proteins (Okazaki et al. 2002). Recently, the ENCODE project revealed that roughly 75% of the genome was transcribed in at least one cell type (ENCODE 2012).

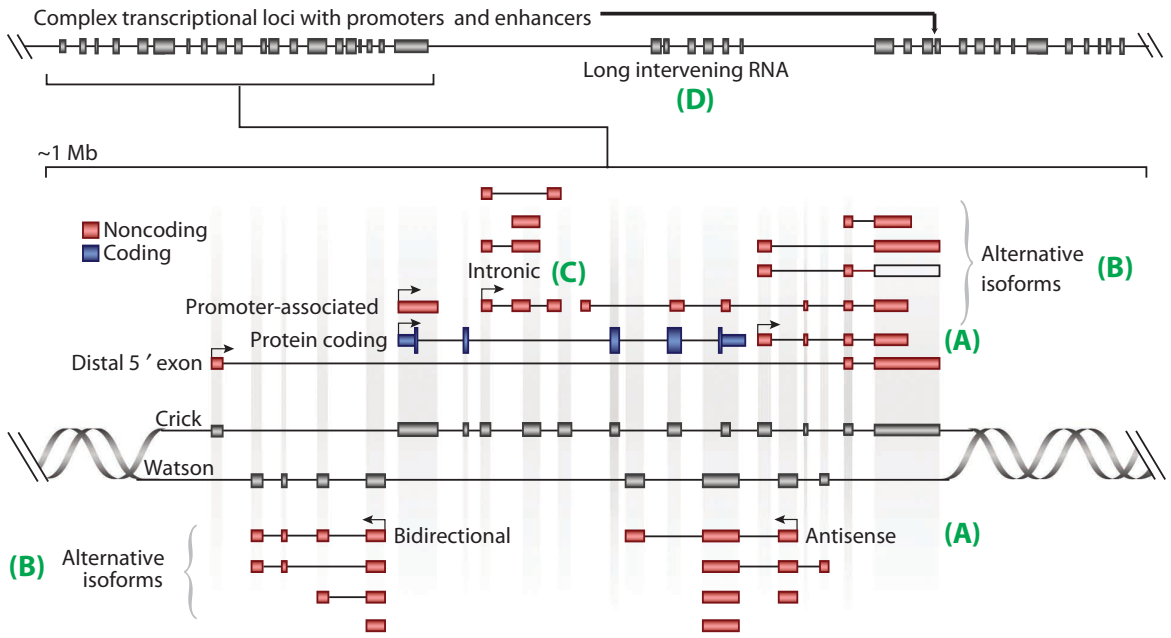

Figure 1.3: Origin of non-coding RNAs (ncRNAs) from multiple modes of transcription
(A) Transcription in sense, anti-sense or both directions (bidirectional). **(B)** Diversification in transcripts due to the use of alternate promoters, splicing and termination. **(C)** ncRNAs, such as microRNAs, originating from introns. **(D)** inter-genic regions as source of ncRNAs known as long intervening RNAs (lincRNAs). (adapted from Mercer and Mattick 2013)

With the advent of recent technologies such as tiling microarrays[¶] and RNA sequencing (RNA-seq), it is clear that most of the genome is actively transcribed. As shown in Figure 1.3, transcription could occur in sense and anti-sense directions, or be bidirectional. In fact, more than half of the human genes are transcribed in an anti-sense direction (Katayama et al. 2005). The use of alternate promoters, splicing and termination further diversify the transcripts. Eukaryote protein coding sequences are interrupted by non-coding regions (introns) that are transcribed but excised during maturation of the mRNAs. Surprisingly, the transcription of introns was found to be tissue-specific and responsive to physical stimuli, and, consequently, a significant proportion of intronic non-coding RNAs (ncRNAs) may have some function (Louro, Smirnova, and Verjovski-Almeida 2009). Roughly a quarter of small ncRNAs known as microRNAs are found to be of intronic origin (Kim and Kim 2007; Rodriguez et al. 2004). The regions between protein-coding genes (intergenic regions) are also transcribed into a plethora of ncRNAs collectively known as long interven-

[¶]Tiling microarray is a modification of the standard microarray platform employed for quantifying gene expression. Instead of using the probes covering the entire genome, probes with an overlap of one nucleotide are utilised for the entire locus of interest, exposing transcription from the locus.

Category	Symbol	Functions	References
3′ UTR-derived RNAs	uaRNAs	*cis* and *trans* regulation of protein expression or lncRNAs	Mercer et al. 2011
Antisense termini associated short RNAs	aTASRs	Unknown	Kapranov et al. 2007, 2010
Human Y RNA	hY RNA	DNA replication	Christov et al. 2006; Zhang et al. 2011a
microRNAs	miRNAs	Post-transcriptional gene silencing	Esteller 2011; Lin and Gregory 2015
PIWI-interacting RNAs	piRNAs	Suppression of transposable elements	Lin 2007; Stefani and Slack 2008
Promoter-associated short RNAs	PASRs	Epigenetic regulation of gene expression	Fejes-Toth et al. 2009; Han, Kim, and Morris 2007
Ribosomal 5S and 5.8S RNAs	rRNAs	Protein synthesis	Stults et al. 2008
Small interfering RNAs	siRNA	Post-transcriptional gene silencing	Kawaji and Hayashizaki 2008
Small nuclear RNAs	snRNAs	RNA splicing	Valadkhan 2005
Small nucleolar RNAs	snoRNAs	Maturation of rRNA	Williams and Farzaneh 2012
Termini-associated short RNAs	TASRs	Unknown	Kapranov et al. 2007, 2010
Tiny transcription initiation RNAs	tiRNAs	Epigenetic regulation of gene expression	Taft et al. 2009, 2010
Transcription start site antisense RNAs	TSSa-RNAs	Transcription initiation	Seila et al. 2008
Transfer RNAs	tRNAs	Protein synthesis	Phizicky and Hopper 2010

Table 1.2: Functions and classification of small non-coding RNAs

ing RNAs (lincRNAs), many of which bind to chromatin-modifying complexes and affect gene expression (Khalil et al. 2009; Ulitsky and Bartel 2013). Furthermore, genomic regions such as centromeres of chromosomes, which were thought to be transcriptionally inactive due to the presence of the silencing histone mark trimethyl-histone-3-lysine-9 (H3K9me3), were not only found to transcribe RNAs but this transcription was found to be required for proper chromosome formation during differentiation (Casanova et al. 2013; Probst et al. 2010). Essential gene regulatory units on DNA such as promoters and enhancers are also found to be transcriptionally active (Mercer and Mattick 2013).

ncRNAs are broadly grouped into two categories based on their length: small (<200 nucleotides) and long non-coding RNAs (lncRNAs) (>200 nucleotides). This classification is largely based on the RNA purification protocols that use different buffers to enrich small or long RNAs (Mattick and Rinn 2015; Mercer, Dinger, and Mattick 2009; Spizzo et al. 2012). According to a recent genomic analysis, the human genome houses roughly 21,000 protein coding genes and 58,000 lncRNAs (Iyer et al. 2015). Although investigating the role of lncRNAs is a vigorous area of research, functions of only a small number of lncRNAs are currently known (see subsection 1.2.2) and, as a result, a classification scheme based on functions of lncRNAs is currently missing (Mattick and Rinn 2015). In contrast, small ncRNAs are *marginally* better understood (Table 1.2). Roles of small RNAs known as microRNAs, PIWI-interacting RNAs (piRNAs) and small nucleolar RNAs (snoRNAs) have been well-established in post-transcriptional gene silencing, suppression of transposable elements and maturation of ribosomal RNA (rRNA), respectively (Table 1.2) (Esteller 2011; Patil, Zhou, and Rana 2014; Stefani and Slack 2008; Williams and Farzaneh 2012). A complete discussion on the roles of each of the different types of small RNAs is out of the scope of this thesis. Only microRNAs and lncRNAs are discussed in detail because experiments described in this thesis tests their utility to predict the surgical outcome of HGSOC patients, roles in cisplatin resistance and the effect of mutant-p53 on lncRNAs (see section 1.3).

1.2.1 microRNAs

1.2.1.1 Biogenesis and mechanisms

microRNAs are a group of small ncRNA with an average length of ~22 nucleotides that play a pivotal role in post-transcriptional gene suppression (Lin and Gregory 2015). Most microRNAs are transcribed from RNA polymerase II (Pol II) from dedicated gene loci whereas ~25% of microRNAs originate from introns (Kim and Kim 2007; Lee et al. 2004; Rodriguez et al. 2004). The newly transcribed RNA known as primary microRNA (pri-miRNA) is processed by enzymes into the precursor microRNA (pre-miRNA) and, subsequently, the mature form. Upon transcription, pri-miRNAs are capped, spliced and polyadenylated. The secondary structure of the pri-miRNA, consisting of a hairpin stem of 33 base pairs, a terminal loop and single-stranded regions upstream and downstream of the hairpin, is critical for its recognition and processing by the Microprocessor complex (Denli et al. 2004; Gregory et al. 2004; Han et al. 2004; Lee et al. 2003). The double-stranded RNase III enzyme Drosha and its essential binding partner DiGeorge syndrome

critical region 8 (DGCR8) are the core components of the Microprocessor complex. The Microprocessor complex is capable of recognising the single-stranded regions of the pri-miRNA as well as their distance from the terminal loop. With DGCR8 acting as a 'molecular ruler', Drosha cleaves the hairpin structure ~11 nucleotides away from the single-stranded junction, liberating the pre-miRNA of ~60-70 nucleotides (Han et al. 2004; Lee et al. 2003; Winter et al. 2009). The pre-miRNA is exported to the cytoplasm by Exportin-5 and Ran-GTP (Yi et al. 2003).

The exported pre-miRNA is further processed by the RNAse III enzyme Dicer, cutting the pre-miRNA close to the terminal loop and resulting in a double-stranded RNA of ~22 nucleotides with overhangs of 2 nucleotides at each 3' end (Lin and Gregory 2015). Transactivation-responsive RNA-binding protein (TRBP) is associated with Dicer during this process and bridges Dicer to Argonaute proteins (Ago1-4) to participate in the assembly of microRNA-induced silencing complex (miRISC) (Chendrimada et al. 2005). One strand of the duplex is retained by Ago proteins (the guide strand) while the other stand is typically degraded (Lin and Gregory 2015). The guide strand bound to Ago protein binds to the 3' untranslated region (UTR) of mRNAs. In a minority of cases where this pairing is 100% complementary, the mRNA is degraded through Ago2, the only catalytically active Ago protein in humans (Ipsaro and Joshua-Tor 2015). In other cases, nucleotides 2-7 from the 5' end of a microRNA, known as the 'seed sequence', are found to be complementary to 3' UTR of mRNAs, and the dominant mode of gene silencing is through suppression of mRNA translation or mRNA decay by deadenylation and decapping (Fabian and Sonenberg 2012; Ha and Kim 2014; Jonas and Izaurralde 2015).

The human genome is estimated to encode more than 3,500 microRNAs (Londin et al. 2015), which collectively regulate more than half of all protein coding genes (Friedman et al. 2009). Thus, it is not surprising that deregulation of microRNA expression is linked to various human diseases including cancer (Hesse and Arenz 2014).

1.2.1.2 microRNAs in cancer

The first evidence of the role of microRNAs in cancer was provided by Croce and colleagues in 2002, who demonstrated that the miR-15/16 cluster of microRNAs were frequently deleted or downregulated in chronic lymphocytic leukaemia (CLL) (Calin et al. 2002). Subsequently, a ground breaking study in 2005 demonstrated that microRNA profiling could classify human cancers (Lu et al. 2005). Later in the same year, the miR-17-92 cluster of microRNAs were found to co-operate with c-myc in promoting human B-cell lymphomas

(He et al. 2005). In addition, microRNAs were found to be downregulated in cancers, indicating their profound role in cancer biology. (Lu et al. 2005).

The mammalian genome contains two copies of *Dicer* (Winter et al. 2009). Loss of *Dicer* is selected against in mouse cancer models and loss of heterozygosity is almost never observed in human cancers, suggesting that *Dicer* works as a haploinsufficient tumour suppressor (Kumar et al. 2009). Interestingly, missense mutations in the RNase IIIB domain of Dicer occur frequently in nonepithelial ovarian cancer (Heravi-Moussavi et al. 2012). The mutant Dicer was unable to cleave the 5' end of pre-miRNAs, resulting in a global loss of microRNAs produced from this end ('5p' microRNAs), but the maturation of microRNAs from the 3' end ('3p' microRNAs) was unaffected (Anglesio et al. 2013). This bias towards the loss of '5p' microRNAs could lead to reduced expression of the tumour suppressor family of microRNAs let-7, all of which are derived from the 5' end (Lin and Gregory 2015). Moreover, loss of microRNAs could also be achieved by genomic deletion or epigenetic mechanisms such as DNA methylation in promoters and loss of histone acetylation (Lujambio and Lowe 2012). While microRNAs are generally downregulated in cancers, oncogenic microRNAs or 'oncomiRs', such as miR-21, miR-155, miR-210, miR-17-92 cluster and miR-221, are upregulated in cancer (Rupaimoole and Slack 2017).

Crucial proteins implicated in cancer biology are subjected to regulation by microRNAs. For example, the tumour suppressor phosphatase and tensin homolog (*PTEN*) is targeted by miR-21 (Meng et al. 2007; Zhang et al. 2012a), miR-214 (Fata et al. 2012; Penna, Orso, and Taverna 2015), miR-17-92 cluster (Xiang and Wu 2010), miR-93 (Kawano et al. 2015) and miR-221/222 (Zhang et al. 2011b). In primary neuroblastomas, *TP53* remains wild-type, but tends to be downregulated by miR-380-5p (Swarbrick et al. 2010). In fact, more than 20 microRNAs, including miR-504 (Hu et al. 2010a) and miR-125b (Le et al. 2009), are known to directly target p53 (Feng et al. 2011; Hermeking 2012). The oncogene *MYCN* is targeted by tumour suppressor microRNAs let-7 (Johnson et al. 2007; Sampson et al. 2007) and miR-34a (Cole et al. 2008; Wei et al. 2008; Welch, Chen, and Stallings 2007). Finally, miR-182 (Moskwa et al. 2011), miR-146a (Garcia et al. 2011; Shen et al. 2008), miR-15a (Zhu et al. 2009), miR-16 (Zhu et al. 2009), miR-638 (Li et al. 2011) and miR-17 (Shen et al. 2008) negatively regulate *BRCA1*.

microRNAs are becoming an attractive therapeutic option because of their profound role in cancer and their ability to influence levels of a large number of mRNAs (Friedman et al. 2009). There are two major types of approaches to the therapy: replenishing tumour suppressive microRNAs, and silencing disease-associated overexpressed microRNAs or oncomiRs (reviewed in Rupaimoole and Slack 2017). Several pre-clinical studies have

demonstrated the efficacy of restoring expression of the miR-34 family of microRNAs in inhibiting tumour growth in mouse models of lung (Kasinski and Slack 2012; Wiggins et al. 2010), pancreatic (Pramanik et al. 2011) and prostate cancers (Liu et al. 2011a). Currently, the effect of restoring miR-34 expression in cancers by lipid nanoparticles is being evaluated in a phase I clinical trial (NCT01829971). Inhibiting miR-122 by locked nucleic acids (LNA) is also being tested in clinical trials for the potential treatment of hepatitis C viral infections (Rupaimoole and Slack 2017).

1.2.1.3 microRNAs in OC

One of the earliest studies of EOC reported that ~15% and at least 36% of microRNAs are downregulated by genomic deletions and epigenetic silencing, respectively (Zhang et al. 2008). miR-15a, miR-34a and miR-34b were some of the downregulated microRNAs in late versus early stages of EOC. In particular, the *Dlk1-Gtl2* locus on chromosome 14 is commonly deleted in EOC, resulting in a loss of 8 microRNAs (miR-337, miR-376a, miR-376b, miR-432, miR-368, miR-495, miR-377 and miR-410) (Zhang et al. 2008). A total of 17 microRNAs were found to be differentially expressed between normal ovaries and HGSOC samples in the TCGA-OV dataset (Miles et al. 2012). Amongst them, 8 microRNAs (miR-183-3p, miR-590-5p, miR-16, miR-15b-3p, miR-15b, miR-18a, miR-18b and miR-96) were found to be upregulated while 9 microRNAs (miR-133a, miR-140-3p, miR-145-3p, miR-143-5p, miR-34b-5p, miR-145, miR-139-5p, miR-34c-3p, and miR-34c-5p) were downregulated (Miles et al. 2012). Furthermore, let-7b showed hemizygous and homozygous deletion in 86% and 7% of the samples, respectively. In contrast, the miR-31 family of microRNAs were focally amplified (Creighton et al. 2012).

1.2.1.4 Serum microRNAs as biomarkers

Each tissue-type has a specific pattern of microRNA expression, and microRNA profiling can distinguish various tissue-types as well as their cancers (Lu et al. 2005). Expression of microRNAs can separate healthy ovaries from EOC (Iorio et al. 2007) and different subtypes of HGSOC (Bell et al. 2011). Surprisingly, microRNAs were detected in twelve body fluids including serum, plasma, urine, saliva and tears (Weber et al. 2010), which was unexpected because microRNAs are short, RNA is chemically labile and most biofluids contain RNases. Moreover, serum microRNAs can withstand extreme conditions such as extended storage, multiple freeze-thaw cycles, high and low pH and even boiling (Becker and Lockwood 2013; McDonald et al. 2011). The encapsulation of microRNAs into

vesicles (exosomes, microvesicles and high-density lipoproteins), chemical modifications or association with protein complexes such as Ago2 are currently thought to provide protection against potent endogenous RNases present in the blood (Arroyo et al. 2011; Kosaka, Iguchi, and Ochiya 2010; Turchinovich et al. 2011). A combination of disease-specific expression and extraordinary stability in serum and other fluids led circulatory microRNAs to be described as a 'gold mine' of non-invasive biomarkers (Cortez et al. 2011).

Indeed, circulatory microRNAs have been able to detect colorectal (Cheng et al. 2011; Ng et al. 2009; Yong, Law, and Wang 2013; Zanutto et al. 2014), breast (Farazi et al. 2011; Heneghan et al. 2010; Madhavan et al. 2012; Volinia et al. 2012), prostate (Mahn et al. 2011; Mitchell et al. 2008; Nguyen et al. 2013; Selth et al. 2013; Shen et al. 2012), lung (Aushev et al. 2013; Hu et al. 2010b; Yu et al. 2008), gastric (Komatsu et al. 2013; Liu et al. 2011b; Tsujiura et al. 2010), and ovarian cancers as well as predicting OS, disease progression, stage, recurrence and distinguishing between good or bad prognosis, depending on the cancer. The literature on utility of circulatory microRNAs in detecting OC has been summarised in Table 3.8. Briefly, Taylor and Gercel-Taylor 2008 first demonstrated that the microRNA profile of blood-derived exosomes was similar to their expression in OC tissue, and circulating microRNAs could be used for detecting OC. Resnick et al. 2009 reported upregulation of 5 (miR-21, miR-92, miR-93, miR-126 and miR-29a) and downregulation of three microRNAs (miR-155, miR-127 and miR-99b) in EOC compared to healthy serum. Our laboratory has previously reported elevation of members of the miR-200 family of microRNAs in the serum from patients of serous EOC versus healthy individuals (Kan et al. 2012).

Despite the ease of access, serum microRNAs are easily swayed by pre-analytical variables and a careful approach is required for their accurate quantification. First, serum microRNAs are present at extremely low levels and may require large starting material for their quantification by real-time quantitative PCR (RT-qPCR). Unfortunately, blood components, such as haemoglobin (Akane et al. 1994), immunoglobin G (Al-Soud, Jönsson, and Rådström 2000) and lactoferrin (Al-Soud and Rådström 2001), also tend to be co-purified with RNA in low levels. Their effect on RT-qPCR is negligible when a small amount of RNA is used in RT-qPCR. However, these contaminants can significantly inhibit reverse transcriptase or Taq polymerase when an excessive amount of RNA is used, which is often the case for microRNAs given their low abundance (Blondal et al. 2013). Second, McDonald et al. 2011 discovered that differences in RNA extraction protocols were the least reproducible factor in microRNA quantification, which resulted in a high level of intra-assay imprecision. Third, release of the microRNA content of red blood cells (RBC)

upon haemolysis can dramatically alter the profile of disease-associated serum microRNAs. The extent of alteration of microRNA levels due to haemolysis in plasma is provided by two independent studies that have reported haemolysis affecting 58 - 65% of detectable microRNAs (Kirschner et al. 2013; Pritchard et al. 2012). Finally, miR-16, often used as a reference microRNA for quantification of serum microRNAs, is also affected by haemolysis (Kirschner et al. 2013).

1.2.2 Biology of lncRNAs

1.2.2.1 General features of lncRNAs

LncRNAs were found to have little protein-coding potential based on criteria such as the presence of open reading frames (ORFs) encoding peptides of >100 amino acids in length, evolutionary selection against the mutations that disrupt the coding sequence and homology of the putative protein product to known protein families (Derrien et al. 2012; Guttman and Rinn 2012; Lin, Jungreis, and Kellis 2011). Potential limitations of approaches based on comparative genomics include an apparent lack of conservation in lncRNAs due to their absence in less complex organisms or the encoded proteins representing newly evolving proteins (Derrien et al. 2012). Intriguingly, application of a new technique known as ribosome footprinting, which identifies RNAs bound to the ribosome, revealed that lncRNAs were frequently associated with ribosomes (Ingolia, Lareau, and Weissman 2011; Ruiz-Orera et al. 2014). To complicate the matter further, lncRNAs such as H19 and TUG1[⊠], which have not presented any evidence of protein production in independent studies (Brannan et al. 1990; Cai and Cullen 2007; Khalil et al. 2009; Yang et al. 2011), were also found to be associated with the ribosomes, indicating that association with ribosomes does not always result in protein production (Guttman and Rinn 2012; Ingolia, Lareau, and Weissman 2011). Recently, there is some evidence emerging that lncRNAs may code for short peptides. For example, a muscle-specific 46 amino acid transmembrane peptide myoregulin, originating from a lncRNA, was shown to regulate muscle physiology in mouse by regulating SERCA, a pump which transports Ca^{2+} from the cytoplasm to the sarcoplasmic reticulum following muscle contraction (Anderson et al. 2015). In addition, an 11 amino acid peptide torsal-less, translated from what was previously thought to be a ncRNA, was found to control tissue folding in *Drosophila* (Galindo et al. 2007). A recent genomic analysis suggested roughly 10% (~5,000/50,000) of lncRNAs could encode short

[⊠]The names of the lncRNA are not italicised when referring to as the expressed RNA form, whereas they are italicised when referring to the gene on the DNA, as in mutations in *H19*.

peptides termed transcripts of unknown coding potentials (TUCPs), and some of them could be biologically active as exemplified by myoregulin and torsal-less (Iyer et al. 2015).

GENCODE version 7 is perhaps the most comprehensive resource to elucidate general properties of lncRNAs (Derrien et al. 2012). Like mRNAs, lncRNAs are transcribed by Pol II, and have features such as 5' capping and 3' polyadenylation that are hallmarks of Pol II-dependent transcription. In addition, a small fraction of lncRNAs could also be transcribed by Pol III. The majority (98%) of lncRNAs are spliced, but most lncRNAs tend to have only two exons on average (Derrien et al. 2012). LncRNAs are highly enriched in the nucleus and are less abundant than mRNAs. More than half (65%) of mRNAs versus 11% of lncRNAs were present in all 16 human tissue-types tested, suggesting that the expression of lncRNAs is highly tissue-specific (Derrien et al. 2012). Even though most lncRNAs do not code for proteins, their promoters are evolutionarily conserved, suggesting an evolutionary pressure to maintain their expression. Exons of the lncRNAs also exhibit more conservation compared to introns or untranscribed intergenic regions (Derrien et al. 2012; Guttman et al. 2009; Ponjavic, Ponting, and Lunter 2007).

1.2.2.2 Cancer-associated lncRNAs and their mechanisms

Enrichment of lncRNAs in the nucleus suggest their role in regulating gene expression. A 2.1 kb lncRNA HOX transcript anti-sense RNA (HOTAIR) was one of the earliest lncRNAs that excited the field by demonstrating the potential of lncRNAs in cancer biology. HOTAIR is expressed in posterior and distal anatomical locations, where its normal function is to epigenetically silence a ~40 kb region spanning *HOXD8–HOXD11* on chromosome 2 (Rinn et al. 2007). Overexpression of HOTAIR promotes metastasis of breast, pancreatic, endometrial, colorectal, and other cancers (Gupta et al. 2010; He et al. 2014; Kim et al. 2012; Kogo et al. 2011; Lv et al. 2013). HOTAIR recruits two epigenetic writers to deposit silencing marks of the 'histone code' on the chromatin (Figure 1.4). The 5' end of HOTAIR binds to and directs Enhancer of zeste homolog 2 (EZH2), a core protein of the Polycomb repressive complex 2 (PRC2), to target loci, decorating them with H3K27me3 for chromatin condensation (Tsai et al. 2010). Additionally, the 3' end of HOTAIR recruits lysine-specific demethylase 1 (LSD1) that removes methyl groups from H3K4me2, erasing the epigenetic marks of active transcription (Tsai et al. 2010). Thus, by working as a scaffold, HOTAIR tethers two epigenetic modulators to the target loci. Unlike typical transcription factors, the target sites are recognised by HOTAIR itself, not PRC2 or LSD1 (Tsai et al. 2010).

Mammalian females carry double the number of X chromosomes compared to males (XX versus XY) in each nucleated cell; therefore, one copy of the X chromosome needs to

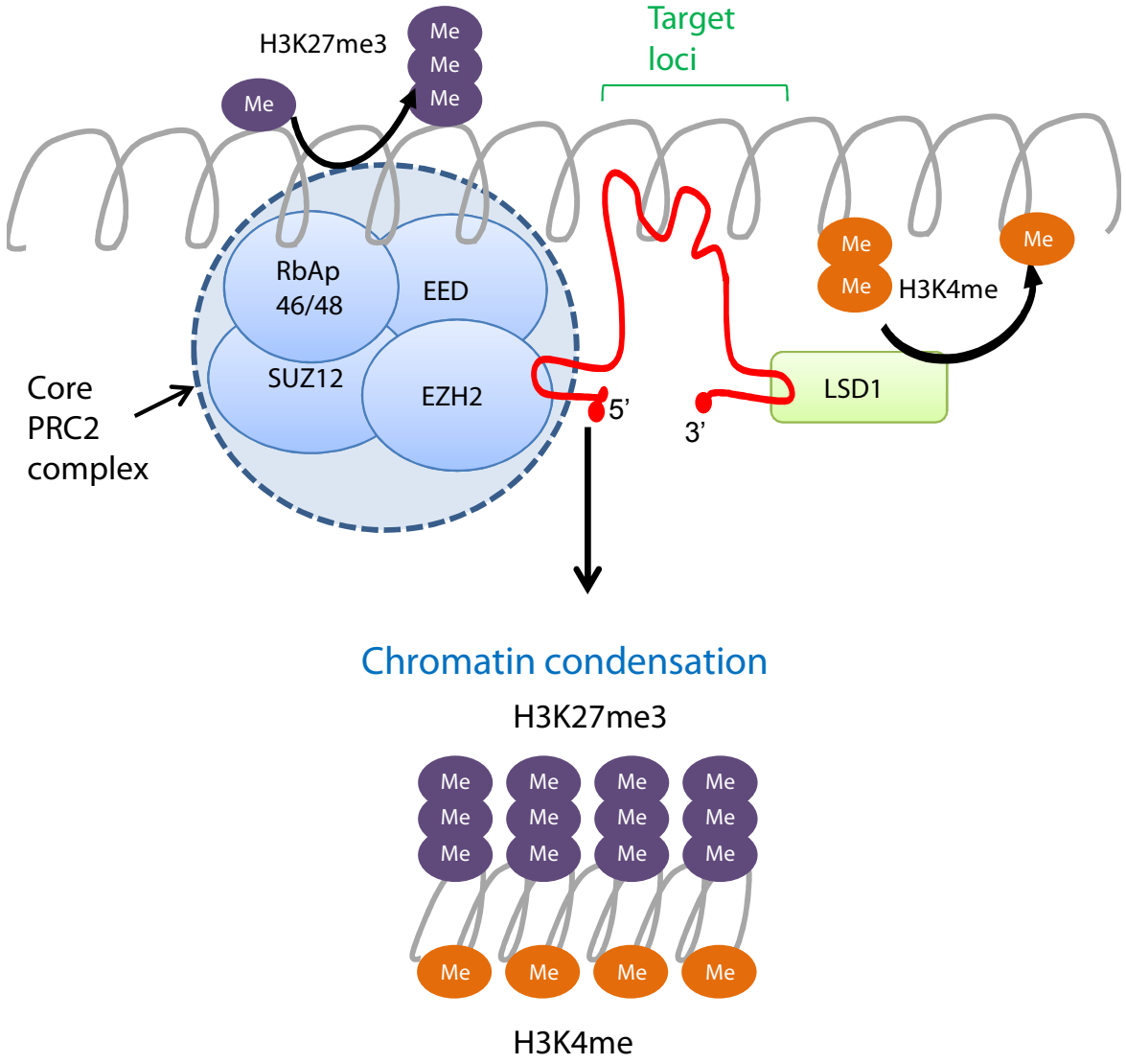

Figure 1.4: Epigenetic regulation of chromatin by lncRNA HOTAIR
Note: The PRC2 complex is comprised of four core proteins: RbAp46/48, EED, SUZ12 and EZH2. Adapted from Marsh, Shah, and Cole 2014.

be silenced in females for dosage compensation of the genes that are on the X chromosome. This remarkable fate is achieved by a 17 kb lncRNA X-inactive specific transcript (XIST), which utilises PRC2 to silence one entire X chromosome. The binding of PRC2 to lncRNAs is not restricted to HOTAIR or XIST. As mentioned previously, a subset of lncRNAs known as long intervening RNAs (lincRNAs) could originate from inter-genic regions (Figure 1.3D). Approximately 20% of lincRNAs were found to be physically associated with the PRC2 complex (Khalil et al. 2009). PRC2 has been referred to as 'promiscuous' in its ability

to bind RNAs by Professor Thomas Cech who was awarded the Nobel Prize in Chemistry in 1989 for discovering the catalytic role of RNA in splicing (Davidovich et al. 2013). Furthermore, ~30% (74/240) of lincRNAs in embryonic stem cells were found to be bound to at least 1 out of 12 chromatin modifying complexes such as epigenetic readers (PRC1, Cbx1, and Cbx3), writers (Tip60/P400, PRC2, Setd8, ESET and Suv39h1), and erasers (Jarid1b, Jarid1c, and HDAC1) (Guttman et al. 2011). LncRNA SChLAP1 overexpressed in a subset of prostate cancers antagonises tumour-suppressive functions of the chromatin-modifying complex SWI/SNF, resulting in metastasis and poor outcomes (Prensner et al. 2013). Taken together, this body of evidence suggests that chromatin regulation by lncRNAs is potentially a widespread phenomena.

LncRNAs can also regulate gene expression by interacting with promoters and enhancers. A significant proportion of enhancers themselves are known to transcribe RNAs termed enhancer RNAs (Mercer, Dinger, and Mattick 2009). A lncRNA transcribed from the upstream minor promoter of the dihydrofolate reductase (*DHFR*) locus could form a RNA:DNA triplex with the major promoter of the gene, suppressing its transcription by interfering with transcription factor binding (Martianov et al. 2007). In the context of cancer, Paupar, a lncRNA transcribed from a locus adjacent to the transcription factor *Pax6* whose expression is restricted to the central nervous system, interacts with distal promoters to regulate the cell cycle and maintain the de-differentiated state of neuroblastoma (Vance et al. 2014). Nuclear enriched abundant transcript 1 (NEAT1), an example of structural RNA that is essential for the formation of paraspeckles (Clemson et al. 2009), was recently discovered as a downstream target of the oestrogen receptor alpha (ERα) in prostate cancer (Chakravarty et al. 2014). ERα is expressed in prostate cancer regardless of the androgen receptor status. Prostate cancers expressing high levels of NEAT1 were resistant to androgen receptor antagonists, and NEAT1 drove oncogenic growth by associating with promoters of genes such as *PSMA* and *GJB1* that resulted in active transcription (Chakravarty et al. 2014). A class of steroid hormone known as glucocorticoids influence cell growth, energy expenditure and survival (Kino et al. 2010). The lncRNA Gas5 was found to be induced in the response to absence of nutrients or growth factors. By binding to the DNA-binding domain of the glucocorticoid receptor, Gas5 could prevent the receptor binding to its normal target sites. Thus, Gas5 inhibited the functions of the glucocorticoid receptor by working as a competitive inhibitor or a 'decoy' (Kino et al. 2010). An 8 kb lncRNA Metastasis Associated Lung Adenocarcinoma Transcript 1 (Malat1) has been shown to influence RNA metabolism, alternative splicing by recruiting serine/arginine (SR) proteins and transcriptional control via binding to Polycomb proteins (Dhamija and Diederichs 2016). Expres-

sion of Malat1 has been found to be altered in lung, liver, renal cell, breast, cervical, colorectal and bladder cancers (reviewed in Gutschner, Hämmerle, and Diederichs 2013).

According to the competing endogenous RNA (ceRNA) hypothesis, RNAs compete for binding sites intracellularly (Salmena et al. 2011). In the traditional sense, microRNAs reduce protein expression as discussed in subsection 1.2.1.1; however, the ceRNA hypothesis predicts that the levels of available microRNAs deflate once they have bound to their cognate sites, probably in the order of their strengths, and, consequently, a subset of mRNAs escape from microRNA-mediated gene silencing. A number of lncRNAs in the cytoplasm have been shown to work as ceRNAs or, informally, 'microRNA sponges'. Upregulation of lncRNA Highly Upregulated in Liver Cancer (HULC) has been shown to work as a microRNA sponge for miR-372 in hepatocellular carcinoma (HCC), rescuing the miR-372 target mRNA PRKACB from suppression (Wang et al. 2010). The PTEN pseudogene 1 (PTENP1) absorbs levels of microRNAs such as miR-21 that usually target the PTEN mRNA. Overexpression of PTENP1 negated actions of miR-21 and reduced cell proliferation, invasion, tumuor growth, and metastasis, which are hallmarks of the functional PTEN protein (Poliseno et al. 2010; Yu et al. 2014a). As expected from its tumour-suppressive functions, *PTENP1* was found to be downregulated in clear cell renal carcinoma by promoter methylation (Yu et al. 2014a) and deletion in melanoma (Poliseno, Haimovic, Christos, et al. 2011). HOTAIR has also been found to work as ceRNA for miR-29b, miR-1, and miR-141 (Bian et al. 2016; Liu et al. 2014; Su et al. 2016; Xu and Zhang 2017; Yu et al. 2017).

Recently, a species of lncRNAs knowns as circular RNAs (circRNAs) have been proposed to function as ceRNAs. A covalent bond between the 5' and 3' ends of an RNA closes the loop, forming a circle (Rong et al. 2017). In particular, circRNA-7 was found to have 70 binding sites for miR-7 (Hansen et al. 2013). Surprisingly, miR-671 could cleave circRNA-7 using Ago2, releasing miR-7 into the cellular pool (Hansen et al. 2011). Thus, circRNA-7 was referred as a buffer for miR-7, ensuring its rapid release when needed (Hansen, Kjems, and Damgaard 2013). Genome-wide circRNA studies have already shown their deregulation in gastric and colorectal cancers as well as squamous cell carcinoma since the first demonstration of the mechanism in 2013 (Sand et al. 2016; Zhao and Shen 2016).

In a short period, lncRNAs have been proven to have crucial roles in promoting cancer by diverse mechanisms, and the field continues to advance rapidly. Although the diagnostic potential of lncRNAs have been omitted from this discussion, the example of the lncRNA prostate cancer antigen 3 (PCA3) is worth noting. A urine test based on PCA3 is already in clinical use for detecting prostate cancer as PCA3 has been found to be superior to the current prostate-specific antigen (PSA)-based methods and overcomes limitations of PSA

such as dependency on the prostate volume (Chandra Gupta and Nandan Tripathi 2017). A deeper understanding and appreciation of the role of lncRNAs in normal physiology and disease aetiology is highly likely to lead to new avenues of diagnostics and therapeutic treatments.

1.2.2.3 LncRNAs in OC and chemoresistance

Compared to other cancers, the research on the role of lncRNAs in OC has been relatively sluggish. A number of lncRNAs have been predicted to have a role in OC, but many of them are not functionally validated (Table 1.3). By identifying the microarray probes in the TCGA-OV dataset corresponding to 10,207 lncRNAs, Du et al. 2013 reported that expression of lncRNAs correlated with OS or PFS of patients with HGSOC. In addition, expression of 1,749 lncRNAs were found to be specific to only one of the four subtypes of HGSOC, reiterating the specificity of lncRNA expression (Du et al. 2013). An independent analysis of the same dataset identified 455 deregulated lncRNAs in HGSOC versus the normal ovary; however, the authors could not define a lncRNA signature that predicted OS (Akrami et al. 2013). By applying principles of network analysis and ceRNA, Malat1, HOTAIR and maternally expressed gene 3 (MEG3) were predicted to have a role in OC (Zhou et al. 2015).

Name	Full Name	*In vivo* and *in vitro* observations	Mechanism	Expression	Reference
ZNF300P1	Zinc Finger Protein 300 Pseudogene 1	Downregulation decreases cell growth	Not described	Down	Gloss et al. 2014
AB073614	NA	Downregulation decreases proliferation, migration, invasion, and promotes apoptosis *in vitro*, and reduces tumour size *in vivo*	Not described	Up	Cheng et al. 2015
HOST2	Human ovarian cancer specific transcript 2	Downregulation decreases proliferation and migration *in vitro*, reduces tumour growth *in vivo*	microRNA sponge for let-7b	Up	Gao et al. 2015
LSINCT5	Long Stress-Induced Non-Coding Transcript 5	Downregulation reduces proliferation	Not described	Up	Silva et al. 2011
FAL1	Focally Amplified Long Non-Coding RNA In Epithelial Cancer	Overexpression suppresses senescence and expression of p21	Chromatin modification through PRC1	Up	Hu et al. 2014
PVT1	Plasmacytoma Variant Translocation 1	Downregulation decreases proliferation and promotes apoptosis	Myc protein stablisation	Up	Guan et al. 2007
XIST	X Inactive Specific Transcript	Downregulation decreases resistance to paclitaxel	Chromatin modification through PRC2	Down	Huang et al. 2002a
HOTAIR	HOX transcript anti-sense RNA	Overexpression increases migration and invasion and promotes EMT	Chromatin modification through PRC2	Up	Qiu et al. 2014
		Downregulation induces cell-cycle arrest *in vitro* and *in vivo*		Up	Qiu et al. 2015a
		Overexpression sensitises cells to carboplatin		Up	Teschendorff et al. 2015
HOXA11-AS	HOXA11 Antisense RNA	Overexpression decreases proliferation, migration, invasion *in vitro*, and reduces tumour size *in vivo*	Not described	Down	Richards et al. 2015
CDKN2B-AS1	CDKN2B Antisense RNA 1 (also known as ANRIL)	Overexpression increases metastasis	Chromatin modification through PRC2	Up	Qiu et al. 2015a
MEG3	Maternally expressed gene 3	Expression suppresses proliferation and promotes apoptosis	Chromatin modification through PRC2, activation of wt-p53	Down	Sheng et al. 2014
H19	H19, Imprinted Maternally Expressed Transcript	Codes miR-675 associated with EMT and chemoresistance	Chromatin modification through PRC2/microRNA production	Up	Matouk et al. 2014; Tanos et al. 1999

Table 1.3: LncRNAs in OC

'Expression' refers to expression of a lncRNA in OC tissues compared to normal ovary/surface epithelia (Adapted from Meryet-Figuière et al. 2016)

As discussed in subsection 1.2.2.2, Malat1 has been implicated in multiple cancers. Malat1 was found to be differentially expressed in SKOV-3.ip1 cells with an increased metastatic potential compared to the parental SKOV-3 cell line (Liu et al. 2013a). However, this was a preliminary *in vitro* study without any *in vitro* or *in vivo* validation of the invasive capabilities of the cells by siRNA knockdown or other methods. A recent study showed that Malat1 expression was stimulated by TGF-β, and siRNA knockdown of Malat1 reduced cell viability, proliferation, migration and invasion of SKOV-3 cells by regulating the MAPK pathway (Zou, Liu, and Wu 2016). Expression of MEG3 reduced levels of MDM2, leading to accumulation of wt-p53 (Zhou et al. 2007), but it is commonly lost or silenced by hypermethylation of its promoter in OC (Sheng et al. 2014).

XIST, H19 and HOTAIR have been implicated in OC biology as well as drug resistance. XIST was found to be downregulated in OC, leading to reactivation of some of the genes on the X chromosome, and correlated with a shorter PFS period (Huang et al. 2002b). Interestingly, decreased XIST expression was linked to increased resistance to paclitaxel, but not cisplatin (Huang et al. 2002b). A 'classic' lncRNA, H19, discovered in the 1990s (Brannan et al. 1990) was found to be overexpressed in cisplatin-resistant A2780cisR cells compared to its sensitive counterpart A2780 (Matouk et al. 2014). By acting as a pri-miRNA for miR-675, H19 promoted epithelial-mesenchymal transition (EMT), a phenomena that often promotes drug resistance in cancers (Singh and Settleman 2010), through the actions of miR-675 (Matouk et al. 2014). Silencing of HOTAIR reduced migration and invasion of EOC cells *in vitro*, and inhibited metastasis of OC to the peritoneum in mice (Qiu et al. 2014). The expression of HOTAIR was higher in serous OC samples compared to the normal ovary and correlated with stage and grade of the tumour (Kogo et al. 2011; Qiu et al. 2015b). Additionally, patients with elevated levels of HOTAIR had a shorter OS period (Qiu et al. 2015b). Like H19, HOTAIR was overexpressed in A2780cisR versus A2780 cells (Ozes et al. 2013). Mechanistically, HOTAIR promoted cisplatin resistance by activating the wnt/β-catenin pathway (Li et al. 2016).

1.2.3 The effect of p53 on lncRNAs

p53 is a well-studied transcription factor influencing the expression of a plethora of protein-coding genes. He et al. 2007 first demonstrated that p53 also affects expression of non-coding RNAs, namely the miR-34 family of microRNAs. Notably, tumour-suppressive functions of p53 were partially mediated through miR-34 (He et al. 2007). Within five years, John Rinn's laboratory at the Harvard University, USA, showed that p53 also regulates

lncRNAs, by identifying lincRNA-p21 transcribed from a locus upstream of *CDKN1A* (p21) on chromosome 17 in mouse (Huarte et al. 2010). lincRNA-p21 was shown to be associated with heterogeneous nuclear ribonucleoprotein K (hnRNP-K) to suppress a subset of genes that are usually suppressed by p53 (Huarte et al. 2010). Global transcription factor-binding analysis (ChIP-seq) showed that half of the DNA regions bound by p53 were located outside the protein-coding genes (Idogawa et al. 2014). Consequently, the list of lncRNAs directly affected by p53 is growing. PANDA (Hung et al. 2011), Pint (Huarte et al. 2010), PR-lncRNA-1 (Sánchez et al. 2014), PR-lncRNA-10 (Sánchez et al. 2014), NORAD (Lee et al. 2016), TUG1 (Guttman et al. 2009; Khalil et al. 2009), PVT1 (Barsotti et al. 2012), LINP1 (Zhang et al. 2016c), DDSR1 (Sharma et al. 2015) and DINO (Schmitt et al. 2016) have been reported to be transcribed directly or indirectly by p53, aiding the 'guardian of the genome' in its tumour-suppressive functions.

Despite the remarkable progress in understanding the effect of p53 on ncRNAs, effects of mutant-p53 on lncRNAs remain largely unexplored. As discussed in subsection 1.1.2.3, mutant-p53 can inactivate members of the p53 family of proteins as well as may offer new capabilities that significantly enhance carcinogenesis. Therefore, it is likely that mutant-p53 orchestrates a dramatically different transcriptomic 'symphony' than its wild-type counterpart, and expression of lncRNAs could be a significant part of it.

1.3 Thesis aims

The overall goal of this thesis is to apply the power of non-coding RNAs, both microRNAs and lncRNAs, to OC with the following aims:

1. To assess the diagnostic role of serum microRNAs in separating patients with HGSOC from healthy women as well as predict their surgical outcome.
2. To assess whether lncRNAs have a role in promoting cisplatin resistance.
3. To investigate the influence of the mutant-p53 targeting drug APR-246 on coding and non-coding RNAs.

Chapter 2

Materials & methods

2.1 Detection of serum microRNAs

2.1.1 Collection of cell-free serum

Written informed consent was obtained and blood collected from 56 women with HGSOC (64.1 $\pm$ 3.4 years) and 30 healthy females age matched within 5 years (61.0 $\pm$ 4.7 years) under a protocol approved by the Northern Sydney Local Health District Human Research Ethics Committee (Protocol # 0310-209B). For women undergoing surgical resection of their tumour, blood was collected from the peripherally inserted central catheter (PICC line) prior to the induction of anaesthesia. Blood from healthy volunteers was collected using a 21 gauge needle. In both cases, samples were transferred or collected into a 9 ml BD Vacutainer serum tube (BD). Blood was allowed to clot for 15 - 30 minutes at 4 °C and centrifuged at 3000 rpm for 15 minutes at 4 °C. Serum was carefully withdrawn without disturbing the buffy coat and immediately stored at -80 °C in 500 µl aliquots as part of the Kolling Institute Gynaecological Tumour Bank. Samples were rapidly thawed in a 37 °C water bath as required. Additional centrifugation at 3000 g for 5 minutes resulted in the cell-free fraction. Samples were randomised and remaining procedures performed in a single-blind manner to avoid bias.

Table 2.1: List of chemicals and reagents

Name	Supplier	Catalogue number	City	State	Country
4-12% NuPAGE® Novex Bis-Tris gel	ThermoFisher Scientific	NP0321BOX	Scoresby	Victoria	Australia
Acetic Acid (Glacial)	Bacto Laboratories	A1-2.5L GL	Mt Pritchard	NSW	Australia
Agarose, molecular biology grade	Bio-Rad	1613102	Gladesville	NSW	Australia
AllStars Negative Control	Qiagen	SI03650318	Chadstone	Vic	Australia
Ampicillin Sodium Salt	Sigma-Aldrich	A9518-5G	Castle Hill	NSW	Australia
APR-246/PRIMA-1^{MET}	Cayman Chemicals	9000487	Ann Arbor	Michigan	USA
BD Horizon Fixable Viability Stain 450 (FVS450)	BD	562247	North Ryde	NSW	Australia
Bromophenol blue	Sigma-Aldrich	114391-25G	Castle Hill	NSW	Australia
Chloroform:Isoamyl alcohol (24:1)	Sigma-Aldrich	25666-100ML	Castle Hill	NSW	Australia
Cisplatin	Sigma-Aldrich	P4394-25MG	Castle Hill	NSW	Australia
DMEM, high glucose	HyClone/GE life sciences	SH30243.01	Logan	Utah	USA
dimethyl sulfoxide (DMSO)	Sigma-Aldrich	D8418-50ML	Castle Hill	NSW	Australia
DpnI enzyme	New England BioLabs	R0176S	Ipswich	MA	USA
Ethylenediaminetetraacetic acid (EDTA)	Astral Scientific	0105-5009	Caringbah	NSW	Australia
Electroporation cuvettes	Bio-Rad	1652086	Gladesville	NSW	Australia
Fetal bovine serum (FBS)	AusGeneX	FBS500-S	Molendinar	QLD	Australia
Glycerol	Sigma-Aldrich	15524	Castle Hill	NSW	Australia
Glycine	Sigma-Aldrich	VWRC10119CU-5KG	Castle Hill	NSW	Australia
HiPerFect Transfection Reagent	Qiagen	301707	Chadstone	Vic	Australia
Amersham Protran Supported 0.45 Nitrocellulose membrane	Sigma-Aldrich	GE10600016	Castle Hill	NSW	Australia
LoBind microcentrifuge tubes	Sigma-Aldrich	Z666548-250EA	Castle Hill	NSW	Australia
Methanol	ThermoFisher Scientific	5005-10L	Scoresby	Victoria	Australia
3 (N-Morpholino) propanesulfonic acid (MOPS)	Sigma-Aldrich	M1254-1KG	Castle Hill	NSW	Australia
Sodium chloride	Astral Scientific	BIOSB0476-5kg	Caringbah	NSW	Australia
Opti-MEM® Reduced Serum media	ThermoFisher Scientific	31985-062	Scoresby	Victoria	Australia

Name	Supplier	Catalogue number	City	State	Country
PfuUltra II Fusion HS DNA Polymerase	Agilent Technologies	600670	Mulgrave	Vic	Australia
Pierce ECL Dura reagent	ThermoFisher Scientific	32106	Scoresby	Victoria	Australia
Pierce ECL Pico reagent	ThermoFisher Scientific	34080	Scoresby	Victoria	Australia
Ponceau S	Bio-Rad	P7170-1L	Gladesville	NSW	Australia
Propan-2-ol (isopropanol)	ThermoFisher Scientific	425-2.5L	Scoresby	Victoria	Australia
QIAzol lysis reagent	Qiagen	79306	Chadstone	Vic	Australia
RNA 6000 Nano Assay	Agilent Technologies	5067-1511	Mulgrave	Vic	Australia
RNA from MS2 bacteriophage	Sigma-Aldrich	10165948001	Castle Hill	NSW	Australia
RNaseZap® RNase Decontamination Solution	ThermoFisher Scientific	AM9780	Scoresby	Victoria	Australia
ROX reference dye	ThermoFisher Scientific	12223-012	Scoresby	Victoria	Australia
RPMI-1640	HyClone/GE life sciences	SH30027.01	Logan	Utah	USA
Sodium dodecyl sulfate (SDS)	Sigma-Aldrich	L3771-500G	Castle Hill	NSW	Australia
SeeBlue® Plus2 protein standard (range 4-250 kDa)	ThermoFisher Scientific	LC5925	Scoresby	Victoria	Australia
SeeBlue® Plus2 Pre-stained Protein Standard	ThermoFisher Scientific	LC5925	Scoresby	Victoria	Australia
Sucrose	Sigma-Aldrich	S0389-1KG	Castle Hill	NSW	Australia
SYBR Safe Nucleic Acid Stain	ThermoFisher Scientific	S33102	Scoresby	Victoria	Australia
SYBR safeDNA gel Stain	ThermoFisher Scientific	S33102	Scoresby	Victoria	Australia
Tris	Astral Scientific	77-86-1/0497-1KG	Caringbah	NSW	Australia
Trypsin-EDTA	Sigma-Aldrich	T4049	Castle Hill	NSW	Australia
Tryptone	Bacto Laboratories	211705	Mt Pritchard	NSW	Australia
Tween-20	Sigma-Aldrich	P5927-500ML	Castle Hill	NSW	Australia
Vacutainer serum tube	BD	455092	North Ryde	NSW	Australia
X-tremeGENE 9 DNA Transfection Reagnt	Sigma-Aldrich	6365809001	Castle Hill	NSW	Australia
Yeast extract	Bacto Laboratories	212750	Mt Pritchard	NSW	Australia

Table 2.2: List of commercial kits

Name	Supplier	Catalogue number	City	State	Country
Cell Line Nucleofector® Kit T	Lonza	VCA-1002	Mt Waverley	Victoria	Australia
CellTiter 96® AQueous One Solution	Promega	G3581	Alexandria	NSW	Australia
DNA High Sensitivity Reagent Kit	PerkinElmer	CLS760672	Notting Hill	Victoria	Australia
ExiLENT SYBR Green master mix	Exiqon	203420	Vedbaek		Denmark
iTaq™ Universal Probes Supermix	Bio-Rad	1725134	Gladesville	NSW	Australia
Maxima H Minus Reverse Transcription kit	ThermoFisher Scientific	K1652	Scoresby	Victoria	Australia
miRCURY RNA Isolation Kit - Biofluids	Exiqon	300112	Vedbaek		Denmark
miRNeasy Mini Kit	Qiagen	217004	Chadstone	Vic	Australia
mirVana™ PARIS™ RNA isolation kit	ThermoFisher Scientific	AM1556	Scoresby	Victoria	Australia
MitoProbe™ DiIC1(5) Assay Kit	ThermoFisher Scientific	M34151	Scoresby	Victoria	Australia
NucleoBon'd® Plasmid Purification Kit	Clontech	PC100	Mountain View	CA	USA
Pick-&-Mix microRNA PCR panel	Exiqon	203802	Vedbaek		Denmark
PureYield™ Plasmid Miniprep System	Promega	A1222	Alexandria	NSW	Australia
Quant-iT™ RNA Assay Kit, broad range	ThermoFisher Scientific	Q10213	Scoresby	Victoria	Australia
RNA Spike-In Kit	Exiqon	203203	Vedbaek		Denmark
SensiMix™ SYBR® Hi-ROX Kit	Bioline	QT605-05	Alexandria	NSW	Australia
Serum/Plasma Focus microRNA PCR panel	Exiqon	203843	Vedbaek		Denmark
SuperScript® III First-Strand Synthesis System	ThermoFisher Scientific	18080051	Scoresby	Victoria	Australia
The LncProfiler qPCR Array Kit	System Biosciences	RA910A-1	Palo Alto	CA	USA
TruSeq Stranded Total RNA Library Prep Kit	Illumina	RS-122-2201	Scoresby	Victoria	Australia
Universal cDNA Synthesis kit	Exiqon	203301	Vedbaek		Denmark
Universal KAPA Library Quantification Kit for Illumina Sequencing Platforms	KAPA Biosystems	KK4824	North Ryde	NSW	Australia

Table 2.3: List of software and equipments

Name	Supplier	City	State	Country
Applied Biosystems 7900HT Fast Real-Time PCR System	ThermoFisher Scientific	Scoresby	Victoria	Australia
Agilent 2100 Bioanalyzer	Agilent Technologies	Mulgrave	Vic	Australia
DNA Engine®Peltier Thermal Cycler	Bio-Rad	Gladesville	NSW	Australia
FACS Diva software V8.0.1	BD	North Ryde	NSW	Australia
epMotion 5070 liquid handling system	Eppendorf	North Ryde	NSW	Australia
ExpressionSuite V1.1	ThermoFisher Scientific	Scoresby	Victoria	Australia
Fujifilm LAS-4000 imaging system	Fujifilm	Brookvale	NSW	Australia
Gene Pulser Electroporator	Bio-Rad	Gladesville	NSW	Australia
GenEX software V6	Exiqon	Vedbaek		Denmark
LabChip GX	PerkinElmer	Notting Hill	Victoria	Australia
Moxi Z	Gene Target Solutions	Dural	NSW	Australia
NanoDrop™ 1000 spectrophotometer	ThermoFisher Scientific	Scoresby	Victoria	Australia
Nucleofector™ 2b Device	Lonza	Mt Waverley	Victoria	Australia
QuantStudio™ 7 Flex Real-Time PCR System	ThermoFisher Scientific	Scoresby	Victoria	Australia
Qubit® 2.0 Fluorometer	ThermoFisher Scientific	Scoresby	Victoria	Australia
SDS RQ Manager software V2.4	ThermoFisher Scientific	Scoresby	Victoria	Australia
SmartView Pro 2100 Gel Documentation System	Major Science	Saratoga	CA	USA
Synergy HT Microplate Reader	BioTek	Winooski	VT	USA

2.1.2 RNA extraction

RNA was extracted from 200 µl serum using the miRCURY RNA isolation kit for Biofluids (Exiqon) according to the manufacturer's instructions. Low nucleic acid binding (marketed as 'LoBind') 1.5 ml eppendorf tubes were used to minimise loss of RNA due to adsorption to tube walls (Sigma-Aldrich). All centrifugation steps were performed at 11,000 g at room temperature for the indicated period. The RNA Spike-in kit consisted of two parts: spike-into be added during RNA extraction (UniSp2, 4 and 5) and for reverse transcription (RT) (UniSp6 and cel-miR-39-3p).

Briefly, the designated bench for RNA work was cleaned using RNaseZap® RNase Decontamination Solution (ThermoFisher). Lysis was performed by adding 60 µl Lysis Solution for BioFluids (BF), 1µl (1 µg) RNA Spike-In Kit (UniSp2, 4 and 5; Exiqon) and 2.5 µl (1 µg) MS2 bacteriophage carrier RNA (Sigma-Aldrich). To remove proteins, 20 µl Protein Precipitation Solution BF was added to the sample, vortexed for 5 seconds, incubated for 1 minute at room temperature and centrifuged for 3 minutes. The clear lysate was transferred to an eppendorf tube, 270 µl isopropanol was added and mixed by vortexing for 5 seconds. The mixture was transferred to microRNA mini spin column BF, incubated for 2 minutes at room temperature and centrifuged for 30 seconds. Flow through was discarded. The column was washed by adding 100 and 700 µl wash solutions 1 and 2, respectively, with a centrifugation step of 30 seconds after addition of each solution. An additional wash was performed by adding 250 µl wash solution followed by centrifugation for 2 minutes. Next, the column was transferred to a fresh eppendorf tube. RNA was eluted in 25 µl nuclease-free water twice (final volume 50 µl) and stored at -80 °C in aliquots.

2.1.3 RT-qPCR

The study was split into the 'Discovery' phase using the Serum/Plasma Focus microRNA PCR panel (Exiqon) containing locked nucleic acid (LNA) primers for 186 microRNAs, of which 170 were target microRNAs, while the rest were primers to measure various factors such haemolysis that may influence the accuracy of RT-qPCR. The 'Validation' phase was designed using a miRCURY LNA Universal RT microRNA PCR Ready-to-Use PCR panel with custom selection of LNA microRNA primer sets (Exiqon). For the Validation phase, 48 microRNAs were measured for each sample including the controls. Because fewer microRNAs were measured in the Validation phase, RT for this phase was performed in 10 µl volume, and the RT-qPCR master mixed was scaled down without changing the ratio of the constituents.

RT was performed in either 20 µl or 10 µl for the Discovery and Validation phase, respectively, using 2 µl RNA template per 10 µl RT reaction as instructed by the Universal cDNA Synthesis kit (Exiqon). A 20 µl RT reaction contained 4 µl of 5X reaction buffer, 9 µl nuclease-free water, 4 µl RNA, 2 µl Enzyme mix and 1 µl Spike-in synthetic RNAs (UniSp6 and cel-miR-39-3p). RT was performed on a DNA Engine® Peltier Thermal Cycler (Bio-Rad) according to the following programme: 42 °C for 60 minutes followed by 95 °C for 5 minutes. The sample was first cooled at 4 °C , followed by storage at -20 °C. Three independent RT reactions were performed for each sample, and one PCR conducted for each RT.

The RT-qPCR master mix sufficient to run one sample on a Discovery Panel contained 1.04 ml of 2X ExiLENT SYBR Green master mix (Exiqon), 20 µl cDNA, 42 µl of 50X ROX dye (ThermoFisher) and 980 µl nuclease-free water. Ten µl of the master mix was transferred to each well of a Serum/Plasma Focus microRNA PCR panel or Pick-&-Mix microRNA PCR panel using the epMotion 5070 liquid handling system (Eppendorf). RT-qPCR was performed on a 7900HT Fast Real-Time PCR System (ThermoFisher) according to the following conditions: 95 °C for 10 minutes; 40 amplification cycles of 95 °C for 10 seconds and 60 °C for 1 minute, followed by melting curve analysis.

2.1.4 Data processing and analysis

Data was imported into the GenEx software V6 (Exiqon). An experimental design table containing grouping information for each sample was also imported into GenEx. In GenEx, plate-to-plate variations in RT-qPCR was normalised to the expression of UniSp3, an interplate calibrator present on each plate. Data points that differed in standard deviation by >1 for each gene per sample were removed. In addition, microRNAs amplified in no template control (NTC) or amplified at C_t > 37 were removed. Following the manufacturer's guidelines missing data was filled with the averages of the biological replicates. In cases where technical replicates for a microRNA in a sample were missing, the missing data were filled with averages of the remaining technical replicates. Global normalisation was applied to the Discovery panel. The NormFinder algorithm was used to identify reference microRNAs to normalise data in the Validation phase or when both sets were pooled and processed together. Missing data on a gene in patients were filled with averages of the biological group for that gene. No microRNA was consistently absent or not amplified in any particular biological group. Technical replicates (3 RTs) were averaged for each gene/patient. The normalised data now resembled ΔC_t of the widely used $2^{-\Delta\Delta C_t}$

method to analyse RT-qPCR data (Livak and Schmittgen 2001). Data was normalised to 'nothing', i.e. no specific biological group, which was calculated in GenEx by evaluating $2^{-\Delta C_t}$. Finally, the data was $\log_2$-transformed and used for subsequent analysis. Thus, last two steps of the processing was essentially $\log_2 (2^{-\Delta C_t}) = -\Delta C_t$. As a result of this, most of the data were negative.

2.2 Cell culture experiments

2.2.1 Cell lines and culture protocols

All cell lines were available in the laboratory upon commencement of this thesis. Their histology, origin and culture methods are listed in Tables 2.4 and 2.5. For passaging, cells were cultured in humidified incubators at 37 °C with 5% CO_2 and passaged at 70 - 90% confluency. Cells were washed once with warm PBS, treated with 0.25% Trypsin/EDTA solution (usually 1 ml) at 37 °C until detached. Approximately 10-times volume of the trypsin of pre-warmed culture media (usually 10 ml) containing FBS was added to the tube to neutralise trypsin followed by centrifugation at 300 g for 5 minutes at room temperature. Supernatant was replaced with fresh pre-warmed media, and cells were plated in cell culture flasks according to the split ratio. Cells were maintained for up to 10 passages after thawing.

2.2.2 Cryopreservation of cells

Cells were harvested at the confluency of 70 - 90% as described above. After neutralising trypsin, cells were preserved in their respective culture media containing a final concentration of 10% DMSO and aliquotted into 2 ml cryovials depending on the doubling time and the split ratio. Cryovials were transferred to the freezing containers and stored at -80 °C for at least 24 hours, after which they were transferred to liquid nitrogen vessels for long term storage. To revive frozen cells, the aliquots were rapidly thawed at 37 °C, washed once with warm culture media containing FBS, and plated in suitable cell culture flasks.

2.2.3 Mycoplasm testing

Cells were routinely tested for Mycoplasma contamination by using 1 ml of conditioned media from cultured cells on the MycoAlet™ Mycoplasma detection kit. This detection system relies on an enzyme produced by Mycoplasma to convert ATP to ADP, giving a luminescent signal which was read on the Veritas™ Microplate luminometer.

2.2.4 Cell typing

Cell typing to confirm their authenticity was performed on a fee-for-service basis at CellBank Australia (Children's Medical Research Institute, Westmead, Australia) using an AmpFLSTR® Identifiler® PCR Amplification Kit.

Table 2.4: Ovarian cancer cell lines used in this study

Cell line	Histology	Origin	Morphology	Reference
A2780	Undifferentiated carcinoma	Tumour	Epithelial	Bohrens et al. 1987
A2780CISR	Undifferentiated carcinoma; derived from A2780 by gradually increasing exposure to cisplatin *in vitro*	Tumour	Epithelial	Bohrens et al. 1987
CAOV4	Papillary serous adenocarcinoma	ovary; derived from metastatic site: subserosa of the fallopian tube	Epithelial	Karlan et al. 1988
COV318	Serous adenocarcinoma	Ascites	Epithelial	Berg-Bakker et al. 1993
H1299	Large cell carcinoma	lung; derived from metastatic site: lymph node	Epithelial	Giaccone et al. 1992
KURAMOCHI	Ovarian carcinoma	Ascites	Epithelial-like	Motoyama 1982
OAW28	Ovarian cystadenocarcinoma	Ascites	Epithelial	Hills et al. 1989
OVCAR-3	Poorly differentiated papillary epithelial ovarian cancer	Ascites	Epithelial	Hamilton et al. 1983
OVCAR4	Adenocarcinoma	Ovary	Epithelial	Hamilton, Young, and Ozols 1984
OVKATE	Adenocarcinoma	Ovary	Epithelial-like	Gorai et al. 1995
OVSAHO	Adenocarcinoma	Ovary	Epithelial-like	Gorai et al. 1995
PEO1	Poorly differentiated serous adenocarcinoma	Ascites	Epithelial	Cooke et al. 2010; Langdon et al. 1988
PEO4	Poorly differentiated serous adenocarcinoma; derived from the same patient as PEO1 after she developed resistance to cisplatin, 5-fluorouracil and chlorambucil	Ascites	Epithelial-like	Cooke et al. 2010; Langdon et al. 1988
SKOV-3	Serous adenocarcinoma	Ascites	Epithelial	Andre et al. 2002

Table 2.5: Cell culture conditions

Cell line	Medium	Culture method	*TP53* mutation
A2780	RPMI-1640 + 10% FCS	1:20 split every 3-5 days	wt
A2780CISR	RPMI-1640 + 10% FCS	1:20 split every 3-5 days	wt
CAOV4	RPMI-1640 + 10% FCS	1:2 to 1:3 split every 6-8 days	p.V147D
COV318	DMEM + 10% FCS	1:4 to 1:10 split every 4-7 days	p.I195F
H1299	RPMI-1640 + 10% FCS	1:10 every 4 days	p53 deletion
KURAMOCHI	RPMI-1640 + 10% FCS	1:10 every 7 days	p.D281Y
OAW28	DMEM + 20 IU/l Insulin + 10% FCS	1:3 to 1:6 every 4-7 days	p.P152fs
OVCAR-3	RPMI-1640 + 10% FCS	1:3 to 1:8 split every 3-5 days	p.R248Q
OVCAR4	RPMI-1640 + 10% FCS	1:4 to 1:5 split every 4 days	p.L130V
OVKATE	RPMI-1640 + 10% FCS	1:4 to 1:10 every 4-7 days	p.R282W
OVSAHO	RPMI-1640 + 10% FCS	1:4 to 1:10 every 4-7 days	p.R342*
PEO1	RPMI-1640 + 10% FCS	1:4 to 1:8 every 4-7 days	p.G244D
PEO4	RPMI-1640 + 10% FCS	1:4 to 1:8 every 4-7 days	p.G244D
SKOV-3	RPMI-1640 + 10% FCS	1:3 to 1:8 split every 3-5 days	c.267del1

2.2.5 Cell proliferation assays using MTS reagent

MTS assays were performed in 96 well plates with all 4 sides filled with sterile water to avoid the 'edge effect'. Cells were seeded in 100 µl culture media, plated for 8 - 24 hours, and treated with 100 µl media containing 2X of the intended drug concentration. Three technical replicates were performed for at each data point. In addition, each plate contained wells filled only with the culture media (blanks) and cells treated with the solvent of the drug (vehicle control) for normalisation (3 technical replicates). At the end of the treatment period, 100 µl media was removed and 20 µl of CellTiter 96® AQueous MTS solution (Promega) was added to each well. Plates were incubated for 1 - 3 hours in the dark at 37 °C, ensuring the produced brown colouration remained in the quantitative range of the assay. Air bubbles were removed, the plate was gently shaken and absorbance at 490 nm was read on a Synergy HT Microplate Reader (BioTek). For data analysis, the average of technical replicates was calculated, absorbance of the 'blank' well was removed from each well, and data were normalised to the vehicle control ($\frac{\text{Treatment}}{\text{Vehicle}} \times 100\%$). Data analysis was automated by a custom programming script written by the candidate in the statistical language R (Appendix C).

2.2.6 Determination of IC_{50}

Cell proliferation data was normalised to the vehicle control in R as mentioned in subsection 2.2.5. The 'drc' package (Ritz et al. 2015) was used to calculate IC_{50} using the 4-parameter (minimum, maximum, the point of inflection and Hill's slope) logistic regression model (see Appendix C for the code). In addition, the 'compParm()' function of the package was used to test whether IC_{50} values of two dose response curves (DRCs) were statistically different using non-linear regression. Cells treated with at least 5 drug concentrations in serial dilutions were used in the calculations.

2.2.7 Transfection of plasmids into mammalian cells

Cells were seeded in a 6 well plate in 2 ml culture media for 18 - 24 hours according to the seeding density required by the experiment. In general, cells were 70 - 90% confluent on the day of transfection. X-tremeGENE 9 DNA Transfection Reagent (Sigma-Aldrich), Opti-MEM media (ThermoFisher) and plasmid DNA were warmed at room temperature. The ratio of 3 µl X-tremeGENE to 1 µg plasmid DNA was used unless stated. X-tremeGENE was diluted with Opti-MEM to a total of 100 µl in an eppendorf tube, 1 µg of DNA

was added, the solution gently mixed by pipetting and incubated for 15 minutes at room temperature. The transfection mixture was added to the wells in a drop-wise manner and swirled gently to mix.

2.3 Molecular biology experiments

2.3.1 RNA

2.3.1.1 RNA extraction using the miRNeasy Mini kit

A maximum of 1 $\times 10^7$ adherent cells were washed once with warm PBS and harvested in 700 µl QIAzol lysis reagent (Qiagen) with a scraper. The sample was transferred to an eppendorf tube and mixed thoroughly by vortexing. The lysate was incubated at room temperature for 5 minutes, 140 µl chloroform:isoamyl alcohol (24:1) was added and vigorously mixed by vortexing for 15 seconds. The sample was briefly (2-3 minutes) incubated at room temperature followed by centrifugation at 12,000 g for 15 minutes at 4 °C. The mixture separated into a clear aqueous phase containing RNA (at top), a middle interphase containing DNA and a bottom pink organic phase containing proteins and lipids. The aqueous phase containing RNA was carefully transferred to a 2 ml eppendorf tube, and total RNA was extracted using the miRNeasy Mini kit (Qiagen) on a QIAcube robotic workstation according to manufacturer's instructions. RNA was eluted in 30 - 50 µl nuclease-free water and stored at -80 °C.

2.3.1.2 RNA extraction using the RNeasy Mini kit

A maximum of 1 $\times 10^7$ adherent cells were washed once with warm PBS and harvested in 350 µl RLT buffer (Qiagen) with a scraper. The lysate was transferred to a 2ml eppendorf tube, and total RNA was extracted using the manufacturer's protocol for the RNeasy Mini kit on a QIAcube robotic workstation. RNA was eluted in 30 - 50 µl nuclease-free water and stored at -80 °C.

2.3.1.3 Assessment of RNA concentration and quality using the NanoDrop™ spectrophotometer

The pedestal of the NanoDrop™ spectrophotometer (ThermoFisher) was washed once and blanked with 2 µl nuclease-free water prior to use. Two µl RNA was used to measure

its concentration and quality. A sample with both 260/280 and 260/230 ratios of > 2 was accepted as "pure" with negligible amounts of proteins and salts that may interfere with downstream analyses.

2.3.1.4 Assessment of RNA integrity using The Bioanalyzer

The integrity of RNA was checked using the RNA 6000 Nano Assay (Agilent Technologies) according to the manufacturer's instructions. Briefly, 1 µl Nano dye was mixed with 65 µl filtered Nano gel. Nine µl of the dye-gel mixture was pipetted into corresponding wells on the chip, and the chip was primed as described in the protocol*. One µl of total RNA (25–500 ng/µl) and the ladder were loaded into their respective wells on the chip, and the gel was run on an Agilent 2100 Bioanalyzer (Agilent Technologies). The virtual RNA gel and the RNA Integrity Numbers (RINs) are reported in this when appropriate.

2.3.2 RT-qPCR

2.3.2.1 Reverse transcription using the Maxima H Minus kit

RT was performed a final volume of 10 µl using the Maxima H Minus Reverse Transcription kit (ThermoFisher). Up to 2.5 µg total RNA, 0.5 µl random hexamers and 0.5 µl dNTP were adjusted with nuclease-free water to a total volume of 7.5 µl. The mixture was incubated at 65 °C for 5 minutes on a DNA Engine® Peltier Thermal Cycler (Bio-Rad) to denature secondary structures followed by 2-3 minutes of incubation on ice. Next, 2 µl of 5X RT buffer and 0.5 µl of the Maxima H Minus reverse transcriptase were added to the tube, resulting in the final volume of 10 µl. The final concentrations of the RT primers and dNTP were 5 µM and 0.5 mM, respectively. The sample was incubated at 25 °C for 10 minutes followed by 50 °C for 30 minutes. cDNA was diluted 10X with nuclease-free water and stored at 4 °C for short term or -20 °C for long term storage.

2.3.2.2 Reverse transcription using SuperScript® III First-Strand Synthesis System

The following components were added into a PCR tube: up to 5 µg of total RNA, 1 µl random hexamers, 1 µl 10 mM dNTPs and nuclease-free water to 10 µl. The tube was heated at 65 °C followed by >1 minute incubation on ice. Next, 10 µl of master mix

*http://www.agilent.com/cs/library/usermanuals/public/G2938-90034_RNA6000Nano_KG.pdf

Stage	Temp (°C)	Time
1	95	10 minutes
2 (40 cycles)	95	15 seconds
	60	30 seconds
	72	30 seconds
3 (melt curve)	95	30 seconds
	60	60 seconds
	95	30 seconds

Table 2.6: Conditions for RT-qPCR using SYBR green dye

containing 2 µl 10X RT buffer, 4 µl 25 mM $MgCl_2$, 2 µl DTT, 1 µl RNaseOUT^{TM} and 1 µl SuperScript III enzyme (ThermoFisher) were added to the same tube. The tube was briefly centrifuged, and incubated according to the following programme: 25 °C for 10 minutes, 50 °C for 50 minutes and 85 °C for 5 minutes. The cDNA was usually diluted at 10X and stored at 4 °C when usage was anticipated for short-term, with long-term storage -20 °C.

2.3.2.3 RT-qPCR using SYBR green dye

RT-qPCR was performed in 10 µl reactions in 384 well plates on an Applied Biosystems 7900HT Fast Real-Time PCR System (ThermoFisher). Typically, 8 µl of master mix was prepared for each primer pair followed by addition of 2 µl diluted template. The composition of the 8 µl master mix was as follow: 5 µl of 2X SensiMix SYBR Hi-ROX master mix (Bioline), 1.33 µl of forward and reverse primers (final concentration = 0.4 µM) and 1.67 µl nuclease-free water. PCR conditions are shown in Table 2.6.

2.3.2.4 RT-qPCR using TaqMan probes

RT-qPCR was performed in 10 µl reactions in 384 well plates on an ABI7900 PCR system (ThermoFisher). Typically, 8 µl of master mix was prepared for each TaqMan probe followed by addition of 2 µl of diluted template. The composition of the 8 µl master mix is as follow: 5 µl of 2X iTaq^{TM} Universal Probes Supermix (Bio-Rad), 0.5 µl of 20X TaqMan probe and 2.5 µl nuclease-free water. PCR conditions are shown in Table 2.7, and TaqMan probes used in this thesis are shown in Table 2.8.

Stage	Temp (°C)	Time
1	95	1 minute
2	95	15 seconds
(40 cycles)	60	60 seconds

Table 2.7: Conditions for RT-qPCR using TaqMan probes

TaqMan Probe	Supplier	Cat. No	City	State	Country
GAPDH-FAM	ThermoFisher Scientific	Hs02758991_g1	Scoresby	Victoria	Australia
TP53-FAM	ThermoFisher Scientific	Hs01034249_m1	Scoresby	Victoria	Australia
UCA1-FAM	ThermoFisher Scientific	Hs01909129_s1	Scoresby	Victoria	Australia

Table 2.8: TaqMan probes used in this study

2.3.2.5 Analysis of the RT-qPCR data

On completion of the RT-qPCR run, plates were added to a project in the SDS RQ manager software V1.2.2. The baseline and the C_t were manually adjusted for each gene if required. Further analyses were performed in the GenEX V6 or ExpressionSuite V1.1 softwares. Glyceraldehyde-3-Phosphate Dehydrogenase (GAPDH) was used as a reference gene for relative quantification of genes using the $2^{-\Delta\Delta C_t}$ method (Livak and Schmittgen 2001). For each sample, ΔC_t was calculated by subtracting the C_t of the GAPDH from each gene of interest. The $\Delta\Delta C_t$ was calculated by subtracting the ΔC_t of the calibrator sample from each sample. Since C_t was measured on the $\log_2$ scale, $2^{-\Delta\Delta C_t}$ operation transformed it back to the linear scale in terms of fold-changes.

Table 2.9: SYBR Green primers used for RT-qPCR.

Gene	Forward	Reverse	Catalogue Number	Gene ID	RefSeq ID
BAX	aac tgg aca gta aca tgg ag	ttg ctg gca aag tag aaa ag	H_BAX_1	581	NM_004324
BBC3	gta aga tac tgt ata tgc gct g	ttt tcc act gtt cca atc tg	H_BBC3_1	27113	NM_001127240
C12orf5	aag gac aag gag tag atg aac	ctg gag aaa gca tga gta aac	H_C12orf5_1	57103	NM_020375
CDKN1A	cag cat gac aga ttt cta cc	cag ggt atg tac atg agg ag	H_CDKN1A_1	1026	NM_000389
GAPDH	aca gtt gcc atg tag acc	ttt ttg gtt gag cac agg	H_GAPDH_1	2597	NM_002046
GCLC	tta tta gag acc cac tga cac	ttc tca aaa tgg tca gac tc	H_GCLC_1	2729	NM_001197115
MDM2	cct tag ctg act att gga aat g	tgt tga gtt ttc cag ttt gg	H_MDM2_1	4193	NM_002392
TP53I3	atc ttg tgg gaa atg ttc ag	cat ttg aag ctt ctt ctg gg	H_TP53I3_1	9540	NM_001206802
UCA1	agg aac atc tca cca att tc	tct tca tat ggc tgg gaa tc	H_UCA1_1	652995	NR_015379

Note: All primers were pre-designed by Sigma-Aldrich, Castle Hill, NSW, Australia

2.3.3 DNA

2.3.3.1 Gel electrophoresis

Agarose (Bio-Rad) was dissolved in Tris-acetate-EDTA (TAE) buffer by heating in a microwave (see Table 2.10 for composition of the buffer). When the solution was cold enough to touch by hand, a 1:10,000 dilution of SYBR safe DNA gel stain (ThermoFisher) was added and poured immediately into a molding plate. DNA was mixed with 6X DNA loading dye and electrophoresed at 100 V for 30-60 minutes in TAE buffer. The gel was visualised on a SmartView Pro 2100 Gel Documentation System (Major Science).

2.3.3.2 Precipitation of DNA using ethanol

Milli-Q water was added to the sample to give a final volume of 50 µl. Next, 5 µl (10% of 50 µl) of 3M sodium acetate (pH 5.2) and 120 µl (~2X volume) were added. The sample was gently mixed by pipetting and incubated at -20 °C overnight. The tube was centrifuged at maximum speed for 15 minutes and the supernatant removed. The DNA pellet was washed once with 500 µl of cold (-20 °C) 80% ethanol, and dried at room temperature by keeping the lid open for ~15 minutes. The pellet was then dissolved in the desired volume of Milli-Q water.

2.3.4 Protein

2.3.4.1 Western blotting

Buffer composition is shown in Table 2.10. Cells were washed once with ice-cold PBS, lysed on ice in Laemmli buffer and transferred to an eppendorf tube. The lysate was sonicated for 30 seconds by directly submerging a metal probe in the sample and heating at 95 °C for 5 minutes. 10-20 µl of the lysate and SeeBlue® Plus2 protein standards (range 4-250 kDa) were run on a pre-casted 4-12% NuPAGE® Novex Bis-Tris gels for 1 hour in MOPS running buffer. Protein was transferred on to a nitrocellulose membrane for 90 minutes at 100 V in cold blotting buffer. The membrane was blocked for at least 30 minutes at room temperature in 5% (w/v) skim milk dissolved in the blocking buffer followed by incubation with the primary antibody overnight at 4 °C. The membrane was washed 3 times (10 minutes each time) with washing buffer, incubated with secondary antibody for at least 2 hours at room temperature followed by 3 $\times$ 10 minute washes. Finally, chemiluminescence was detected

Table 2.10: Composition of buffers

Name	Constituents	Final concentration
TAE	Tris-Base Acetic acid EDTA (pH 8.0) (in Milli-Q water)	40 mM 20 mM 1 mM
6X DNA loading dye	Bromophenol blue Sucrose (in Milli-Q water)	0.25% (v/v) 40% (v/v)
Luria broth (LB)	Bacto-tryptone Bacto-yeast extract NaCl (in Milli-Q water) (Adjust pH to 7.5 with NaOH. Autoclave.) *For LB agar plates, add 15 g/L agar before autoclaving.*	10 g/L 5 g/L 10 g/L
MOPS running buffer	MOPS Tris-Base SDS EDTA (pH 7.7)	50 mM 50 mM 0.1% (w/v) 1 mM
Blotting buffer	Tris-Base Glycine Methanol	25 mM 152 mM 20% (v/v)
Blocking buffer	Tris, pH 7.4 Tween-20	40 mM 0.1% (v/v)
Wash buffer	Tris, pH 7.4 Tween-20 NaCl	20 mM 0.1% (v/v) 150 mM

using Pierce ECL Pico or Dura reagent (ThermoFisher) on a LAS-4000 imaging system (FujiFilm).

Table 2.11: Primary and secondary antibodies used in this study

Antibody	Host	Dilution	Diluent	Molecular mass (KDa)	Type	Catalogue number	Supplier	City	State	Country
GAPDH (14C10)	Rabbit	1:10,000	5% skim milk	37	Primary	2118	Cell Signaling	Danvers	MA	USA
p53 (1C12)	Mouse	1:2,000	5% skim milk	53	Primary	2524	Cell Signaling	Danvers	MA	USA
Phospho-p53 (Ser15)	Rabbit	1:1,000	5% BSA	53	Primary	9284	Cell Signaling	Danvers	MA	USA
p21 (WAF1-C1P1)(DCS60)	Mouse	1:2,000	5% skim milk	21	Primary	2946	Cell Signaling	Danvers	MA	USA
anti-mouse IgG HRP	Sheep	1:2,500	5% skim milk	NA	Secondary	NA931	GE Healthcare Life Sciences	Parramatta	NSW	Australia
anti-rabbit IgG HRP	Donkey	1:2,500	5% skim milk	NA	Secondary	NA934	GE Healthcare Life Sciences	Parramatta	NSW	Australia

2.4 Bacterial work

2.4.1 Growing bacteria

Small amounts of *Escherichia coli* (*E.coli*) from the frozen glycerol stocks were transferred to a starter culture of ~5 ml LB in a 50 ml Falcon tube, and grown overnight at 37 °C at roughly 225 rpm in a shaking incubator. Ampicillin was used at a final concentration of 0.1 mg/ml as a selection marker when required, i.e growing *E.coli* carrying a plasmid containing a transgene. All steps were performed under aseptic conditions using a bunsen burner.

2.4.2 Bacterial transformation using the heat shock method

Aliquots of commercially available α-Select Chemically Competent Cells were thawed on ice, and mixed with gentle flicking. Plasmid DNA (1-5 µl) was added, cells were mixed by gentle flicking and incubated on ice for 30 minutes. The heat shock treatment was performed for 45 seconds in a pre-warmed water bath set at 42 °C, and cells were immediately returned to ice for ~2 minutes. One ml LB without antibiotics was added to each tube, and incubated for 1 hour in a shaking incubator set at 225 rpm at 37 °C to allow expression of the antibiotic resistance gene. A small volume (50-100 µl) of this culture was spread on LB agar plates containing antibiotics (usually ampicillin at 0.1 mg/ml), inverted and incubated overnight at 37 °C. Resistant colonies were selected for future work on the following day.

2.4.3 Bacterial transformation using electroporation

Electroporation cuvettes (Bio-Rad) were cooled on ice. The electrocompetent *E.coli* strain JM109 was thawed on ice, and 1-2 µl (50-100 ng) plasmid DNA was added to the cells and mixed gently. Cells were electroporated on a Gene Pulser Electroporator (Bio-Rad) using default settings. Immediately after electroporation, 1 ml LB was added to the cuvette and pipetted up and down to mix cells. This solution was transferred to a 1.5 ml eppendorf tube. As described in the previous subsection, the tube was incubated for 1 hour in a shaker incubator set at 225 rpm at 37 °C, spread on LB agar plates containing antibiotics (usually ampicillin at 0.1 mg/ml), grown overnight and colonies were picked for future work.

2.4.4 Plasmid isolation from bacterial cells

Plasmids from 3 ml bacterial cultures grown overnight in the presence of ampicillin were isolated using PureYield™ Plasmid Miniprep System (Promega) according to manufacturer's protocol. Briefly, bacteria were centrifuged at the maximum speed, the supernatant was discarded and the bacterial pellet was re-suspended in 600 µl of water. Cells were lysed by adding 100 µl Lysis buffer and mixed by gently inverting the tube 6 times. Three hundred and fifty µl cold of Neutralisation solution was added and mixed by inverting. The eppendorf tube was centrifuged at the maximum speed for 3 minutes, and the clear lysate was transferred to a PureYield™ Minicolumn. The minicolumn was placed inside a collection tube and centrifuged at the maximum speed for 15 seconds. Two hundred µl of Endotoxin removal solution was added to the minicolumn followed by centrifugation at the maximum speed for 15 seconds. Next, the minicolumn was washed by adding 400 µl Column wash solution followed by centrifugation at the maximum speed for 30 seconds. Finally, the minicolumn was transferred to a fresh eppendorf tube, DNA was eluted in 30 µl Elution buffer by centrifugation and stored at -20 °C.

2.5 Flow cytometry

2.5.1 Cell viability using DilC1(5)/FVS450 dyes

All centrifugation steps were performed at 300 g for 3 minutes at room temperature. The MitoProbe™ DilC1(5) dye (ThermoFisher) was re-constituted at 1 mg/ml in DMSO. DilC1(5) accumulates in the mitochondria with active membrane potential, a hallmark of viable cells, whereas FVS450 (BD) is a membrane impermeable dye analogous to propidium iodide.

Supernatant was transferred to a round bottom flow cytometry tube and centrifuged to collect dead cells and debris. Adherent cells were washed once with PBS, and harvested with trypsin as described in subsection 2.2.1. Supernatant and the adherent fractions were pooled and washed 2 times with PBS. Samples were suspended in 250 µl PBS, 50 µl of staining buffer [44.5 µl PBS + 5 µl 1X DilC1(5) + 0.5 µl FVS450] was added and the sample was incubated in the dark at room temperature for 15 minutes.

Flow cytometry analyses were performed using the BD Fortessa cell analyser (BD). FVS450 and DilC1(5) were excited with violet (405 nm) and red (640 nm) lasers, respectively, and their emission was measured by 450/50 and 670/14 filters, respectively. Compensation was calculated by staining an identical sample, comprising both dead and live

cells, with both dyes individually. Technically, compensation was found to be unnecessary due to little overlap in emission spectra of both dyes as well as different lasers, which were spatially separated, used for excitation; however, it was occasionally used for improving visualisation of the populations. Data was analysed on FACS Diva software V8.0.1 (BD).

DilC1(5) and FVS450 mark viable ($DilC1(5)^+/FVS450^-$; top left quadrant), late apoptotic/dead ($DilC1(5)^-/FVS450^+$; bottom right quadrant) or early apoptotic ($DilC1(5)^-/FVS450^-$; bottom left quadrant) cells. The $DilC1(5)^+/FVS450^+$ cells (top right quadrant) represent artefact of trypsin digestion where cell membrane became permeable while the mitochondrial membrane potential remained intact. In majority of cases, this fraction remained unchanged up on various drug treatments.

2.5.2 Statistical analysis

All statistical analyses were performed in R. The student's t-test was usually two-tailed assuming equal variance in the two biological groups. Analysis of variance (ANOVA) was followed by Tukey's honest significance post-hoc test. Error bars in all Figures represent standard error of mean (SEM). A P-value < 0.05 was considered significant unless stated.

Chapter 3

Prediction of surgical outcome of patients with HGSOC using serum microRNAs

3.1 Introduction

Size of the residual tumour at the conclusion of cytoreductive surgery remains one of the most important factors influencing the overall survival (OS) and progression-free survival (PFS) of ovarian cancer (OC) patients (Bristow et al. 2002; Fader and Rose 2007; Griffiths 1975). Bristow et al. 2002 reported a 5.5% increase in median OS for every 10% increase in maximal cytoreduction*. Historically, 'optimal' cytoreduction status of the surgery was defined as <1.5 cm of residual disease at the conclusion of the surgery because residual tumour size beyond this cut-off, i.e. suboptimal cytoreduction, did not improve OS significantly (Griffiths 1975). Although 'optimal' is currently defined as <1 cm of residual tumour, recent evidence suggests that achieving 'no macroscopic' residual disease (0 mm; also known as R0 resection) improves OS even further compared to the presence of any visible tumour mass after the completion of surgery (>0 mm) (du Bois et al. 2009; Winter et al. 2008). Specifically, Winter et al. 2008 reported a doubling in median OS of the patients achieving R0 status (median OS: 64 months) compared to any residual disease (0.1 - 5 cm; median OS: 30 months). As a result, R0 resection is increasingly becoming recognised

*maximal cytoreduction effort was graded from 0-100%, with >2 cm residual tumour as 0% and <0.5 cm as 100%.

as 'optimal', and surgeons are encouraged to be aggressive in the cytoreductive surgery to achieve R0 resection when possible (Chang et al. 2013; Horowitz et al. 2015; Jayson et al. 2014; Nick et al. 2015).

Prediction of surgical outcome is critical as it helps with timing of the surgery. Patients with >1 cm of residual disease may experience little to no overall benefits from the primary cytoreductive surgery considering the possible significant morbidity resulting from the extensive surgery (Bristow 2006; Bristow et al. 2007). In fact, it may be better to avoid surgery all together and rely purely on chemotherapy in cases with extensive disease (Bowtell et al. 2015). Neoadjuvant chemotherapy (NACT) could be a suitable option for patients likely to have suboptimal cytoreduction (Kehoe et al. 2015; Morice et al. 2003; Schwartz et al. 1999; Vergote et al. 2010). Although OS remains unchanged for these patients (Kehoe et al. 2015; Morice et al. 2003; Schwartz et al. 1999; Vergote et al. 2010), they tend to have less morbidity, improving the quality of their lives.

Computed tomography, laparoscopy, aberrant expression of certain genes in tumour tissue, measurement of serum proteins CA-125 and HE4, machine learning/artificial intelligence and obtaining a two-surgeon opinion on the resectability of ovarian tumours (The Anderson Algorithm) have been used to predict surgical outcome (see subsection 1.1.1.6); however, a reliable method remains elusive. Serum microRNAs have not yet been tested to address this challenge. microRNAs are a class of small RNAs with a profound biological role in normal physiology as well as diseases such as cancer (Hayes, Peruzzi, and Lawler 2014; Lin and Gregory 2015; Lu et al. 2005; Schickel et al. 2008). Notably, microRNAs are present in a variety of biological fluids, and can withstand extreme conditions such as boiling, multiple freeze-thaw cycles and extended storage (Cortez et al. 2011; McDonald et al. 2011; Wang et al. 2014; Weber et al. 2010), making them a strong choice for biomarkers. The overall aim of this chapter was to assess the diagnostic role of serum microRNAs by testing whether pre-operative levels of certain serum microRNAs could identify patients with HGSOC from healthy women as well as predict their surgical outcome.

Since serum microRNAs are influenced by a number of pre-analytical factors (McDonald et al. 2011; Witwer 2015), development and implementation of a thorough quality control protocol was necessary prior to the microRNA profiling. Traditional predictive tools such as logistic regression (LR) were tested against modern machine learning (ML) methods [†] for their predictive power. As proof-of-principle, the analytical pipeline was first ap-

[†]LR was performed by the candidate whereas ML was conducted by Professor Jean Yang of the School of Mathematics and Statistics, University of Sydney, Australia.

plied to identify microRNAs that could separate HGSOC patients from healthy women, followed by an assessment of these models to predict surgical outcome.

3.2 Materials and methods

Since this work is presented over Chapters 3 and 4, common methodologies for both chapters, such as collection of cell-free serum, RNA extraction, RT-qPCR, data processing and analysis, can be found in Chapter 2, section 2.1.

3.2.1 Cohort Information

As detailed in Chapter 2, subsection 2.1.1, blood was collected from all individuals according to a protocol approved by the Northern Sydney Local Health District Human Research Ethics Committee (Protocol # 0310-209B). The composition of the cohort is shown in Table 3.1. Optimal cytoreduction was defined as R0 resection, i.e. no macroscopic residual tumour, whereas suboptimal was defined as >1 cm residual tumour. Patients achieving 1 - 10 mm residual tumour were excluded from analyses to potentially observe clear differences in serum microRNA profiles of a relatively small number of optimally/suboptimally cytoreduced patients (N = 56).

3.2.2 Quantification of CA-125 levels in serum

CA-125 (also known as MUC16) concentrations were determined using the Quantikine® ELISA Human CA-125/MUC16 Immunoassay kit (R&D Systems #DCA125, Minneapolis, United States) according to the manufacturer's instructions. Serum was diluted 5 – 5000 times in Calibrator Diluent RD5P supplied with the kit. One hundred µl of Assay Diluent RD1X was added to each well followed by addition of 100 µl of the diluted samples, 7 standards (0.5 to 32 U/ml in a 2-fold dilution series) or zero controls. The plates were incubated for 2 hours at room temperature on a plate shaker set at 500 rpm, and washed 4 times with Wash Buffer. Next, 200 µl of the CA-125 conjugate was added to each well, incubated for 2 hours at room temperature on a plate shaker set at 500 rpm and washed 4 times. To develop colouration 200 µl of Substrate Solution was added to each well, incubated for 30 minutes at room temperature followed by the addition of 50 µl of Stop Solution. All samples were performed in 2 technical replicates. Absorbance was read at 450 nm on a VICTOR^3 1420 multilabel plate reader (PerkinElmer). For each plate absorbance the average of the zero controls was removed from all wells and the averages of technical

	Discovery (N= 43)	Validation (N= 43)
Cohort information (N = 86)		
Healthy*	15	15
Optimally cytoreduced	15	15
Suboptimally cytoreduced	13	13
Mean age (yr)* ± SEM		
Healthy	61.1 ± 3.4	61 ± 3.3
Optimally cytoreduced	60.5 ± 3.8	59.1 ±3.1
Suboptimally cytoreduced	68.7 ± 2.5	67.9 ± 2.8
FIGO Stage		
I	1 (3.6%)	3 (10.7%)
II	1 (3.6%)	4 (14.3%)
III	21 (75%)	17 (60.7%)
IV	1 (3.6%)	0 (0%)
Unknown	4 (14.3%)	4 (14.3%)
Interval Debulking		
Suboptimally cytoreduced	4 (14.3%)	3 (10.7%)

Table 3.1: Cohort information

*: Samples from healthy women were age-matched within 5 years to samples from women with ovarian cancer. 'Interval debulking': patients underwent primary surgery followed by a few cycles of chemotherapy. A secondary surgery was performed to excise more tumour mass prior to resuming additional cycles of chemotherapy. Optimal: R0 resection; suboptimal >1 cm residual disease. Patients achieving 1 - 10 mm residual tumours were excluded

FIGO Stage	Optimal (N=30)	Suboptimal (N=26)
I	3 (10%)	1 (3.8%)
II	3 (10%)	2 (7.7%)
III	22 (73.3%)	16 (61.5%)
IV	1 (3.3%)	0 (0%)
Unknown	1 (3.3%)	7 (26.9%)

Table 3.2: Tumour Stage according to the surgical outcome.

replicates were calculated. The standard curve was constructed and the concentrations of the samples were read off. All standard curves were of high quality ($R^2 > 0.99$). Log_2-transformed CA-125 values were used in calculations.

3.2.3 Data analysis

3.2.3.1 Empirical Bayesian test

A typical high-throughput experiment in 'omic' technologies measures a much greater number of variables, ie genes, than the number of samples. The empirical Bayes test (also known as the moderated t-test) proposed by Smyth 2004 and offered by the R (R Core Team 2016) package 'limma' (Ritchie et al. 2015) modifies the SEM of the student's t-test by applying the Baye's rule on the observed variance of *all* genes, resulting in a robust estimate of the SEM.

A matrix containing gene expression values in 'genes × samples' format and a design matrix specifying grouping of the samples to treatments groups were constructed in R. A linear model was built using 'lmFit()' function of 'limma' based on the two matrices followed by 'eBayes()' with the 'trend' option set to 'TRUE'. Benjamini–Hochberg (BH) procedure was applied to control for false discovery rate (FDR) at 5% unless stated otherwise.

3.2.3.2 Feature selection and evaluating their performances

Using the R package MASS (Venables and Ripley 2002), the 'stepAIC()' function was employed for performing stepwise logistic regression in both directions as a feature selection[‡] method identifying predictive biomarkers. A threshold that maximised the sum of sensitivity and specificity was used to calculate the area under curve (AUC) of the receiver operator characteristic (ROC) curve as well as the accuracy of prediction using the R package pROC (Robin et al. 2011). A 1000 bootstraps with replacement was calculated using the R package boot (Davison and Hinkley 1997), and the median values of AUC or accuracy were reported.

3.2.3.3 Machine learning

The applications of ML algorithms for this thesis were established by Professor Jean Yang of University of Sydney, and were modified extensively by the candidate. Machine learning was performed using the R package ClassifyR (Strbenac et al. 2015). In addition, 'dlda()' and 'svm()' functions of R package sparsediscrim (Ramey 2016) and e1071 (Meyer et al. 2015) were used to run diagonal linear discriminatory analysis (DLDA) and support

[‡]'feature selection' is the technical term to describe the process of identifying the most important variables in predicting an outcome.

vector machine (SVM) algorithms, respectively — both were implemented in the ClassifyR package.

3.3 Results

Overview of the experimental design is presented in Figure 3.1.

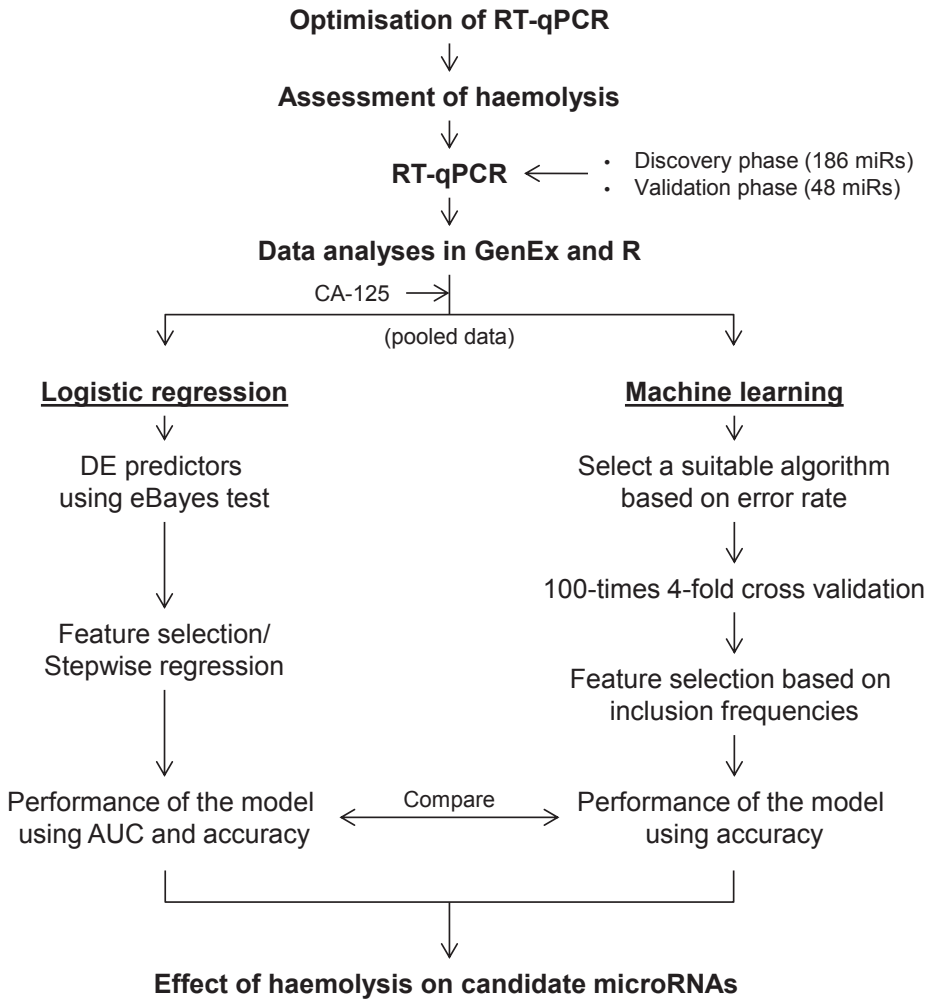

Figure 3.1: Overview of the study design
'DE' refers to differentially expressed and 'miRs' refer to microRNAs

3.3.1 Optimisation and quality control

3.3.1.1 Optimisation of RT-qPCR

First, the selection of small or total RNA was addressed. Since separate buffers are required for extracting total versus small RNAs, it was not clear whether to follow protocols to extract total RNA, which may not enrich for small RNAs, compared to specific protocols designed

to enrich small RNAs such as microRNAs but may compromise the levels of large RNAs. The choice of enriching for small RNAs seemed obvious for a microRNA study. However, ours and the adjacent laboratory (Cancer Genetics, Kolling Institute) that works on serum microRNAs have traditionally used total RNA for quantifying serum microRNA. I also contacted Dr. Kai Wang of the Institute for Systems Biology, Seattle, Washington, United States of America, who has co-authored 8 studies on circulating microRNAs since 2013, to ask his opinion on small versus total RNA for serum microRNA profiling. He also suggested using total RNA for profiling. Based on the experience of researchers in our and the adjacent laboratory, as well as an external researcher, total RNA from serum was used in this study.

Our laboratory had previously used the mirVana™ PARIS™ RNA isolation kit to quantify microRNAs from serum (Kan et al. 2012). However, a recent study reported that the Exiqon miRCURY™ Biofluid RNA Isolation kit was superior in terms of yield of RNA extracted and removal of inhibitors of PCR out of five commercially available kits tested: miRCURY™ RNA Isolation Kit – Cell and Plant, miRCURY™ RNA Isolation Kit – Biofluid, mirVana™ PARIS™, Qiagen miRNeasy Serum/Plasma Kit and TRIzol reagent LS for Liquid Samples (McAlexander, Phillips, and Witwer 2013). To compare the performance of mirVana™ PARIS™ and Exiqon miRCURY™ Biofluid RNA extraction kits, RNA from 200 µl of serum pooled from three HGSOC patients was extracted using both kits, and the yields were measured using a NanoDrop™ 1000 spectrophotometer. The mirVana™ PARIS™ kit resulted in a higher yield of RNA (1.68 µg/200 µl serum) compared to the miRCURY™ Biofluid kit (150 ng/200 µl serum). The NanoDrop™ measurements are known to be inaccurate for serum microRNAs due to their low concentrations; therefore, RT-qPCR was used to measure the abundance of endogenous hsa-miR-103 (Kan et al. 2012) as a stable surrogate marker of microRNA levels in RNA extracted from serum.

Haemoglobin, immunoglobin G and lactoferrin tend to be co-purified in low levels with RNA extracted from serum, which can significantly inhibit reverse transcriptase or Taq polymerase when high amounts of RNA is used for RT-qPCR (Akane et al. 1994; Al-Soud, Jönsson, and Rådström 2000; Al-Soud and Rådström 2001). To identify the maximum amounts of RNA that could be used for RT-qPCR without affecting its efficiency, six different amounts of RNA were reverse transcribed in a total of 20 µl using the Universal cDNA Synthesis kit (Exiqon), and levels of miR-103 was quantified using RT-qPCR. RNA extracted using miRCURY™ Biofluid and mirVana™ PARIS™ kits as well as pooled RNA from both kits in a 1:1 ratio was used. As shown in Figure 3.2A, miR-103 extracted using the miRCURY™ Biofluid kit consistently resulted in a lower C_t than from the mirVana™ PARIS™ kit and pooled RNA of both kits, suggesting that the miRCURY™ Biofluid kit was

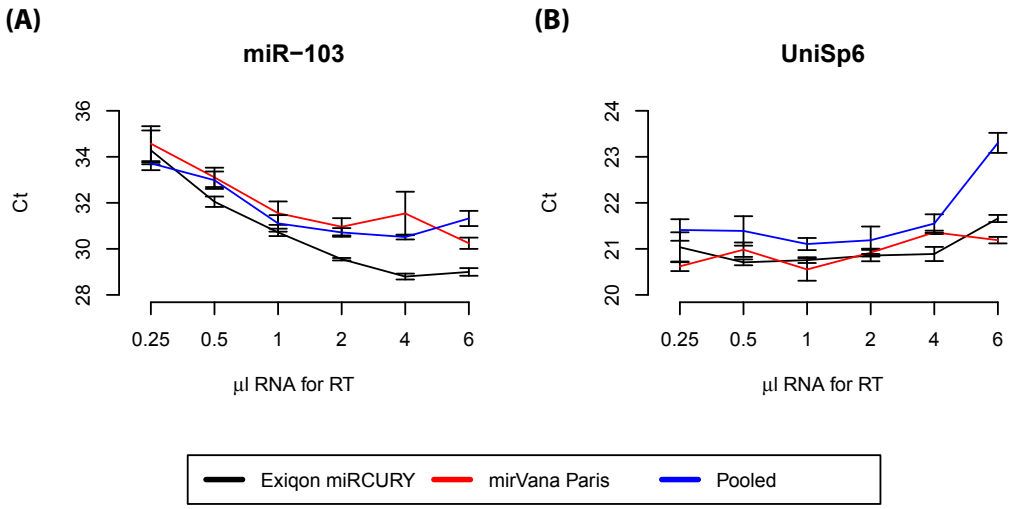

Figure 3.2: Selection of RNA extraction kit and RT protocol for serum microRNA profiling
Two questions were answered by one experiment: (1) identifying the maximum amount of RNA that does not inhibit RT-qPCR as inhibitors of RT-qPCR tend to be co-purified with RNA, and (2) Selection of a superior RNA extraction kit between miRCURY^{TM} Biofluid and mirVana^{TM} PARIS^{TM} kits. **(A)** miR-103 extracted using the miRCURY^{TM} Biofluid kit consistently resulted in a lower C_t than from the mirVana^{TM} PARIS^{TM} kit and pooled RNA of both kits, suggesting that the miRCURY^{TM} Biofluid kit was indeed better for RT-qPCR. Additionally, a linear decrease in the C_t of hsa-miR-103 was observed when up to 4 µl of RNA extracted using the miRCURY^{TM} Biofluid kit was used as template for RT. **(B)** Spike-in RNA UniSp6 was equally added to each RT reaction; therefore, it should be amplified at the same level in all reaction, which was the case when up to 4 µl RNA was used for RT. Both miR-103 and UniSp6 indicated that RT-qPCR was not affected using up to 4 µl of serum RNA. Error bars represent SEM of 3 technical replicates.

indeed better for RT-qPCR. Next, a linear decrease in the C_t of hsa-miR-103 was observed when up to 4 µl of RNA extracted using the miRCURY^{TM} Biofluid kit was used as template for RT, indicating an insignificant amount of inhibitors of RT and PCR up to this point. Furthermore, the spike-in RNA UniSp6, which was utilised to monitor efficiency of RT (subsection 2.1.2), was added to all RT reactions in equal amounts, and amplified using RT-qPCR. The C_t values of UniSp6 also remained unchanged for up to 4 µl of serum RNA (Figure 3.2B), which is consistent with results obtained on miR-103.

RT was performed in 20 µl volumes using 4 µl RNA for the Discovery phase where 186 microRNAs (170 candidates + 16 controls) were profiled. Because a small number of microRNAs (N = 48) were amplified in the Validation phase, we proposed to conduct RT in a 10 µl volume using 2 µl RNA. To assess the applicability of both protocols to a large number of samples prior to microRNA profiling, three and two samples were prepared according to the protocol for the Discovery and Validation phases, i.e 20 µl or 10 µl RT

(A)

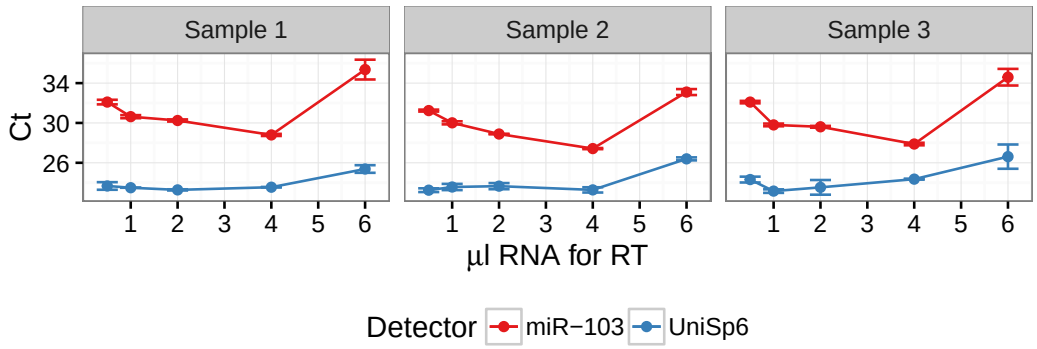

(B)

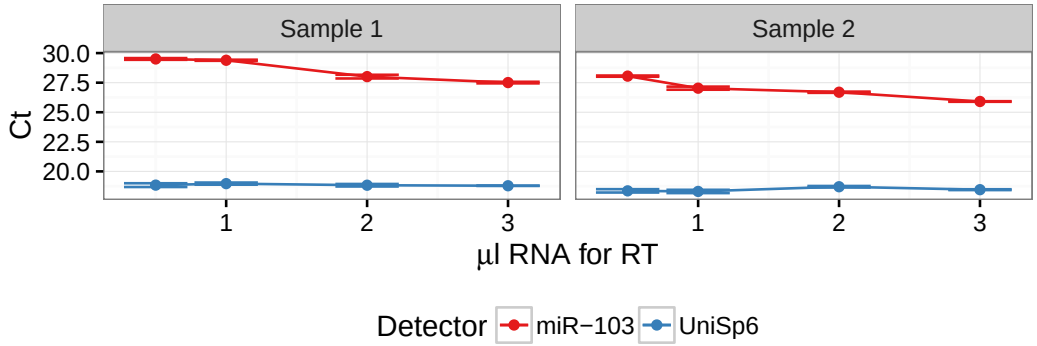

Figure 3.3: Testing of the RT protocol in multiple biological samples
(A) Confirming lack of inhibitors for the RT protocol for the Discovery phase. RT was performed in a total of 20 µl volume using 4 µl RNA as template. No inhibition in miR-103 and UniSp6 levels was observed, suggesting that this protocol was applicable to a large number of samples. **(B)** Due to the smaller number of microRNAs amplified in the Validation phase relative to the Discovery phase, RT was carried out in a 10 µl volume using 2 µl RNA. Again, no significant inhibition was observed using this protocol in 2 samples. Error bars represent SEM of 3 technical replicates.

volume using varied amounts of RNA, respectively, and hsa-miR-103 and UniSp6 were amplified. As shown in Figure 3.3, no inhibition was seen when 4 µl (Figure 3.3A) and 2 µl (Figure 3.3B) of RNA were used in a total of 20 and 10 µl RT reactions, respectively.

3.3.1.2 Assessment of haemolysis

Release of the microRNA content of RBC upon haemolysis has the potential to interfere with screening processes (Kirschner et al. 2011, 2013; McDonald et al. 2011; Pritchard et al. 2012). As an essential quality control step for this study, I compared sensitivities of four

different methods to detect low levels of haemolysis: Coulter® AcT diff™ Analyzer, visual inspection, the absorbance of haemoglobin measured by spectrophotometry at 414 nm and the ratio of red blood cell-enriched miR-451a to the reference microRNA miR-23a-3p (referred to as the 'miR ratio'). These methods have been described in the literature (Blondal et al. 2013; Kirschner et al. 2011, 2013), but a direct study comparing their sensitivities was missing. This work has been described in detail in Chapter 4 and is published in *Plos One* (Shah, Soon, and Marsh 2016).

The 'miR ratio' was found to be the most sensitive method to measure low levels of haemolysis (Shah, Soon, and Marsh 2016), and was used to measure haemolysis in this cohort. A 'miR ratio' of <5, 5-7 and >7 indicate a sample with low, moderate or high risk, respectively, of being affected by haemolysis (Blondal et al. 2013). Next, haemolysis amongst the three biological groups was assessed by one-way ANOVA. No differences were observed and no further samples were excluded from the study (P = 0.365; Figure 3.10A). Finally, differentially expressed microRNAs was tested to see if they are affected by haemolysis (subsection 3.3.4; Figure 3.10).

3.3.2 Using logistic regression to identify predictive biomarkers

3.3.2.1 Predictors of HGSOC from healthy women

The levels of 27 of 170 (16%) microRNAs measured in the Discovery phase using the Serum/Plasma Focus microRNA panel were found to be significantly different between healthy and HGSOC serum samples ($P < 0.05$; Figure 3.4A and marked with '¶' in Supplementary Table B.1), of which the 10 most highly (5.9%) differentially expressed (DE) microRNAs were selected for independent validation in the Validation phase (Table 3.3). Table 3.4 summarises candidate microRNAs when Discovery and Validation phases were analysed separately or as a single pooled dataset. In the pooled dataset, levels of CA-125 were approximately 40-fold higher ($\log_2$ FC = 5.5) in HGSOC compared to healthy samples ($P = 4.24 \times 10^{-14}$, Figure 3.4D and Table 3.4). Overall, miR-375, miR-150-5p, miR-210 and miR-181a-5p were amongst the most DE microRNAs between healthy and HGSOC samples in the pooled data after selection based on 5% FDR (Figure 3.4A-C, E and Table 3.4). miR-200c-3p was found to be strongly upregulated by approximately 5-fold in HGSOC compared to healthy samples in the Discovery phase ($P = 3.55 \times 10^{-9}$; Figure 3.4A), but this was not confirmed in the Validation phase (P = 0.116, Figure 3.4E and Table 3.4). miR-200c-

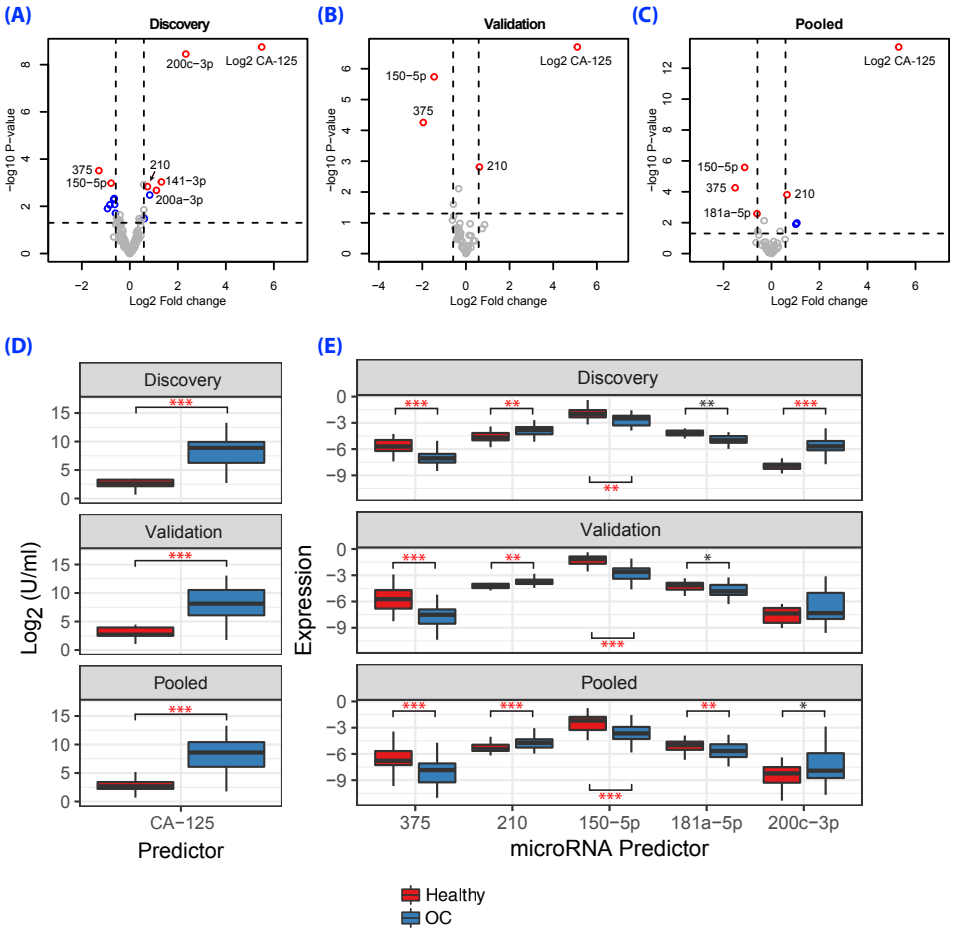

Figure 3.4: Identification of the predictors separating HGSOC patients from healthy women.

Volcano plots showing DE predictors identified from **(A)** Discovery, **(B)** Validation and **(C)** Pooled phases (N=86; Table 3.4 and Supplementary Table B.1). Vertical and horizontal dashed lines mark the absolute fold-change of 1.5 and *P* value of 0.05, respectively. Blue and red circles represent predictors with > 1.5 absolute fold-change with either unadjusted $P < 0.05$ or were significant after 5% false discovery rate (FDR), respectively. Only 'red circles' are labelled for simplicity. **(D, E)** Levels of CA-125 and candidate microRNAs in Discovery, Validation and the Pooled dataset. The expression of miR-375, miR-210, miR-150-5p and miR-181a-5p are shown in **(E)** because they were found to be DE after FDR-correction in the pooled data whereas miR-200c-3p is shown as it was DE only in the Discovery phase (Table 3.4). * P <0.05, ** $P < 0.005$ and *** $P < 0.0005$. Biomarkers that remained significant after FDR-correction are marked with a red asterisk according to the criteria above.

3p, as a result, was not found to be significant at 5% FDR in the pooled dataset (FDR-*P* value = 0.7; Table 3.4).

Given the relatively small cohort sizes of Discovery and Validation phases, data was pooled and stepwise regression analysis was employed to determine microRNA levels in

Purpose	microRNAs	N
Haemolysis	miR-451a, miR-16-5p, miR-15b-3p, miR-142-3p, miR-146a-5p	6
Healthy versus OC	miR-200c-3p, miR-92b-3p, miR-150-5p, miR-210, miR-181a-5p, miR-200b-3p, miR-200a-3p, miR-99b-5p, miR-141-3p	10
Optimal versus suboptimal cytoreduction	miR-34a-5p, miR-145-5p, miR-551b-3p, miR-629-5p, miR-20b-5p, let-7i-3p, miR-361-3p, miR-505-3p, miR-122-5p, miR-605, miR-29a-5p, miR-222-3p, miR-29b-2-5p, miR-30a-5p	15
References	miR-93-5p, miR-106b-5p, miR-106a-5p, miR-20a-5p, miR-144-3p, miR-22-3p, miR-101-3p, miR-29c-3p, miR-19a-3p, miR-103a-3p, miR-29a-5p	11
Efficiency of RT-qPCR	UniSp2, UniSp4, UniSp5, UniSp6, cel-miR-39-3p	6

Table 3.3: microRNAs tested in the Validation Phase.

healthy versus HGSOC cohorts. This analysis was undertaken to determine whether data from Validation and Discovery phases analysed separately could be replicated, and/or new DE microRNAs identified. Akaike information criterion (AIC) is often used to rank competing statistical models. AIC computes loss in information by a given model, and the model minimising AIC usually represents the best prediction model (Burnham and Anderson 2004; Kuha 2004; Lindsey and Jones 1998; Symonds and Moussalli 2011). Stepwise regression, a feature selection method, identified CA-125, miR-375 and miR-210 as the most important predictors of all 10 possible predictors identified with $P < 0.05$ in the pooled data ($\log_2$ CA-125, miR-150-5p, miR-375, miR-210, miR-181a-5p, miR-141-3p, miR-200c-3p, miR-106b-5p, miR-551b-3p and miR-629-5p; Table 3.4), reducing the initial AIC of 48.22 to 37.12 When compared individually, $\log_2$ CA-125 had the highest median AUC of 0.929 in the ROC curve followed by miR-375 (0.765) and miR-210 (0.750; Figure 3.5A and Table 3.5). Similarly, $\log_2$ CA-125 alone had a higher accuracy (0.895) of prediction whereas both miR-375 and miR-210 alone resulted in the identical accuracy of 0.756 (Figure 3.5C). AUC and accuracy of the prediction model comprising $\log_2$ CA-125, miR-375 and miR-210 were found to be 0.984 and 0.965, respectively (Figure 3.5B, D; Table 3.5).

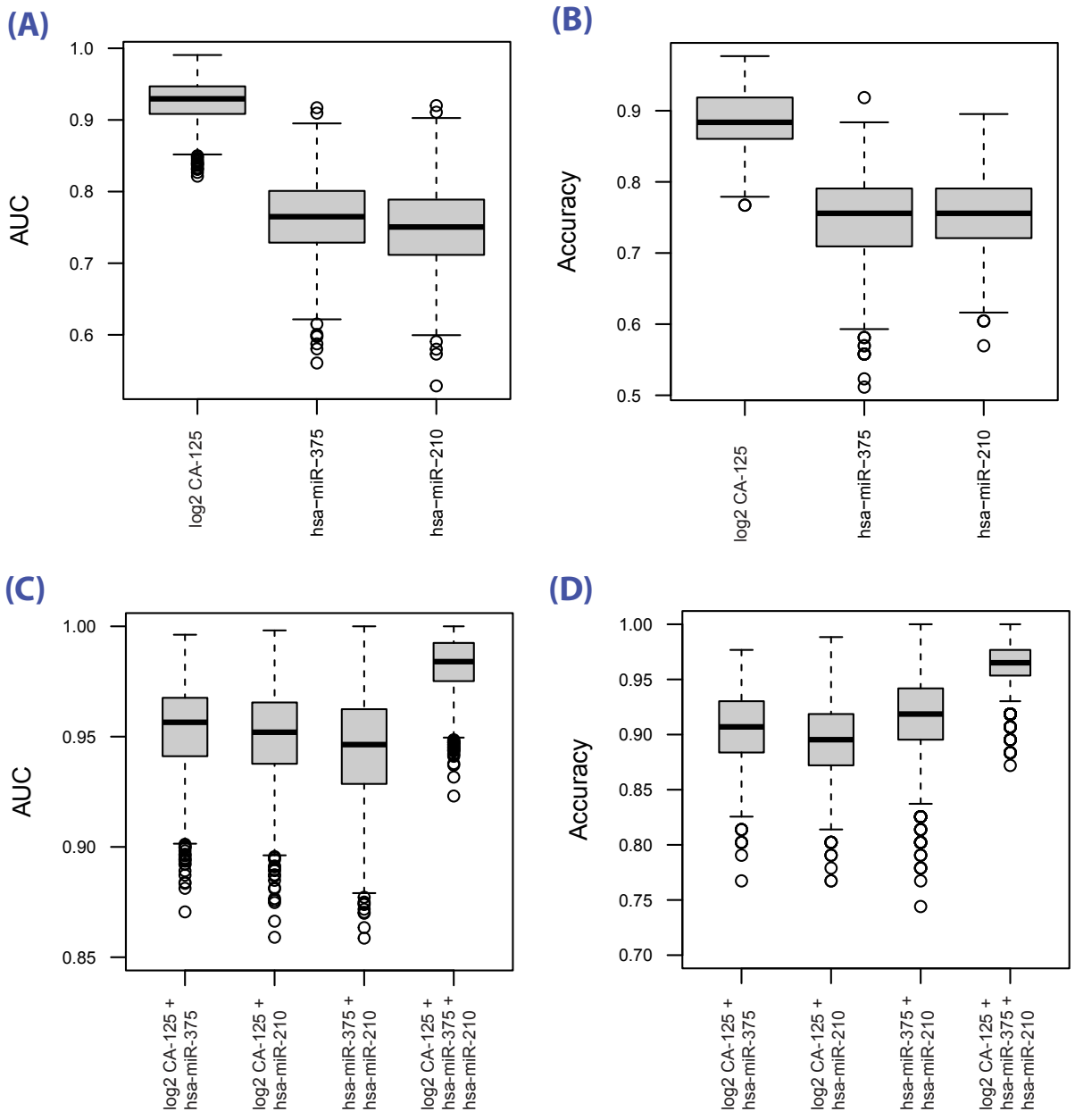

Figure 3.5: Performance of predictors separating HGSOC patients from healthy women. Area under curve (AUC) and accuracy of the most significant markers identified from stepwise regression from the pooled data (N=86; 30 healthy + 56 HGSOC samples) to predict healthy versus HGSOC status: **(A, B)** when markers are used individually, or **(C, D)** in combination. Boxplots represent values of 1000 bootstraps with replacement.

	Discovery			Validation			Pooled		
	logFC	***P***	**FDR-*P***	**logFC**	***P***	**FDR-*P***	**logFC**	***P***	**FDR-*P***
Log_2 CA-125	**5.494**	**1.79E-09**	**3.02E-07**	**5.105**	**1.97E-07**	**9.46E-06**	**5.300**	**4.24E-14**	**2.00E-12**
150-5p	**-0.780**	**0.001**	**0.034**	**-1.455**	**1.83E-06**	**4.40E-05**	**-1.118**	**2.63E-06**	**6.19E-05**
375	**-1.288**	**3.09E-04**	**0.018**	**-1.954**	**5.55E-05**	**0.001**	**-1.514**	**5.50E-05**	**0.001**
210	**0.734**	**0.001**	**0.036**	**0.619**	**0.002**	**0.019**	**0.648**	**1.54E-04**	**0.002**
181a-5p	-0.650	0.005	0.079	-0.577	0.025	0.201	**-0.602**	**0.003**	**0.024**
141-3p	**1.315**	**0.001**	**0.034**	0.749	0.154	0.466	1.060	0.010	0.070
200c-3p	**2.332**	**3.55E-09**	**3.02E-07**	0.855	0.116	0.47	1.014	0.013	0.07
92b-3p	0.572	0.001	0.034	0.064	0.815	0.910	0.124	0.619	0.873
200a-3p	**1.108**	**0.002**	**0.045**	0.406	0.384	0.596	0.566	0.121	0.472
99b-5p	0.829	0.003	0.063	-0.197	0.610	0.818	0.290	0.351	0.720
Identified from Pooled Data									
106b-5p	-0.267	0.361	0.748	-0.337	0.008	0.075	-0.304	0.007	0.058
551b-3p	-0.676	0.005	0.080	-0.561	0.061	0.416	-0.573	0.035	0.168
629-5p	0.585	0.014	0.159	0.236	0.263	0.525	0.357	0.036	0.168

Table 3.4: Summary statistics of microRNAs that can separate healthy women from HGSOC patients

Predictors with absolute FC > 1.5-fold are filled with background colour while those meeting FDR-corrected $P < 0.05$ are shown in bold face. FC: fold-change, FDR: false discovery rate.

	AUC	Accuracy
Log_2 CA-125	0.929	0.884
miR-375	0.765	0.756
miR-210	0.751	0.756
Log_2 CA-125 + miR-375	0.956	0.907
Log_2 CA-125 + miR-210	0.952	0.895
miR-375 + miR-210	0.946	0.919
Log_2 CA-125 + miR-375 + miR-210	0.984	0.965

Table 3.5: Performance of biomarkers that can separate healthy women from HGSOC patients
Log_2 CA-125, miR-375 and miR-210 were found to be the most significant predictors of disease status, i.e. patients with HGSOC or healthy women, from stepwise regression. Their performances in predicting the binary outcome was tested by systematically adding additional features in the predictive model. A model comprising Log_2 CA-125, miR-375 and miR-210 resulted in a higher AUC and accuracy compared to each predictor individually. AUC: area under curve

3.3.2.2 Predictors of the surgical outcome

Thirteen microRNAs of 170 tested (7.6%) were found to be DE between sera of optimally and suboptimally cytoreduced (abbreviated as Opt and Subopt hereafter) patients in the Discovery phase (unadjusted-$P < 0.05$; Table 3.6 and marked with '§' in Supplementary Table B.2). In addition to the 13 microRNAs, we included 5 predictors (Log_2 CA-125, miR-222-3p, miR-30a-5p, miR-29a-5p and miR-29b-2-5p), which failed to reach statistical significance but showed a trend (P between 0.05 and 0.17), for the Validation phase only (Table 3.6). Log_2 CA-125 levels were elevated in Subopt compared to Opt samples by approximately 4.4 fold (log_2 FC = 2.1) in the pooled data; however, this biomarker failed to achieve statistical significance at 5% FDR (Figure 3.6D and Table 3.6). In contrast, miR-34a-5p was consistently found to be at a higher level in Subopt versus Opt samples when Discovery and Validation phases were analysed separately or pooled, satisfying the criterion of 5% FDR in the pooled data (Figure 3.6C, E and Table 3.6).

Eight of 18 (13 miRs with $P < 0.05$ + 5 miRs showing a trend) predictors (log_2 CA-125, let-7b-3p, miR-34a-5p, 222-3p, 141-3p, 30a-5p, 29a-5p and 29b-2-5p) were found to be statistically significant in the pooled data ($P < 0.05$; Table 3.6). Three additional microRNAs (miR-92b-3p, 200a-3p and 200c-3p), which were not found to be statistically significant in the Discovery or Validation data tested individually, also reached the P-value of 0.05 in the pooled data, resulting in a total of 11 predictors for the feature selection (Table 3.6). Stepwise regression analysis on the pooled data identified miR-34a-5p and log_2 CA-125 as the most

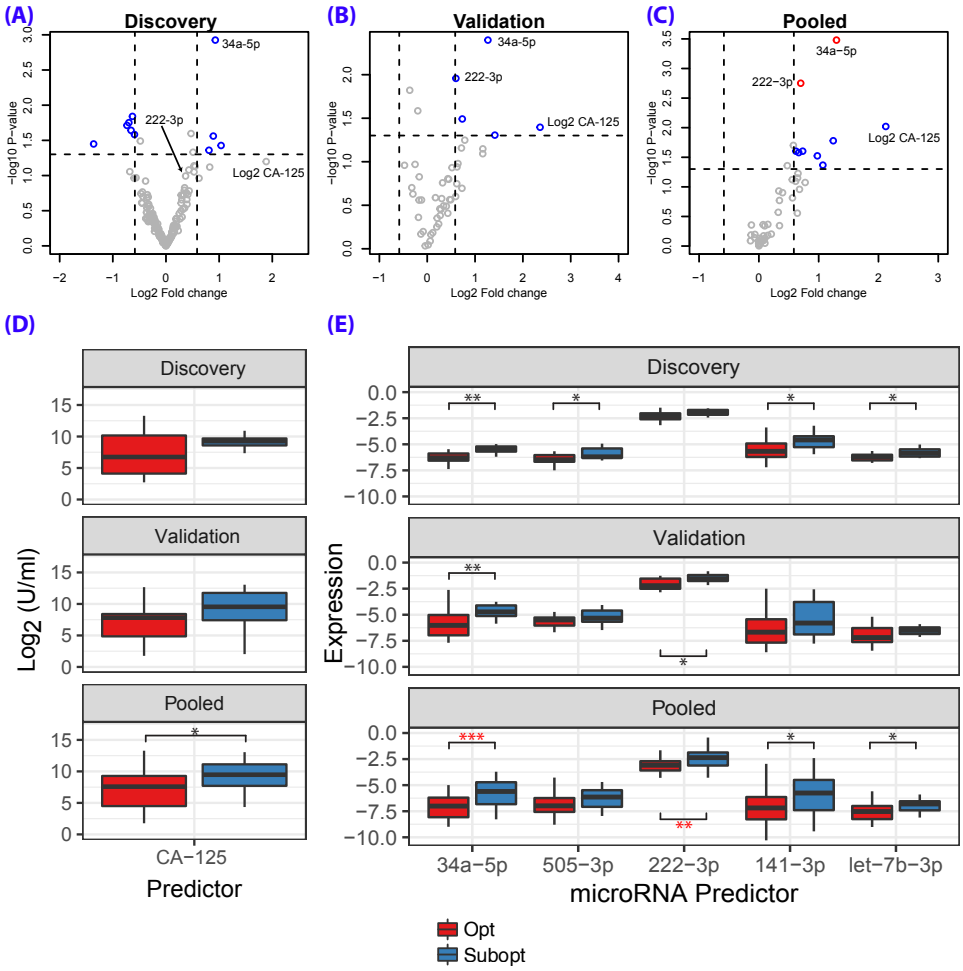

Figure 3.6: Identification of the markers that predict surgical outcome for women with HGSOC.

Volcano plots showing differentially expressed predictors identified from **(A)** Discovery, **(B)** Validation or **(C)** Pooled set. Vertical and horizontal dashed lines mark the absolute fold-change of 1.5 and *P* value of 0.05, respectively. Blue and red circles represent predictors with > 1.5-fold absolute change with either unadjusted $P < 0.05$ or were significant after 5% false discovery rate (FDR), respectively. Only CA-125, miR-34a-5p and miR-222-3p are labelled for simplicity. **(D, E)** Levels of CA-125 and candidate microRNAs in Discovery, Validation and the Pooled dataset. microRNAs in **(E)** were chosen based on their DE (Table 3.6). * P <0.05, ** $P < 0.005$ and *** $P < 0.0005$. Biomarkers that remained significant after FDR-correction are marked with a red asterisk according to the criteria above.

important predictors of surgical outcome out of all 11 predictors, reducing the AIC from 78.04 to 65.64. miR-34a-5p also had a slightly higher bootstrapped median AUC (0.779) and accuracy (0.750) compared to CA-125 (AUC: 0.700 and accuracy: 0.714, Figure 3.7 and Table 3.7). A prediction model comprising both predictors resulted in AUC and accuracy of 0.818 and 0.786, respectively (Figure 3.7 and Table 3.7).

	Discovery			Validation			Pooled		
	logFC	***P***	**FDR-*P***	**logFC**	***P***	**FDR-*P***	**logFC**	***P***	**FDR-*P***
34a-5p	0.928	0.001	0.202	1.269	0.004	0.192	**1.298**	**3.31E-04**	**0.016**
222-3p	0.431	0.083	0.755	0.600	0.011	0.241	**0.700**	**0.002**	**0.042**
Log_2 CA-125	1.886	0.063	0.755	2.359	0.040	0.321	2.123	0.010	0.150
141-3p	1.037	0.037	0.578	1.161	0.081	0.351	1.244	0.017	0.155
let-7b-3p	0.471	0.025	0.578	0.433	0.157	0.402	0.577	0.020	0.155
30a-5p	0.549	0.074	0.755	0.518	0.117	0.351	0.733	0.025	0.155
29a-5p	0.346	0.162	0.905	0.448	0.159	0.402	0.620	0.025	0.155
29b-2-5p	0.369	0.102	0.773	0.303	0.265	0.427	0.475	0.044	0.187
145-5p	-0.698	0.018	0.578	0.472	0.273	0.427	0.345	0.452	0.766
551b-3p	-0.631	0.014	0.578	0.200	0.560	0.656	0.083	0.797	0.946
629-5p	-0.593	0.026	0.578	0.208	0.444	0.547	-0.072	0.722	0.946
20b-5p	-0.657	0.023	0.578	0.063	0.814	0.850	0.021	0.902	0.953
let-7i-3p	-0.733	0.019	0.578	0.321	0.175	0.409	0.065	0.813	0.946
361-3p	-0.483	0.032	0.578	0.266	0.347	0.484	0.101	0.736	0.946
505-3p	0.509	0.047	0.610	0.284	0.353	0.484	0.558	0.076	0.248
122-5p	0.890	0.027	0.578	0.595	0.251	0.427	0.774	0.084	0.248
605	-1.361	0.036	0.578	0.400	0.324	0.472	-0.140	0.815	0.946
375	0.809	0.044	0.610	0.430	0.391	0.521	0.679	0.110	0.305
Identified from Pooled Data									
92b-3p	0.046	0.837	0.966	0.733	0.032	0.310	0.666	0.026	0.155
200a-3p	-0.057	0.903	0.973	0.727	0.202	0.421	0.978	0.030	0.156
200c-3p	0.231	0.608	0.962	1.414	0.049	0.339	1.070	0.043	0.187

Table 3.6: Summary statistics of microRNAs that could predict Optimal/Suboptimal cytoreduction

Predictors with absolute FC > 1.5-fold are filled with background colour while those meeting FDR-corrected $P < 0.05$ are shown in bold face. FC: fold-change, FDR: false discovery rate.

	AUC	Accuracy
Log_2 CA-125	0.693	0.714
miR-34a-5p	0.777	0.750
Log_2 CA-125 + miR-34a-5p	0.818	0.786

Table 3.7: Performance of biomarkers that can separate Optimal/Suboptimal samples
miR-34a-5p and log_2 CA-125 were found to be the most significant predictors of the surgical outcome from stepwise regression. Their performances in predicting the binary outcome was tested by systematically adding additional features in the predictive model. A model comprising both predictors resulted in a higher AUC and accuracy compared to each predictor individually. AUC: area under curve

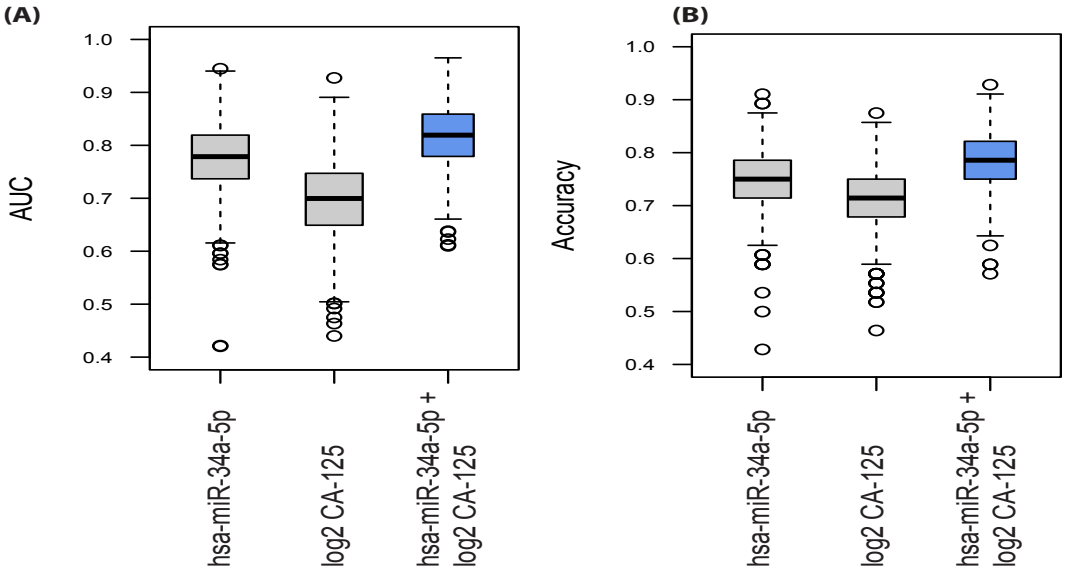

Figure 3.7: Performance of predictors that predict the surgical outcome of women with HGSOC.
(A) Area under curve (AUC) and **(B)** accuracy of the most significant markers identified from stepwise regression from the pooled data to predict the optimal versus suboptimal cytoreduction (N=56; 30 Opt + 26 Subopt samples) when markers are used individually or in combination. Boxplots represent values of 1000 bootstraps with replacement.

3.3.3 Using machine learning to identify predictive biomarkers

3.3.3.1 Predictors of HGSOC from healthy women

Two ML algorithms were used to separate patients with HGSOC from healthy women: DLDA and SVM. Both algorithms were trained on the Discovery dataset and tested on the Validation dataset by incrementally increasing the number of features[§] used for the classification. Error rates (1 - accuracy) for both algorithms were calculated as a function of the number of features (Figure 3.8A). Compared to SVM, DLDA showed less fluctuations in the error rate for predicting healthy or HGSOC status; therefore, was subsequently selected for 100-times 4-fold[¶] cross validation (CV). The top 10 features from each round of CV were pooled into a frequency table. Ranking the inclusion frequencies of the features from CV suggested their order of importance for the binary classification (Figure 3.8B). For example, if a feature is strongly predictive of an outcome, it will tend to be selected more often compared to others in the CV and present with a high inclusion frequency.

CA-125 had the highest inclusion frequency followed by microRNAs when both phases were pooled, suggesting that CA-125 was superior to microRNAs in predicting HGSOC (Figure 3.8B). Performance of DLDA by incrementally adding more features is shown in Figure 3.8C, starting with a combination of Log_2 CA-125 and miR-150-5p as DLDA requires at least two features. Overall, the median accuracy of DLDA using a combination of 10 microRNAs with the highest inclusion frequencies was 0.883 and Matthews correlation coefficient (MCC), a measure of quality of binary classification with a value of 1 for perfect prediction, was 0.770 (Figure 3.8C).

[§] 'features' is the technical term to refer to predictor variables in machine learning

[¶] 4-fold means that the data was split into 4 equal parts or 'folds'; 3 folds were used for training the algorithm and the remaining 1 fold was used to test the performance of the model. This procedure was repeated 100-times with randomisation, ultimately using all data for training and testing the algorithm.

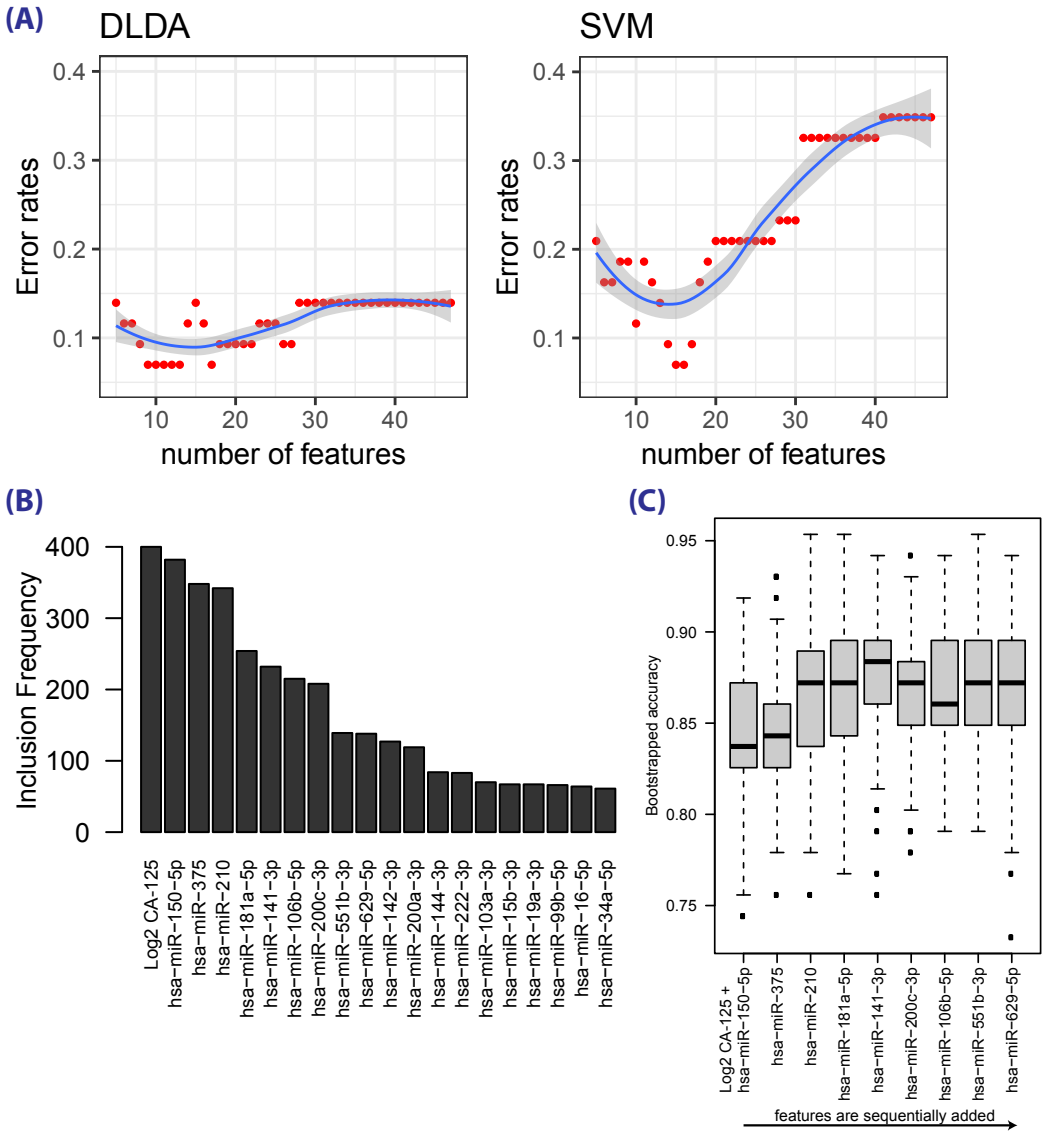

Figure 3.8: Applying machine learning algorithms to separate patients with HGSOC from healthy women

(A) Selection of two ML algorithms, diagonal linear discriminatory analysis (DLDA) and support vector machine (SVM), to separate patients with HGSOC from healthy women. DLDA was selected for further analyses as it resulted in a lower error rate than SVM. **(B)** Inclusion frequencies of features using 100-times 4-fold cross validation (CV). **(C)** Accuracy of prediction using DLDA and multiple features.

3.3.3.2 Predictors of the surgical outcome

DLDA was also found to have less fluctuations in the error rate of predicting the surgical outcome compared to SVM, and was selected for 100-times 4-fold CV (Figure 3.9A). Both miR-34a and miR-222 had higher inclusion frequencies compared to Log_2 CA-125, indicating that microRNAs were superior to Log_2 CA-125 in predicting the surgical outcome (Figure 3.9B). Performance of DLDA by incrementally adding more features is shown in Figure 3.9C, starting with a combination of miR-34a-5p and miR-222-3p. The median accuracy of DLDA using a combination of the top 10 microRNAs with highest inclusion frequencies was 0.688 with MCC of 0.362 (Figure 3.9C).

3.3.4 The effect of haemolysis on DE microRNAs

Numerous microRNAs are found to be affected by haemolysis due to the emptying of microRNA content of red blood cells into serum (Kirschner et al. 2011, 2013; Pritchard et al. 2012). We have previously shown that the ratio of miR-451a to miR-23a-3p (delta Cq (miR-23a-3p - miR-451a)), referred to as the 'miR ratio', is the most sensitive method to monitor low levels of haemolysis in serum (Shah, Soon, and Marsh 2016). As discussed previously, the miR ratio of <5, 5-7 and >7 is indicative, respectively, of a sample at a low, moderate or high risk of being affected by haemolysis (Blondal et al. 2013). We tested whether the microRNAs identified to predict surgical outcome or differentiate serum from healthy women or ovarian cancer patients were affected by haemolysis. No significant differences in haemolysis levels in the three groups (Healthy, Opt and Subopt) were found in pooled data (one-way ANOVA, $P = 0.365$; Figure 3.10A). One-way ANOVA also suggested that miR-210 was significantly affected by haemolysis ($P < 0.05$) whereas $\log_2$ CA-125, miR-375 and miR-34a-5p remained unaffected ($P > 0.05$; Figure 3.10B-F).

3.4 Discussion

Prediction of surgical outcome for HGSOC women prior to surgery has a potentially crucial role in personalising therapeutic options yet remains difficult to achieve. This study used serum microRNAs to predict the completeness of surgical resection. As proof-of-principle that serum microRNAs could potentially differentiate disease state, we also employed our analytical pipeline to identify differentially expressed (DE) microRNAs in HGSOC patients compared to healthy age-matched women

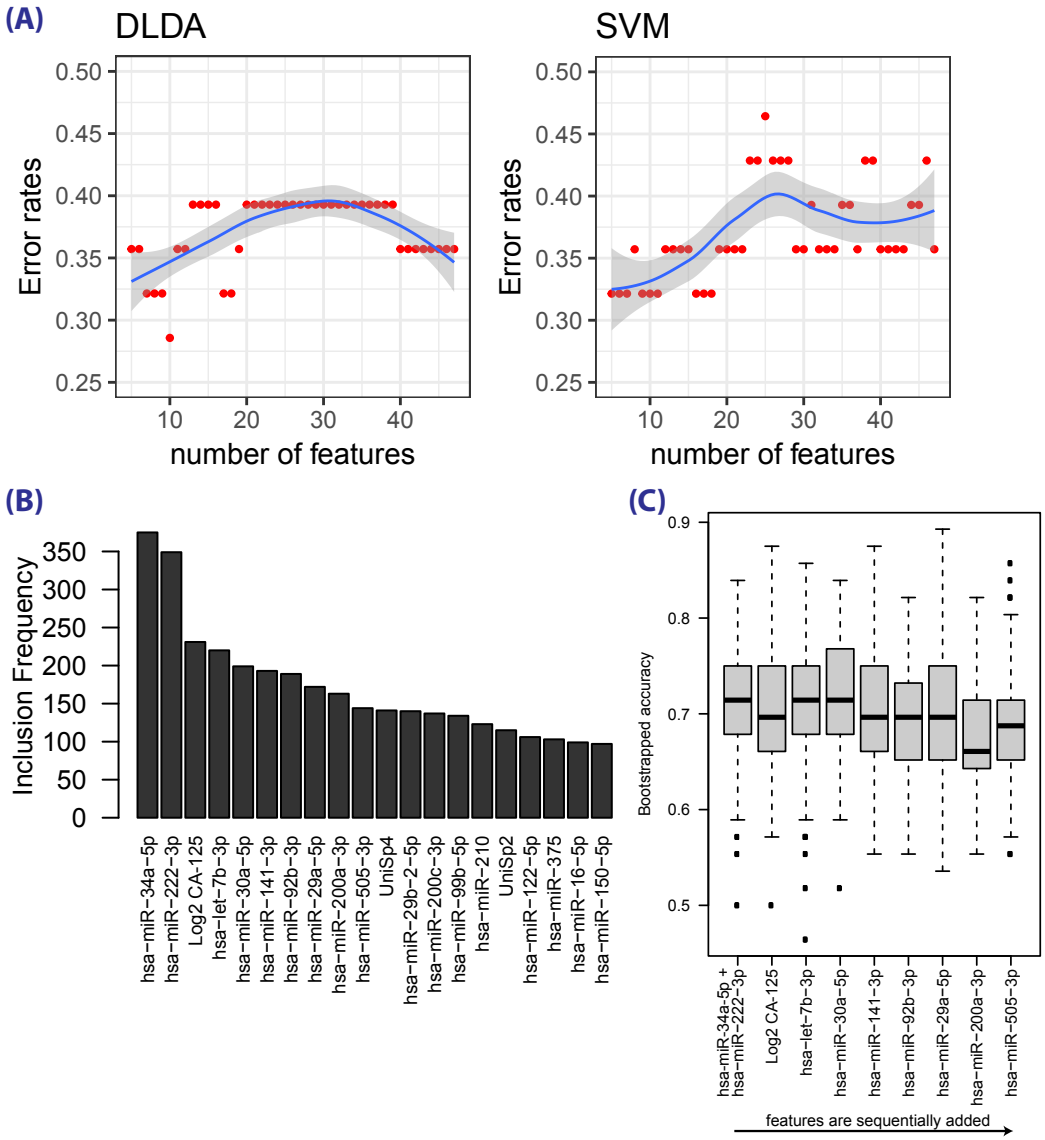

Figure 3.9: Applying machine learning algorithms to predict surgical outcome
(A) Selection of two ML algorithms, DLDA and SVM, to predict surgical outcome for women with HGSOC. DLDA was selected for further analyses as it resulted in a lower error rate than SVM. **(B)** Inclusion frequencies of features using 100-times 4-fold CV. **(C)** Accuracy of prediction using DLDA and multiple features.

3.4.1 Identifying HGSOC patients from healthy women

Serum microRNAs miR-375 and miR-210 were consistently found to be differentially expressed in HGSOC patients versus healthy women in this study. To our knowledge, these microRNAs have not previously been reported to discriminate healthy women from patients with ovarian cancer (Table 3.8). miR-375 levels in circulation has been found to be

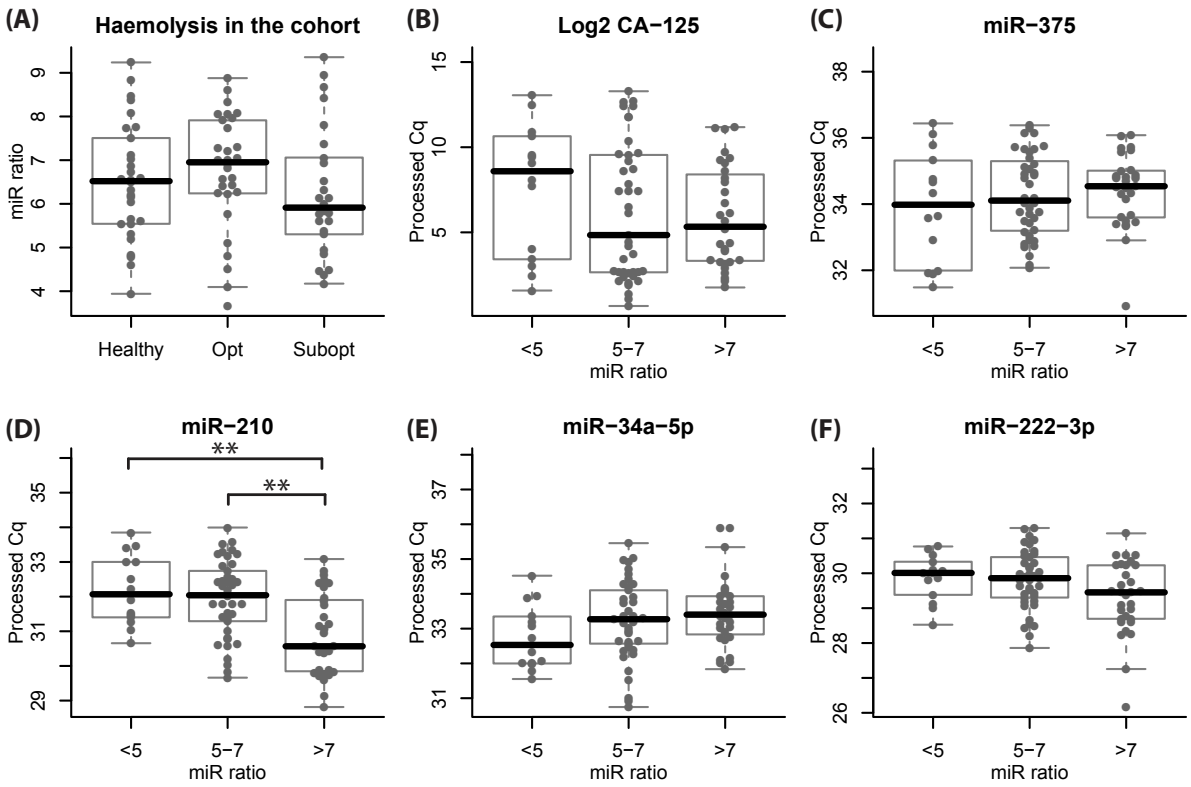

Figure 3.10: Effect of haemolysis on candidate predictors.
(A) Haemolysis levels in the three biological groups (Healthy, Optimally and Suboptimally cytoreduced) in this cohort measured by the 'miR ratio' (delta Cq (miR-23a-3p—miR-451a)), the most sensitive method of detecting low levels of haemolysis (Shah, Soon, and Marsh 2016) **(B-F)** Effect of haemolysis on the candidate predictors including $\log_2$ CA-125. Log_2 CA-125, miR-375, miR-34a-5p and miR-222-3p were not affected by haemolysis, suggesting that they are suitable for routine clinical use where haemolysis is frequent (Hawkins 2010; Lippi et al. 2009).

altered in patients with prostate (Cheng et al. 2013; He et al. 2015; Kachakova et al. 2015; Selth et al. 2012; Wach et al. 2015), breast (Huo et al. 2016), gastric (Zhang et al. 2012b), pancreatic (Carlsen et al. 2013) and non-small-cell lung cancers (Yu et al. 2014b) compared to healthy individuals. Circulating miR-210 has also been suggested as a biomarker of early recurrence of melanoma (Ono et al. 2015), colorectal (Wang et al. 2016b), pancreatic (Ho et al. 2010; Yingxia et al. 2015) and clear cell renal cancers (Iwamoto et al. 2014).

Serum protein CA-125 levels had a higher AUC (0.929) and accuracy (0.884) for predicting the HGSOC status compared to either miR-375 or miR-210 alone that had AUCs and accuracies of approximately 0.750 each. A combination of CA-125, miR-375 and miR-210 increased AUC and the accuracy of prediction to 0.984 and 0.965, respectively. Since we and others (Kirschner et al. 2013) have shown that miR-210 was affected by haemolysis,

it may not be suitable for clinical use where haemolysis is common (Hawkins 2010; Lippi et al. 2009). In contrast, miR-375 was not affected by haemolysis, and a combination of CA-125 and miR-375 marginally improved AUC (0.953) and accuracy (0.907) of prediction of HGSOC patients versus healthy women compared to CA-125 alone.

The performance of miR-375 is comparable with the previous study published by our group that reported a combination of miR-200b and miR-200c in predicting HGSOC from healthy women (AUC: 0.784; Kan et al. 2012), and by other laboratories (summarised in Table 3.8). Hausler et al. 2010 reported that miR-343-3p could separate OC patients from healthy women with an AUC of 0.86. Assuming that a diagnostic test would be unlikely to rely on a single biomarker, the authors used a panel of 40 microRNAs using SVM that resulted in an AUC of ~0.85. Nonetheless, microRNA predictive of OC from the study of Hausler et al. 2010 and others (Table 3.8) were found to be inferior to CA-125, which, in our study, could predict HGSOC with an AUC of 0.929.

Currently, a population-wide screening test for OC is missing due to high sensitivity (>0.75) and specificity (0.996) required of the test to attain a PPV of 0.10, a minimum value for a screening test (Clarke-Pearson 2009; Hennessy, Coleman, and Markman 2009). CA-125 is also known to be nonspecific and its levels in blood are affected by multiple factors such as menopausal status, uterine fibroids, ovarian cysts and liver disease (Felder et al. 2014; Matulonis et al. 2016; Verheijen et al. 1999). Any biomarker that is likely to replace CA-125 in the diagnosis of OC should at least perform as well as CA-125 before being tested in wider settings that could overcome its limitations. HE4 is increasingly becoming a promising biomarker with performance reported to be equivalent to CA-125 (Chen et al. 2016; Ferrarow et al. 2013; Hu et al. 2016). A meta-analysis of 9 published studies (N = 1,807; Wu et al. 2012) reported that HE4 could separate OC from healthy samples with AUC of 0.927, sensitivity of 0.83 and specificity of 0.90, which is comparable with a sensitivity of 0.80 and specificity of 0.75 reported by an earlier meta-analysis performed on CA-125 (17 studies, N = 2,374; Medeiros et al. 2009)[⊠].

Serum microRNAs have, so far, been unable to match the performance of CA-125 or HE4 in identifying OC from healthy samples. Most reviews in this field only report the differentially expressed microRNAs, not their performance in predicting the healthy/OC status. A meta-analysis evaluating predictive power of reported microRNAs (similar to Table 3.8) is needed to identify microRNAs reported from independent studies and to

[⊠] Medeiros et al. 2009 reported AUC of 0.888 for CA-125's ability to differentiate malignant versus benign lesions; however, a healthy versus OC comparison was missing, making it difficult to compare AUCs of HE4 and CA-125 directly. Nonetheless, HE4 outperformed CA-125 in sensitivity and specificity in this study, making it at least comparable, if not superior, to CA-125.

evaluate their predictive potential in a large cohort. miR-200a, -b or -c have been reported for their predictive power from at least three independent studies (Kan et al. 2012; Selth et al. 2012; Taylor and Gercel-Taylor 2008). Differences in cohort compositions, methodologies to quantify serum microRNAs as well as choice of the quality control protocols may explain why miR-200a, -b or -c were not discovered in other studies. This study and the study conducted by Kan et al. 2012 — both from our laboratory — had numerous methodological differences. The current study used miRCURY RNA isolation kit for Biofluids (Exiqon) whereas Kan et al. 2012 used miRVANA PARIS kit (Ambion, Applied Biosystems). Additionally, LNA primers were used in qPCR in the current study versus pre-amplification using the Taqman PreAmp Master Mix (Applied Biosystems) used by Kan et al. 2012. Of the samples analysed in the current study, 19 HGSOC and 3 healthy volunteer serums were also included in this earlier study conducted by Kan et al. 2012. In this study, miR-200c displayed a strong upregulation in HGSOC sera (FC: ~5-fold, FDR-$P = 3.02 \times 10^{-7}$) in the Discovery phase, but this diminished when all data were pooled (FDR-$P = 0.07$; Table 3.4). miR-200a was not found to be DE in the pooled data, and miR-200b was present only in the Validation phase at a statistically non-significant level (FDR-$P = 0.8$; Supplementary Table B.1). It remains to be tested whether other ncRNAs such as lncRNAs or circular RNAs could improve or outperform CA-125 or HE4 in diagnosing OC.

microRNA	Source	Volume	Highest value					Reference	Comments
			AUC	Acc	Sens	Spec	FC		
miR-200b + miR-200c	Serum	500 µl	0.784		0.786	0.464	2.5	Kan et al. 2012	
miR-343-3p	Whole blood	5 ml	0.86					Hausler et al. 2010	
A panel of 40 miRs				0.85*	0.85*	0.85*			miR-375 and miR-210 were not present on this list.
miR-21, -141, -200a, -200b, -200c, -203, -205 and -214	Exosomes	2.5ml serum						Taylor and Gercel-Taylor 2008	Reported 8 DE miRs, but diagnostic statistics were missing
miR-21, -92, -93, -126 and -29a (upregulated)	Serum	250 µl					5.4*	Resnick et al. 2009	miR-92 had the highest FC of 5.4*.
miR-155, -127 and -99b (downregulated)							-9.2*		miR-99b had the highest FC of -9.2*.
miR-21	Plasma	400 µl					3.4	Xu et al. 2013	Investigated early diagnosis of OC
miR-92	Serum	200 µl	0.803				1.3*	Guo et al. 2013	Although miR-92 was DE in EOC versus healthy samples (P <0.05; N = 100), the FC seemed low (read-off the graph). Haemolysis-sensitive miR-16 used as reference.
miR-205 + let-7f	Plasma	250 µl	0.726 - 0.831		0.62 - 0.64	0.72 - 0.929		Zheng et al. 2013	Statistics on multiple validation sample reported, but a pooled analysis was lacking.
miR-132, -26a, -143, -145 and let-7b	Plasma	500 µl					>-2	Chung et al. 2013	All 5 miRs were downregulated. Diagnostic statistics were missing
miR-1290	Plasma	1 ml	0.87				14.57	Shapira et al. 2014	
miR-92a	Urine exosomes						31.97	Záveský et al. 2015	
miR-106b							-3.7		
miR-100							-3.3		
miR-206	Plasma						21.26	Ayaz et al. 2014	Used plasma of 3 ml blood
miR-200c	Serum		0.79		0.72	0.7	1.8*	Gao and Wu 2015	
miR-141			0.75		0.69	0.72	1.7*		

Table 3.8: Summary of microRNAs predictive of OC

Only highest values of performance indicators are reported. * exact values were not reported in the manuscript, but they were read-off the graphs. AUC: Area under curve, Acc: accuracy, Sens: sensitivity, Spec: specificity, FC: fold-changes. Positive and negative FC represent up- or down-regulation of a miR in OC compared to healthy controls.

3.4.2 Prediction of surgical outcome

Serum levels of miR-34a-5p and $\log_2$ CA-125 were found to be predictive of surgical outcome for women with HGSOC, with miR-34a-5p performing slightly better than $\log_2$ CA-125 (AUC: 0.779 versus 0.700, and accuracy: 0.750 versus 0.714, respectively). The final AUC and accuracy of 0.818 and 0.786, respectively, were achieved by combining both markers (Figure 3.7 and Table 3.7).

The identification of miR-34a-5p in predicting surgical outcome is intriguing. Independent studies have established that miR-34a-5p is a potent tumour suppressor microRNA and a direct transcriptional target of the wild-type (wt) p53, resulting in cell cycle arrest and apoptosis upon induction (Adams, Parsons, and Slack 2016; He et al. 2007; Hermeking 2012; Rokavec et al. 2014). Several pre-clinical studies have demonstrated the efficacy of restoring expression of the miR-34 family of microRNAs in inhibiting tumour growth in mouse models of lung (Kasinski and Slack 2012; Wiggins et al. 2010), pancreatic (Pramanik et al. 2011) and prostate cancers (Liu et al. 2011a). In fact, restoring expression of the miR-34 family of microRNAs is currently being tested as a cancer therapy in a clinical trial (NCT01829971). miR-34a-5p was found to be downregulated in late versus early stages of EOC (Eitan et al. 2009; Zhang et al. 2008) as well as EOC compared to the normal ovarian surface epithelial cells by promoter hypermethylation (Corney et al. 2010; Schmid et al. 2016). Of note, these studies were conducted in EOC, of which HGSOC is the most common subtype (Matulonis et al. 2016) and their findings should translate well to HGSOC. Given the downregulation of miR-34a-5p in EOC, it remains unlikely that miR-34a-5p is released at elevated levels from presumably more aggressive suboptimally cytoreduced HGSOC.

Besides cancer, miR-34a-5p has been shown to play a crucial role in normal physiology and diseases such as metabolic syndromes (Lovis et al. 2008; Rottiers and Näär 2012; Yang, Cappello, and Wang 2015), senescence of endothelial cells (Qin, Yang, and Xiao 2012), aging of cardiac cells (Boon et al. 2013) and platelet production (Gatsiou et al. 2012). Therefore, the observed elevation in miR-34a-5p could be a result of the body's response to suboptimally cytoreduced tumours.

The current study highlights ongoing challenges in predicting the surgical outcome. A range of modalities such as CT, laparoscopy, expression of mRNAs from tissues, surgical management using the two-surgeon opinion approach (The Anderson Algorithm), circulatory proteins CA-125 and HE4 have been attempted as well as the use of serum microRNAs as conducted in this study. A reliable method of predicting surgical outcome to identify patients that are either likely, or unlikely, to respond well to the primary cytoreductive surgery

remains elusive. The challenge could partly be attributed to variations in skills of surgeons, attitudes as well as policies of institutes towards aggressive surgeries. Modalities such as CT have been found to be promising in predicting the surgical outcomes in single centre studies (Bristow et al. 2000; Dowdy et al. 2004) but failed to attain sufficient performance in multicentre trials (Axtell et al. 2007; Borley et al. 2015; Mackintosh et al. 2014), partially due to variability in radiologists' skills (Mackintosh et al. 2014). Thus, inconsistencies in patient management are a significant hurdle to overcome.

Standardised patient care is the crux of 'The Anderson Algorithm' which uses laparoscopy with at least 2 surgeons' opinions on the surgical resectability of the tumour (Nick et al. 2015). Although the study has not been officially published yet, the initial results reported in a review by Nick et al. 2015 have been promising, with the rate of R0 increasing from 20% to 84% since implementation of the protocol. The effect of laparoscopy combined with either one surgeon or multiple surgeons' opinions on the likelihood of R0 resection also remains to be seen, which would indicate the effect of unstandardised protocols on the rate of R0 resection. Given the low prevalence of OC, implementing a two-surgeon opinion approach may be difficult to achieve in smaller centres. However, if approaches such as The Anderson Algorithm are proven to be effective in multicentre studies, they would represent strong evidence for streamlining the surgical management of OC patients.

3.4.3 A commentary on statistical methods

Traditional methods such as LR and ML algorithms originated as different branches of statistics with their own jargon to often describe the same concepts (Iterson, Haagen, and Goeman 2012). Briefly, traditional statistics put significant emphasis on accuracy of the probability distribution function, such as the Gaussian ('normal') distribution, and estimates of the parameters (e.g. mean and standard deviation); performance measures are calculated afterwards. In contrast, ML algorithms aim to maximise accuracy of the prediction based on linear or non-linear functions that separate the binary outcomes (Wale 2011). I have used accuracies predicted by LR and ML to compare their performances.

The consulting statistician, Professor Jean Yang of The University of Sydney, Australia, found it appropriate to use two ML algorithms (DLDA and SVM) to model the data. SVM resulted in significantly more variations in the accuracy of prediction than DLDA for classifying healthy/HGSOC and Opt/Subopt outcomes. In both predictions, LR resulted in a higher accuracy of the prediction than DLDA. However, this is not a criticism of ML algorithms. DLDA performed reasonably well in separating HGSOC from healthy samples

(median accuracy: 0.883), where there were obvious differences between the two biological groups. In addition, only 2 algorithms were attempted in this study whereas ML consists of an exhaustive number of algorithms, with >200 algorithms implemented in a single R package 'caret' (Jed Wing et al. 2016).

3.5 Conclusions

Pre-operative prediction of surgical outcome has the potential to improve clinical management of patients with HGSOC by optimising the timing of the surgery, i.e. before chemotherapy (current standard treatment) or after 'shrinking' tumours with a few rounds of chemotherapy (neoadjuvant chemotherapy). Although prediction of the surgical outcome using serum microRNAs was the primary aim of this study, a thorough quality control protocol, including measurements of low levels of haemolysis, was first developed for reliable quantification of serum microRNAs (Chapter 4). This study identified that levels of miR-375 and miR-210 in serum can separate patients with HGSOC from healthy women, both have not been reported in the literature for this purpose previously to our knowledge. In addition, serum miR-34a-5p was found to be slightly superior to CA-125 in predicting the surgical outcome. Finally, miR-375 and miR-34a-5p were not affected by haemolysis, suggesting their suitability for routine use as circulating biomarkers.

Chapter 4

Detecting low levels of haemolysis in serum

4.1 Introduction

Since serum microRNAs and their extracellular carriers (exosomes, microvesicles and high-density lipoproteins) bathe in blood, the microRNA content of blood cells could interfere with analyses of disease-associated microRNA profiles due to haemolysis. Leakage of the content of RBC is potentially a grave source of contamination given the vast abundance of RBCs in blood compared to other blood cells such as leukocytes, although lymphocyte-derived microRNAs such as miR-150 could also be affected by haemolysis to a lesser extent (Pritchard et al. 2012). Recent studies have shown that 58% (46/79) of proposed microRNA biomarkers for solid cancers were highly expressed in one or more blood cell types (Pritchard et al. 2012), and up to 65% of detectable microRNAs in plasma were affected by haemolysis (Kirschner et al. 2013). Although certain diseases such as chronic lymphocytic leukaemia can cause haemolysis *in vivo*, blood collection protocols and processing seem to be a common cause of haemolysis (Kirschner et al. 2013). According to a study on 111,780 clinical samples, up to 43% of the clinical samples were found to be haemolysed based on free haemoglobin levels >0.5 g/L (Hawkins 2010). On the other hand, only 5.6% manifested the pink discolouration visible to the naked eye (Lippi et al. 2009). Taken together, haemolysis has the potential to lead to inaccurate quantification of microRNAs in a significant proportion of samples, including the current study. As an example, the reference miR-16 used for normalising data in some serum/plasma studies

was found to be severely affected by haemolysis, questioning its suitability as a reference microRNA (Kirschner et al. 2013; McDonald et al. 2011).

Determining robust methods to enable sensitive detection of haemolysis that may affect the identification of disease-associated microRNA was essential for the microRNA studies presented in Chapter 3 of this thesis. Earlier studies by others employed the presence of pink discolouration of serum as a marker of haemolysis; however, it was later discovered that plasma samples can already be affected by haemolysis before manifesting this discolouration (Kirschner et al. 2011, 2013). For example, Kirschner et al. 2011 established that RBC concentration of up to 0.125% (v/v) of plasma could be detected as visually pink indicating that haemolysis had occurred. The levels of haemolysis-sensitive miR-16 and miR-451; however, could be detected at just 0.031% (v/v) haemolysis in plasma (Kirschner et al. 2011). Alternative methods, such as measuring the peak absorbance of haemoglobin at 414 nm by spectroscopy, or quantifying levels of miR-451a, the most abundant microRNA in RBC, compared to the reference microRNA miR-23a (the 'miR ratio') were proposed in the literature, but a direct comparison to determine the sensitivities of these was lacking (Blondal et al. 2013; Kirschner et al. 2011).

In this chapter, I present a detailed analysis of different methods to detect haemolysis, including use of a cohort of serum collected from healthy women and women with HGSOC. The utility of routinely used equipment to determine haemoglobin levels in the clinic such as the Coulter®AcT diff™ Analyzer as well as visual inspection for pink discolouration in serum were investigated to determine their ability to robustly detect low levels of haemolysis.

Declaration: This study has been published (see Shah, Soon, and Marsh 2016). The text in Materials & Methods, Results, Discussion and Conclusion of this chapter is identical to the work originally published in American English, but has been re-formatted to Australian English for this thesis. In-text citations have been updated to match the references in the bibliography. American English has been retained within the published figures.

The following methodology described in the published paper is expanded elsewhere:

- Blood collection and ethics information: Chapter 2, subsection 2.1.1, p. 36
- RNA extraction from serum: Chapter 2, subsection2.1.2, p. 41
- RT-qPCR for detecting serum microRNAs: Chapter 2, subsection 2.1.3, p. 41

- Data analysis: Chapter 2, subsection 2.1.4, p. 42

Complete citation: Shah JS, Soon PS and Marsh DJ. Comparison of Methodologies to Detect Low Levels of Hemolysis in Serum for Accurate Assessment of Serum microRNAs, *PloS One* (2016). doi: `http://dx.doi.org/10.1371/journal.pone.0153200`

4.2 Materials and methods

4.2.1 Haemolysis dilution series

Whole blood, 0.5 ml collected from a healthy volunteer, was allowed to clot in an eppendorf tube, and sonicated until the sample was completely fluid and bright red, indicative of a high degree of haemolysis. Serum was isolated from the blood of a healthy volunteer as per the healthy volunteers' protocol. This sample, collected under optimal conditions, was classified as unhaemolysed for the purpose of this study. A haemolysis dilution series comprising 100%, 20%, 4%, 1%, 0.25%, 0.062%, 0.016%, 0.004%, 0.001% haemolysed and unhaemolysed samples (v/v) was prepared by serial dilution of the 100% haemolysed sample with unhaemolysed serum.

4.2.2 Assessment of haemolysis

Haemolysis in serum samples was measured using 4 methods. The first method measured haemoglobin concentration using the Coulter® AcT diff™ Analyzer and the Tainer Reagent Kit (Beckman Coulter Inc # 8547135, Lane Cove, NSW, Australia). Three technical replicates were performed for each sample. The second method to assess haemolysis was simple visual inspection of serum samples for pink discolouration indicative of free haemoglobin against a white background. Visual discolouration of each sample was scored from 0 (unhaemolysed serum) to 5 (100% haemolysed serum). The third method was measurement of the absorbance of haemoglobin at 414 nm using a NanoDrop™ 1000 spectrophotometer (Thermo Scientific, Scoresby, Victoria, Australia), averaging two technical replicates per sample. Lastly, the fourth method used determined the ratio of miR-451a to miR-23a-3p (delta C_t (miR-23a-3p - miR-451a)) referred to hereon as the "miR ratio"), with RT-qPCR. Three RT reactions were performed for each sample followed by one PCR per RT.

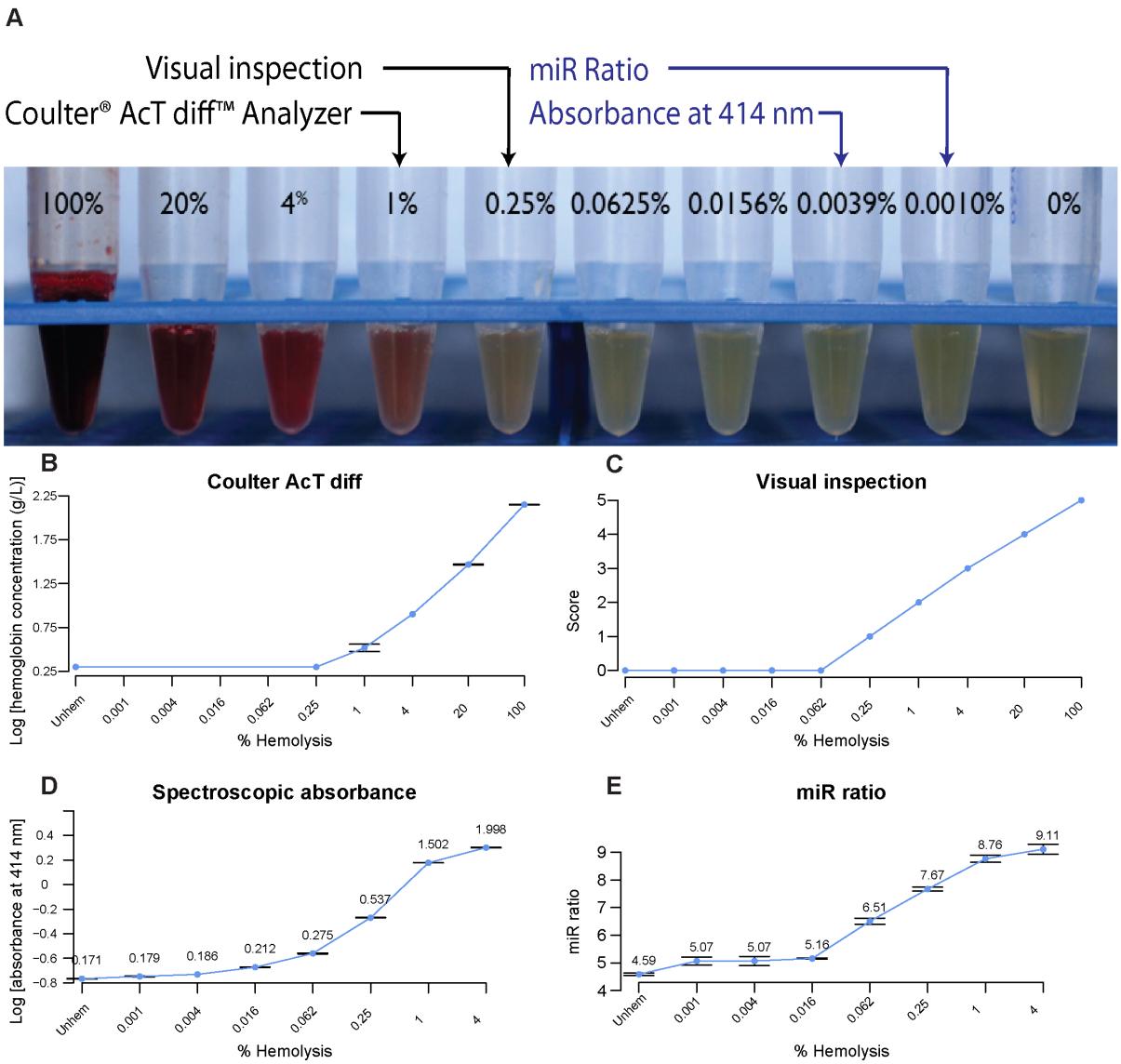

Figure 4.1: Sensitivities of four methods to detect haemolysis.
(A) A haemolysis series was prepared by diluting 100% haemolysed sample with unhaemolysed serum (0%), and the sensitivity of each method determined by its ability to detect haemolysis (indicated by arrows). **(B - E)** Detection of haemolysis using four methods. For visual inspection, samples were scored from 0 (unhaemolysed sample) to 5 (100% haemolysis). Averages of technical replicates are shown where appropriate. 'Unhem' denotes unhaemolysed serum. Absorbance measures (D) and miR ratios (E) are noted on the graphs.

4.3 Results

4.3.1 Sensitivities of four methods to detect haemolysis

Four methods for the detection of haemolysis were compared using the haemolysis dilution series as described. The Coulter® AcT diff™ Analyzer measurement of haemoglobin could detect down to 1% haemolysis, while the 0.25% haemolysed and the unhaemolysed sample remained indistinguishable (Figure 4.1B). By visual inspection alone, the pink discolouration of free-haemoglobin could be detected down to 0.25% haemolysis (Figure 4.1A, C). In contrast, the spectrophotometric method could detect down to 0.004% haemolysis (Figure 4.1D). The calculated miR ratio could detect down to 0.001% haemolysis, the lowest point tested, making it the most sensitive method (Figure 4.1E). The Coulter® AcT diff™ method was excluded from further analyses due to its low sensitivity. Therefore, in order of decreasing sensitivity, the methods used can be ranked as miR ratio > spectrophotometry > visual inspection > Coulter® AcT diff™ Analyzer.

Next, we determined the haemolysis levels of 86 samples (56 women with ovarian cancer and 30 age-matched, healthy females) using visual inspection, spectrophotometric absorbance and the miR ratio. Using the miR ratio as the 'gold standard', 16% (14/86), 48% (41/86) and 36% (31/86) of the samples were found to have low (miR ratio <5), moderate (miR ratio between 5 and 7) or severe (miR ratio >7) haemolysis, respectively, according to the criteria defined by Blondal et al. 2013, highlighting haemolysis as potentially a problematical factor, even when serum samples are collected under optimal conditions (Figure 4.2A). The miR ratio of the unhaemolysed sample used to construct the dilution series was 4.59 ± 0.10. In contrast, the miR ratio for the 0.25% haemolysed sample, the limit of visual inspection, was 7.67 ± 0.14. Furthermore, 100% of the samples with pink discolouration (8/8) had a miR ratio >7, suggesting that any samples with visible pink discolouration were already severely affected by haemolysis (Figure 4.2A).

4.3.2 Identification of severely haemolysed samples using visual inspection and the absorbance of haemoglobin

Since the majority of the severely haemolysed samples based on the miR ratio (74%; 23/31) were visually undetectable, we investigated whether the absorbance of haemoglobin could be utilised to detect additional severely haemolysed samples, i.e miR ratio >7. The samples

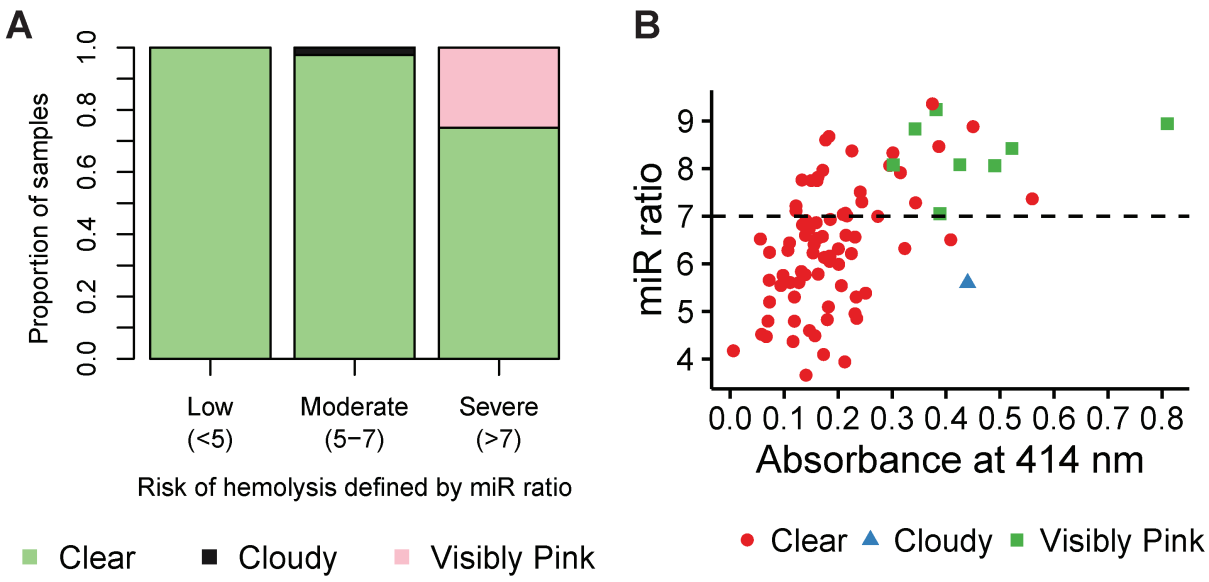

Figure 4.2: Comparison of methodologies for determining haemolysis in serum samples. **(A)** Serum samples (N=86) categorised by low (miR ratio <5; N=14), moderate (miR ratio 5-7; N=41) and severe (miR ratio >7; N=31) haemolysis. Results of visual inspection are recorded for each category as the proportion of samples that are clear, cloudy or visibly pink. **(B)** Absorbance at 414 nm and the miR ratio of the cohort (N=86). The dotted line represents the threshold above which samples are considered to be severely haemolysed according to the miR ratio (>7). Samples are colour-coded according to their visual appearance (clear, cloudy or visibly pink).

with pink discolouration had both higher absorbance (0.46 ± 0.11) and miR ratios (8.29 ± 0.51; Figure 4.2B).

No significant differences were observed between the absorbance of low and moderate haemolysed samples as classified by the miR ratio (P = 0.13; Figure 4.3A); however, low and moderately haemolysed samples were significantly different from the severely haemolysed samples (P <0.001 & <0.0001, respectively). In other words, the miR ratio could further quantify haemolysis in the samples that were indistinguishable by absorbance. Severely haemolysed samples (miR ratio >7) had 1.85-fold higher absorbance than low and moderately haemolysed samples combined together (miR ratio <7; P <0.0001;Figure 4.3B), indicating that the absorbance of haemoglobin could have predictive value in discriminating severely haemolysed (miR ratio >7) samples. The ROC curve separated severely haemolysed samples from the rest with an AUC of 0.8038 (P <0.0001; Figure 4.3C). The cut-off absorbance of 0.3 identified 48.4% (15/31) of haemolysed samples, of which 8 were visually undetectable. The accuracy of prediction using this cut-off $\left(\frac{\text{True Positive + True Negative}}{\text{Positive+Negtive}}\right)$ was 0.779.

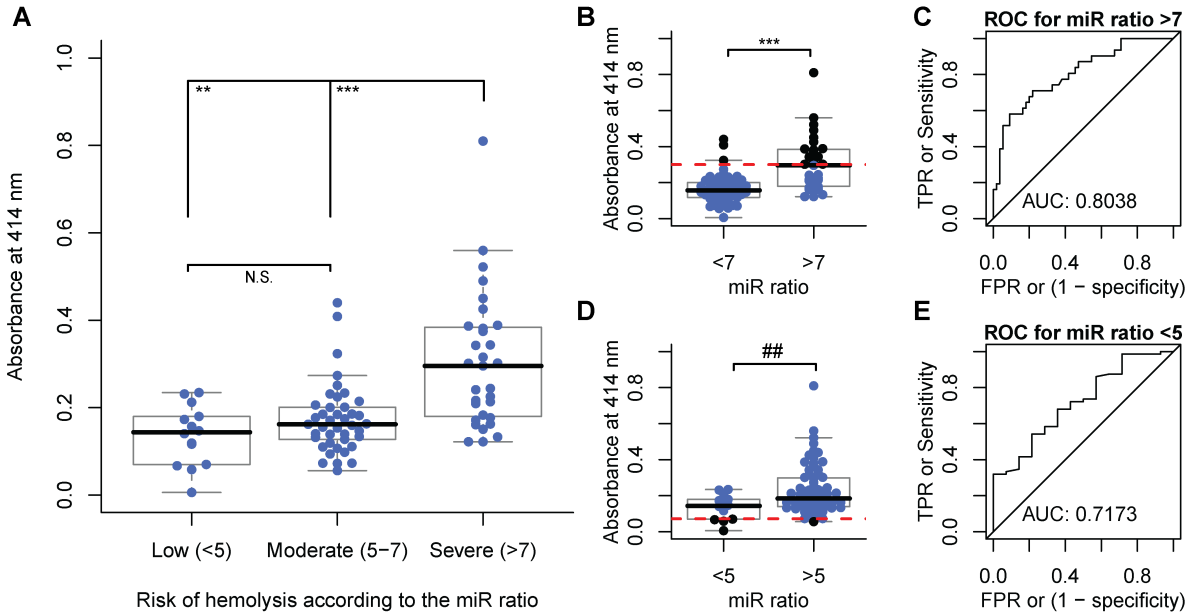

Figure 4.3: Identification of samples with low or severe haemolysis by spectrophotometric absorbance

(A) Cohort (N=86) is grouped by low (miR ratio <5; N=14), moderate (miR ratio 5-7; N=41) and severe (miR ratio >7; N=31) predicted risk of haemolysis, and absorbance at 414 nm was compared between groups. No significant differences in absorbance of samples were observed between the low and moderate groups; however, both were significantly different to the severe haemolysis group. **(B-C)** Absorbance of samples with miR ratio >7 was 1.85-fold higher than those with miR ratio <7. ROC analysis suggested that absorbance could predict severely haemolysed samples (miR ratio >7). The cut-off for absorbance of 0.3 identified by ROC is shown as a dotted red line. **(D-E)** ROC analysis revealed a cut-off for absorbance of 0.072 (depicted as a dotted red line) below which samples would be predicted to have low levels of haemolysis (miR ratio <5). ** $P < 0.001$, *** $P < 0.0001$ and ## Mann-Whitney U test $P < 0.001$. 'TPR' and 'FPR' refer to true and false positive rates, respectively.

We tested whether a similar analysis could identify an absorbance cut-off below which a sample is likely to have low levels of haemolysis (miR ratio <5; Figure 4.3D). Despite similar median values between the two groups (miR ratio <5 and >5), the cut-off absorbance of 0.072 could identify samples with a low risk of haemolysis with AUC of 0.7173 (Figure 4.3E). In general, absorbance-based tests to predict haemolysis suffered from low sensitivity, but offered high specificity and moderate positive and negative predictive values (Table 4.1 and Figure 4.5).

	Low risk (miR ratio <5)		Severe risk (miR ratio >7)	
	All samples (N=86)	Clear samples* (N=77)	All samples (N=86)	Clear samples* (N=77)
Cut-off absorbance	0.072	0.072	0.300	0.300
AUC	0.717	0.733	0.804	0.756
Accuracy	0.849	0.831	0.779	0.779
Sensitivity	0.250	0.250	0.484	0.333
Specificity	0.986	0.984	0.946	0.981
PPV	0.800	0.800	0.833	0.889
NPV	0.852	0.833	0.765	0.765

Table 4.1: Assessment of performance of the spectrophotometric absorbance of haemoglobin at 414 nm for predicting the miR ratio.

Absorbance measurements of samples were split into two groups for each comparison: (I) prediction of low risk of haemolysis (miR ratio <5): <5 versus >5, and (II) prediction of high risk of haemolysis (miR ratio >7): >7 versus <7. ROC analysis was performed for each comparison, and the cut-off absorbance that maximised the accuracy of prediction was selected. Sensitivity, specificity, PPV and negative predictive value (NPV) were calculated based on the chosen cut-off. *refers to samples that did not have a pink discolouration or were cloudy.

4.3.3 Impact of haemolysis on haemolysis-sensitive microRNAs

Since the microRNAs affected by haemolysis originate predominantly from the rupture of RBC, the extent to which a specific microRNA is altered may depend on its abundance in RBC. Using RBC-derived miR-16-5p and miR-15b-3p surrogates for haemolysis-sensitive high and low abundant microRNAs based on C_t values in the cohort as a whole (Figure 4.4), we calculated differences in their levels across the 3 categories defined by the miR ratio, especially for miR-15b-3p as most microRNAs in serum are likely to be present at moderate or low levels. The levels of miR-16-5p and miR-15b-3p increased as the miR ratio increased (Figure 4.4A, B). miR-16-5p and miR-15b-3p were found to be altered by 5.9-fold (P <0.0001) and 4.5-fold (P <0.0001), respectively, in the samples at severe risk of haemolysis (miR ratio >7) compared to those at low risk (miR ratio <5). Both microRNAs were also found to be elevated by approximately two-fold between miR ratio categories <5 compared to 5-7, as well as 5-7 compared to >7. Thus, both high and low abundant microRNAs susceptible to haemolysis are significantly altered amongst 3 categories defined by the miR ratio. miR-23a-3p was present at a similar level in each of the 3 categories as expected (Figure 4.4C).

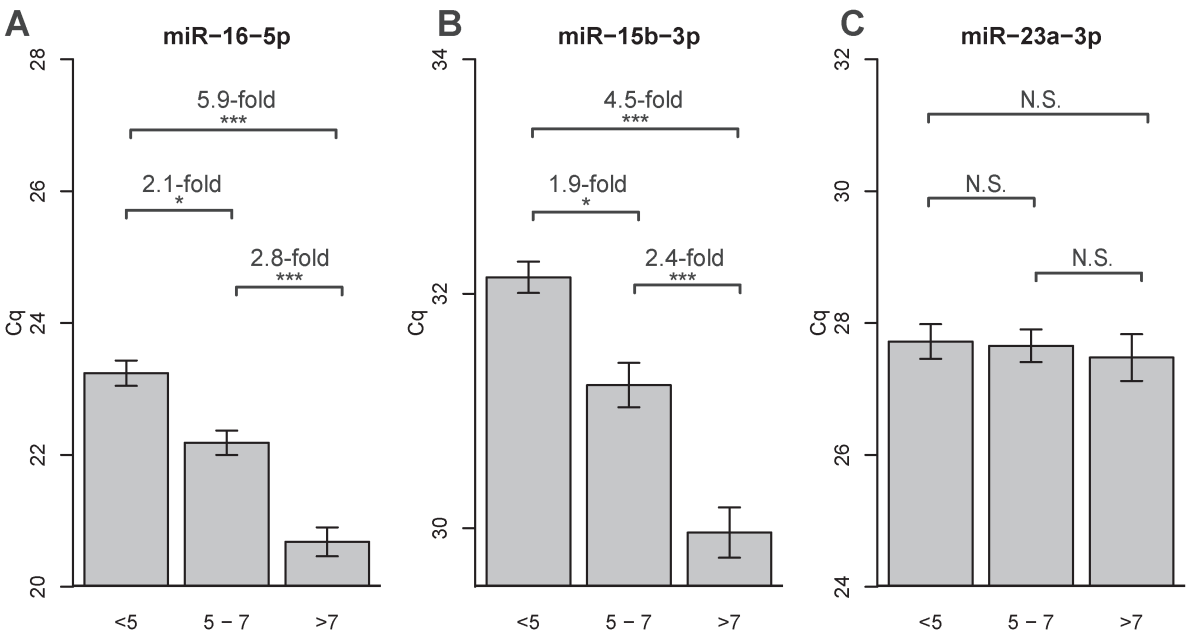

Figure 4.4: Haemolysis-sensitive high and low abundant microRNAs are significantly altered between categories defined by the miR ratio.
(A) Levels of haemolysis-sensitive highly abundant serum microRNA miR-16-5p was found to be significantly altered across low, moderate and severely haemolysed serum samples defined by miR ratios **(B)** Levels of a haemolysis-sensitive low abundant microRNA miR-15b-3p were also different across all miR ratio categories. **(C)** miR-23a-3p was present at a similar level amongst three categories, supporting its use as a reference microRNA in determining the miR ratio. * P <0.05, ** P < 0.001 and *** P < 0.0001.

4.4 Discussion

Serum microRNAs are attractive non-invasive biomarkers because of their disease-specific expression and stability in a wide range of conditions. However, a series of pre-analytical and analytical variables must be considered in the development of robust and reliable microRNA-based tests (Becker and Lockwood 2013; Calin and Croce 2006; Cortez and Calin 2009; Cortez et al. 2011; Lin and Gregory 2015; Lu et al. 2005; McDonald et al. 2011; Schickel et al. 2008; Witwer 2015). The effect of release of the microRNA content of blood cells upon haemolysis dramatically alters the level of specific serum microRNAs. Recent studies have shown that 58% (46/79) of proposed microRNA biomarkers (Pritchard et al. 2012) for solid cancers were highly expressed in one or more blood cell types, and up to 65% of detectable microRNAs in plasma were affected by haemolysis (Kirschner et al. 2013). Haemolysis in clinical samples is common. Reports have suggested that approximately 43% of clinical samples are haemolysed as determined by free haemoglobin >0.5 g/L, whereas

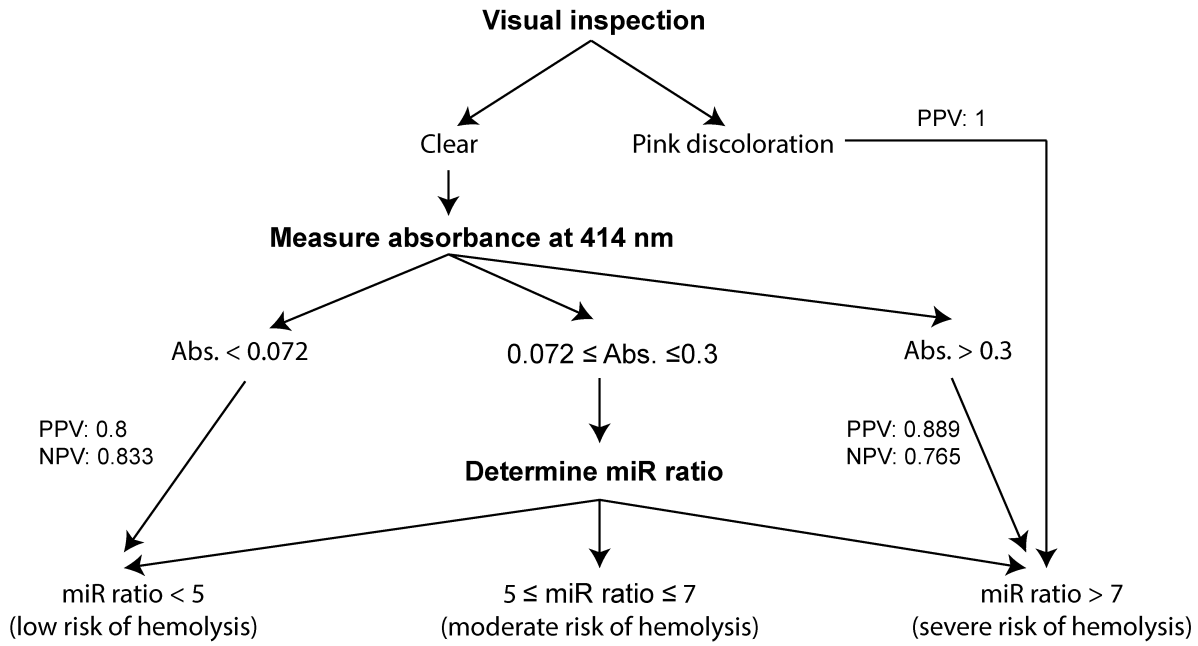

Figure 4.5: Assessment of haemolysis in serum samples.
All serum samples exhibiting pink discolouration were found to be strongly affected by haemolysis for microRNA profiling according to the miR ratio. After exclusion of the visibly haemolysed samples, samples with absorbance at 414 nm of >0.3 are also likely to be have miR ratio >7, predicting severe haemolysis. In contrast, samples with an absorbance at 414 nm of <0.072 are predicted to have a miR ratio <5. Samples meeting these criteria may be excluded from miR ratio for the purpose of determining haemolysis; however, the miR ratio should be determined for samples with absorbance between 0.072 and 0.3. PPV and NPV refer to positive and negative predictive values after removal of visibly haemolysed or cloudy samples, respectively.

visual detection indicated by the presence of a pink discolouration is seen in less than 6% of samples (Hawkins 2010; Lippi et al. 2009). Therefore, quantifying haemolysis is an essential step for any procedure measuring circulatory microRNAs for diagnostic purposes or biomarker discovery. A number of methods to measure haemolysis in serum have been described; however, a direct comparison assessing their sensitivities has not been reported.

In our study of serum, using a 4-fold dilution series, visual inspection could only detect down to 0.25% haemolysis (v/v). This is comparable to the detection limit of 0.125% (v/v) identified by Kirschner et al. 2011 using a 2-fold dilution series of plasma (Kirschner et al. 2013). We and others have shown that visual inspection, i.e. identification of visible pink, as a measure of haemolysis is insufficient as levels of haemolysis-sensitive microRNA such as miR-451a are already compromised prior to visual detection (Blondal et al. 2013; Kirschner et al. 2013).

The ratio of miR-451a to miR-23a-3p was found to be the most sensitive method that could detect down to 0.001% haemolysis in serum. We quantified haemolysis levels of 86 samples using the miR ratio, and discovered that haemolysis-sensitive microRNAs miR-15b-3p and miR-16-5p were significantly affected in the categories of haemolysis (low, moderate and severe) defined by Blondal et al. 2013. In particular, the levels of low abundant, haemolysis-sensitive miR-15b-3p were approximately 4.5-fold higher in the samples with low (miR ratio <5) versus severe (miR ratio >7) risk of haemolysis. The differences were greater for the more abundant miR-16-5p between the same groups (5.9-fold).

While the miR ratio was the most sensitive method to detect low levels of haemolysis, it may not be suitable for all large-scale screening for haemolysis due to additional cost and a relatively large requirement for starting material (200 µl serum). The absorbance of haemoglobin at 414 nm, on the other hand, is a suitable alternative as it overcomes these restrictions and was found to be more sensitive than visual inspection in our dataset. We tested whether absorbance could identify samples that are at a severe risk of haemolysis (miR ratio >7) but remained undetectable by visual inspection. ROC analysis revealed that absorbance at 414 nm >0.3 (water as blank) identified severely haemolysed samples with accuracy, PPV and NPV of approximately 80% (Figure 4.5). Over half (8/15) of the samples were visually undetectable. Similarly, Kirschner et al. 2013 suggested use of absorbance at 414 nm >0.2 (unhaemolysed plasma as blank) to identify haemolysis in plasma as it reduced variability in miR-451 levels (Kirschner et al. 2013). The different choices of blanks and serum versus plasma may have led to the differences observed. Interestingly, some samples in our study had lower absorbance than the unhaemolysed serum used in the dilution series; therefore, water seemed to be an appropriate choice of blank. Similarly, based on our data, samples with absorbance less than 0.072 are likely to be at low risk of haemolysis (miR ratio <5).

Given that a substantial number of circulatory microRNAs are known to be affected by haemolysis, the miR ratio is recommended as the final quality control step unless clearly indicated in the literature that the microRNA of interest is not affected by haemolysis, for example miR-122 (Ding et al. 2012; McDonald et al. 2011; Qiu and Dai 2014). If a promising microRNA is found to be sensitive to haemolysis, clinical interpretation of the test should evaluate the extent to which it is modified by the underlying condition or disease as well as haemolysis. Since haemolysis is common in clinical samples, this comparison will also help identify levels of haemolysis that are acceptable in the samples without significantly affecting the performance of a given test. Failure to meet quality standards would jeopardise

accuracy of measurement in the context of a disease specific relationship of any microRNA known to be affected by haemolysis. Measuring absorbance of haemoglobin at 414 nm can identify samples that are likely to be at either a low or severe risk of haemolysis, reducing the total number of samples that would require testing by miR ratio to determine haemolysis. Despite high specificity, we have shown that the absorbance-based method is inaccurate for predicting haemolysis between absorbance readings at 414 nm of 0.3 and 0.072, and suggest that the miR ratio should be used to test for haemolysis in samples that fall within this range. Further, bilirubin is known to interfere with the absorbance of haemoglobin, rendering this method inaccurate in conditions such as jaundice where serum bilirubin levels are elevated (Noe, Weedn, and Bell 1984).

4.5 Conclusions

The pivotal role of haemolysis as a quality control measure in any serum microRNA profiling cannot be underestimated. The ratio of miR-451a to miR-23a-3p proposed by Blondal et al. 2013 was found to be the most sensitive method to detect low levels of haemolysis, and should be routinely employed. High and low abundant microRNAs sensitive to haemolysis are significantly altered in the three categories of haemolysis (low, moderate and severe) defined by Blondal et al. 2013. Visual inspection to detect haemolysis is insufficient as microRNA in serum samples that do not display a visible pink discolouration can still show effects of haemolysis, as shown by a miR ratio >7. Measuring haemoglobin's absorbance at 414 nm can identify samples that are likely to be at a low or high risk of haemolysis, therefore reducing the total number of samples that should be further analysed for haemolysis using the miR ratio test.

4.6 Additional conclusions

The finding that the 'miR ratio' is the most sensitive method to detect low levels of haemolysis has been integrated as an essential quality control step for all experiments analysing serum microRNAs in this thesis (Chapter 3, subsection 3.3.1.2). The expression of candidate microRNAs identified in Chapter 3 was tested against the 'miR ratio' to determine that candidate microRNAs were not influenced by haemolysis (Chapter 3, subsection 3.3.4).

Chapter 5

Role of lncRNAs in promoting cisplatin resistance

5.1 Introduction

Cisplatin was the first platinum-containing drug approved for treatment of cancers by the FDA in 1978. Although second- and third- generation platinum-containing agents such as carboplatin and oxaliplatin were subsequently developed to reduce toxicities associated with cisplatin (McWhinney, Goldberg, and McLeod 2009; Rabik and Dolan 2007), platinum-containing agents still remain crucial for treatment of some cancers nearly forty years after their first application. Primary cytoreductive surgery followed by platinum and taxane-based chemotherapy remains the standard therapy for patients with OC, with carboplatin-paclitaxel being the most common combination (Coleman, Ramirez, and Gershenson 2017; Matulonis et al. 2016; Raja, Chopra, and Ledermann 2012). OC is initially sensitive to chemotherapy; however, most patients develop resistance within two years of the treatment (Agarwal and Kaye 2003; Hennessy, Coleman, and Markman 2009; Romero and Bast 2012), resulting in recurrent disease that is difficult to treat (Coleman, Ramirez, and Gershenson 2017).

Small noncoding RNAs such as the miR-200 family of microRNAs are known to promote cisplatin resistance in OC (Samuel et al. 2016); however, the roles of long non-coding RNAs (lncRNAs) remain poorly understood. To address this gap, ninety lncRNAs

were profiled by the candidate in two independent cell lines that model the development of cisplatin resistance. Functional studies assessing the role of a lncRNA known as Urothelial Cancer Associated 1 (UCA1) discovered from these profiling experiments is presented in this chapter.

5.2 Materials & methods

5.2.1 lncRNA profiling

LncRNA profiling was conducted using the LncProfiler qPCR Array Kit (System Biosciences). The kit contained reagents for reverse transcription (RT) and SYBR-green primers for 90 lncRNAs.

5.2.1.1 Reverse transcription

RNA was extracted from cells using the miRNeasy Mini kit (subsection 2.3.1.1), and reconstituted at the final concentration of 400 ng/µl. Addition of poly(A) tails to 3' ends of the RNAs was performed in a PCR tube by incubating the following constituents at 37 °C for 30 minutes: 5 µl total RNA (2 µg) + 2 µl 5X polyA buffer + 1 µl 25 mM $MnCl_2$ + 1.5 µl 5 mM ATP + 0.5 µl PolyA polymerase. Next, 0.5 µl oligo-dT adapters were added to the PCR tube and incubated at 60 °C for 5 minutes followed by 2 minutes at room temperature. The RT mixture was prepared as follows: 4 µl 5X RT buffer + 2 µl dNTP mix + 1.5 µl 0.1M DTT + 1.5 µl random primer mix + 1 µl reverse transcriptase, incubated at 42 °C for 60 minutes followed by 95 °C for 10 minutes.

5.2.1.2 Real-time RT-qPCR

Lyophilised primers were purchased in a 96 well-plate format (System Biosciences). The plate was briefly centrifuged and the primers were reconstituted in 132 µl nuclease-free water. RT-qPCR was performed in 384 well-plates in a total of 10 µl reactions. Eight µl of the master mix containing cDNA was transferred to each well followed by addition of 2 µl of the reconstituted primers. Composition of the master mix was as follows: 3.125 ml 2X SensiMix SYBR Hi-ROX master mix (Bioline) + 40 µl cDNA + 1.835 ml nuclease-free water. RT-qPCR was performed on an ABI7900 PCR system using the standard PCR program (Table 2.6).

Gene	Supplier	Catalogue Number
UCA1, siRNA #13	Qiagen	SI05450340
UCA1, siRNA #17	Qiagen	SI05463353
TP53, siRNA #9	Qiagen	SI02655170
AllStars Negative Control	Qiagen	SI03650318
AllStars Negative Control-Alexa Fluor 488	Qiagen	1027292

Table 5.1: List of siRNAs

Three biological replicates were used for each cell line, and 1 RT-qPCR was performed for each lncRNA. GAPDH, Hydroxymethylbilane Synthase (HMBS) and β-actin (ACTB) were tested for their potential use as the reference gene. However, they all performed equally well (data not shown) and GAPDH was chosen as the reference gene. Data was analysed using the $2^{-\Delta\Delta C_t}$ method using the ExpressionSuite software (ThermoFisher).

5.2.2 siRNA transfection

5.2.2.1 siRNA transfection using HiPerFect Reagent

siRNA were transfected using HiPerFect reagent (Qiagen) according to the 'fast-forward' protocol. Cells were seeded in a 6 well plate in 2 ml culture media for 18 - 24 hours prior to the transfection. Cells were approximately 50-80% confluent on the day of transfection. siRNA (usually 100 nmol) were diluted with Opti-MEM media (ThermoFisher) to 100 µl in an eppendorf tube and 12 µl of HiPerFect reagent was added. Reagents were mixed by vortexing, incubated for 10 minutes at room temperature and added to the well in a drop-wise manner. The plate was swirled gently and returned to the incubator. The AllStars Negative Control (Qiagen) was included as a control (Table 5.1).

5.2.2.2 siRNA transfection using electroporation

Cells were harvested from T75 flasks using trypsin as described. 1×10^6 cells underwent electroporation using Nucleofactor (Lonza). Cells were centrifuged and resuspended in 100 µl Opti-MEM media, and 10 µl (100 nmol) siRNA was added. Cells were mixed gently by pipetting, transferred to an electroporation cuvette and electroporated using the Nucleofactor program X-005 for epithelial cells. Following electroporation, cells were immediately transferred to an eppendorf tube containing warm media and plated in 6 well plates. AllStars Negative Control (Qiagen) was included as a control.

Cell line	Cells/well for MTS assay	Cells/well for clonogenic assay
PEO1	4000	1000
PEO4	10,000	1000
OVCAR-3	6000	2000
OVCAR4	5000	500
Kuramochi	10,000	NA

Table 5.2: Seeding densities for MTS and clonogenic assays
MTS and clonogenic assays were performed in 96 and 6 well-plates, respectively.

5.2.3 Clonogenic assays

Cells were seeded at low density in a 6 well plate to allow colonies to grow from single cells as described in subsection 2.2.1. Seeding density and growth period were optimised for each cell line (Table 5.2). For drug treatments, cells were seeded in 1.5 ml media and 0.5 ml media containing 4X drug concentration was added after 18-24 h. Media was replaced at the end of drug treatment (usually 3 days), and cells were grown for 10-21 days with weekly addition of 1 ml of fresh media. Colonies were stained with crystal violet for 5 minutes. Excess stain was removed by washing the plates 2-3 times with water. The plates were dried and colonies were counted. A cluster of at least 50 cells was considered as a colony.

5.2.4 Determining siRNA transfection efficiency using flow cytometry

Cells were seeded and transfected with 100 nmol AllStars Negative Control siRNA labelled with Alexa Fluor 488 (AS-488) (Qiagen) using HiPerFect reagent as described in subsection 5.2.2.1. Unlabelled AllStars Negative Control siRNA (AS-UNL) (Qiagen) was used as a control. Cells were cultured for 24 h after the siRNA transfection and harvested using trypsin. Cells were washed once in PBS and suspended in 300 µl PBS. Flow cytometry was conducted as described in subsection 2.5. Alexa Fluor 488 was excited with a blue (488 nm) laser and its emission was measured using a 530/30 filter.

5.2.5 Site-directed mutagenesis

The wt *TP53* was isolated from HEK293 cells and cloned into the mammalian expression vector pcDNA4/To by Dr. Michael Hahn, a previous postdoctoral fellow in our laboratory. To introduce a desired mutation, PCR was conducted using forward and reverse primers of

TP53 mutation	Direction	Primer sequence (5′ → 3′)
C176Y	Forward	gac gga ggt tgt gag gcg ct**a** ccc cca cca tga gcg ctg ctc ag
C176Y	Reverse	ctg agc agc gct cat ggt ggg gg**t** agc gcc tca caa cct ccg tc
H179R	Forward	ggt tgt gag gcg ctg ccc cca cc**g** tga gcg ctg ctc aga tag cga tgg
H179R	Reverse	cca tcg cta tct gag cag cgc tca **c**gg tgg ggg cag cgc ctc aca acc
I195T	Forward	ctg gcc cct cct cag cat ctt a**c**c cga gtg gaa gga aat ttg cgt g
I195T	Reverse	cac gca aat ttc ctt cca ctc gg**g** taa gat gct gag gag ggg cca g
R175H	Forward	cat gac gga ggt tgt gag gc**a** ctg ccc cca cca tga gcg ctg c
R175H	Reverse	gca gcg ctc atg gtg ggg gca g**t**g cct cac aac ctc cgt cat g
R248Q	Forward	cct gca tgg gcg gca tga acc **a**ga ggc cca tcc tca cca tca tc
R248Q	Reverse	gat gat ggt gag gat ggg cct c**t**g gtt cat gcc gcc cat gca gg
R248W	Forward	cct gca tgg gcg gca tga ac**t** gga ggc cca tcc tca cca tca tc
R248W	Reverse	gat gat ggt gag gat ggg cct cc**a** gtt cat gcc gcc cat gca gg
R273C	Forward	gac gga aca gct ttg agg tg**t** gtg ttt gtg cct gtc ctg gga g
R273C	Reverse	ctc cca gga cag gca caa ac**a** cac acc tca aag ctg ttc cgt c
R273H	Forward	gac gga aca gct ttg agg tgc **a**tg ttt gtg cct gtc ctg gga g
R273H	Reverse	ctc cca gga cag gca caa aca **t**gc acc tca aag ctg ttc cgt c
V157F	Forward	cac ccc cgc ccg gca ccc gc**t** tcc gcg cca tgg cca tct aca agc
V157F	Reverse	gct tgt aga tgg cca tgg cgc gga **a**gc ggg tgc cgg gcg ggg gtg
Y220C	Forward	cga cat agt gtg gtg gtg ccc t**g**t gag ccg cct gag gtt ggc tct g
Y220C	Reverse	cag agc caa cct cag gcg gct ca**c** agg gca cca cca cac tat gtc g

Table 5.3: Primer sequences to introduce mutations into *TP53* using site-directed mutagenesis
This work was equally shared with Mr. Alexander Cole, a PhD student in the laboratory. The introduced mutation is shown in slightly larger fonts in bold face.

30-44 nucleotides in length harbouring the desired mutation roughly in the middle (Table 5.3). High fidelity DNA polymerase Pfu Ultra II (Agilent) was used for amplification. Final composition of the 50 µl PCR reaction was as follows: 5 µl of 10X reaction buffer + 6 µl of 2.5 mM dNTPs + 1 µl (100 ng) DNA template + 5 µl of 2 µM forward primer + 5 µl of 2 µM reverse primer + 2.5 µl of 100 % molecular grade DMSO + 24.5 µl nuclease-free water + 1 µl Pfu Ultra II polymerase. PCR cycling conditions: 95 °C for 30 seconds and 16 cycles of 95 °C for 30 seconds + annealing temperature of 62-65 °C for 1 minute + extension at 68 °C for 7 minutes, roughly 1 minute/kb of the insert length. Amplification of the product was confirmed using electrophoresis on a 1% agarose gel.

Since the template DNA was isolated from *E.coli* strain JM109, it was methylated by the bacteria to mark it as 'self' compared to a foreign piece of DNA such as bacteriophage during infection. The template DNA was digested using the methylation-specific restriction enzyme Dpn I (New England BioLabs) by incubating 40 µl PCR product with 1 µl Dpn I at 37 °C for 1 hour. DNA was purified using the ethanol precipitation method described

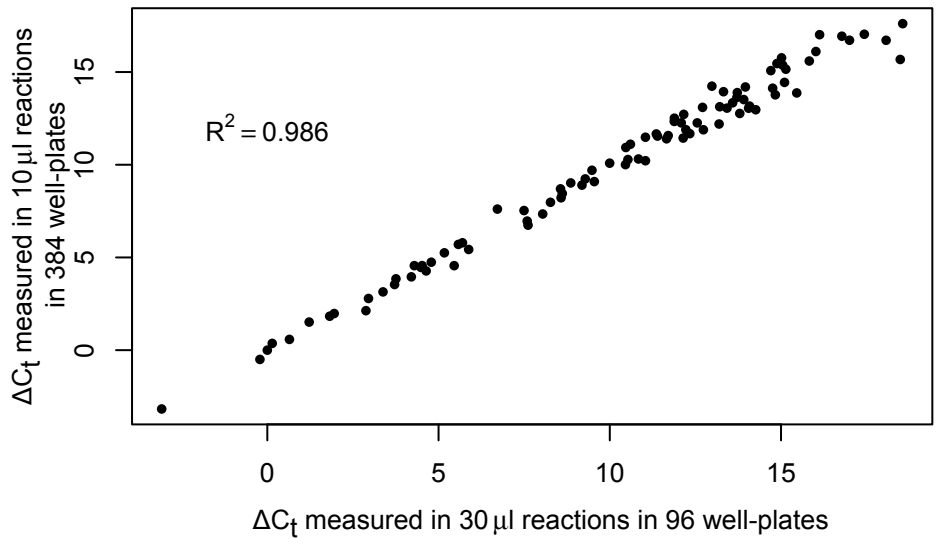

Figure 5.1: Strong correlation between lncRNA profiling performed in 96 and 384 well plates

in subsection 2.3.3.2. Competent JM109 bacteria were transformed using electroporation, selected based on resistance to Ampicillin and propagated as described in section 2.4. Finally, mutation status was confirmed using Sanger sequencing commercially performed at the Australian Genome Research Facility (AGRF), Westmead, NSW, Australia.

5.3 Results

5.3.1 lncRNA profiling

5.3.1.1 Optimisation

The LncProfiler qPCR Array Kit (System Biosciences) was used to evaluate expression of 90 lncRNAs from 4 cell lines. The 90 lncRNAs measured by the kit were selected by the supplier based on their association with cancer (see lncRNAdb,Amaral et al. 2010). The manufacturer advised to conduct RT-qPCR in a 30 µl volume in a 96 well plate format, which would limit the number of biological replicates for profiling due to the large amount of SYBR green required. I first tested whether the profiling performed equally in a 10 µl volume in a 384 well plate using cDNA from A2780 cells (Figure 5.1). The manufacturer suggested to reconstitute the lncRNA primers in 44 µl of nuclease-free water, transferring

(A)

Well	Cell line	Replicate	RIN
1	A2780	1	10
2	A2780	2	9.8
3	A2780	3	10
4	A2780cisR	1	10
5	A2780cisR	2	10
6	A2780cisR	3	10
7	PEO1	1	9.8
8	PEO1	2	9.9
9	PEO1	3	9.8
10	PEO4	1	9.8
11	PEO4	2	9.7
12	PEO4	3	9.9

(B)

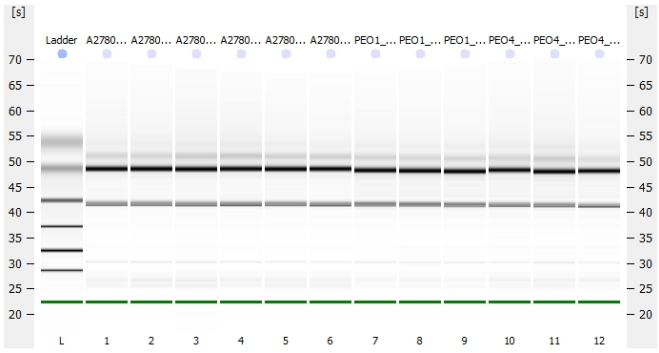

Figure 5.2: Assessment of RNA integrity of the samples used for lncRNA profiling
(A) RNA quality of each sample. Three biological replicates were profiles for each cell line. **(B)** Virtual RNA gel exported from the Bioanalyzer 2100 (Agilent). RIN: RNA Integrity Number.

2 µl of primers to the 28 µl master mix comprising cDNA and RT-qPCR master mix comprising SYBR-green dye. Scaling this ratio down to a 10 µl total reaction volume corresponded with pipetting 0.67 µl primers/well, which would be too low for accurate pipetting. To overcome this limitation, primers were reconstituted in 132 µl (scaled up 3 times) water instead, and 2 µl (3×0.67 µl) and 6 µl (3×2 µl) were used in a total volume of 10 µl and 30 µl RT-qPCR reactions. The final concentration of primers in both reactions was 600 nM. A strong correlation ($R^2 = 0.986$) was seen in ΔC_t generated from 30 µl or 10 µl volume, suggesting that both protocols were comparable in performance (Figure 5.1).

5.3.1.2 lncRNA profiling of 2 pairs of cisplatin sensitive/resistant cell lines

A2780/A2780cisR and PEO1/PEO4 cell lines were used for identifying lncRNAs that could be promoting drug resistance. The A2780 and PEO1 cells were derived from untreated patients with HGSOC. A2780cisR was developed from A2780 by gradual exposure to cisplatin *in vitro* (Bohrens et al. 1987) whereas the PEO4 cell line was established from the same patient as PEO1 after she naturally acquired resistance to cisplatin (Langdon et al. 1988). RNA was extracted using the miRNeasy kit and integrity was checked using a Bioanalyzer 2100 (Agilent) as described in subsections 2.3.1.1 and 2.3.1.4, respectively. All RNA had a RNA Integrity Number (RIN) >9.5, indicating an excellent quality of RNA (Figure 5.2). Ninety lncRNAs were profiled from a total of twelve samples (three

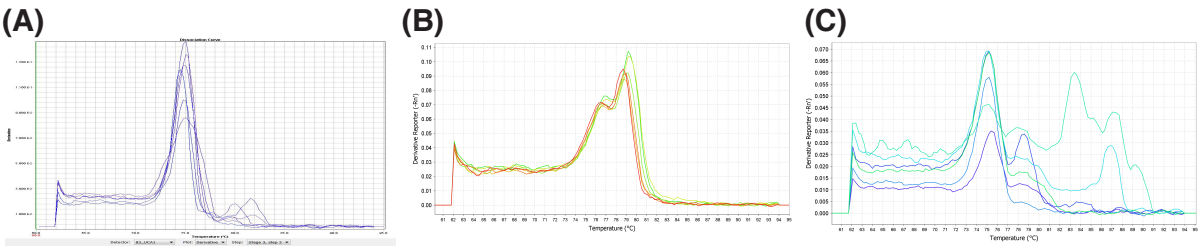

Figure 5.3: Representative melt curves used for grading the quality of lncRNA primers
(A) Excellent melt curve with only one peak;UCA1 amplified from in A2780/A2780cisR cells, **(B)** Acceptable melt curve with one major peak and additional 1-2 small peaks; Gas5 amplified from A2780/A2780cisR cells, and **(C)** Poor melt curve with multiple peaks of significant heights; HOTAIR amplified from A2780/A2780cisR cells

biological replicates/cell line), and one RT-qPCR was performed for each lncRNA/sample. The reference gene GAPDH was amplified in three technical replicates/sample for accurate quantification. In addition, a no template control (NTC) was included using GAPDH primers to monitor contaminants in the reagents.

GAPDH was amplified at a C_t of 34.04 ± 0.42 in the NTC compared to the C_t of 20.25 ± 0.11 for the actual samples, indicating lack of contamination in water and the PCR master mix. The data was normalised to the sensitive cell line of each cisplatin resistant counterpart using the $2^{-\Delta\Delta C_t}$ method. The following selection criteria were used to identify candidate lncRNAs for further analysis.

1. Each primer pair must display only one peak in the melt curve.
   The melt curve of each primer pair was graded as excellent (only one peak), acceptable (one major peak with 1-2 additional smaller peaks) or poor (multiple peaks of significant heights). A representative melting curve for each grade is shown in Figure 5.3. In addition, the proportion of each grade of melting curves in the cell lines are shown in Table 5.4. Roughly, 40% of the lncRNA primers exhibited excellent melt curves; the rest displayed acceptable or poor quality of the melt curves, which could be due to generally low abundance of lncRNAs compared to mRNAs (Derrien et al. 2012).

	A2780	A2780cisR	PEO1	PEO4
Excellent	41 (42.7%)	41 (42.7%)	37 (38.5%)	37 (38.5%)
Acceptable	28 (29.2%)	30 (31.3%)	36 (37.5%)	37 (38.5%)
Poor	27 (28.1%)	25 (26.0%)	23 (24.0%)	22 (22.9%)
Total primer pairs	96	96	96	96

Table 5.4: Quality of primer pairs based on their melt curves

2. A lncRNA must amplify at C_t < 35 as RT-qPCR tends to be unreliable at late cycles.
3. A lncRNA must be altered by at least 1.5-fold in at least one out of two resistant cell lines.
4. A lncRNA must be significantly different ($P < 0.05$) in at least one out of two drug resistant cell lines.
5. A lncRNA must show the same trend of differential expression in both drug resistant cell lines.

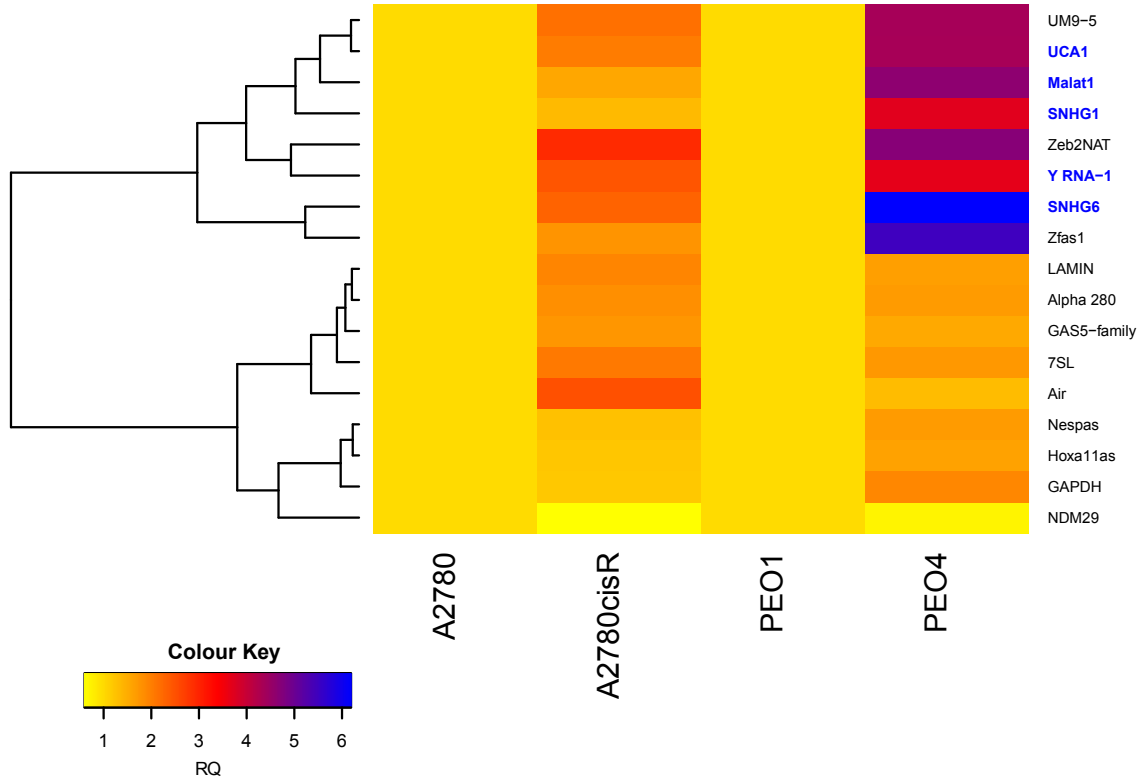

Figure 5.4: Overview of lncRNA expression in two pairs of cisplatin resistant/sensitive cell lines.

LncRNAs meeting criteria 1 (excellent melt curve) and 2 (C_t < 35) are shown as a heatmap diagram to provide an overview of lncRNA expression in two pairs of cisplatin resistant/sensitive cell lines. LncRNAs highlighted in blue met all five criteria (Table 5.5). RQ: relative quantification.

Five lncRNAs shown in Table 5.5 and Figure 5.4 satisfied the above selection criteria. LncRNA HOTAIR* was excluded from further analyses at it presented with a poor melt curve (Figure 5.3C). Urothelial Cancer Associated 1 (UCA1) was selected for further biological validation based on its emerging role in promoting cisplatin resistance in bladder cancer, as described in the next subsection.

	A2780cisR normalised to A2780				PEO4 normalised to PEO1			
	Melt curve	RQ	*P*	Mean C_t	Melt Curve	RQ	*P*	Mean C_t
SNHG1	Excellent	1.35	0.59	30.14	Acceptable	3.71	0.02	30.60
SNHG6	Excellent	2.32	0.10	27.66	Excellent	6.19	0.04	27.53
Malat1	Excellent	1.58	0.41	28.61	Excellent	4.62	0.03	27.32
Y RNA-1	Excellent	2.47	0.04	20.20	Excellent	3.68	0.07	21.62
UCA1	Excellent	2.04	0.03	32.64	Acceptable	4.35	0.14	30.01

Table 5.5: Candidate lncRNAs that were differentially expressed between drug resistant and non-drug resistant cell line pairs.

Excellent melt curve: only one peak; acceptable: one major peak with 1-2 additional smaller peaks. RQ: relative quantification

5.3.1.3 LncRNAs identified by profiling resistant/sensitive pairs of cell lines

This project started in 2013 and many things that are known now were unknown at that time. However, the following information reflects the current knowledge on the candidate lncRNAs.

5.3.1.3.1 SNHG1 & SNHG6

Role in cancer: Both snoRNAs and snoRNA host genes (SNHGs) have been implicated in cancer biology (reviewed in Stepanov et al. 2015; Williams and Farzaneh 2012). SNHG1 was found to be upregulated in non-small cell lung cancer (NSCLC) cell lines and its knockdown reduced the ability of the cells to form colonies in clonogenic assays (You et al. 2014). Similarly, SNHG1 was also found to be upregulated in HCC, and its overexpression enhanced proliferation, invasion and migration of HCC cells through suppressing levels of miR-195 (Zhang et al. 2016a; Zhang et al. 2016b). Higher expression of SNHG1 in neuroblastoma was found to be associated with poor patient survival as well as an independent prognostic marker for progression-free

*The names of the lncRNA are not italicised when referring to as the expressed RNA form, whereas they are italicised when referring to the gene on the DNA, as in mutations in *HOTAIR*.

survival (Sahu et al. 2016). SNHG6 was also found to be upregulated in HCC (Chang et al. 2016).

Role in promoting cisplatin resistance: Unknown.

Mechanism: snoRNAs and SNHGs encode noncoding transcripts that predominantly associate with the nucleolus where they play a vital role in maturation of rRNA. By directly base-pairing with the rRNA, snoRNAs guide the enzymes that catalyse 2'-*O*-ribose methylation or pseudouridylation to their target sites on the rRNA (Williams and Farzaneh 2012).

5.3.1.3.2 Malat1

Role in cancer: The role of Malat1 in cancer is relatively well-studied (reviewed in Gutschner, Hämmerle, and Diederichs 2013 and Dhamija and Diederichs 2016). Briefly, the expression of Malat1 was found to be associated with late stages and metastasis in NSCLC (Ji et al. 2003), enhanced cell migration and tumour growth in mouse models (Schmidt et al. 2011). Malat1 is highly expressed in pancreatic cancer and its expression was found to correlate with clinical stage, tumour size, lymph node and distant metastases (Jiao et al. 2014; Pang et al. 2015). In pancreatic cancer cells, knockdown of Malat1 inhibited cell proliferation and invasion through downregulation of EMT and induction of G2/M cell cycle arrest (Jiao et al. 2014). Malat1 also induced EMT in NSCLC, enhancing metastasis to the brain (Shen et al. 2015). Malat1 has been reported to increase cell proliferation in clear cell renal carcinoma (Zhang et al. 2015), multiple myeloma (Cho et al. 2014) and osteosarcoma (Dong et al. 2015). Malat1 expression is correlated with poor outcome in multiple cancers from a meta-analysis (Wei and Niu 2015).

Role in promoting cisplatin resistance: A study reported that cisplatin suppressed Malat1 expression in laryngeal squamous cell carcinoma (Chen et al. 2014). HIF-2α has been found to stimulate Malat1 expression under hypoxic conditions. As described in Chapter 1, subsection 1.2.2.2, many lncRNAs can act as competing endogenous RNAs (ceRNAs) and absorb levels of microRNAs. Working as a ceRNA, Malat1 absorbs the levels of miR-216b, a negative regulator of autophagy in HCC, promoting multidrug resistance by upregulating autophagy that resulted from the downregulation of miR-216b (Mimeault and Batra 2013). Malat1 was found to be overexpressed in cisplatin resistant tumours as well as cancer stem cells of NSCLC (Lopez-Ayllon et al. 2015).

Interactions between Bcl-2 and Malat1 in NSCLC have also been proposed, implicating its potential role in regulating apoptosis (Schmidt et al. 2014).

Mechanism: Malat1 binds to the serine/arginine (SR) splicing factors, affecting their distribution in the nuclear speckle domains and regulating splicing of a subset of mRNAs (Tripathi et al. 2010). In addition, Malat1 has been found to interact with Polycomb proteins and control gene expression of cell cycle genes (Yang et al. 2011).

5.3.1.3.3 Y RNA-1

Y RNAs are technically considered as small ncRNAs given their length of 83-112 nucleotides (Christov, Trivier, and Krude 2008).

Role in cancer: Y RNA-1 to 5 have been found to be over-expressed in solid cancers, of which Y RNA-1 and 3 were the most upregulated Y RNAs in bladder, cervix, colon, kidney, lung and prostate cancers (Christov, Trivier, and Krude 2008). siRNA knockdown of Y RNA-1 reduced the proportion of replicating cells (Christov et al. 2006).

Role in promoting cisplatin resistance: Unknown.

Mechanism: Y RNAs are required for initiation of the chromosomal DNA replication by interacting with components of the pre-replicative complex (Hall, Turnbull, and Dalmay 2013; Zhang et al. 2011a). Y RNAs have been found to be associated with autoantigen protein Ro60, influencing its subcellular localisation (Sim and Wolin 2011). Y RNAs have been proposed as potential sources of microRNAs such as miR-1975 from Y RNA-5 and miR-1979 from Y RNA-3 (Hall, Turnbull, and Dalmay 2013; Verhagen and Pruijn 2011).

5.3.1.3.4 UCA1

Role in cancer: A study in 2006 reported upregulation of UCA1 in bladder cancer compared to the adjacent normal tissue. In addition, levels of UCA1 in urine were found to be predictive of bladder transitional cell carcinoma (Wang et al. 2006). Subsequently, UCA1 was found to be associated with multiple cancers including breast cancer, colorectal cancer, lung squamous cell carcinoma, oesophageal sqamous cell carcinoma, gastric cancer, HCC and ovarian cancer (Xue, Chen, and Li 2016). A pan-cancer analysis, incorporating RNA-seq data on 2,878 tumour samples of 8 cancer types as well as 349 matched normal tissues, confirmed overexpression of UCA1

in colorectal cancer and lung squamous cell carcinoma (Cabanski et al. 2015). Notably, ovarian cancer was excluded from this analysis due to missing RNA-seq data on normal ovaries. UCA1 was also one of the 5 differentially expressed lncRNAs between SKOV-3 and its derivative cell line with enhanced metastatic capabilities (SKOV-3.ip1) (Liu et al. 2013a).

Role in promoting cisplatin resistance: Multiple studies have confirmed that overexpression of UCA1 promotes cisplatin resistance in bladder cancer (Fan et al. 2014; Pan et al. 2016; Wang et al. 2008). A report in 2015 showed that UCA1 was upregulated in ovarian cancer compared to normal ovaries, and its forced overexpression promoted migration, invasion and cisplatin resistance of SKOV-3 cells through interactions with SR Protein Kinase 1 (SRPK1) (Wang et al. 2015). Knockdown of UCA1 restored cisplatin sensitivities of 2 cell lines of tongue squamous cell carcinoma (Wang et al. 2016a).

Mechanism: UCA1 promoted cell proliferation by inducing cAMP response-element binding protein (CEBP) and phosphoinositide-3-kinase (PI3K)/Akt pathways (Yang et al. 2012). Further, activated transcription factor CEBP induced expression of miR-196a-5p in bladder cancer cells, which then suppressed the expression of the cell cycle inhibitor $p27^{kip1}$ through microRNA-miRISC axis (Pan et al. 2016). Overexpression of UCA1 was found to downregulate regulators of apoptosis Fas and ataxia telangiectasia mutated (ATM) (Wang et al. 2012).

5.3.1.4 Selection of UCA1 for further investigations

All 5 candidate lncRNAs have been implicated in cancer biology. Further, Malat1 and UCA1 were found to have roles in promoting cisplatin resistance. Malat1 has been studied extensively as it is normally present at a high level compared to other lncRNAs whereas UCA1 remains understudied. While Malat1 could be knocked down using siRNA or similar technologies for functional studies, its long size of ~8 kb could pose difficulties in conducting rescue experiments involving transfection of cloned expression vector or virus-mediated transduction. In contrast, all 3 isoforms of UCA1 (1.4, 2.2 and 2.7 kb) (Xue, Chen, and Li 2016) are much shorter than Malat1 . As described above, UCA1 has been shown to work through the PI3K/Akt pathway — a pathway that has been extensively studied in our laboratory previously with antibodies and TaqMan probes for its key members available for further downstream investigation. Therefore, UCA1 was selected for further studies. The

1.4 kb isoform of UCA1 is most abundant, and has been the focus of most studies (Xue, Chen, and Li 2016) including the current one.

5.3.2 Investigating the role of UCA1 in promoting cisplatin resistance in PEO1 and PEO4 cells

To provide an overview of the experimental approach, the expression of UCA1 in A2780, A2780cisR, PEO1 and PEO4 quantified from the lncRNA profiling was validated using sensitive TaqMan probes. Next, the transfection efficiencies of the cells were tested using labelled-siRNAs in flow cytometry. Finally, the effect of UCA1 knockdown on cisplatin sensitivities was determined using MTS and clonogenic assays.

5.3.2.1 Validation of UCA1 expression using TaqMan probes

One µg RNA was reverse transcribed using SuperScript III enzyme, and the expression of UCA1 quantified in 4 cell lines using TaqMan probes (N = 6/cell line; Figure 5.5). GAPDH was used as the reference gene. In contrast to the SYBR green primers used for lncRNA profiling, no significant differences were observed in UCA1 levels between A2780 and A2780cisR cells (P = 0.07). However, UCA1 was found to be elevated by approximately 3-fold in PEO4 compared to PEO1 cells (P = 0.0005). It remains unclear why conflicting results were obtained using the SYBR-green primers and the TaqMan probes. All three biological replicates used in the lncRNA profiling were used when quantifying expression of UCA1 using the TaqMan probes and passaged less than ten times since revival from the liquid nitrogen stocks. The manufacturer of the LncProfiler qPCR Array Kit (System Biosciences) did not disclose the sequence of UCA1 SYBR-green primers, making it difficult to compare the regions of UCA1 amplified with the SYBR-green primers and the TaqMan probes. Nevertheless, results obtained using the TaqMan probes should be more reliable because TaqMan-based RT-qPCR is much more sensitive than SYBR green-based assays. Given that UCA1 levels did not differ in the A2780/A2780cisR paired cell lines, they were excluded from further validation.

5.3.2.2 Testing siRNA transfection efficiency in PEO4 and PEO1 cells using flow cytometry

The siRNA transfection efficiency of PEO4 cells was tested by transfecting 100 nmol AllStars Negative Control siRNA labelled with Alexa Fluor 488 (AS-488) using the HiPerFect

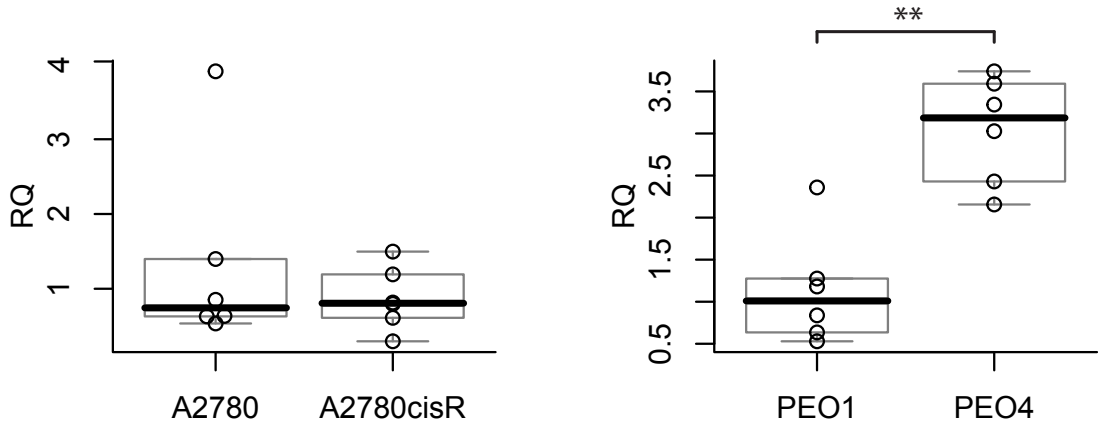

Figure 5.5: TaqMan Validation of UCA1 in 4 ovarian cancer cell lines
** $P < 0.005$.

reagent. Unlabelled AllStars Negative Control siRNA (AS-UNL) was transfected as a control. Cells were prepared for flow cytometry as described in subsection 5.2.4. When compared to the AS-UNL cells, approximately 80% of the single cells (gate P1 in Figure 5.6 B and E) transfected with AS-488 were positive for Alexa Fluor 488 at 24 h post-transfection (N = 3; Figure 5.6 A and D; gate Q4 in Figure 5.6 C and F), suggesting a high transfection efficiency of PEO4 cells. Similarly, PEO1 cells also exhibited a high transfection efficiency using HiPerFect reagent (N = 1; Figure 5.7 A and B).

5.3.2.3 Optimising UCA1 knockdown in PEO4 and PEO1 cells

Although the flow cytometry experiment above used 100 nmol siRNA, the levels of siRNA used to knockdown an actual gene should be kept to a minimum in order to avoid possible off-target effects. Two independent siRNAs (#13 and #17) targeting different regions of the 3' UTR of UCA1 were used to knockdown UCA1. Fifty nmol of siRNAs #13 and #17 each was transfected into PEO4 cells using 12 µl HiPerFect reagent (as for flow cytometry experiments described above), but UCA1 levels, quantified by TaqMan probes using RT-qPCR, were not significantly reduced at 16 and 88 h post-transfection (N = 3; Figure 5.8 A). These time points mimic start and end points of a typical experiment involving cisplatin treatments for 3 days. To reduce UCA1 levels further, the siRNA concentration was increased to 100 nmol as well as transfected with two different volumes (12 or 18 µl) of the HiPerFect reagent (N = 3), and UCA1 levels were measured at 24 h post-transfection. As shown in Figure 5.8B, increasing the siRNA concentration indeed further reduced the UCA1 levels compared to the 50 nmol siRNA regardless of the amount of HiPerFect used for transfection; however, the final knockdown levels of ~40% in PEO4 cells were still found

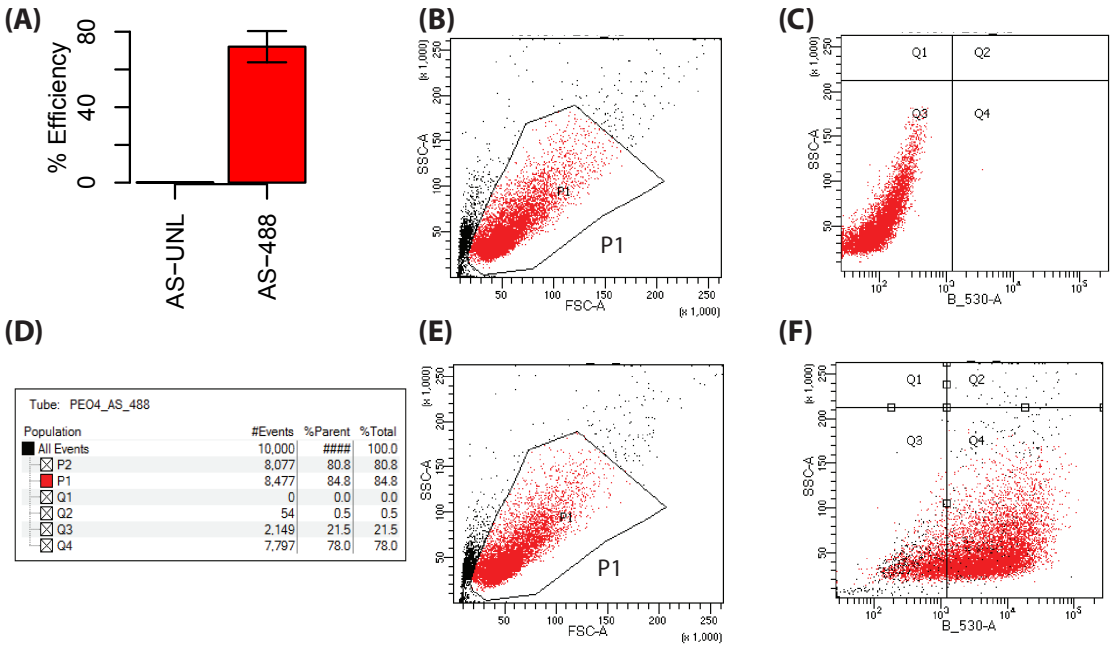

Figure 5.6: Determining siRNA transfection efficiency using HiPerFect reagent in PEO4 cells measured by flow cytometry

(A) Transfection efficiency of PEO4 cells using HiPerFect measured by flow cytometry (N=3), (B-C) PEO4 transfected with AS-UNL, (D) Typical transfection efficiencies achieved in PEO4 cells using HiPerFect reagent measured by flow cytometry, and (E-F) PEO4 transfected with AS-488. FCS-A and SSC-A represent areas of the forward and side scatter, respectively. B_530-A represents area for the fluorescence of Alexa Fluor 488. AS-UNL: unlabelled AllStars Negative Control siRNA, AS-488: AllStars Negative Control siRNA labelled with Alexa Fluor 488.

to be unsuitable for functional validation. UCA1 levels were found to be even less affected upon siRNA treatment in PEO1 cells (100 nmol siRNA + 12 µl HiPerFect; N = 3; Figure 5.9), suggesting that other methods to knockdown UCA1 should be investigated.

In contrast to HiPerFect reagent that utilises lipid-based chemistry to deliver siRNA-infused complexes to the cell, electroporation relies on momentary generation of holes in the cell's lipid bilayer upon electric shock, during which siRNAs enter the cell because of its high extra-cellular concentration. Nucleofactor Kit T (Lonza) for electroporation was tested for it suitability to knockdown UCA1 in PEO4 cells. In addition, serum-free Opti-MEM media was also tested for the purpose of cost-efficiency. Kit T resulted in 86% and 83% knockdown at 24 and 48 h post-electroporation using 100 nmol siRNA, respectively (N=1; data not shown). A similar knockdown efficiency of 87% at 24 h post-electroporation was achieved just by using Opti-MEM media (N=1; data not shown); therefore, Opti-MEM media was used in electroporation for the rest of the study. Electroporation resulted

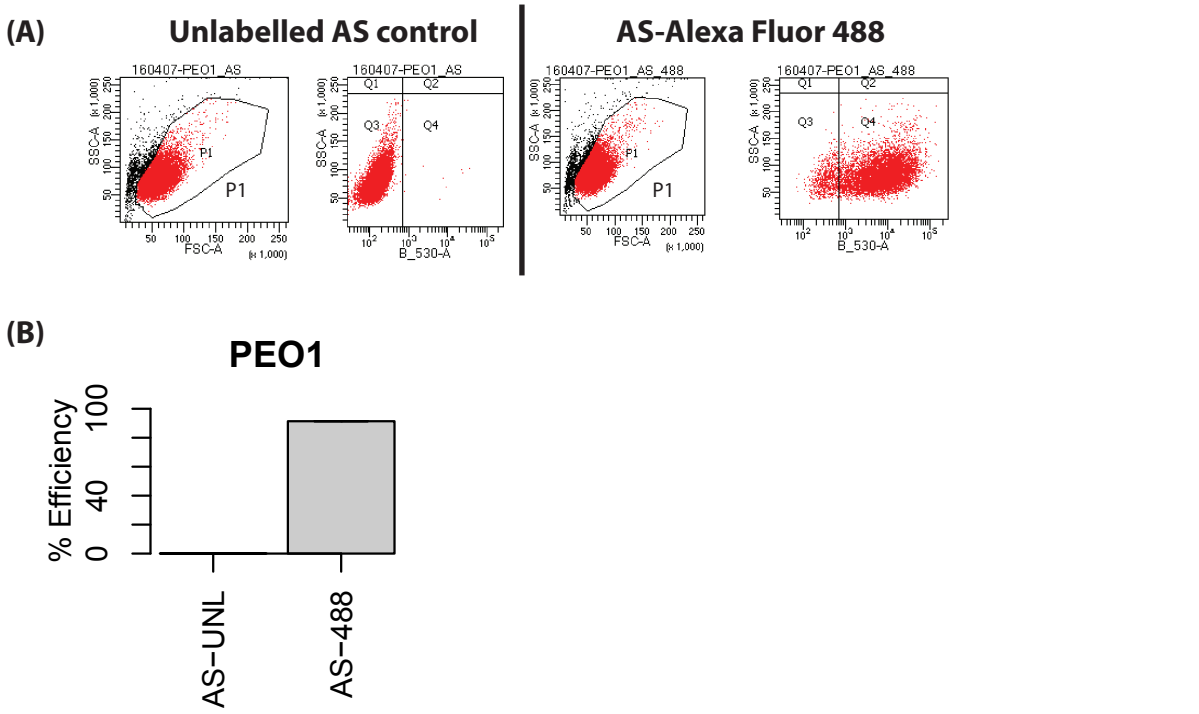

Figure 5.7: Determining siRNA transfection efficiency using HiPerFect reagent in PEO1 cells measured by flow cytometry

(A) PEO1 cells transfected with AS-UNL or AS-488 using HiPerFect reagent, and transfection efficiency was measured using flow cytometry (N=1). **(B)** Quantification of the transfection efficiency (N=1). FCS-A and SSC-A represent areas of the forward and side scatter, respectively. B_530-A represents area for the fluorescence of Alexa Fluor 488. AS-UNL: unlabelled AllStars Negative Control siRNA, AS-488: AllStars Negative Control siRNA labelled with Alexa Fluor 488.

in slightly higher cell death compared to the HiPerFect reagent, which was compensated by increasing seeding densities in experiments. The knockdown efficiencies of UCA1 by electroporation in PEO1 and PEO4 cells are depicted in Figure 5.10A (N = 3).

5.3.2.4 The effect of UCA1 knockdown on cisplatin sensitivity of PEO4 and PEO1 cells

Cisplatin sensitivity of PEO1 and PEO4 cells following UCA1 knockdown was determined by MTS and clonogenic assays. One million cells were electroporated with 100 nmol AllStars (AS) Negative Control and UCA1 siRNAs #13 and #17 using Opti-MEM media (Figure 5.10 A), seeded overnight for MTS or clonogenic assays at the densities outlined in Table 5.2, subsections 2.2.5 and 5.2.3. Cells were treated with cisplatin for 3 days (N = 3). No difference in cisplatin DRCs were observed using the MTS assay upon UCA1 knockdown

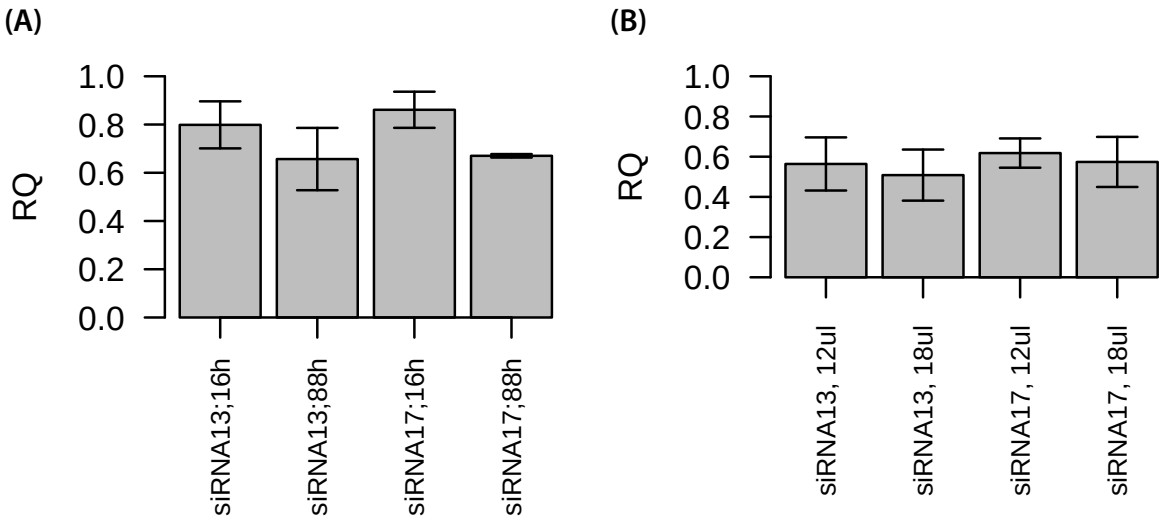

Figure 5.8: Knockdown of UCA1 in PEO4 cells using the HiPerFect reagent
(A) Fifty nmol of siRNAs #13 or #17 were transfected using 12 µl of HiPerFect reagent, and UCA1 expression was measured at 16 and 88 h post-transfection using TaqMan RT-qPCR (N=3). **(B)** To achieve a higher knockdown, 100 nmol siRNAs were transfected using 12 or 18 µl HiPerFect reagent, and UCA1 levels were measured at 24 h post-transfection using TaqMan RT-qPCR (N=3). In both cases, UCA1 knockdown achieved using the HiPerFect reagent were unsuitable for functional assays. RQ: relative quantification.

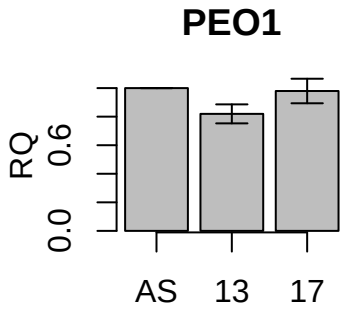

Figure 5.9: siRNA transfection efficiency using HiPerFect reagent in PEO1 cells
One hundred nmol siRNAs were transfected using 12 µl HiPerFect reagent and UCA1 knockdown was measured at 24 h post-transfection using by TaqMan RT-qPCR (N=3). RQ: relative quantification.

in both cells (Figure 5.10B and D). Further, the calculated IC_{50} also remained unchanged (Figure 5.10C and E; N = 3; $P > 0.05$).

Long-term effects of UCA1 knockdown on cell survival were measured by clonogenic assays (Figure 5.11). This assay was initially seeded in N = 3 for both cell lines according to the densities in Table 5.2, but some wells in one biological replicate for PEO1 cells were

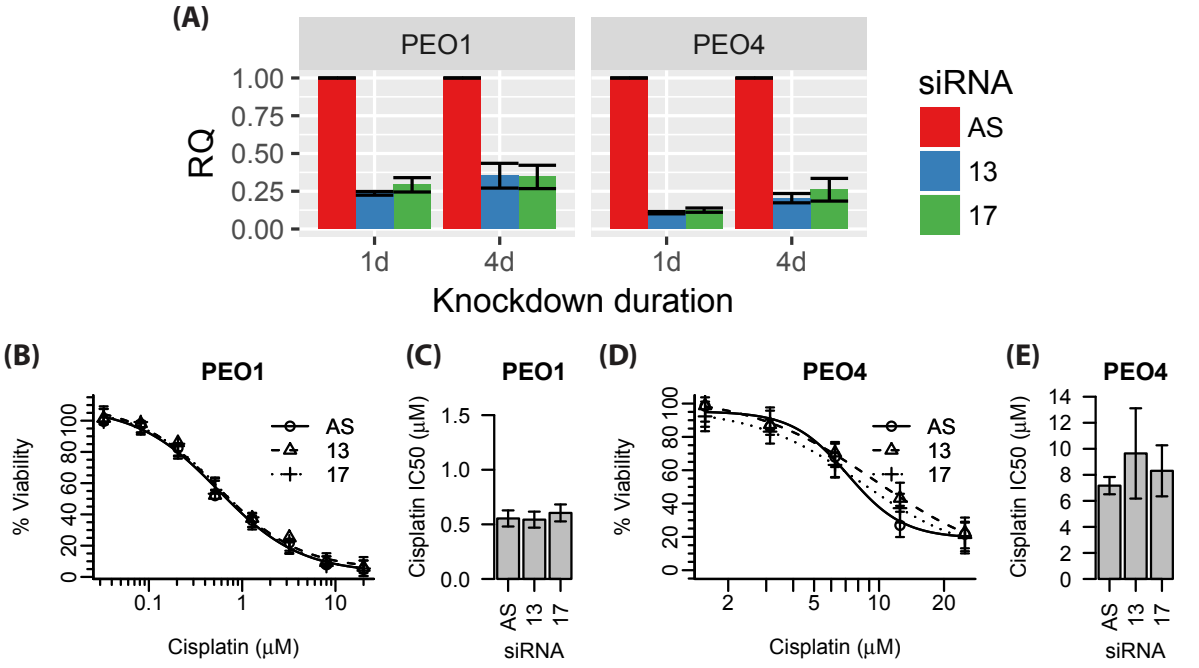

Figure 5.10: Cisplatin sensitivities of PEO1 and PEO4 cells upon UCA1 knockdown measured by MTS assay

(A) The efficiencies of UCA1 knockdown using electroporation (N=3). (**B-C**) Cisplatin dose response curves (DRCs) and IC_{50} in PEO1 cells upon UCA1 knockdown, respectively. **(D-E)** Cisplatin DRCs and IC_{50} in PEO4 cells upon UCA1 knockdown, respectively. 'AS': AllStars Negative Control, RQ: relative quantification.

dried, resulting in inaccurate quantification and were ignored. The only statistical difference was observed in PEO4 cells electroporated with AS control or siRNA #17 treated with 0.08 µM cisplatin; however, no differences were observed between AS and siRNA #13 treated at the same cisplatin concentration. Further, this difference disappeared at higher concentrations, suggesting that the difference observed might be inconsistent. Therefore, we concluded that UCA1 does not affect survival of PEO1 and PEO4 cells upon cisplatin treatment.

5.3.3 Functional validation of UCA1 knockdown in additional HGSOC cells

5.3.3.1 UCA1 expression in 8 HGSOC cell lines

To broadly investigate the role of UCA1 in promoting drug resistance, 8 cell lines ranked as 'likely high-grade serous' according to Domcke et al. 2013 were chosen, representing rele-

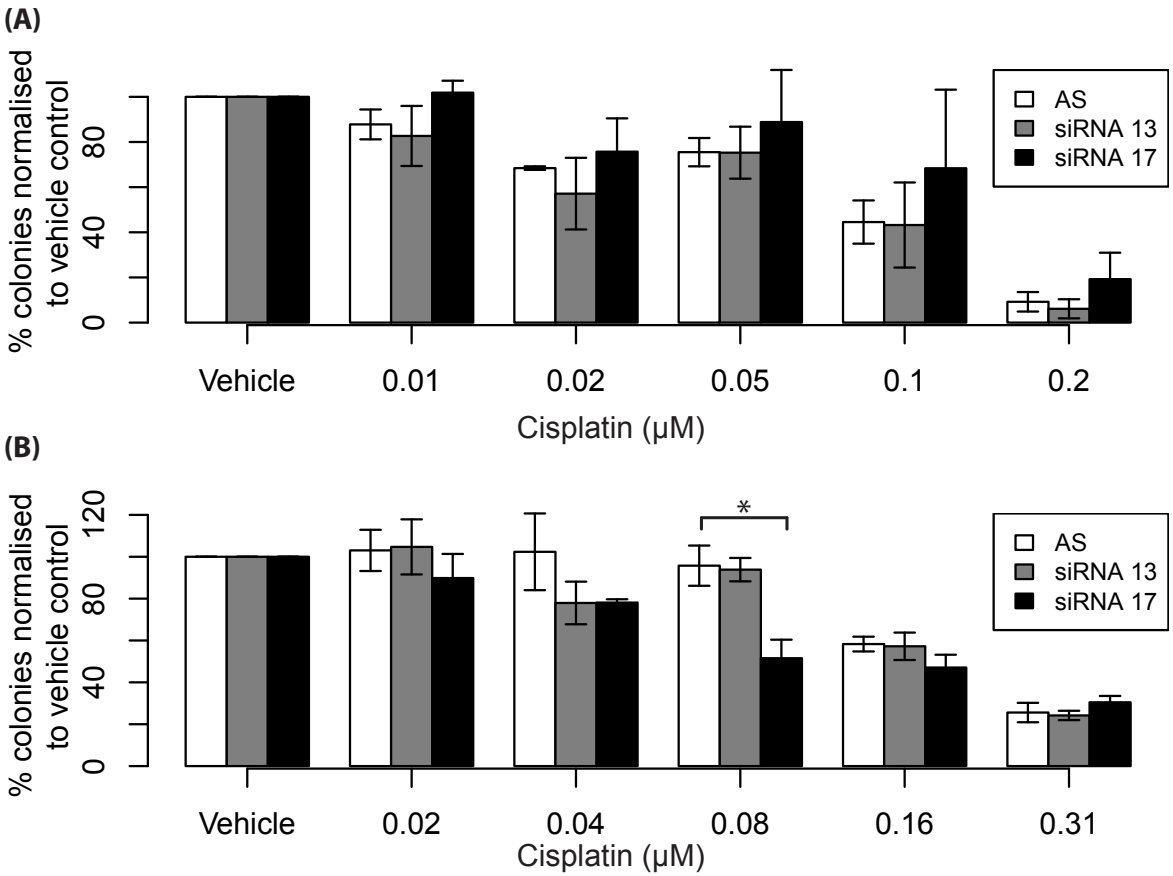

Figure 5.11: Long-term effects of UCA1 on cell survival upon cisplatin treatment in PEO1 and PEO4 cells measured by clonogenic assays

(A) PEO1 cells (N=2; some wells in the 3rd biological replicate were dried out and excluded.) **(B)** PEO4 cells (N=3). * $P < 0.05$.

vant models to study drug resistance. UCA1 expression was determined using SYBR-green primers (N = 3; Figure 5.12)†. GAPDH was used as the reference gene whereas Kuramochi cells were used as the calibrator cell line. Amongst the 8 cell lines, Kuramochi and OAW28 were excluded from the clonogenic assays as they did not form colonies upon 21 days of growth *in vitro*. Nonetheless, Kuramochi cells were selected for investigation by the MTS assay as it is arguably the closest match to primary HGSOC patient samples (Domcke et al. 2013). CaOV4, COV318 and OVKATE had a doubling time of approximately 6 days, making them difficult to grow. OVSAHO was a suitable cell line but it was excluded because its abilities to form colonies had not been tested previously. Kuramochi, OVCAR-3 and

†The UCA1 primers used in this experiment were pre-designed by Sigma-Aldrich (Table 2.9) whereas UCA1 primers used for lncRNA profiling were supplied by the kit. Results obtained using primers from Sigma-Aldrich were comparable to UCA1 Taqman probes (data not shown)

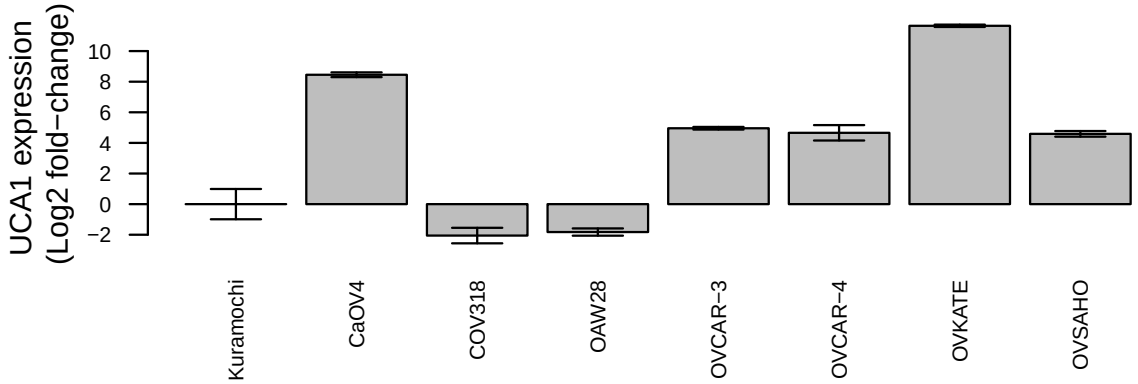

Figure 5.12: UCA1 levels relative to the Kuramochi cells in 8 HGSOC cell lines

OVCAR4 were chosen for further validation due to their ease of handling and amenability for drug sensitivity assays.

5.3.3.2 Effect of UCA1 knockdown on cisplatin sensitivity in additional HGSOC cell lines

The overall approach in investigating the effects of UCA1 knockdown in additional HGSOC cell lines was similar to the experiments conducted in PEO1/PEO4 cells: optimisation of UCA1 knockdown in Kuramochi, OVCAR-3 and OVCAR4 cell lines followed by functional assays to determine sensitivities to cisplatin upon UCA1 knockdown. Like PEO1 and PEO4 cells, ~80% of Kuramochi, OVCAR-3 and OVCAR4 cells were found to be positive for AS-488 following its transfection using HiPerFect reagent (Supplementary Figure A.1). Despite a high level of transfection capabilities, UCA1 knockdown in OVCAR-3 and OVCAR4 cells using HiPerFect reagent was found to be insufficient (~40-60%) for functional experiments (Supplementary Figure A.2). It was empirically observed that Kuramochi cells were difficult to transfect using HiPerFect reagent (data not shown), and were excluded from this experiment.

Kuramochi, OVCAR-3 and OVCAR4 cells were tested for electroporation to knock-down UCA1. Electroporation resulted in an excellent UCA1 knockdown in OVCAR-3 and OVCAR4 cells that was sustained for up to 4 days post-electroporation, indicating that the knockdown persisted throughout the experiment (Figure 5.13A. Unfortunately, UCA1 was not found to be knocked down in Kuramochi cells even using electroporation.

One million OVCAR-3, Kuramochi and OVCAR4 cells were electroporated with 100 nmol siRNAs, seeded for MTS and clonogenic assays, and treated with cisplatin for 3

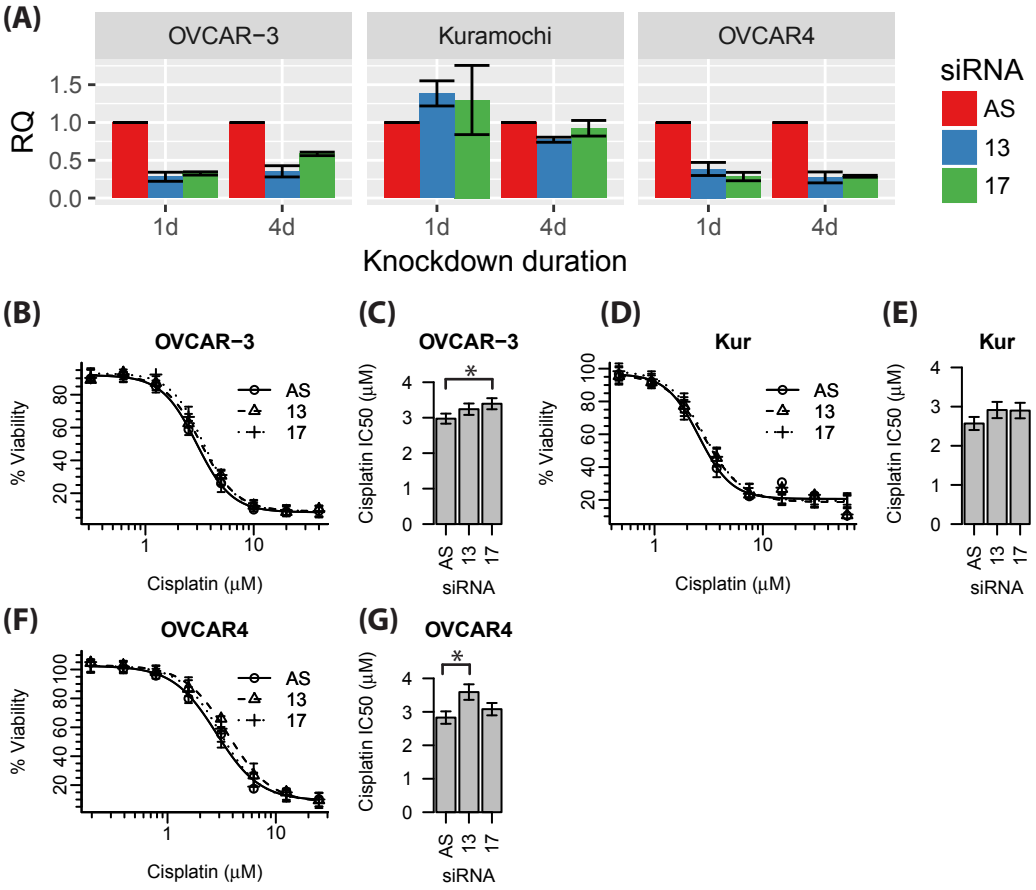

Figure 5.13: Effect of UCA1 knockdown on cisplatin sensitivity in 3 additional HGSOC cell lines

(A) UCA1 knockdown using electroporation. **(B, D and F)** Cisplatin DRC upon UCA1 knockdown in OVCAR-3, Kuramochi and OVCAR4 cells, respectively. **(C, E and G)** IC_{50} of cisplatin upon UCA1 knockdown in OVCAR-3, Kuramochi and OVCAR4 cells, respectively. Kur: Kuramochi cells. * $P < 0.05$.

days as previously described. Despite an excellent UCA1 knockdown in OVCAR-3 and OVCAR4 cells (Figure 5.13A), cisplatin DRCs and IC_{50} remained relatively unchanged. A statistical difference between IC_{50} values of AS and siRNA #17 in OVCAR-3 cells was observed (Figure 5.13C); however, this translated into a marginal increase of 12.4% in the IC_{50}. Similarly, a statistically significant difference of 21% in IC_{50} of AS and siRNA #13 was observed in OVCAR4 cells (Figure 5.13G). The observed differences, however, were not replicated in the second siRNA treatment despite the excellent knockdown using both siRNAs individually. No differences in IC_{50} values upon siRNA treatments were observed in Kuramochi cells (Figure 5.13D, E), which is expected because these cells were resistant to siRNA electroporation (Figure 5.13A). Nonetheless, this experiment could be interpreted

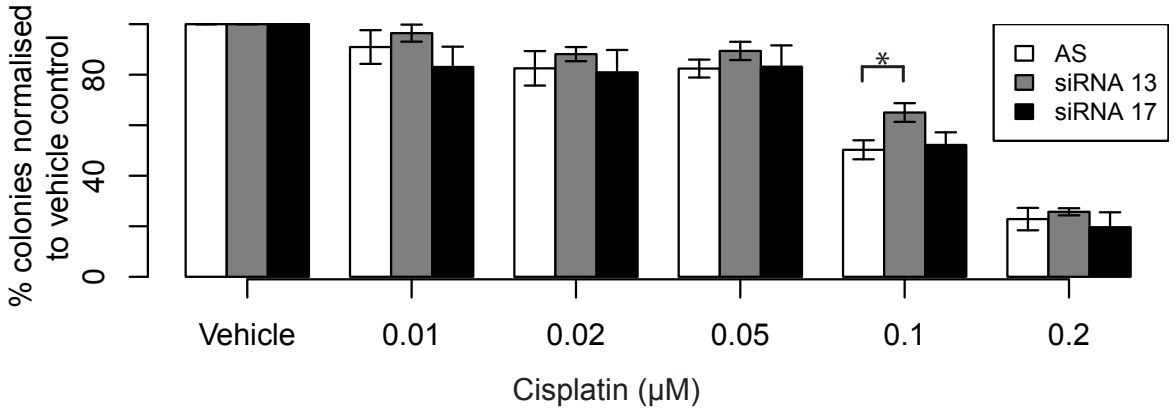

Figure 5.14: Long-term effects of UCA1 on cell survival upon cisplatin treatment in OVCAR4 cells measured by clonogenic assays
* $P < 0.05$.

as a scenario where the null hypothesis is true, and, indeed, no differences were observed, reflecting robustness of the assay.

OVCAR-3 and OVCAR4 cells were seeded to perform clonogenic assays following siRNA electroporation (N = 3). Kuramochi cells were not seeded for clonogenic assays as they lacked an ability to form colonies. Unfortunately, media of some wells, including the vehicle control used for normalisation, in all 3 biological replicates for OVCAR-3 cells were dried out, making them unusable. The data on OVCAR4, on the other hand, were reliable and have been presented in Figure 5.14. A statistically significant difference was observed between AS and siRNA #13 treated with 0.1 μM cisplatin. However, no statistical difference was observed between AS and siRNA #17 under the same conditions. Thus, no consistent difference upon UCA1 knockdown in cisplatin sensitivity was observed.

5.3.4 Effect of p53 on UCA1

Mr. Alexander Cole, a fellow PhD student in the lab, studied transcriptome-wide effects of wt p53 upon cisplatin treatment in the A2780 cells. UCA1 was found to be induced by ~20-fold in the A2780 cells treated at the IC^{75} value of cisplatin (9.9 μM) for 24 hours in his dataset (FDR-adjusted $P = 0.0001$). *CDKN1A* encoding p21, a canonical downstream target of wild-type p53, was also found to be upregulated by 21.4-fold under the same conditions (FDR-adjusted $P = 0.0001$). Since A2780 harboured wt p53 that was stabilised by cellular stressors such as cisplatin and given the induction of p21 upon cisplatin treatment, I tested whether UCA1 was a downstream target of wt p53 and, further, whether it was affected by mutant-p53.

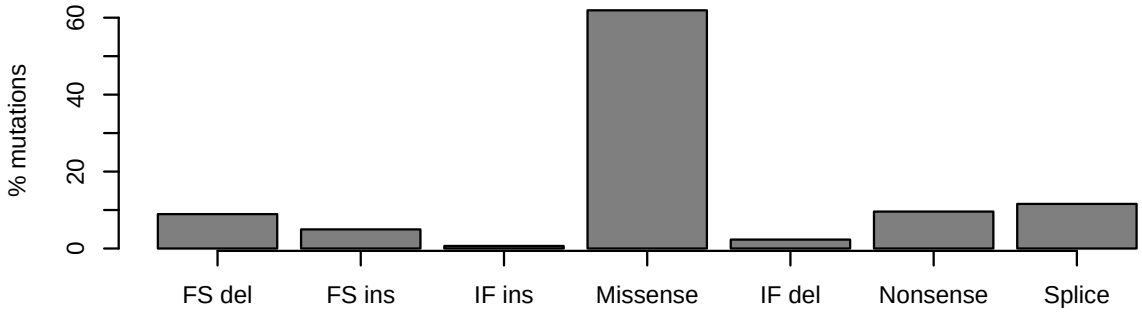

Figure 5.15: Frequency of types of *TP53* mutation observed in the TCGA-OV dataset
(FS = frame shift, IF = in-frame, ins = insertion and del = deletion)

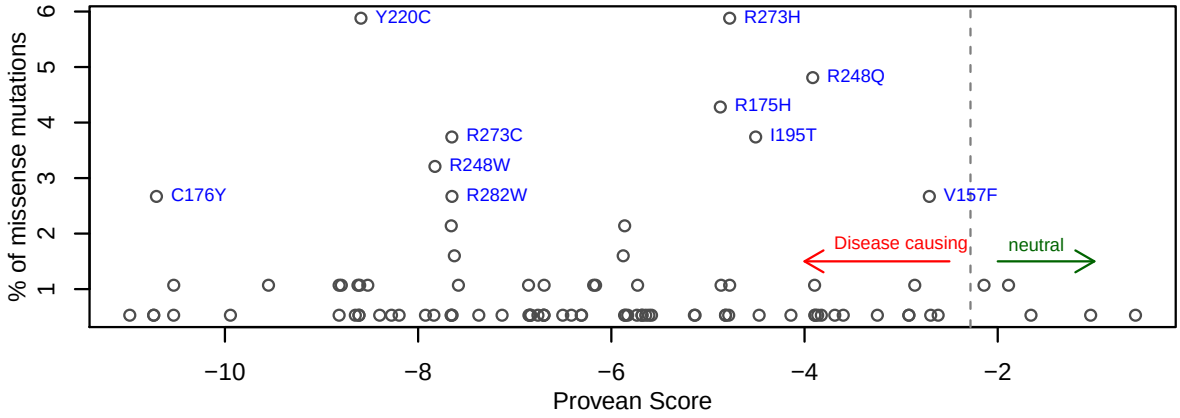

Figure 5.16: Prioritising the p53 mutations based on their evolutionary conservation predicted by the algorithm PROVEAN and their observed frequency in the TCGA-OV dataset

5.3.4.1 Identifying high priority *TP53* mutations in TCGA-OV dataset

Information on the *TP53* mutations in a total of 302 patients of the TCGA-OV dataset were downloaded from cBioportal on June 6, 2013. Missense mutations were found to be the most common type (~62%; Figure 5.15). There were 94 unique missense mutations reported in the TCGA-OV dataset, and it was important to prioritise a small number of *TP53* mutations for further studies.

Algorithms, such as SIFT, polyphen2 and mutation assessor, based on evolutionary conservation of amino acids have been employed to predict whether mutations are neutral or could be disease-causing (Rebbeck, Spitz, and Wu 2004). In general such algorithms first identify evolutionary conserved residues because of their essential role in protein functions. In addition, these algorithms also compare the chemical properties (electric charge, hydrophobicity and so on) of the wild-type versus the mutated residue in calculating

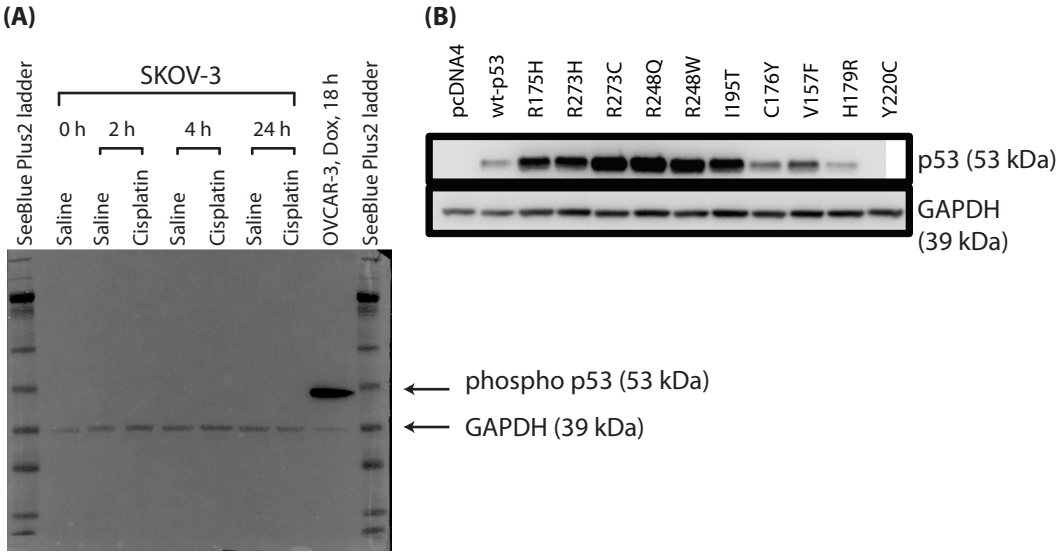

Figure 5.17: Validating protein expression of mutant-p53 constructs in p53-null SKOV- 3 cells

(A) Comfirming that SKOV-3 are p53-null by stimulating these cells with cisplatin for up to 24 h and blotting for phospho-p53, as its antibody was more sensitive than the total p53. OVCAR-3 cells were stimulated with doxorubicin for 18 h as a positive control. GAPDH was used as reference. 'Dox' refers to doxorubicin. **(B)** Protein expression of mutant-p53 transfected into SKOV-3 cells to show that the transfected plasmids carrying mutant-p53 were expressed in the cells. (B) was generated by Mr. Alexander Cole.

a score (Rebbeck, Spitz, and Wu 2004). When the SIFT algorithm was run on the *TP53* mutations reported in the TCGA-OV dataset, almost all of them were predicted to be disease-causing (data not shown), rendering this software incapable in prioritising mutations. A recent algorithm known as Protein Variation Effect Analyzer (Provean) could evaluate the effects of up to 6 mutations in a given protein (Choi et al. 2012). Importantly, the Provean scores could segregate the disease-causing mutations into a broader range than SIFT, making this an appropriate algorithm for this purpose.

Since a lethal mutation would be less tolerated by the cell, it was hypothesised that lethality of a mutation should inversely correlate with its observed frequency. Surprisingly, the data revealed this not to be the case, and certain mutations stood out distinctively from the rest (highlighted in blue in Figure 5.16). Their higher frequency in independent patients ascertain favourable outcomes for the cancer cell. In fact, the *TP53* mutations R175H, R273H and R248Q are amongst the most frequently occurring mutations and have been reported as 'gain-of-function' mutations (Bieging, Mello, and Attardi 2014).

Using the pcDNA4/TO mammalian expression vector harbouring the wt-p53 cloned by a previous laboratory member as template, the following 10 mutations were generated using site-directed mutagenesis[‡]: R175H, R273H, R273C, R248Q, R248W, I195T, V157F, Y220C, R282W and C176Y. All mutations were confirmed by Sanger sequencing. Several attempts were made to synthesise R282W; however, the mutated p53 also showed extra unintended mutations in addition to R282W, leading us to exclude this mutation from further studies.

The expression vector containing wild-type or mutant-p53 was transfected into the functionally p53-null ovarian cancer cell line SKOV-3 (c.267del1, resulting in a frame-shift (Bamford et al. 2004)). To confirm that SKOV-3 cells are *bona fide* p53-null, 5×10^5 SKOV-3 cells were treated with 16.6 µM (5 µg/ml) cisplatin for 2, 4 or 24 h and blotted for phospho-p53. A treatment of stressors such as cisplatin would be expected to increase phosphorylation and subsequent accumulation of p53, if present. OVCAR-3 cells harbouring the *TP53* mutation R248Q were treated with 1 µM doxorubicin for 18 h as a positive control. GAPDH was used as the reference. Either total p53 or phospho-p53 could be blotted to answer the question. However, the phospho-p53 antibody was used because it was found to be more sensitive than total p53 antibody in our experience. Phospho-p53 was not detected in SKOV-3 cells upon the cisplatin treatment (Figure 5.17A), confirming that they are p53-null.

Next, 1 µg of plasmid containing wild-type or mutant-p53 were transfected into SKOV-3 cells using X-tremeGENE 9 DNA Transfection Reagent, and total protein was harvested 48 h post-transfection. As shown in Figure 5.17B, most mutants produced the protein in SKOV-3 cells. Interestingly, the levels of R175H, R273H, R273C, R248Q, R248Q, I195T and V157F were higher than the wt-p53, similar to the clinical HGSOC samples where mutant-p53 is expressed at a higher level. The levels of Y220C mutations were undetectable, and the mutation was excluded.

5.3.4.2 Effect of p53 on UCA1

In a 6 well-plate 2.5×10^5 SKOV-3 cells were seeded overnight, and transfected with 1 µg plasmid harbouring empty vehicle (pcDNA4), wt-p53 or 4 mutant-p53 (R175H, R248Q, R248W AND R273H). RNA was harvested 48 h post-transfection using the Qiazol reagent. Expression of UCA1 and p53 mRNA was quantified by TaqMan probes using RT-qPCR, and was normalised to the vehicle control (Figure 5.18A). As expected, the levels of wt-p53 and mutant-p53 were more than 500-fold higher compared to the vehicle control ($P < 0.05$). Interestingly, the levels of mutant-p53 were also higher than the wt-p53 ($P < 0.05$),

[‡]This work was shared equally with Mr. Alexander Cole.

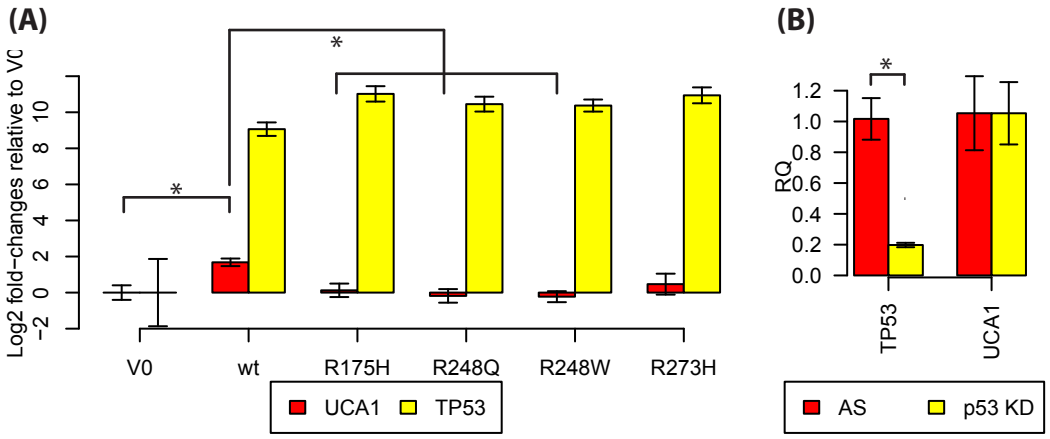

Figure 5.18: Effect of p53 on UCA1

(A) SKOV-3 cells were transfected with 1 µg empty pcDNA4 (V0) or pcDNA4 containing wild-type or mutant-p53, and the expression of *TP53* (to confirm successful transfection) and UCA1 were determined 48 h post-transfection using TaqMan RT-qPCR. **Note:** The levels of all 4 mutant-p53 were statistically higher than wt-p53, but the figure has not been marked with '*' for simplicity. **(B)** The effect of p53 knockdown in OVCAR-3 cells naturally harbouring the *TP53* mutation R248Q. UCA1 was not affected despite ~80% knockdown in p53 levels.

consistent with the protein expression of mutant-p53 shown in Figure 5.17B. The statistical significance of p53 expression was not marked with '*' on Figure 5.18A to focus on UCA1.

When compared to the vehicle control, UCA1 was found to be upregulated only by the wt-p53 by 3.2-fold (N = 3; $P = 0.01$; Figure 5.18A). Importantly, the UCA1 expression induced by wt-p53 remained higher than the mutant-p53 R175H, R248Q and R248W ($P < 0.05$). Although UCA1 expression upon wt-p53 transfection was statistically not different compared with the R273H mutation, it was found to be upregulated in wt-p53 with a trend ($P = 0.077$; Figure 5.18A). This experiment was repeated in an independent p53-null cell line H1299 (lung cancer), but it was not fruitful as UCA1 was not found to be expressed at the basal level in H1299 cells as well as upon transfection of wild-type and mutant-p53 (data not shown).

To confirm that UCA1 was not induced by mutant-p53, *TP53* was knocked down in OVCAR-3 cells endogenously harbouring mutant-p53 R248Q (Figure 5.18B). 2×10^5 OVCAR-3 cells were transfected with 100 nmol p53 siRNA #9 using HiPerFect reagent, RNA was harvested 48 h post-transfection followed by quantification of gene expression using TaqMan probes. Intriguingly, the p53 mRNA was found to be reduced by 80% ($P = 0.001$), which contradicted the previous experiments attempted to knockdown UCA1 in OVCAR-3 cells (Supplementary Figure A.2). Nonetheless, UCA1 levels remained unchanged upon p53 knockdown ($P = 0.7$).

5.4 Discussion

Adjuvant chemotherapy based on the agents containing platinum and taxane, such as a combination of carboplatin and paclitaxel, remain the cornerstone for treatment of patients with OC. Although OC is responsive to these agents initially, most patients develop resistance to chemotherapy within the first two years of the treatment (Agarwal and Kaye 2003; Hennessy, Coleman, and Markman 2009; Romero and Bast 2012). Therefore, understanding the mechanisms of drug resistance is crucial. The possible role of lncRNAs in promoting cisplatin resistance was investigated in this chapter.

The experimental approach utilised two independent pairs of cisplatin sensitive/resistance cell lines, A2780/A2780cisR and PEO1/PEO4, to identify candidate lncRNAs. The sensitive cell lines A2780 and PEO1 cells were derived from untreated HGSOC patients. A2780cisR was developed from A2780 by gradual exposure to cisplatin *in vitro* (Bohrens et al. 1987) whereas the PEO4 cell line was established from the same patient as PEO1 after she naturally acquired resistance to cisplatin (Langdon et al. 1988). A total of 90 lncRNAs were profiled using SYBR-green primers in RT-qPCR. By optimising the RT-qPCR conditions, we were able to profile each cell line in three biological replicates for the amount of one. In addition, five types of selection criteria, ranging from assessing the qualities of the lncRNA primers to consistent differential expression of lncRNAs in both pairs of cell lines, were implemented to identify the robust candidates for functional studies.

Five of 90 lncRNAs (SNHG1, SNHG6, Y RNA-1, Malat1 and UCA1) satisfied the selection criteria. Notably, the prominent lncRNA HOTAIR was excluded as it manifested poor melt curves. Amongst the 5 candidates, both SNHG1 and SNHG6 were previously demonstrated to have a role in promoting NSCLC (You et al. 2014), HCC (Chang et al. 2016; Zhang et al. 2016a; Zhang et al. 2016b) and neuroblastoma (Sahu et al. 2016), but their potential role in promoting cisplatin resistance remains unknown. Y RNA-1 was found to be a small ncRNA given its length of 83-112 nucleotides (Christov, Trivier, and Krude 2008). In comparison, Malat1 is a relatively well-studied lncRNA in promoting cancer (Dhamija and Diederichs 2016; Gutschner, Hämmerle, and Diederichs 2013) as well as dug resistance by mechanisms such as increasing autophagy (Mimeault and Batra 2013). Interactions between Bcl-2 and Malat1 in NSCLC have also been proposed, implicating its potential role in regulating apoptosis (Schmidt et al. 2014). The role of UCA1 in promoting cancer and cisplatin resistance began to emerge recently. It was found to be upregulated in bladder cancer compared to the adjacent healthy tissue, and its level in urine could predict

bladder transitional cell carcinoma (Wang et al. 2006). Subsequently, UCA1 was found to be associated with multiple cancers including breast cancer, colorectal cancer, lung squamous cell carcinoma, oesophageal squamous cell carcinoma, gastric cancer, HCC and ovarian cancer (Xue, Chen, and Li 2016), and to promote cell proliferating by inducing CEBP and PI3K/Akt pathways (Yang et al. 2012). Furthermore, Wang et al. 2008 showed that overexpression of UCA1 promoted cisplatin resistance in bladder cancer. Based on these pieces of evidence in bladder cancer, especially its role in promoting cisplatin resistance, as well as novelty in OC, UCA1 was chosen to investigate its possible role in promoting cisplatin resistance in OC when the project started in 2013. Importantly, the PI3K/Akt pathway had been extensively studied in our laboratory previously with antibodies and TaqMan probes for key members of the pathway available for further investigation.

Prior to the functional analyses, we validated the overexpression of UCA1 observed in the resistant cell lines from the lncRNA profiling conducted using SYBR-green-based RT-qPCR with more sensitive TaqMan probes. In the lncRNA profiling, UCA1 was found to be differentially expressed only in the A2780/A2780cisR pair. However, this finding was reversed when TaqMan probes were used to quantify UCA1 expression, and UCA1 was found to be overexpressed in PEO4 compared to PEO1 cells. According to a study published in 2013, A2780/A2780cisR ranked as 'unlikely HGSOC' when their various '-omic' profiles were compared to the primary HGSOC tissues of the TCGA-OV cohort (Bell et al. 2011; Domcke et al. 2013) whereas the PEO1/PEO4 pair remain untested as models that strongly mimic HGSOC. Based on the functional evidence of UCA1 in promoting cisplatin resistance in bladder cancer, we continued the investigation in the PEO1/PEO4 cell lines, and subsequently three additional cell lines (Kuramochi, OVCAR-3 and OVCAR4) that closely matched primary HGSOC tissues (Domcke et al. 2013).

Efficient knockdown of UCA1 was challenging. Roughly 80% of the cells were found to be positive for fluorescently labelled AllStars Negative Control (AS-488) 24 h post-transfection, suggesting high transfection efficiencies of the cell lines using HiPerFect reagent. In contrast, transfection of two independent siRNAs targeting separate regions of the 3' UTR of UCA1 reduced its levels by only ~50% in most cell lines at 16 - 24 h post-transfection, which was insufficient for functional assays. Additionally, *TP53* was found to be knocked down at higher levels (~80%) in OVCAR-3 cells 48 h post-HiPerFect transfection, whereas UCA1 levels were mildly affected under the same conditions at 24 h post-transfection in the same cell line, pointing to the fact that OVCAR-3 cells were adequately transfected using the HiPerFect reagent. This led us to question whether both UCA1 siRNAs were functional *in vitro*. Approximately 80% of knockdown in UCA1 levels

was achieved using electroporation of the same siRNAs in all cell lines except Kuramochi 24 h post-electroporation, suggesting that both siRNAs were functional. Therefore, it appears that the time-point of 24 h was perhaps too early to measure knockdown in UCA1 when HiPerFect Reagent was used for transfection, but it was necessary to quantify the knockdown levels prior to further experiments.

Electroporation proved to be surprisingly efficient and cheap (cost in addition to siRNAs: Opti-MEM media and recycled electroporation cuvettes) in knocking down UCA1, and was used for the rest of experiments. UCA1 levels were measured on 1 and 4 days post-electroporation to confirm the knockdown throughout the experiment. A slightly higher cell death was observed using electroporation compared to the HiPerFect reagent, which was adjusted by empirically increasing the seeding densities.

UCA1 knockdown did not affect cisplatin resistance in PEO1, PEO4, OVCAR-3 and OVCAR4 cells as tested by MTS assays (N=3). Specifically, the IC_{50} values remained unchanged when UCA1 was knocked down compared to the AS control. The IC_{50} values were statistically different between treatments in some cases, but the differences in absolute fold-changes were marginal (~1.2-fold). No significant differences were observed upon UCA1 knockdown in the clonogenic assays performed on PEO1, PEO4 and OVCAR4 cells investigating the long-term effects of UCA1 knockdown on cell survival. Kuramochi cells were found to be unable to form colonies, and results of the clonogenic assays on OVCAR-3 cells were excluded from the analyses because the culture media in some wells evaporated during the experiment.

The conclusion of this study contradicts (Wang et al. 2015) who reported that overexpression of UCA1 promoted cisplatin resistance of SKOV-3 cells. The choice of knocking down UCA1 using siRNA in our case *versus* a forced overexpression from an expression vector performed by Wang et al. 2015 could have led to different conclusions. A key limitation of their study is the use of only one HGSOC cell line SKOV-3, which has already been found to be 'unlikely' to be representative of HGSOC according to Domcke et al. 2013. Although the similarities between PEO1/PEO4 and HGSOC patient samples were not tested by Domcke et al. 2013, OVCAR-3 and OVCAR4 model HGSOC well *in vitro*, therefore, results obtained from these cell lines should immediately be able to be translated.

Transcriptional regulation of *UCA1* also remains largely unknown. Transcription factor Ets-2 was found to induce UCA1 expression by directly binding to its promoter in bladder cancer cell lines (Wu et al. 2013b). In addition, a bioinformatic analysis suggested c-Myb can bind to the promoter of UCA1 (Xue, Li, and Chen 2013). In the dataset generated by Mr. Alexander Cole, a fellow PhD student, UCA1 was induced by roughly 20-fold upon

cisplatin treatment in A2780 cell lines harbouring wt-p53. Remarkably, this induction was as high as CDKN1A/p21, a direct transcriptional target of wt-p53, prompting us to investigate whether UCA1 could be downstream of p53.

A functional approach was undertaken to test whether UCA1 expression was affected by wt-p53 as well as four *TP53* mutations. Ten high priority mutations in *TP53*, identified based on evolutionary approaches, were synthesised using site-directed mutagenesis. UCA1 was found to be induced by ~3-fold in the p53-null cells transfected with wt-p53 compared to the empty vector whereas three (R175H, R248Q and R248W) of the four mutant-p53 tranfected had no significant effect on UCA1 levels ($P < 0.05$). The fourth mutant-p53 (R273H) also showed the same effect with a trend ($P = 0.077$).

To confirm that mutant-p53 was unable to induce UCA1, mutant-p53 was downregulated in OVCAR-3 cells endogenously harbouring the *TP53* mutation R248Q. As shown in Figure 6.2, OVCAR-3 cells express a high level of mutant-p53 and an additional stimulus such as cisplatin treatment was unnecessary. UCA1 levels were not affected by ~80% knockdown in the *TP53* mRNA. Thus, there is some indirect evidence to support the role of wt-p53 in regulation of UCA1, which could have been lost upon *TP53* mutation. However, more experiments are needed to confirm this. In particular, if the hypothesis is correct, downregulation of the mutant-p53 in cells, such as Kuramochi, CaOV4 and OV202 expressing high basal levels of mutant-p53, should not affect levels of UCA1. Knocking down p53 in the cell lines harbouring wt-p53 (HEY and MCF7) in the absence of a DNA damage-type stimulus would probably be unfruitful since the levels of wt-p53 are usually kept low by the E3 ligase MDM2. UCA1 might be induced in these cells upon treatment with stressors such as cisplatin, as shown in A2780 cells. In fact, the A2780 cell line could be a good model to investigate effects of UCA1 following activation of wt-p53. The expression of UCA1 was found to be higher in PEO4 versus PEO1 cells. Both cell lines carry the identical *TP53* mutation G244D (Cooke et al. 2010) as well as harbouring a germline mutation in *BRCA2*; however, PEO4 cells gained an additional mutation in *BRCA2* that restores the wild-type protein sequence (Cooke et al. 2010). While the identical mutation in *TP53* in PEO1/PEO4 may not be responsible for the overexpression of UCA1 seen in PEO4 cells, the possible influence of *BRCA2* status on UCA1 expression remains unclear. Besides cisplatin resistance, a wider role of UCA1 in promoting multiple cancer remains unknown. In the context of OC, UCA1 was also one of the five differentially expressed lncRNAs between SKOV-3 and its derivative cell line with enhanced metastatic capabilities (SKOV-3.ip1) (Liu et al. 2013a), and the potential role of UCA1 in promoting invasiveness remains to be tested in other cell

line models. Finally, if additional evidence supports that UCA1 is a transcriptional target of wt-p53, its role in the p53 network should be investigated.

5.5 Conclusions

Ninety lncRNAs were profiled in two cell line models of cisplatin resistance, and five lncRNAs were found to be differentially expressed between resistant and sensitive cell lines. UCA1 was selected for functional validation given its emerging role in promoting cisplatin resistance in bladder cancer, as well as its association with multiple cancers including ovarian, bladder and breast cancers. However, no differences in cell proliferation and survival were observed upon UCA1 knockdown in a pair of cisplatin sensitive/resistant cell line originally used in the lncRNA profiling as well as two additional HGSOC cell liness. UCA1 was significantly induced, as much as *CDKN1A*, in A2780 cells harbouring wt-p53 treated with cisplatin, indicating that it could be a downstream target of wt-p53. In support of this hypothesis, UCA1 was induced in the p53-null cells transfected with wt-p53, but not mutant-p53, and downregulating mutant-p53 in OVCAR-3 cells did not affect the levels of UCA1. However, further experiments are needed to confirm a potential role for UCA1 in the wild-type p53 network.

Chapter 6

Investigating the effects of mutant-p53 on lncRNAs by using the p53-activating drug APR-246

6.1 Introduction

p53 is a well-studied transcription factor regulating expression of a large number of protein-coding genes. Recently, p53 has also been found to transcribe microRNAs, such as the miR-34 family of microRNAs, (He et al. 2007) and lncRNAs such as lincRNA-p21 (Huarte et al. 2010), PANDA (Hung et al. 2011), Pint (Huarte et al. 2010), PR-lncRNA-1 (Sánchez et al. 2014), PR-lncRNA-10 (Sánchez et al. 2014), NORAD (Lee et al. 2016), TUG1 (Guttman et al. 2009; Khalil et al. 2009), PVT1 (Barsotti et al. 2012), LINP1 (Zhang et al. 2016c), DDSR1 (Sharma et al. 2015) and DINO (Schmitt et al. 2016). In fact, half of the DNA regions bound by p53 were found to be located outside the protein-coding genes by a recent ChIP-seq study (Idogawa et al. 2014). Thus, p53 is likely to dramatically influence transcription of lncRNAs. *TP53* is mutated at a high frequency in cancers (Muller and Vousden 2013; Oren and Rotter 2010; Strano et al. 2007b) and almost universally mutated in HGSOC (Bell et al. 2011). The effect of mutant-p53 on the lncRNA landscape remains largely unexplored.

Mutations in most tumour suppressors result in loss of their functions, which can eventually lead to cancer. Most mutations in p53 are missense mutations that are frequently

expressed at a high protein level. The p53 protein is a tetramer consisting of two dimers. Mutant-p53/wt-p53 heterodimers are considerable impaired in the ability to bind to the p53-response element and transcribe wt-p53-response genes(Goh, Coffill, and Lane 2010; Weinberg et al. 2004). Mutant-p53 can inactivate wt-p53 as well as other members of the p53 family of proteins such as p63 and p73 due to dominant-negative effects (Martynova et al. 2012). In addition, mutant-p53 was found to interact with transcription factors and proteins that do not influence transcription directly, enhancing or preventing their activities, depending on the mutant-p53 and interacting partners (Muller and Vousden 2013). Based on these pieces of evidence, it has been proposed that mutations in p53 do not always equate to the loss of the protein but offer new capabilities that significantly enhance carcinogenesis. In support of this theory, genetically engineered mouse models harbouring mutant-p53 were found to have more aggressive and metastatic tumours than p53-wild-type or p53-null mice (Doyle et al. 2010; Lang et al. 2004; Morton et al. 2010; Olive et al. 2004). Furthermore, patients of Li–Fraumeni syndrome harbouring germline p53 missense mutations developed tumours 9-15 years earlier than those with mutations that resulted in a loss of p53 expression (Bougeard et al. 2008; Zerdoumi et al. 2013).

The aim of the research described in this chapter was to investigate the effects of mutant-p53 on lncRNAs using a small compound known as APR-246 that has been shown to induce wt-p53 activity from mutant-p53 in multiple cancers and is currently undergoing phase Ib/II clinical trial for treatment of recurrent HGSOC (NCT02098343 2014). Furthermore, APR-246 was found to be synergistic with cisplatin in ovarian cancer cell lines and primary cells derived from patients' ascites (Fransson et al. 2016; Mohell et al. 2015). Therefore, we also aimed to investigate mechanisms of synergy between APR-246 and cisplatin.

A combination of two drugs is called synergistic when their combined effect is significantly greater than their addition; therefore, the calculation of the additive effect is of utmost importance and remains complex (see the 60-page review authored by Chou 2006 devoted to this topic). More than 300 mechanism-specific equations have been derived to predict the additive effect (Chou 2010). A simple graphical technique known as an isobologram is often used to interpret drug interactions since its first employment by Loewe 1953. An abridged description of an isobologram is provided in Figure 6.1, and details on its construction can be found in Tallarida 2001 and Grabovsky and Tallarida 2004. Assuming the potency ratio, R, is constant, the additive effect of both drugs results in a linear line ('isobole') connecting the IC_{50} values of both drugs (Figure 6.1). When concentration of drug B is zero ($b = 0$), the equation for the isobole shown in Figure 6.1 results in $a = A$, which is the IC_{50} and the x-intercept of drug A. If a pair of doses is synergistic, the fixed

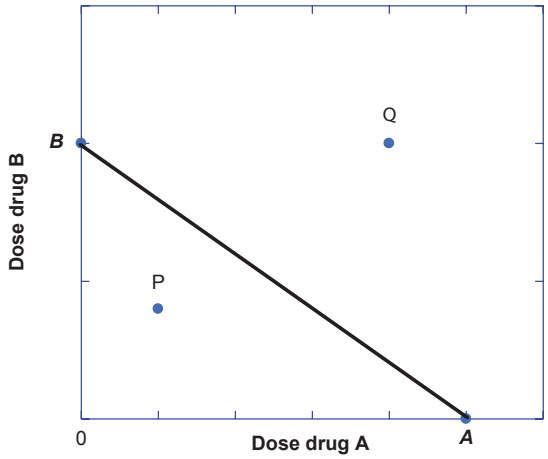

Fixed effect:
reduction in cell viability by 50% (IC_{50})

A : IC_{50} of drug A
B : IC_{50} of drug B
a : dose of drug A
b : dose of drug B

Potency ratio $R = \frac{A}{B}$
Additive isobole: $\frac{a}{A} + \frac{b}{B} = 1$

Figure 6.1: Analysis of drug interactions using isobolograms
A specified effect level observed upon a drug treatment, such as IC_{50}, is fixed for an experiment. The IC_{50} of each drug represents x and y intercepts of the isobologram. Next, the potency ratio, R, is calculated by dividing IC_{50} of drug A and B. The potency ratio enables the calculation of the equivalent dose of drug B to observe the same effect, such as a reduction in cell viability by half, using dose of drug A. When R is constant, the isobole is linear otherwise it is curved. Interaction points below and outside the isobole represent synergism and antagonism, respectively (Grabovsky and Tallarida 2004; Tallarida 2001). *P*: synergistic drug combinations, *Q*: sub-additive or antagonistic drug interactions.

effect level, i.e. IC_{50}, is reached using a lower amount of the total dose and the interaction falls below the isobole (point *P* in Figure 6.1). A drug interaction such as point *Q* in Figure 6.1 represents sub-additivity or antagonism, where a higher dose than the predicted additive effect is required to observe the effect level. The 'Additive model' (explained in subsection 6.2.1) was employed in this study to identify synergistic drug interaction, as advised by the developers of APR-246 (Mohell et al. 2015).

6.2 Materials and methods

6.2.1 Calculations of synergy between two treatments

The additive model (Jonsson et al. 1998) was used to calculate synergy between two drugs. For example, if drug *A* and *B* individually resulted in cell viabilities of 0.4 and 0.6, respectively, the additive model predicts the viability of 0.24 (0.4×0.6) for their combined effect. The ratio of the observed to the predicted viabilities ($\frac{\text{Observed}}{\text{Predicted}}$; also known as the

Survival Index (SI)) dictates whether an interaction is additive ($0.8 \leq SI \leq 1.2$), synergistic ($SI < 0.8$) or sub-additive/antagonist ($SI > 1.2$).

6.2.2 RNA-seq

RNA-seq was performed at the Garvan Institute of Medical Research, Sydney, Australia, by our collaborators on bioinformatics, Dr. Nenad Bartonicek and Mr. James Torpy. A short description is provided below.

6.2.2.1 RNA quality control prior to cDNA library construction

RNA quality was assessed on a LabChip GX instrument (Perkin Elmer) with the Standard RNA Assay kit according to the manufacturer's instructions (Perkin Elmer). RNA concentration was measured using a Qubit 2.0 spectrophotometer (Thermo Fisher) and RNA Broad Range (BR) assay (Thermo Fisher).

6.2.2.2 cDNA library construction

250 ng of total RNA was used as input material for library preparation using the TruSeq Stranded Total RNA Sample Prep Kit (Illumina) according to the manufacturer's instructions. Individual libraries were indexed as recommended by Illumina.

6.2.2.3 Quantification and quality control of cDNA libraries

Indexed DNA libraries were analysed individually using a LabChip GX instrument (Perkin Elmer) with the DNA High Sensitivity Assay kit according to the manufacturer's instructions (Perkin Elmer). Libraries were diluted and pooled to a final concentration of 3 nM in Resuspension Buffer (Illumina). Pooled libraries were analysed using a LabChip GX instrument and DNA High Sensitivity Assay kit according to the manufacturer's instructions. PCR-competent library DNA concentration was verified using the universal KAPA Library Quantification Kit for Illumina Sequencing Platforms according to manufacturer's instructions (KAPA Biosystems). An Applied Biosystems QuantStudio 7 Real-Time PCR machine (Life Technologies) was used for RT-qPCR.

6.2.2.4 Processing of RNA-seq data

The sequenced sample libraries were assessed for quality control and trimmed by Trim Galore (v.0.41). Next, the sequences were mapped to the human genome (hg38) and

transcriptome (Gencode human, v.24) using STAR (v.2.5.0b) and counted with RSEM (v.1.2.25). The counts reported with RSEM were normalised with the R package 'edgeR' (Robinson, McCarthy, and Smyth 2010). Only those genes that had at least 5 reads in at least 3 samples were reported. Differentially expressed genes were calculated as those with FDR <0.05.

6.2.3 Gene Set Enrichment Analysis

Gene Set Enrichment Analysis (GSEA) was performed by the candidate under supervision of the bioinformaticians. The java application for performing GSEA (v.2.2.4) was downloaded from the Broad Institute's website (`http://software.broadinstitute.org/gsea/downloads.jsp`). The 'Hallmarks' and 'C2' gene sets used in this thesis were provided by MSigDB v.6.0, also available through the Broad Institute (Subramanian et al. 2005). A 1000 permutations were performed using the median values of the ranked list L to calculate the P values of a gene set.

6.3 Results

6.3.1 Selection of cell line models

Since APR-246 is thought to work by reactivating wt-p53 activity from the mutant-p53, we hypothesised that the cell line with high basal levels of mutant-p53 might respond well to APR-246. Measurements of basal levels of mutant-p53 were conducted by Mrs. Kristie Dickson and Ms. Joa Manoudian in our laboratory (Figure 6.2). OVCAR-3 cells were selected based on their high basal mutant-p53 expression as well as *TP53* mutation R248Q, which is a gain-of-function and hotspot p53 mutation (Bieging, Mello, and Attardi 2014; Walerych, Lisek, and Del Sal 2015).

6.3.2 Establishing synergistic conditions of the combination of cisplatin and APR-246 at 72 hours post-treatment

Synergistic drug combinations can be determined at any given time point. Our laboratory has routinely treated cells with cisplatin for 72 hours to allow the drug to manifest its effects; therefore, this time period was chosen to determine the synergy between APR-246 and cisplatin. Once synergistic conditions were established, transcript levels of selected

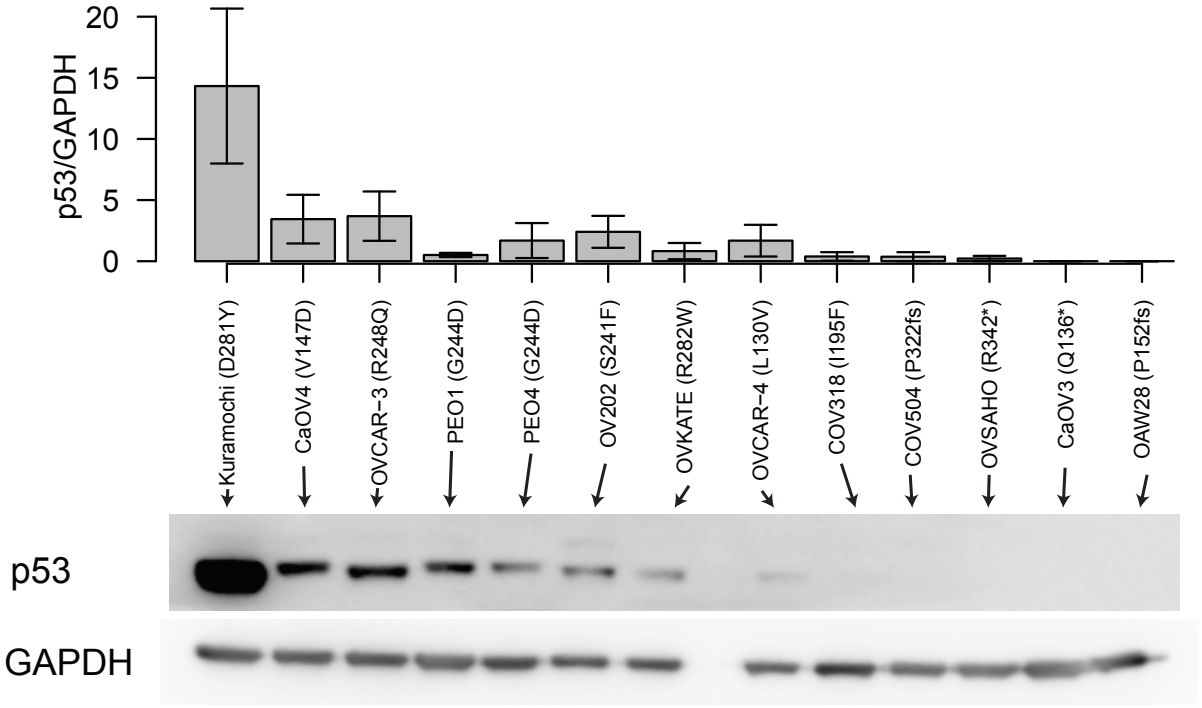

Figure 6.2: Protein expression of mutant-p53 in OC cell lines
Cell lines were grown as described in subsection 2.2.1. Three biological replicates were used for quantifying levels of mutant-p53 using western blotting. *TP53* mutation status is shown in parenthesis after a cell line's name. GAPDH was used for normalisation. A representative western blot is shown in this figure. This data was generated by Mrs. Kristie Dickson and Ms. Joa Manoudian.

p53 target genes were measured as early as 4 hours post-treatment to capture the cellular response to the drugs whose effects were determined to be synergistic after 72 hours.

6.3.2.1 Optimising drug doses using the MTS assay

IC_{50} values of APR-246 and cisplatin were calculated in OVCAR-3 cells. Briefly, 3000 cells were seeded in 96 well-plates overnight, treated with the drugs individually for 72 hours and the MTS assay was performed to assess cell viabilities as described in subsection 2.2.5. As shown in Figure 6.3, the IC_{50} values for APR-246 and cisplatin were found to be 11.7 and 3.31 μM, respectively (N=3). Next, OVCAR-3 cells were treated with a range of combinations of APR-246 and cisplatin in terms of varied ratios of their IC_{50} concentrations. The DRC was calculated for each ratio of IC_{50}. For simplicity, the concentration of APR-246 was fixed at 60 μM whereas the amount of cisplatin was varied to achieve the desired ratio. For example, to prepare the master mix for the IC_{50} ratio of 1:1 for APR-246 and

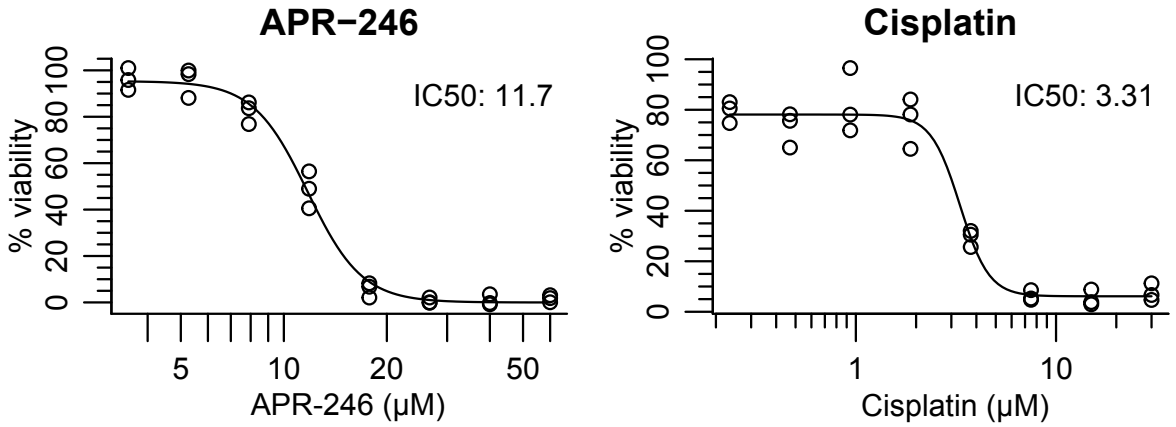

Figure 6.3: Dose response curves (DRCs) and IC_{50s} of APR-246 and Cisplatin in OVCAR-3 cells

OVCAR-3 cells were seeded into 96 well plates overnight and treated with the drugs for 72 hours. The MTS assay was used to infer cell viability. Data was normalised to vehicle controls. A total of 8 drug dilutions were used in calculating IC_{50} values (N = 3).

cisplatin (11.7/3.3 = 3.54), 16.9 μM cisplatin (60/3.54) was added to 60 μM APR-246. Cells were treated with 8 concentrations, in 1.5-fold dilutions from the master mix, for each IC_{50} ratio to obtain the DRC. Cells were treated with the following ratios of APR-246 to cisplatin IC_{50s}: 0.8:1, 1:1, 1:2, 1:2.5, 1.2:1 and 1.4:1. In addition, drug combinations in the format '10 μM APR-246+various concentrations of cisplatin' were also tested. These combinations culminated in a total of 8 × 96 well-plates for each biological replicate. Three biological replicates were performed and each biological replicate included the DRC of each drug treated individually to account for inter-plate variability.

Data analysis was automated by a custom R script written by the candidate (Appendix C). For each biological replicate, the treatment dose was broken down into its APR-246 and cisplatin constituents, and cell viability at the concentrations for each drug was estimated from their respective DRCs. The Additive model was applied to each drug combination to determine whether the drug combination was additive, synergistic or sub-additive (outlined in subsection 6.2.1). Finally, the SEM was calculated for each data point from three biological replicates (Figure 6.4). To visually identify the synergistic drug combinations, the size of the coloured 'bubble' was plotted inversely proportional to the SI whereas SEM was colour-coded. Data points with both small SI and SEM (large bubbles in red, blue or green colour) close to the IC_{50} values of each drug were given a priority. Three points of interest were validated for synergy using the alternative methodology of flow cytometry: 10 μM

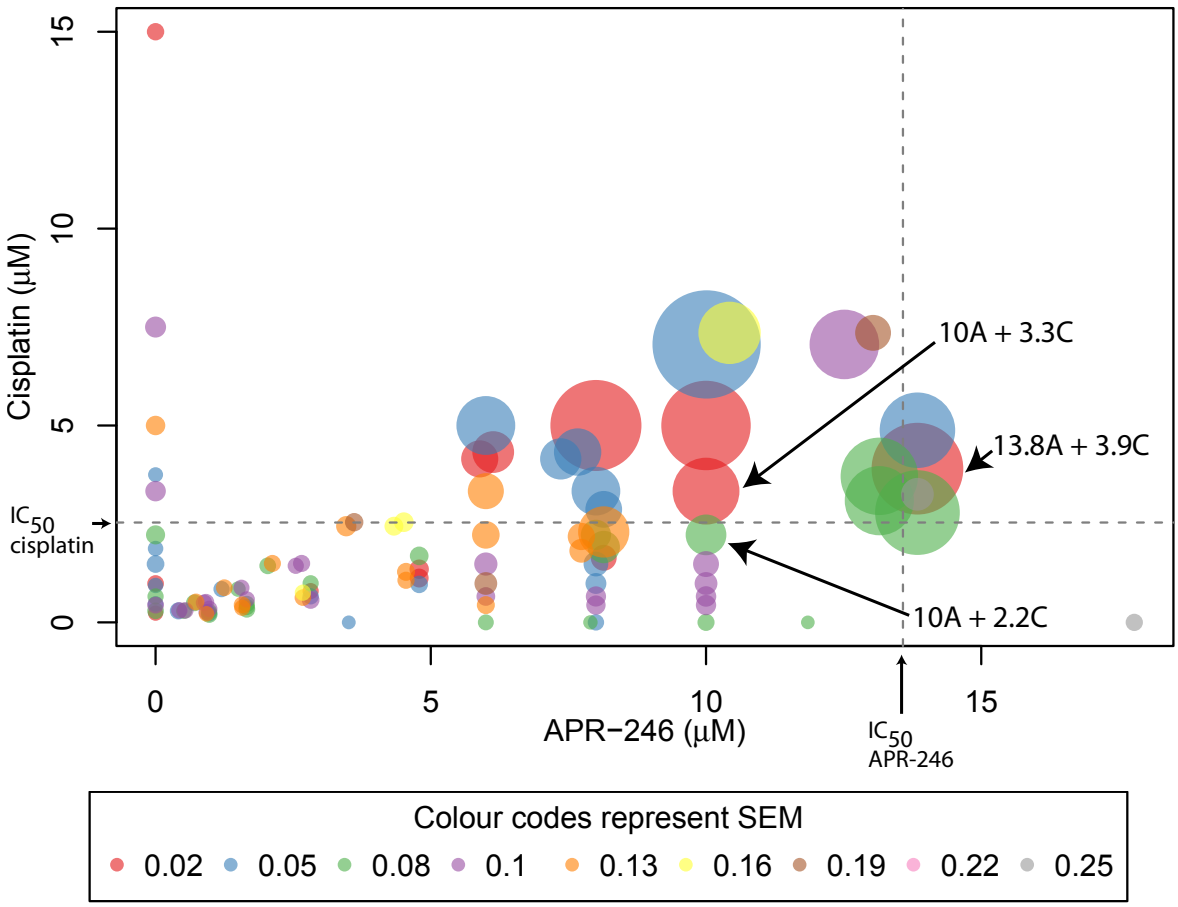

Figure 6.4: Overview of interactions between APR-246 and cisplatin measured using the MTS assay in OVCAR-3 cells.
OVCAR-3 cells were treated with a range of APR-246 and cisplatin concentrations for 72 hours, and the effects on cell viability were measured by MTS assay (N = 3). The size of the coloured bubble is inversely proportional to the SI, hence, larger bubbles represent stronger synergies. Only data matching SI < 1 are shown to put an emphasis on the synergistic conditions. The colour of the bubbles represents SEM of the biological replicates. The bubbles marked with arrows were selected for validating synergy using flow cytometry as their total drug dose was higher compared to other drug interactions. The notation 'A+C' refers to drug combination of APR-246 (A) and cisplatin (C).

APR-246+2.2 μM cisplatin (shortened as 10A+2.2C hereon), 10A+3.3C and 13.8A+3.9C (marked with arrows in Figure 6.4).

6.3.2.2 Validating the synergistic drug interactions using flow cytometry

The synergistic conditions identified from MTS assays were upscaled to T25 flasks to provide sufficient cells to perform flow cytometry. 2.25×10^5 OVCAR-3 cells were seeded into T25 flasks and treated with 10A+2.2C, 10A+3.3C and 13.8A+3.9C, either both drugs

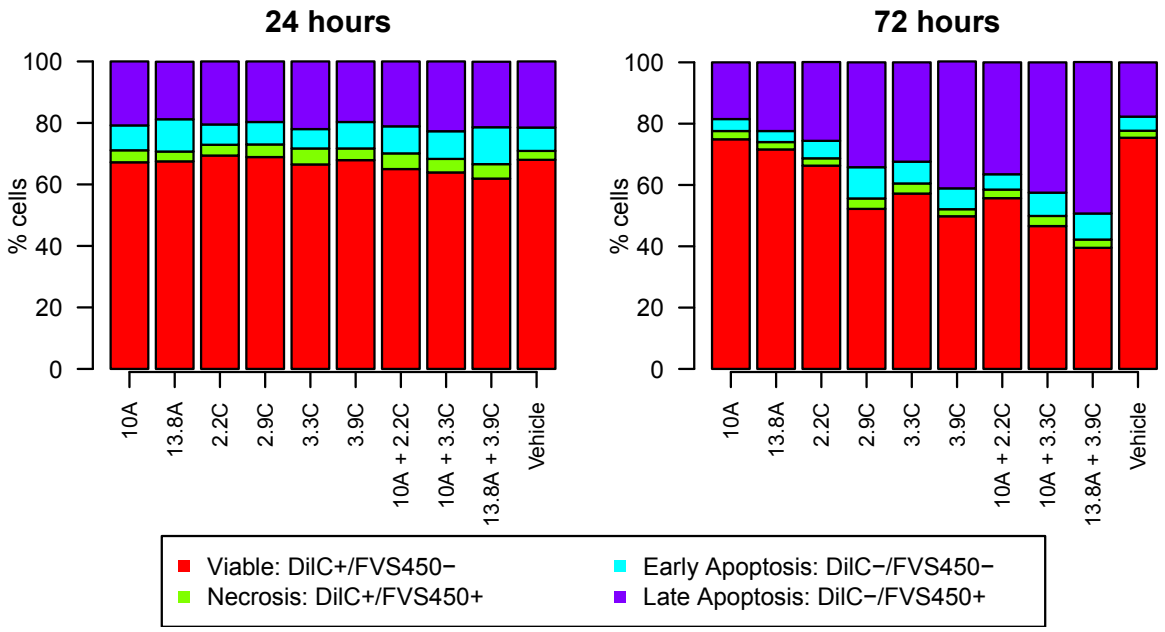

Figure 6.5: Validating synergistic conditions established by MTS assay using flow cytometry at 24 hours and 72 hours post-treatment

Three synergistic drug combinations (10A+2.2C, 10A+3.3C and 13.8A+3.9C) identified from Figure 6.3 were tested for synergy using flow cytometry. OVCAR-3 cells were treated with APR-246 and cisplatin alone or in combination for 24 or 72 hours, and cell viabilities were determined using DilC1(5)/FVS450 dyes (subsection 2.5)

individually or in combination (Figure 6.5). Cells were prepared for flow cytometry to determine cell viability using DilC1(5)/FVS450 dyes at 24 hours and 72 hours post-treatment (subsection 2.5). As shown in Figure 6.5, cell viability at 24 hours post-treatment of all samples treated with drugs was similar to the vehicle control. Although the cell viability was markedly reduced in some drug treated samples for 72 hours, the viability in the dual drug combinations such as 13.8A+3.9C did not seem to be synergistic compared to cells treated with both drugs individually. This simple experiment (N = 1) suggested that the conditions used previously to assess cell viability by MTS assays may not be scalable to T25 flasks. Out of the 3 drug combinations found to be synergistic based on the MTS data, '13.8A+3.9C' contained the highest concentrations of both drugs compared to other combinations and it was tested for synergy in further experiments (N = 4).

Optimising conditions in T25 flasks was also found to be cumbersome, requiring excessive numbers of cells, amount of the drugs and tissue culture consumables; therefore, 6 well-plates were used for subsequent experiments. The seeding density was fixed at 1.5×10^5 OVCAR-3 cells/well, which was found to be sufficient for downstream analyses without

overgrowing the cells. Cells were treated with 20A+4C, 20A+6C, 20A+8C, 30A+4C, 30A+6C or 30A+8C for 72 hours, and cell viability was measured using flow cytometry (Figure 6.6; N = 3). The drug combination 13.8A+3.9C found to be synergistic at 72 hours post-treatment identified from the MTS assays was also tested (N=4).

In standard hypothesis testing procedures, the null hypothesis states that no difference between two treatments is observed, i.e. H_0: average (treated samples) - average (untreated samples) = 0. A $P < 0.05$ is considered as sufficient evidence to reject the null hypothesis. Because the synergistic drug interactions have SI < 0.8, the null hypothesis for this experiment was: H_0: SI < 0.8*, statistical analyses were preformed using a one-tailed one-sample student's t-test. The following drug combinations were found to be synergistic ($P >$ 0.05, insufficient evidence to reject the null hypothesis): 20A+4C, 20A+6C and 30A+4C. When assessed alone, the 30A treatment resulted in a more variable cell viability compared to 20A and was excluded from further analyses. The variability in cell viability was similar between 4C and 6C treatments; however, 20A+6C was found to be more synergistic than 20A+4C and was chosen for subsequent experiments.

6.3.2.3 Assessing drug response under synergistic conditions

Since APR-246 is proposed to activate wt-p53 activity, SYBR green primers were used to quantify the expression of canonical p53-regulated genes (*CDKN1A*, *BBC3*/*PUMA*, *MDM2*, TP53-Induced Gene 3 (*TP53I3*), *BAX* and *C12orf5* after APR-246 treatment (N = 3; Figure 6.7). In addition, Glutamate-Cysteine Ligase Catalytic Subunit (*GCLC*) induced upon oxidative stress was also measured. Data was normalised to the vehicle control, which was omitted from the graphs after normalisation. As shown in Figure 6.7, *CDKN1A*, *BBC3/PUMA*, *BAX* and *C12orf5* were not significantly induced (absolute FC > 2 and P < 0.05) upon 20A and 30A treatments. In contrast to p53-response genes, *GCLC* was significantly induced upon 20A and 30A treatments (Figure 6.7). Although *CDKN1A* and *BBC3/PUMA* were induced at a higher level upon treatment with 30 μM compared to 20 μM APR-246, this treatment was not statistically significant.

Western blotting was performed to test whether APR-246 induced p21 at the protein level regardless of the doses that were found to be synergistic. Since western blotting required more cells than RT-qPCR and significant cell death was observed upon APR-246 treatments, both seeding densities and drug doses were increased for the following

*The H_0: SI = 1 (absence of synergy) was considered. However, a $P < 0.05$ would indicate that the drug interactions are either synergistic (SI < 1) or sub-additive (SI > 1), requiring a one-tailed t-test for further confirmation. Importantly, a synergistic interaction is defined as SI < 0.8, not SI < 1, justifying H_0: SI < 0.8 for this experiment

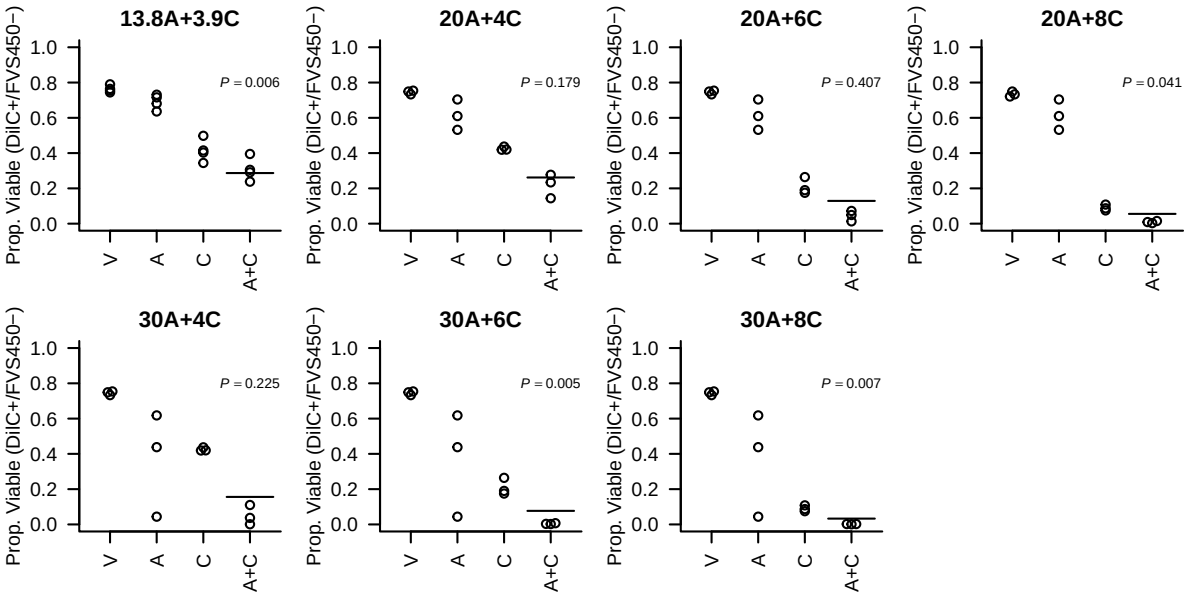

Figure 6.6: Optimisation of synergistic conditions at 72 hours post-treatment using flow cytometry

OVCAR-3 cells were treated with either both drugs alone or in combination for 72 hours, and cell viabilities were measured using DilC5/FVS450 dyes on a flow cytometer. *P* values represent evidence against the null hypothesis H_0: SI < 0.8, which was accepted when $P > 0.05$. The short horizontal lines above 'A+C' combinations indicate predicted viability of the drug combination based on the Additive model, and cell viabilities under the lines usually represent synergy. The notation 'A+C' refers to drug combination of APR-246 (A) and cisplatin (C).

experiment to obtain enough starting material. Briefly, 3×10^5 OVCAR-3 cells were treated with 30 - 50 µM APR-246 for 24 - 48 hours, and both the floating and the adherent fractions were collected in 200 µl Laemmli buffer (N = 1; Figure 6.8A). *TP53*-null H1299 cells (Mitsudomi et al. 1992) transfected with wt-p53 plasmid, which were found to express the wt-p53 and the downstream protein p21, were used as a positive control. OVCAR-3 cells expressed mutant-p53 basally as well as upon APR-246 treatment, although this experiment would not discriminate between wild-type or mutant-p53 upon APR-246 treatment in this experiment. The expression of p21 remained undetectable with or without APR-246 treatment for 24 or 48 hours (Figure 6.8).

If treatment with APR-246 was able to reactivate wt-p53 activity from mutant-p53, there was an expectation that levels of p53-target genes such as *CDKN1A/p21* would be increased, which would be detectable by RT-qPCR. Plus, RT-qPCR also requires lower amounts of starting material for analysis; therefore, RT-qPCR was used for further experiments. In conclusion, canonical p53-response genes, measured by RT-qPCR and western blotting, were not significantly induced in OVCAR-3 cells following treatment with APR-246,

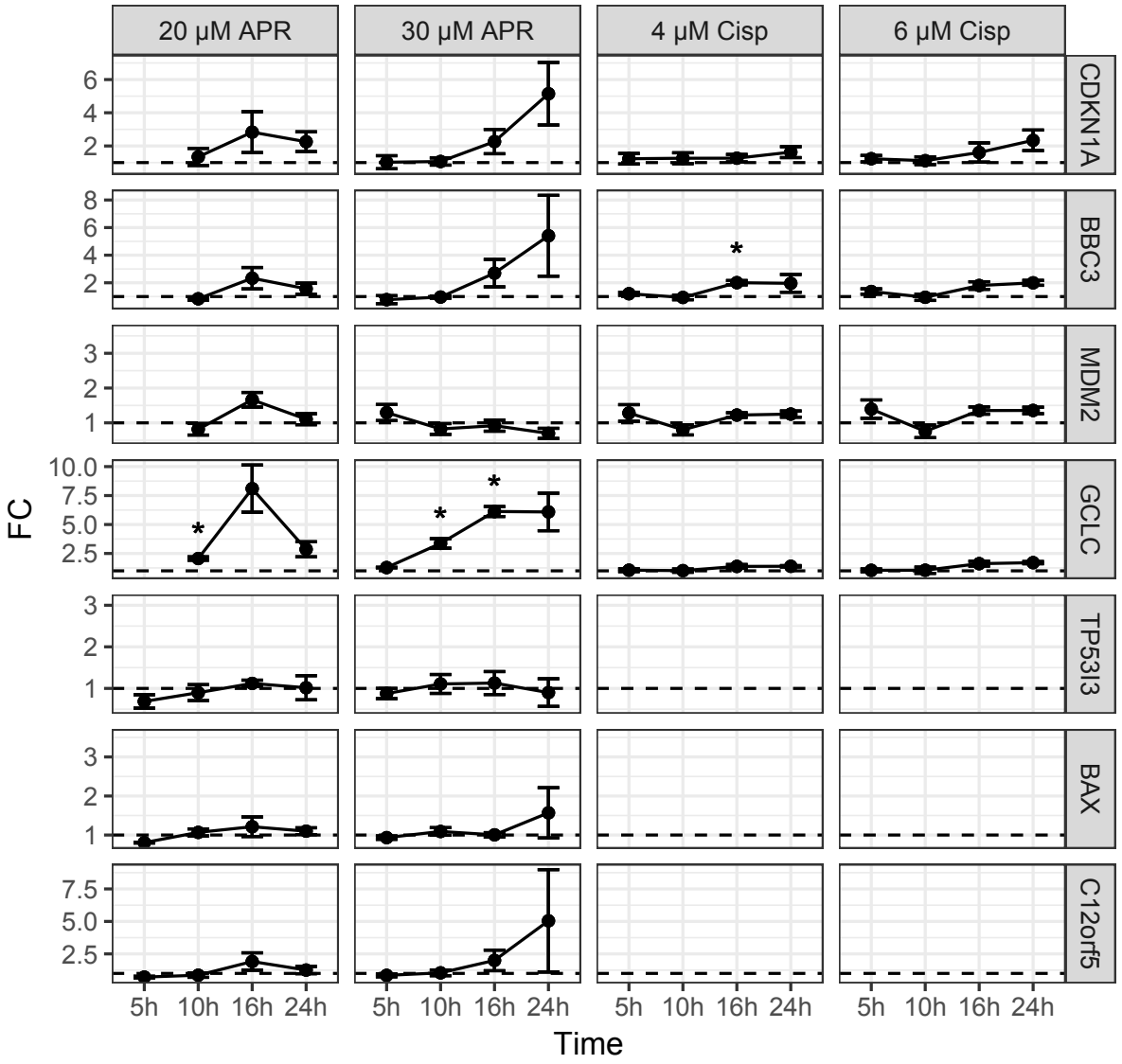

Figure 6.7: Expression of p53- and ROS-responsive genes in OVCAR-3 cells after treatment with APR-246 or cisplatin.

Horizonal dashed lines represent fold-change (FC) of 1, i.e. the vehicle control. Differentially expressed data points (absolute FC > 2 and *P* using student's t-test < 0.05) are decorated with an asterisk. p53-responsive genes *TP53I3*, *BAX* and *C12orf5* were not measured in cisplatin-treated samples.

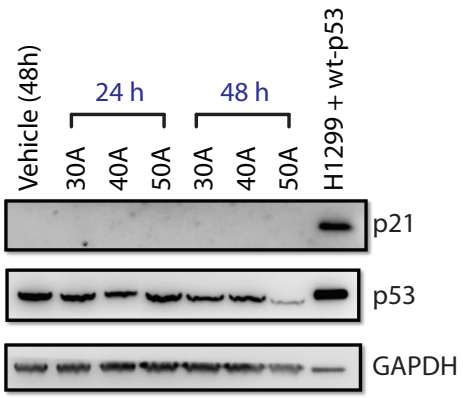

Figure 6.8: Screening for p21 induction in OVCAR-3 cells following APR-246 treatment.
OVCAR-3 cells treated with APR-246 for 24 and 48 hours. H1299 (p53-null) cells transfected with wt-p53 plasmid were used as a positive control for detecting wt-p53 and p21 proteins.

suggesting that the selected APR-246 dose, despite causing a reduction in cell viability as measured by flow cytometry experiments, may not be enough to elicit a strong wt-p53 response, or the drug might be operating through other pathways.

6.3.3 Establishing synergistic conditions of the combination of cisplatin and APR-246 at 48 hours post-treatment

OVCAR-3 cells were treated with higher concentrations of APR-246 to ensure that the dose was sufficiently high to induce a potential p53-response upon treatment. Induction of p21 protein was observed in published studies using ~50 μM APR-246 at 12 - 24 hours post-treatment (Bykov et al. 2005a; Liu et al. 2015; Zandi et al. 2011). Previous experiments showed that ~50 μM APR-246 treatment killed virtually all OVCAR-3 cells at 72 hours post-treatment, and synergistic conditions were optimised at an earlier time point. However, 24 hours of drug treatments may be too early to observe the full extent of cell death; therefore, synergy was optimised at 48 hours post-treatment using higher drug doses. Furthermore, Kuramochi cells, which express mutant-p53 (D281Y) at high levels (Figure 6.2), were also included to investigate effects of APR-246 on a separate cell line.

OVCAR-3 cells were seeded at 4 $\times 10^5$ cells/well in 6 well-plates, treated with high concentrations of APR-246 (50, 60 and 70 μM APR-246) and cell viability was measured at 48 hours post-treatment using flow cytometry (Figure 6.9). Similar experiments were performed on Kuramochi cells (seeding density: 3 $\times 10^5$ cells/well; Figure 6.10). Multiple drug combinations were found to be synergistic in each cell line, amongst which 70A+8C and 80A+20C were chosen for further investigations in OVCAR-3 and Kuramochi cells, respectively (marked with red arrows in Figure 6.11A; N = 3). Next, cell viabilities of OVCAR-3 and Kuramochi cells were measured at 12, 24 and 48 hours post-treatment (Figure 6.11B; N = 3). A reduction in cell viability was evident as early as 12 hours post-APR-246 treatment in OVCAR-3 cells, confirming that cells were responding to the drug dosage. Kuramochi cells, on the other hand, did not show significant reduction in cell viability when treated with both drugs individually for up to 48 hours, but a marked reduction in cell viability was observed in 'A+C' dual drug treatments at 24 and 48 hours.

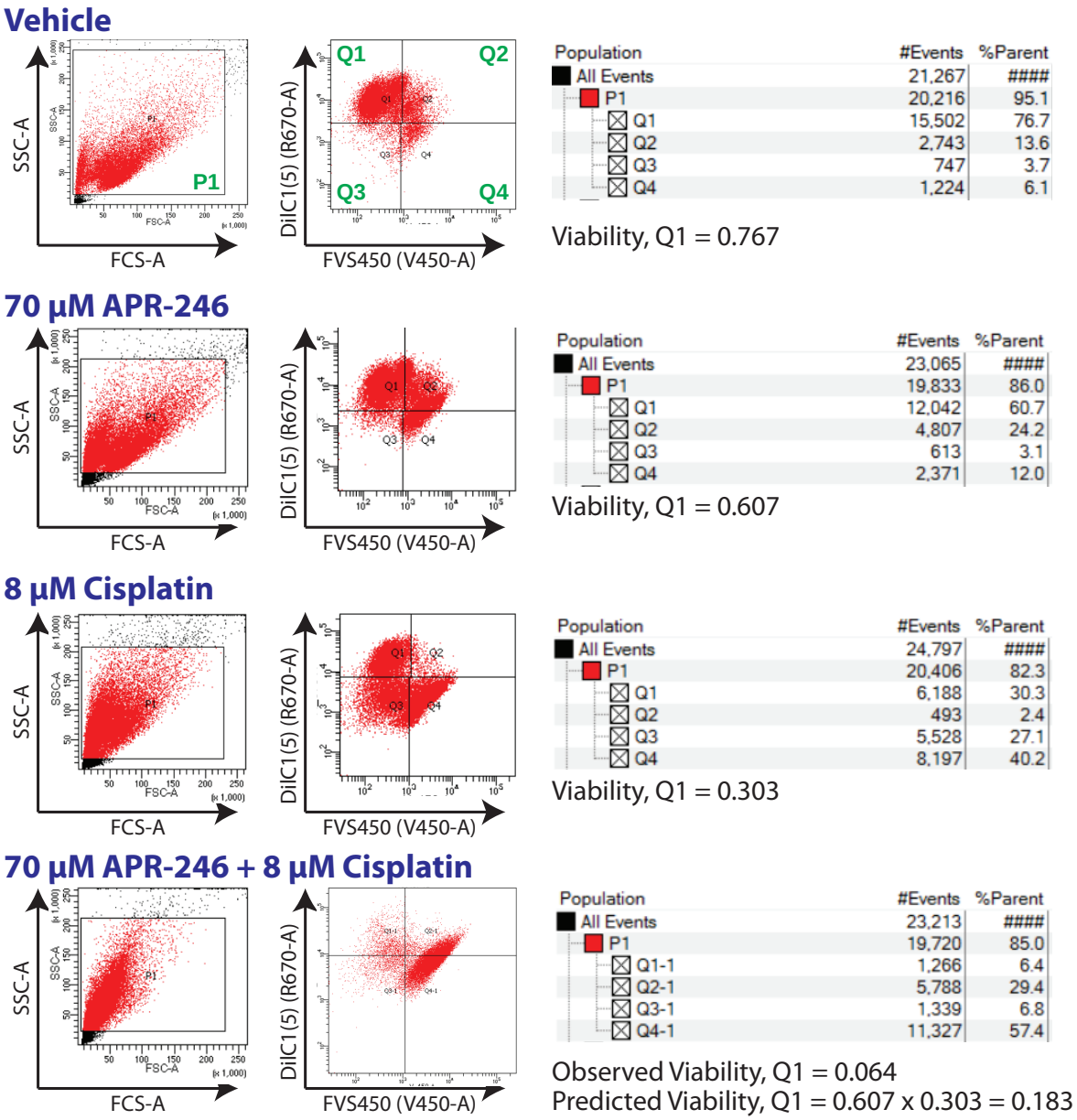

Figure 6.9: Synergistic conditions in OVCAR-3 cells at 48 hours post-treatment
Representative data of the conditions for synergy previously established (Figure 6.11B). OVCAR-3 cells were treated with the vehicle, 70 µM APR-246, 8 µM cisplatin and 70 µM APR-246+8 µM cisplatin for 48 hours. Debris were excluded (Gate P1). Cell viabilities were measured using DilC1(5)/FVS450 dyes in flow cytometry (Gate Q1). Additive model was used to calculate the predicted viability: viability obtained using 70 µM APR-246 × viability obtained using 8 µM cisplatin = 0.607 × 0.303 = 0.183. Survival Index (SI): 0.064 (observed viability of 70 µM APR-246 + 8 µM cisplatin)/0.183 (predicted viability) = 0.350, which is less than 0.8, i.e. synergistic.

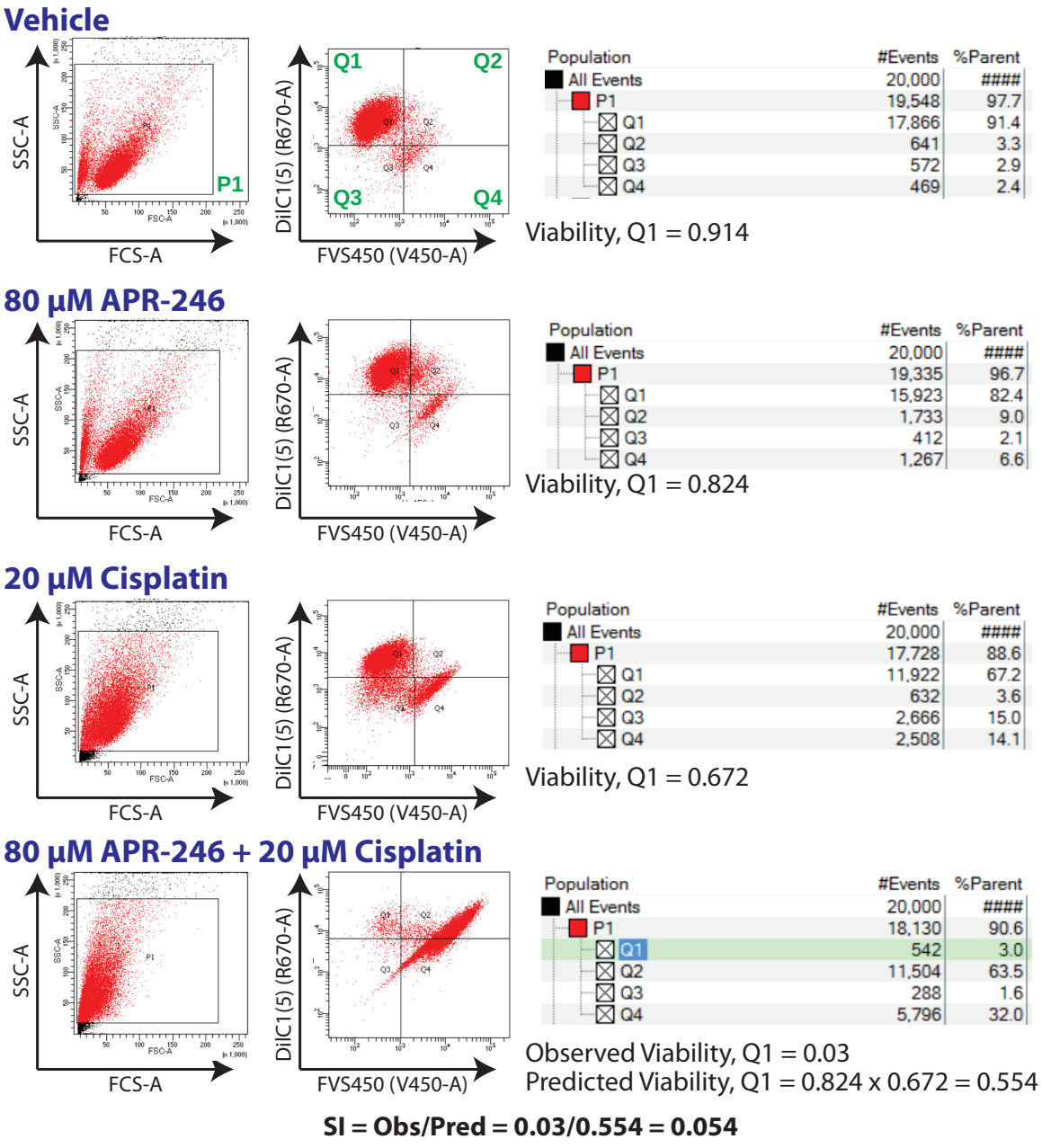

Figure 6.10: Synergistic conditions in Kuramochi cells at 48 hours post-treatment
Representative data of the conditions for synergy previously established (Figure 6.11B). Kuramochi cells were treated with the vehicle, 80 µM APR-246, 20 µM cisplatin and 80 µM APR-246+20 µM cisplatin for 48 hours. Debris were excluded (Gate P1). Cell viabilities were measured using DilC1(5)/FVS450 dyes in flow cytometry (Gate Q1). Additive model was used to calculate the predicted viability: viability obtained using 80 µM APR-246 × viability obtained using 20 µM cisplatin = 0.824 × 0.672 = 0.554. Survival Index (SI): 0.03 (observed viability of 80 µM APR-246 + 20 µM cisplatin)/0.554 (predicted viability) = 0.054, which is less than 0.8, i.e. synergistic.

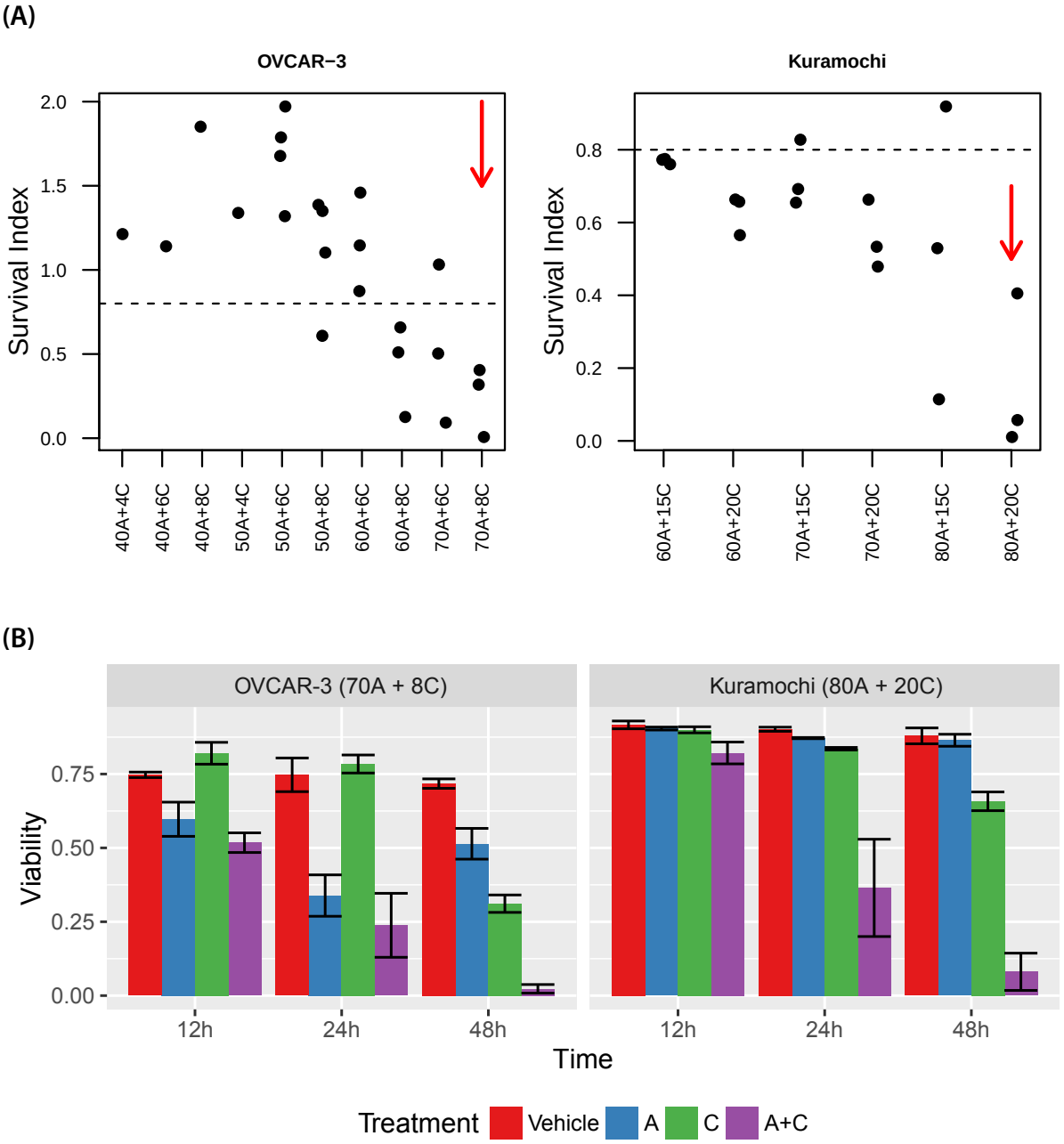

Figure 6.11: Optimisation of synergistic conditions in OVCAR-3 and Kuramochi cells at 48 hours post-treatment using higher drug doses

(A) Screening for synergistic conditions at 48 hours post-treatment in OVCAR-3 and Kuramochi cells using higher APR-246 and cisplatin doses. Red arrows highlight drug combinations that were chosen for further studies in OVCAR-3 (70A+8C) and Kuramochi (80A+20C) cells (N = 3). Dashed lines represent SI of 0.8, below which drug interactions are classified as synergistic. **(B)** Quantification of cell viabilities in OVCAR-3 and Kuramochi cells treated at synergistic combinations for 12, 24 and 48 hours (N = 3).

Expression of *CDKN1A/p21*, *BBC3* and *GCLC* were measured 4, 8, 12, 16 and 24 hours post-treatment (Figure 6.12; N = 3). Again, the p53-responsive gene *CDKN1A* was barely induced by 2-fold whereas *BBC3* remained relatively unaffected in both cell lines treated with APR-246 for up to 24 hours. In contrast, ROS-responsive *GCLC* was induced by ~3-fold following treatment with APR-246 as early as 8 hours in OVCAR-3 cells. These data were consistent with the earlier results optimised at 72 hours for drugs treatments using lower doses (Figure 6.7), supporting the hypothesis that APR-246 failed to activate wt-p53 activities in OVCAR-3 cells. Interestingly, p21 was found to be DE in Kuramochi cells treated with cisplatin for 16 and 24 hours (Figure 6.12), suggesting that transcription of *CDKN1A* may not be entirely exclusive to wt-p53.

RNA-seq was employed to gain a transcriptome-wide overview of the cellular response to the drugs and identify pathways resulting in the synergy observed. OVCAR-3 and Kuramochi cells treated for 12 and 24 hours were selected for RNA-seq, respectively, as they represented the earliest time point where differences in gene expression were observed in the corresponding cell lines. In addition, the viability of OVCAR-3 cells treated for 12 hours was comparable with Kuramochi cells treated for 24 hours (Figure 6.11), representing functionally equivalent points. Both cells were also equivalent in cell viabilities at 48 hours post-treatment where synergy was optimised.

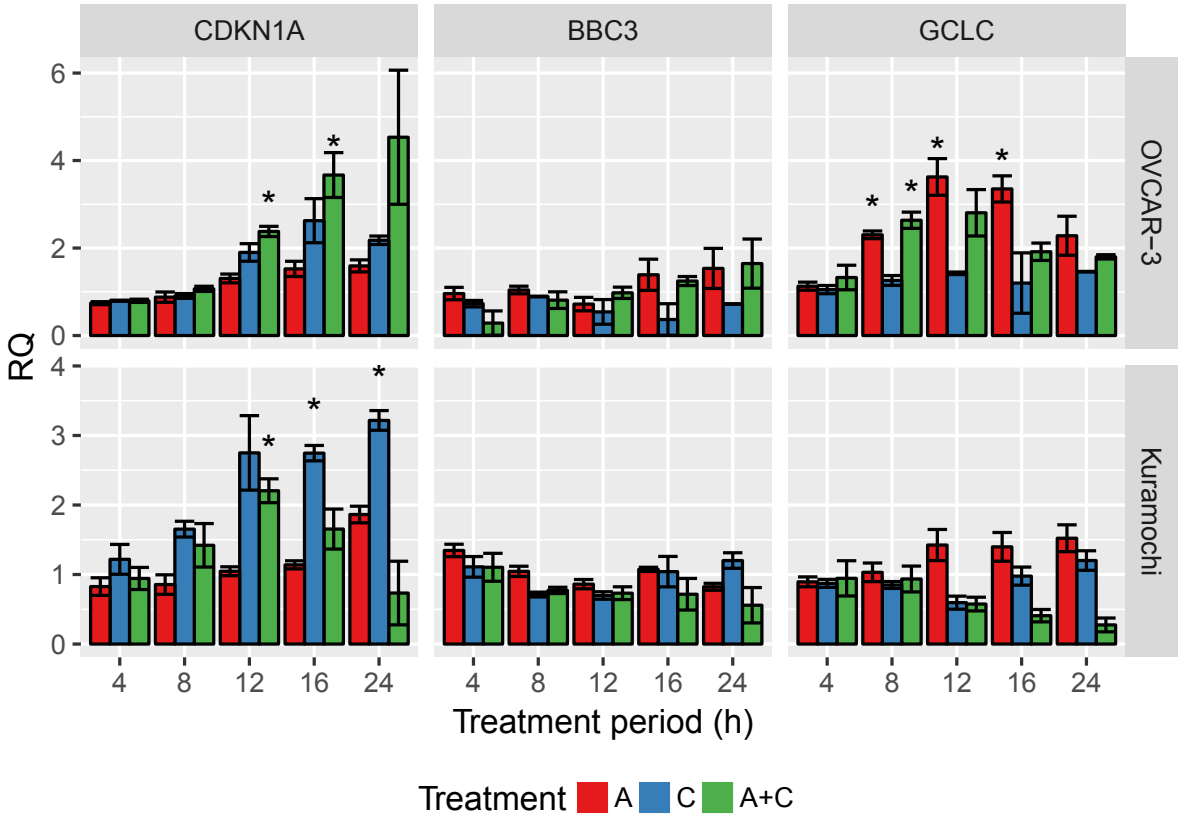

Figure 6.12: Assessing whether higher drug concentrations induced p21 using a time-course

OVCAR-3 and Kuramochi cells were treated with 70A+8C and 80A+20C, respectively, with both drugs individually as well as their indicated combinations. RNA was collected at 4, 8, 12, 16 and 24 hours post-treatment (N=3), and levels of p53-responsive genes *CDKN1A/p21* and *BBC3/PUMA* as well as ROS-responsive *GCLC* were quantified using RT-qPCR. Vehicle control was used for normalisation, and excluded from plots since its RQ = 1. RQ: relative quantification, '*' denotes absolute RQ > 2 and $P < 0.05$, 'A' APR-246, 'C' cisplatin and 'A+C' APR-246 + cisplatin

6.3.4 Investigating transcriptome-wide effects of APR-246 using RNA-seq

RNA-seq was employed to investigate the global changes in transcription in OVCAR-3 and Kuramochi cells following treatment with APR-246 for 12 and 24 hours, respectively. This work was conducted in collaboration with bioinformaticians Dr. Nenad Bartonicek and Mr. James Torpy of The Garvan Institute of Medical Research, Sydney, Australia. Quality control, library preparation, RNA-seq and processing of the data was perform at the Garvan. Analyses presented in this section were conducted by the candidate following consultation with the bioinformaticians.

6.3.4.1 Comparison of RNA-seq results with RT-qPCR

RT-qPCR remains the 'gold standard' to validate results of RNA-seq experiments, and expression of *CDKN1A*, *BBC3* and *GCLC* in OVCAR-3 and Kuramochi cells in a time-course as determined previously could be used as positive controls to validate the results obtained from RNA-seq (Figure 6.12). Expression of *CDKN1A*, *BBC3* and *GCLC* based on RNA-seq (Figure 6.13) were comparable with RT-qPCR, and only *GCLC* was found to be differentially expressed at 12 hours post-APR-246 treatment in OVCAR-3 cells using both methods.

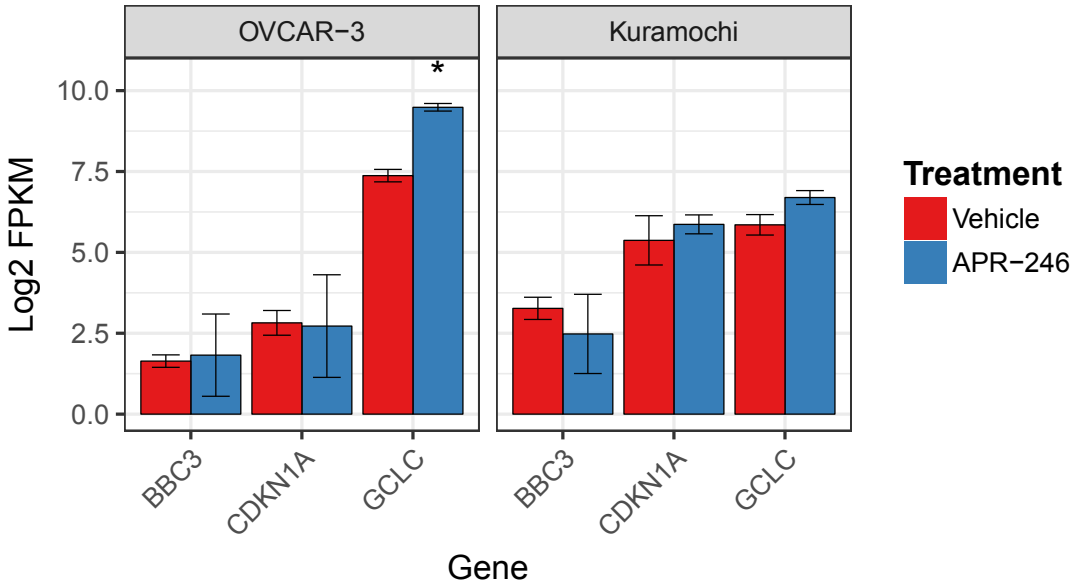

Figure 6.13: Validation of RNA-seq results with RT-qPCR
mRNA levels of BBC3/PUMA, CDKN1A and GCLC were measured by RT-qPCR following 12 and 24 hours of APR-246 treatment in OVCAR-3 and Kuramochi cells, respectively (Figure 6.12). The expression of the three genes quantified by RNA-seq in terms of Fragments Per Kilobase of transcript per Million mapped reads (FPKM). Higher FPKM indicate a higher number of sequences mapped to a gene, hence, higher abundance of a transcript in a sample. Amongst the three mRNAs, only GCLC was found to significantly (absolute fold-changed > 2 and $P < 0.05$) induced upon 12 hours of APR-246 treatment in OVCAR-3 cells, which is comparable with results of the RT-qPCR experiment, suggesting that RNA-seq was comparable to RT-qPCR. Identical RNA samples were used in RT-qPCR and RNA-seq.

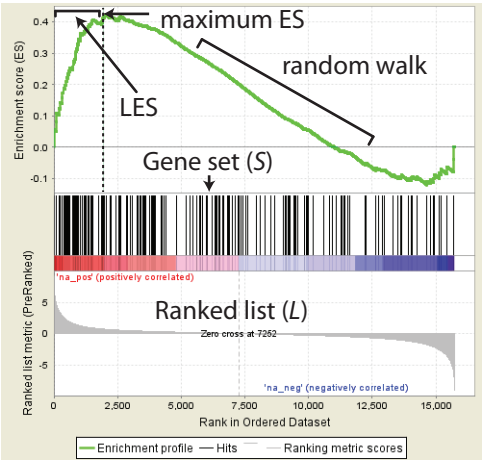

Figure 6.14: Overview of Gene Set Enrichment Analysis
Gene Set Enrichment Analysis (GSEA) calculates whether genes in a pre-determined gene set *S* behave significantly different between two conditions or biological states. More specifically, it measures whether the position of *S* in a ranked list *L* (ordered by Fold-change (FC) or $\log_2$-FC) is non-random and significantly shifted towards upregulated, downregulated genes or both. In our case, *S* and *L* could represent known genes downstream of p53 and FC of all genes measured in an experiment, respectively. A score is calculated by walking down the list *L*. The score of the running-sum statistic is increased upon encountering a member of *S* and decreased when the encountered gene is not in *S*. The Enrichment score (ES) is the maximum deviation from 0 (Subramanian et al. 2005). Genes at or immediately before the ES constitute the leading edge subset (LES) which identifies the genes contributing to the ES.

6.3.4.2 Investigation of the p53-response in the RNA-seq dataset

GSEA (Subramanian et al. 2005) was used to calculate enrichment of the p53 pathway following treatment with APR-246. The calculation of ES is straight forward (explained in Figure 6.14). Numerous pre-designed gene sets representing canonical pathways and the software are available through the Broad Institutes's MSigDB database[†]. Gene sets are grouped into several categories. The 'Hallmark' gene sets summarise and represent well-defined biological states or processes. The 'C2' gene sets are curated from various sources such as online pathway databases, the biomedical literature and knowledge of experts in the field. p53 gene sets from four well-known sources were used for further analyses: one from the 'Hallmark' and three from the 'C2' categories (Biocarta, KEGG and the protein interactions database (PID)).

Since APR-246 was proposed to work by alkylating the cysteine residues irrespective of the missense mutations in *TP53* (Lambert et al. 2009), the expression data from both

[†]`http://software.broadinstitute.org/gsea/msigdb`

cell lines were combined to test if the potential induction of the p53 pathway was common between both cell lines following APR-246 treatment (Table 6.1A). Combining data from both cell lines simplified the analysis and increased the number of biological replicates (N), which then improved the statistical power to detect a change. If a phenomenon, such as enrichment of the p53 pathway, is not consistent in both cell lines, the combined data should have a higher variance and likely to result in statistically non-significant results ($P > 0.05$). In addition, these analyses was repeated on both cell lines individually (Table 6.1B-C).

(A) Both cell lines combined

		Weighted-FC					Weighted-Log2-FC				
Name	**Size (S)**	**ES**	**NES**	***P***	**LES**	**% (LES/S)**	**ES**	**NES**	***P***	**LES**	**% (LES/S)**
Biocarta	16	0.32	0.82	0.56	13	81%	0.45	1.09	0.37	7	38%
KEGG	64	0.26	0.73	0.70	11	16%	0.30	0.99	0.47	15	22%
PID	125	0.62	1.85	0.05	13	10%	0.39	1.44	0.00	19	15%
Hallmark	194	0.25	0.77	0.76	24	12%	0.27	1.05	0.34	32	16%

(B) OVCAR-3

		Weighted-FC					Weighted-Log2-FC				
Name	**Size (S)**	**ES**	**NES**	***P***	**LES**	**% (LES/S)**	**ES**	**NES**	***P***	**LES**	**% (LES/S)**
Biocarta	16	0.26	0.56	0.76	4	19%	0.42	1.03	0.38	4	19%
KEGG	64	0.20	0.43	0.94	8	11%	0.28	0.91	0.63	9	13%
PID	125	0.67	1.52	0.11	4	3%	0.33	1.18	0.13	23	18%
Hallmark	194	0.29	0.66	0.85	16	8%	0.26	0.96	0.59	20	10%

(C) Kuramochi

		Weighted-FC					Weighted-Log2-FC				
Name	**Size (S)**	**ES**	**NES**	***P***	**LES**	**% (LES/S)**	**ES**	**NES**	***P***	**LES**	**% (LES/S)**
Biocarta	16	0.37	0.64	0.76	12	75%	0.50	1.14	0.26	7	38%
KEGG	64	0.28	0.51	0.97	13	20%	0.26	0.76	0.91	13	20%
PID	125	0.56	1.07	0.35	15	12%	0.36	1.17	0.14	38	30%
Hallmark	194	0.30	0.60	0.99	16	8%	0.26	0.88	0.82	51	26%

Table 6.1: GSEA on four p53 pathways using weighted-FC and weighted-$\log_2$-FC

FC: fold-change, Size (S): size of the gene set, ES: enrichment score, NES: normalised ES, LES: number of genes in the leading edge set, %(LES/S): percentage of genes used to calculate the ES.

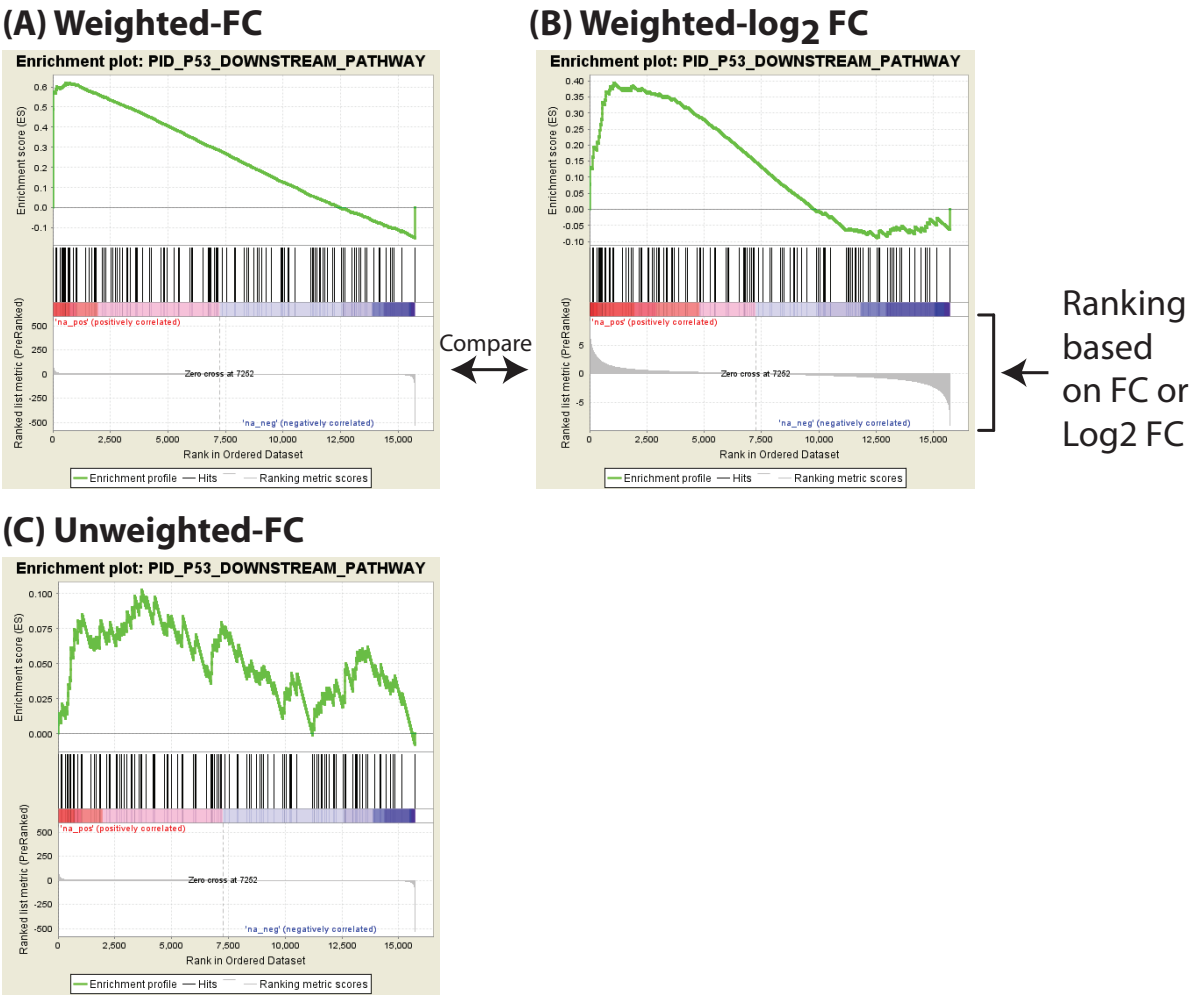

Figure 6.15: Enrichment plots for the p53 gene set from the Protein Interaction Database (PID) using various parameters in GSEA

Gene Set Enrichment Analysis (GSEA) performed using the p53 downstream genes provided by the protein interactions database (PID) weighted by their **(A)** fold-change (FC) or **(B)** $\log_2$-FC in our experiment. Using $\log_2$-FC resulted in more uniform changes in fold-changes as seen in the waterfall plots under the 'barcode'-like plots in (A-B). **(C)** GSEA was performed on the PID-p53 gene set using unweighted-FC.

The list L could be sorted by FC, $\log_2$-FC or simply by the rank or position of a gene in L. Preliminary analysis showed that 'weighted' analysis, which used a magnitude of FC/$\log_2$-FC in calculating the ES, was superior to unweighted analysis based purely on ranking of the genes in L (Figure 6.15C). Weighted GSEA using four gene sets was performed on the combined data and each cell line individually as well as FC or $\log_2$-FC (Table 6.1).

As shown in Table 6.1, only one gene set (the PID p53 gene set; shortened as PID-p53 hereafter) out of four was found to be significantly upregulated when GSEA was performed

	Weighted-Log2-FC					
Cells	**Size (S)**	**ES**	**NES**	***P***	**LES**	**% (LES/S)**
Combined	114	0.31	1.12	0.179	15	13%
OVCAR-3	114	0.32	1.16	0.169	18	15%
Kuramochi	114	-0.32	-1.01	0.429	36	31%

Table 6.2: p53 pathway eEnrichment scores for cell lines treated with APR-246 based on a published consensus list of p53-responsive genes (Fischer 2017).

on the combined dataset using FC or $\log_2$-FC; none of the gene sets were statistically enriched when cell lines were analysed individually. Enrichment plots for PID-p53 are shown in Figure 6.15A, B. Although GSEA based on FC and $\log_2$-FC gave similar results, results of $\log_2$-FC should be more reliable because (1) log-transformation is often employed to convert skewed data to normally-distributed data, (2) the waterfall plots for ranked list L under the gene set S ('barcode'-like plots in Figure 6.15A, B) look more uniform using $\log_2$-FC, and (3) on average, a higher number of genes were used to calculate the ES using $\log_2$-FC versus FC (compare LES/S in Table 6.1), making the analysis more robust.

6.3.4.3 Meta-analysis of p53-target genes

Fischer 2017 curated a list of potential 3,509 p53-target genes from 13 genome-wide studies. Interestingly, a majority of the genes (2261 out of 3509; 64.4%) were specific to only one dataset, even when multiple studies were analysed under the same conditions, i.e. HCT116 cells treated with 5-Fluorouracil or MCF-7 cells treated with Nutlin-3a (Fischer 2017). This variance suggests the presence of false positive and false negative results when relying on only one dataset. To identify a consensus list of p53-responsive genes, Fischer 2017 suggested a list of 116 genes that were found to be upregulated by p53 in at least six datasets. Canonical p53-response genes *CDKN1A/p21*, *RRM2B*, *BAX* and *MDM2* were included in the list (see Table 6.3 for their general role in the p53 pathway). The candidate created a custom gene set consisting of these genes, and performed GSEA using weighted $\log_2$-FC on the data from both cell lines combined or treated individually (Table 6.2). Two genes out of 116 were not detected in our dataset, resulting in the size of the gene set of 114 genes. The p53 pathway was not found to be enriched in all combinations tested (Table 6.2 and Figure 6.16).

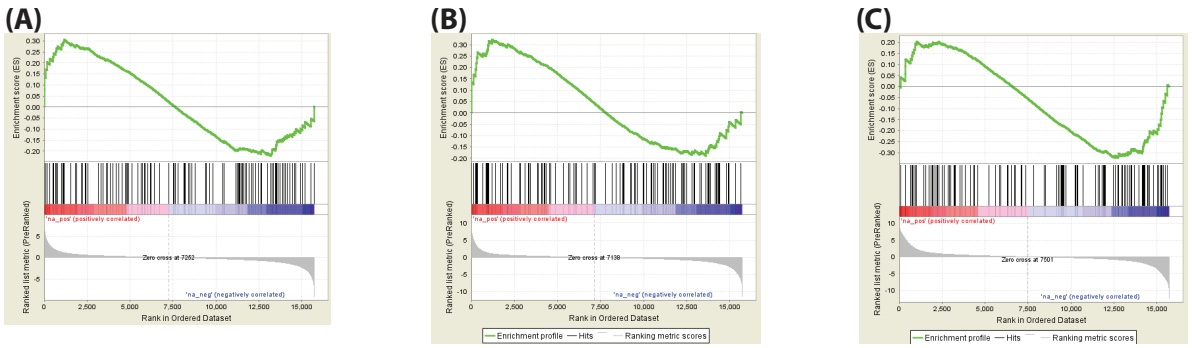

Figure 6.16: Enrichment plots for the 114 p53-responsive genes present in at least six studies curated by Fischer 2017.
Fischer 2017 identified 116 genes that were present in at least six genome-side studies that quantified cellular response to activation of wt-p53. 114 out of 116 genes were present in our dataset. GSEA was performed using weighted $\log_2$-FC on the data from both cell lines combined or treated individually. **(A)** OVCAR-3 and Kuramochi cells combined, **(B)** OVCAR-3 cells and **(C)** Kuramochi cells.

Gene	Function
RRM2B	DNA repair by supplying pre-cursors
CDKN1A/p21	p53-dependent downregulation of cell cycle genes
MDM2	E3 ligate, mediates degradation of p53
GDF15	member of TGF-B family, inflammation and apoptosis
GADD45A	controls G2/M progression
BAX	control mitochondria membrane permeabilisation
BBC3/PUMA	regulator of apoptosis
PMAIP1/NOXA	regulator of apoptosis

Table 6.3: Functions of some of the canonical p53-response genes
RRM2B: ribonucleotide reductase regulatory TP53 inducible subunit M2B, *CDKN1A/p21*: Cyclin Dependent Kinase Inhibitor 1A, *MDM2*: Mouse double minute 2 homologue , *GDF15*: Growth/differentiation factor 15, *GADD45A*: Growth Arrest And DNA Damage Inducible Alpha, *BAX*: BCL2 Associated X, *BBC3/PUMA*: BCL2 Binding Component 3 and *PMAIP1/NOXA*: Phorbol-12-Myristate-13-Acetate-Induced Protein 1. Data for this table was supplied by Bieging and Attardi 2012; Zilfou and Lowe 2009 and Fischer 2017.

	Weighted-Log2-FC					
Cells	**Size (S)**	**ES**	**NES**	***P***	**LES**	**% (LES/S)**
Combined	181	0.42	1.65	0	51	28%
OVCAR-3	181	0.32	1.24	0.025	46	25%
Kuramochi	181	0.42	1.43	0.003	51	28%

Table 6.4: Enrichment of genes downstream of NRF2, a ROS-responsive transcription factor

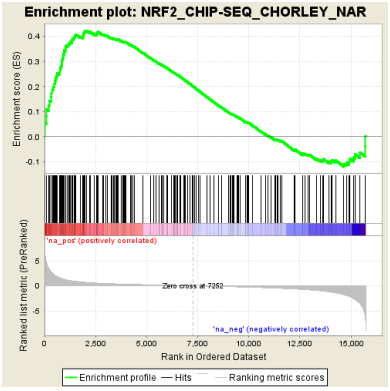

Figure 6.17: Enrichment plot for NRF2-pathway upon APR-246 treatment
Note: Combined data of both cell lines were used in this analysis.

6.3.4.4 Testing upregulation of ROS upon APR-246 treatment

Transcription factor nuclear factor erythroid 2-related factor 2 (NRF2) plays a central role in sensing oxidative stress (Gorrini, Harris, and Mak 2013). Analogous to the p53-MDM2 axis, NRF2 is present at low levels in resting conditions due to actions of the Kelch-like ECH-associated protein 1 (KEAP1)-Cullin 3 E3 ligase complex that marks NRF2 for ubiquitin-mediated protein degradation (Gorrini, Harris, and Mak 2013). KEAP1 is modified under oxidative conditions and unable to bind to NRF2, leading to the stabilisation and translocation of NRF2 to the nucleus where it transcribes key genes responsible for glutathione (GSH) biosynthesis (Gorrini, Harris, and Mak 2013). NRF2 directly transcribes *GCLC* and the Glutamate-Cysteine Ligase Modifier Subunit (*GCLM*) necessary for formation of the glutamate–cysteine ligase — an enzyme conducting the rate-limiting step of GSH synthesis, reaction of glutamate with cysteine (Gorrini, Harris, and Mak 2013). In addition, NRF2 also transcribes cysteine transporter XCT coded by solute carrier family 7 member 11 (*SLC7A11*) to increase intracellular abundance of cysteine (Gorrini, Harris, and Mak 2013).

Using transcription of genes downstream of NRF2 as a proxy for ROS response, GSEA was attempted to test for enrichment of the ROS response followed by quality control check

by visualisation of FPKM using bar plots. Only the Biocarta collection on the MSigDB had a gene set available for ROS compared to other well-known sources such as KEGG. However, the Biocarta NRF2 gene set had only 13 members, which was inadequate for performing GSEA. Some gene sets such as 'HOUSTIS_ROS' had >15 genes but were specific to diseases such as type 2 diabetes, and were excluded for GSEA. A study conducted by Chorley et al. 2012 used ChIP-seq to identify direct transcriptional targets of NRF2 in human lymphoblastoid cells treated with the ROS-inducing agent sulforaphane. Normalised ChIP-seq data was available in Supplementary File 1 of the publication, and a custom gene set was built by selecting 181 genes with high confidence ChIP-seq peaks that had at least one antioxidant responsive element (ARE) in the vicinity. Importantly, *GCLC*, *GCLM* and *SLC7A11* were present in this gene set.

As show in Table 6.4 and Figure 6.17, the NRF2 pathway was found to be significantly upregulated following treatment with APR-246 in OVCAR-3 and Kuramochi cells analysed individually as well as in combination, suggesting a presence of high intracellular levels of ROS. FPKM values of 51 genes comprising the LES in the combined dataset are shown in Figure 6.18 in the order of their ranking used in GSEA. A number of top ranked upregulated genes following APR-246 treatment, shown in the 'left' side of the enrichment plot in Figure 6.17, were genuinely found to be DE (absolute FC >2 and FDR-P < 0.05), validating the result of GSEA.

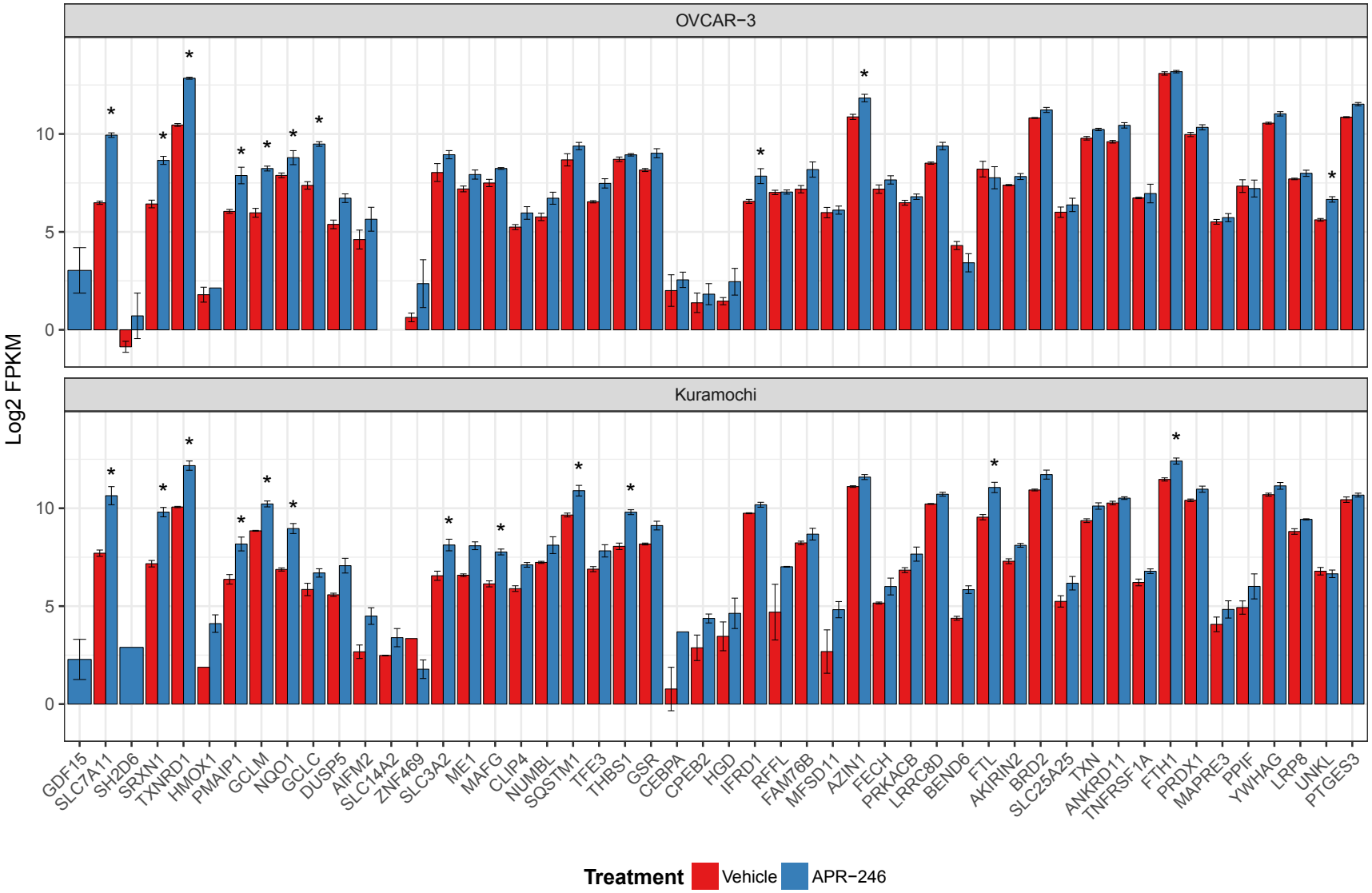

Figure 6.18: Expression of the genes in the leading edge subset (LES) used for calculating enrichment score (ES) for NRF2 pathway.
Genes shown from left to right are sorted in the order of ranking as used by GSEA for a custom gene set of NRF2-responsive genes identified according to the ChIP-seq study by Chorley et al. 2012. '*' absolute FC >2 and FDR-*P* < 0.05

6.3.4.5 Effect of APR-246 on noncoding RNAs

In addition to protein coding genes, p53 also influences expression of microRNAs such as miR-34a (Figure 6.19A), (He et al. 2007) and lncRNAs such as lincRNA-p21 (Huarte et al. 2010), PANDA (Hung et al. 2011), Pint (Huarte et al. 2010), PR-lncRNA-1 (Sánchez et al. 2014), PR-lncRNA-10 (Sánchez et al. 2014), NORAD (Lee et al. 2016), TUG1 (Guttman et al. 2009; Khalil et al. 2009), PVT1 (Barsotti et al. 2012), LINP1 (Zhang et al. 2016c), DDSR1 (Sharma et al. 2015) and DINO (Schmitt et al. 2016). Since the field is still evolving, only seven lncRNAs downstream of p53 (*PANDA*, *Pint*, *NORAD*, *TUG1*, *LOC105371267*, *PVT1*, *LINP1*) were specific to the human species with annotated sequences on the Ensembl genome browser[‡], of which five were detectable in our dataset (Figure 6.19B). Only PVT1 out of five lncRNAs was found to be DE; however, it does not appear DE upon examining its FPKM in Figure 6.19B. The bioinformaticians advised that FPKM and statistics (FC and *P* values) were determined using separate algorithms, and the algorithm calculating statistics (edgeR) was more accurate in their opinion. Even though miR-34a was found to be a direct target of wt-p53 by He et al. 2007, it was not found to be DE following APR-246 treatment in OVCAR-3 ($P = 0.071$) and Kuramochi cells ($P = 0.098$).

6.3.5 Testing the specificity of APR-246 for mutant-p53

p53-null SKOV-3 cells (c.267del1, resulting in a frame-shift (Bamford et al. 2004)) were transfected with 0.25, 0.5 or 1 µg of empty vector (V0) or plasmid harbouring wt-p53 or the R248Q mutation (harboured in OVCAR-3 cells), seeded into 96 well plates at 24 hours post-transfection and treated with a range of APR-246 concentrations for 72 hours to test whether the IC_{50} values, measured by the MTS assay, were dependent on the wild-type or mutant status of p53 as well as the amounts of plasmid transfected. If effects of APR-246 are specific to mutant-p53, higher levels of transfected plasmid should result in a dose-dependent reduction in IC_{50} specific to the R248Q mutation. In contrast, cell death due to other effects such as induction of ROS would be common in all plasmid transfections.

Levels of wild-type and mutant-p53 in SKOV-3 cells at 24 hours post-transfection is shown in Figure 6.20A. As expected, p53 remained undetected in untransfected (UT) cells or cells transfected with different amounts of the empty vector, whereas transfection with wt-p53 or mutant-p53 resulted in higher levels of p53. In the case of wt-p53, the expression of p53 was dependent on the amount of plasmid transfected for all biological replicates (N=3). The same trend was observed in 2 out of 3 replicates of cells transfected

[‡]last checked on 9th June 2017.

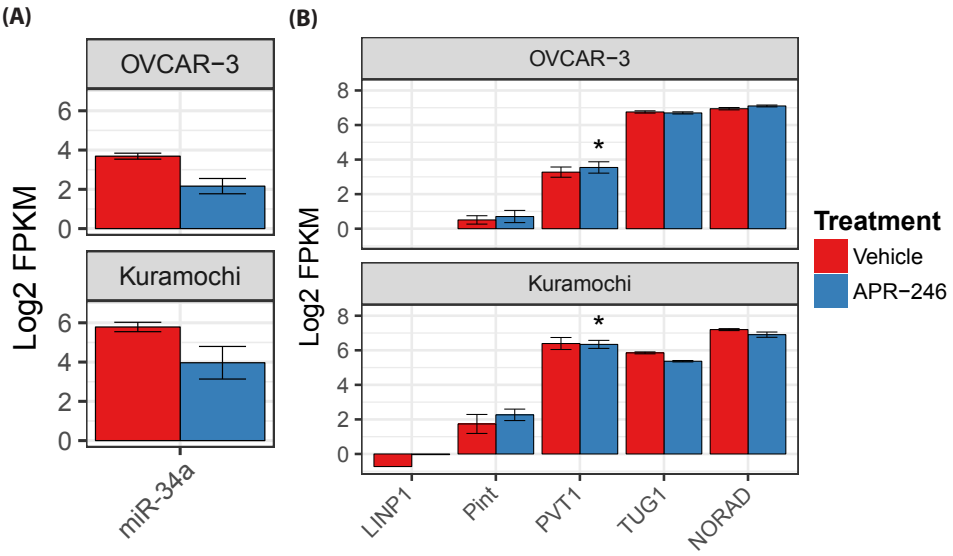

Figure 6.19: Effect of APR-246 on noncoding RNAs
Effect of APR-246 treatment on wt-p53-responsive **(A)** miR-34a and **(B)** five lncRNAs. PVT1 was found to be DE following APR-246 treatment in both cell lines. Although mean FPKM values for PVT1 look similar in both cell lines, bioinformaticians advised that FPKM and FC values were determined using separate algorithms, and the algorithm calculating FC (edgeR) was more accurate in their opinion. '*' absolute FC >2 and FDR-$P < 0.05$.

with mutant-p53. Both wild-type and mutant-p53 had identical molecular weights. p21 downstream of wt-p53 was immunoblotted to confirm that the mutant-p53 was indeed mutant, and p21 was detected only in the cells transfected with wt-p53. Remarkably, p21 was detectable in the cells transfected with 0.25 µg of wt-p53, in which the wt-p53 itself remained undetectable (Figure 6.20A). Thus the positive controls of the experiment showed results as expected. No differences were observed in background-corrected absorbance values for the transfected cells treated with vehicle (one-way ANOVA; $P = 0.252$), suggesting that transfection of V0, wt-p53 or mutant-p53 by itself did not result in significant cell death (Figure 6.20B).

Processed data from the MTS assay used for calculating the IC_{50} values are shown in Figure 6.21. Data was normalised to the vehicle control prior to the calculations. A significant decrease in IC_{50} was observed between cells transfected with 0.25 versus 1 µg of empty vector V0 ($P < 0.05$, marked with the red line over the bar graph in Figure 6.22A). To normalise the reduction in IC_{50} due to the amount of plasmid transfected, IC_{50} for wild-type or mutant-p53 were divided by the IC_{50} of the V0 for a given amount of plasmid (Figure 6.22B).

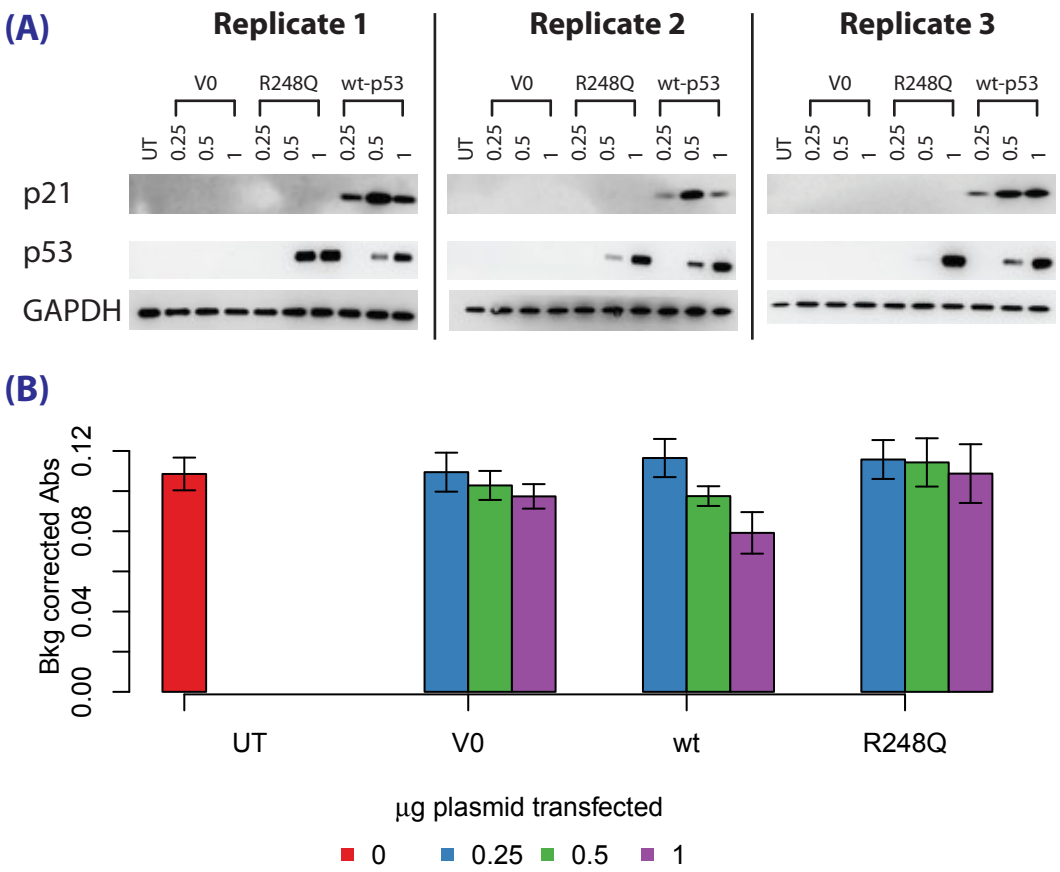

Figure 6.20: Effect of plasmid transfections on the levels of p53 and p21 as well as cell viabilities.

(A) Protein expression of p53 and p21 at 24 hours post-transfection in three biological replicates upon varied amounts of plasmid transfected. **(B)** Background-corrected absorbance values of the MTS assay for transfected cells treated with the vehicle. No difference amongst treatments was observed (one-way ANOVA; $P = 0.252$). UT: untransfected, V0: empty vector.

The degree of wt-p53-like activities restored from mutant-p53 upon APR-246 treatment could be roughly inferred by matching the IC_{50} values of mutant-p53 to wt-p53 obtained using different amounts of transfected plasmid. SKOV-3 cells transfected with 1 µg of plasmid harbouring wt-p53 had a significantly lower IC_{50} compared to V0 for the same amount of plasmid ($P < 0.05$), reflecting the tumour-suppressive actions of wt-p53 and benchmarking the expected IC_{50} if 100% of the transfected 1 µg of mutant-p53 was converted to wt-p53. A statistically significant difference in 1 µg wild-type versus mutant-p53 was observed ($P < 0.05$; highlighted in red lines above the bar plot in Figure 6.22B). However, the IC_{50} of cells transfected with 1 µg mutant-p53 was not only higher than 1 µg wt-p53 but also 0.25 µg mutant-p53 (highlighted in the blue line), which strongly

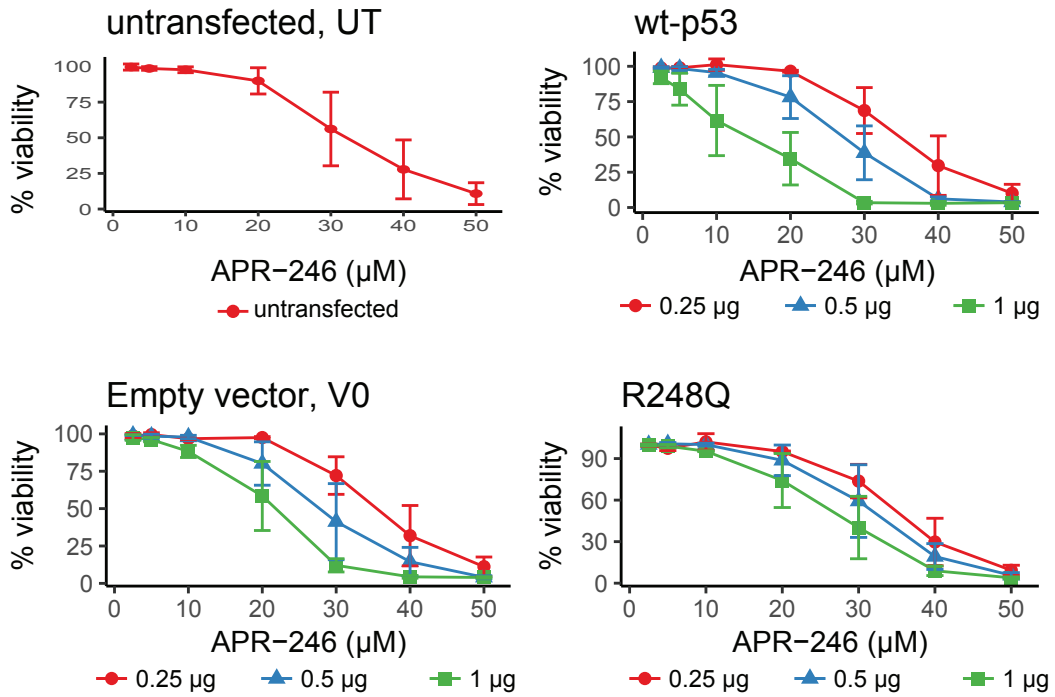

Figure 6.21: DRCs of SKOV-3 cells transfected with varied amounts of empty vector (V0) or plasmid harbouring wt-p53 or the *TP53* R248Q mutation and treated with APR-246.

contradicted the hypothesis that a dose dependent decrease in IC_{50} should be observed by increasing the amounts of mutant-p53 if APR-246 is specific to mutant-p53. Intriguingly, the IC_{50} of 1 μg mutant-p53 was not found to be statistically different to that of 1 μg V0 by one-way ANOVA ($P = 0.10$), but a t-test indicated that this comparison was statistically significant ($P = 0.037$). Nonetheless, an increase of ~30% in IC_{50} values of 0.25 μg and 1 μg mutant-p53 is key evidence that APR-246 is not specific for mutant-p53. Mutant-p53 is likely to promote cellular growth and/or drug resistance, explaining the dose-dependent increase in IC_{50}.

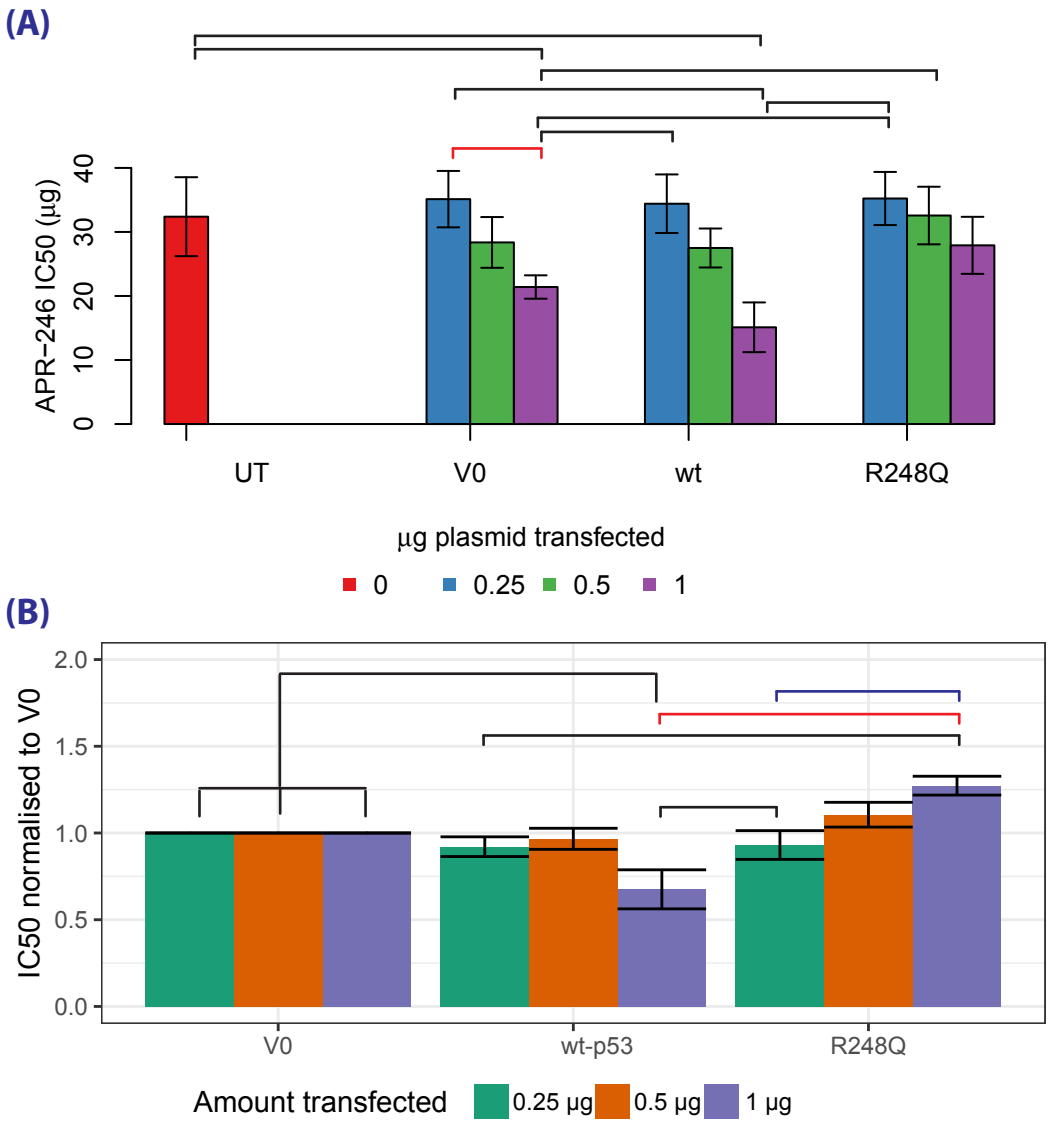

Figure 6.22: Effects of wild-type or mutant-p53 on the IC_{50} of APR-246 in the p53-null SKOV-3 cell line.

(A) IC_{50} obtained by normalising the data with vehicle-treated cells. As marked with red lines, a statically significant difference in IC_{50} values of 0.25 versus 1 µg V0 was observed, suggesting that higher amounts of V0 had a detrimental effect on IC_{50}. **(B)** IC_{50} values for wild-type or mutant-p53 were divided by the IC_{50} of the V0 for a given amount to account for a reduction in IC_{50} due to the amount of plasmid transfected. All statistically significant comparisons ($P < 0.05$) are marked with lines above the graph for completeness whereas key comparisons are marked in red and blue lines above the bar plot.

6.4 Discussion and future directions

The transcription factor p53 influences a myriad numbers of protein-coding and ncRNAs. Given that p53 is mutated at a high frequency in multiple cancers, and almost universally mutated in HGSOC, it is likely that the transcriptomic signature of mutant-p53 is markedly different than wt-p53 and its effects on lncRNAs remain largely unknown. In this chapter, we investigated transcriptome-wide effects of a drug knowns as APR-246 that has been reported to restore wt-p53 activities from mutant-p53 (Bykov et al. 2016; Bykov et al. 2005b; Lambert et al. 2010; Rkaeus et al. 2010; Zache et al. 2008a).

6.4.1 Activation of wt-p53 activity in OC cell lines upon APR-246 treatment

Because APR-246 has been reported to be synergistic with cisplatin in ovarian cancer (Mohell et al. 2015), we reasoned that mechanisms of synergy could be studied using transcriptome-wide analysis by carefully selecting time-points and drug doses. Synergistic conditions were optimised several times to accommodate different end-points and drugs doses. Initially, cells were treated for 72 hours to allow sufficient time for the drugs to exert their effects and cell viability was measured by MTS assays, allowing testing of a wide range of drug combinations to identify synergistic combinations. Although convenient, material extracted from 96 well plates used for MTS assays would not be sufficient for downstream analyses. Further, since cells were cultured for 72 hours, they were seeded at low densities to avoid excessive growth, and the tissue culture vessels had to be large enough to harvest sufficient cells at an earlier point, such as 24 hours post-treatment, to test activation of p53-responsive genes. Both factors led to validating the MTS conditions in T25 flasks using flow cytometry, an independent method. However, the combination of 13.8A+3.9C found to be synergistic at 72 hours post-treatment by MTS assays was not found to be synergistic when tested using flow cytometry, which could be attributed to upscaling the conditions by ~75-times or to differences in methodologies. Optimising conditions in T25 flasks was already found to be cumbersome in these preliminary experiments, requiring excessive numbers of cells, amount of the drugs and tissue culture consumables; therefore, 6 well-plates were used for subsequent experiments. Moreover, only flow cytometry was used to test synergy as it allowed a direct measure of cell viability in cultures treated in 6 well-plates.

The doses of drugs were increased in the next round of experiments, and three combinations were found to by synergistic at 72 hours post-treatment: 20A+4C, 20A+6C and

30A+4C. None of the 6 canonical p53-downstream genes (*CDKN1A*, *BAX*, *BBC3/PUMA*, *MDM2*, *c12orf5* and *TP53I3*) were found to be differentially expressed (DE; absolute FC > 2 and $P < 0.05$) using RT-qPCR when cells were treated with 20 and 30 μM APR-246 in a time-course experiment. In contrast, ROS-responsive *GCLC* was found to be DE as early as 10 hours following APR-246 treatment.

In published studies p53-responsive genes were found to be upregulated by 15 - 100 μM of APR-246 (15-60 μM in Li et al. 2015, 25 μM in Bykov et al. 2005b, 35 μM in Tessoulin et al. 2014 and 100 μM in Zandi et al. 2011). We considered the possibility that 20 - 30 μM APR-246 may not be sufficient to fully activate wt-p53-functions from mutant-p53. Furthermore, the study by Mohell et al. 2015 conducted using APR-246 in OVCAR-3 found that APR-246 was synergistic with cisplatin at 48 hours post-treatment whereas the interaction was only additive at 24 h. Therefore, synergy was optimised again at 2 d post-treatment using drug dose. We also included Kuramochi cells as an additional cell line for subsequent analyses. Much higher doses of drugs (70A+8C for OVCAR-3 and 80A+20C for Kuramochi) were required to observe synergy between APR-246 and cisplatin at 48 h. Consistent with previous results, the p53-responsive genes *CDKN1A* and *BBC3* were not found to be DE at 70 and 80 μM APR-246 treatment in OVCAR-3 and Kuramochi cells, respectively, while *GCLC* was found to be DE at 8 hours post-treatment. A concurrent increase in seeding densities and drug doses may nullify the effect of using a higher drug dose; however, insufficient activation of wt-p53 due to lower drug doses was not a factor contributing to the lack of induction of p53-responsive genes. In addition, we also monitored cell viabilities at 12, 24 and 48 hours and showed that cells were responding to the drugs.

RNA-seq was employed through collaborations with bioinformaticians at the Garvan Institute of Medical Research, Sydney, Australia to investigate transcriptome-wide effects of APR-246. Although OVCAR-3 and Kuramochi responded differently to the drugs, the drug treatments for 12 hours in OVCAR-3 was functionally equivalent to that of 24 hours in Kuramochi cells in terms of cell viability. In addition, both time-points were reasonably early to capture direct changes in gene expression. Enrichment of the p53-responsive genes was tested by Gene Set Enrichment Analysis (GSEA) using the lists/gene sets of canonical p53-responsive genes from four well-known sources: KEGG, Biocarta, PID and 'Hallmark' pathways of MSigDB database maintained by the Broad Institute, USA. Only the PID-p53 gene set was found to be enriched in our data set. Recently, Fischer 2017 identified 116 genes that were commonly induced by wt-p53 in at least six high-throughput studies. GSEA performed using these p53-responsive genes showed that the p53 pathway was not

statistically enriched in both cell lines treated with APR-246. KEGG, Biocarta, PID and 'Hallmark' gene sets shared only six members and Fischer 2017 reported a majority of the genes (2261 out of 3509; 64.4%) were specific to only one dataset, indicating a considerable amount of variation in p53-responsive genes between studies. In short, the p53 pathway was not found to be significantly induced upon APR-246 treatment in 4 out of 5 gene sets.

To directly assess the specificity of APR-246 towards mutant-p53, p53-null SKOV-3 cells were transfected with 0.25, 0.5, 1 μg of empty vector, wt-p53 or p53-R248Q and treated with APR-246 to determine the IC_{50} values. A dose-dependent reduction in IC_{50} of cells transfected with mutant-p53 was predicted if APR-246-dependent cell death was mediated by mutant-p53. Remarkably, the IC_{50} of cells transfected with 1 μg mutant-p53 was higher than cells transfected with 0.25 μg mutant-p53, strongly contradicting the hypothesis. An increase in IC_{50} upon transfecting 1μg mutant-p53 could be attributed to its potential effect on promoting cellular growth and/or drug resistance. Thus, our results consistently showed that APR-246 was not inducing wt-p53 activities in HGSOC cell lines harbouring mutant-p53.

Despite being in phase Ib/II clinical trials (NCT02098343), there are only three published studies, to the best of the candidate's knowledge, testing the effects of APR-246 in OC (Fransson et al. 2016; Mohell et al. 2015; Yoshikawa et al. 2016). None of these studies tested whether p53-response genes such as p21 were induced following APR-246 treatment. p21 was found to be upregulated by more than 2-fold in Kuramochi cells (p53 status: D281Y) upon 16 hours of cisplatin treatment in our time-course experiment, suggesting that its expression was not exclusive to wt-p53. In studies such as Liu et al. 2015, the induction of p21 upon APR-246 was confirmed to be dependent on p53 since siRNA knockdown of p53 demolished activation of p21. However, such experiments did not have much value in our case where p21 was simply not induced by APR-246.

APR-246 has been shown to induce high levels of ROS and kill cells regardless of the p53-status in multiple cancers (Deben et al. 2016; Grellety et al. 2015; Peng et al. 2013; Tessoulin et al. 2014) including OC (Yoshikawa et al. 2016). Our preliminary GSEA consistently showed enrichment of the genes downstream of the ROS-sensitive transcription factor NRF2 upon APR-246 treatment in OVCAR-3 and Kuramochi cells individually as well as their combination, suggesting that APR-246 was inducing oxidative stress. However, this needs to be confirmed in functional assays such as rescue of the APR-246-mediated cell death by the antioxidant/ROS scavenger NAC.

6.4.2 Calculations of synergy

Despite commonly used in publications, the term 'synergy' remains profusely littered with technical terms that are not always clearly defined (Berenbaum 1977). In the absence of a clear understanding of synergy amongst researchers, experiments were found to be poorly designed to detect synergy even if it existed or the cases of additivities, in fact, represented antagonisms (Berenbaum 1977). A recent meta-analysis that evaluated reported cases of synergies between drugs in clinical trials for multiple cancers found that inappropriate methods for evaluation of synergy was common in pre-clinical publications (43% and 56% of phase I and II studies, respectively) (Ocana et al. 2012). Only ~32% of the studies used formal methods to validate synergies between agents using tools such as isobolograms (Ocana et al. 2012). Clearly, the biomedical community should be more vigorous and specific when reporting synergies between compounds.

Isobolograms were not employed to test the synergies between APR-246 and other compounds in the original or subsequent reports describing PRIMA-1 and APR-246 (Bykov et al. 2002, 2005b; Fransson et al. 2016; Mohell et al. 2015). In particular, the potency ratio R (see Figure 6.1) is often not constant in practice, leading to curved isoboles representing drug additivities, which is often mistaken for synergy or antagonism if the fundamental assumptions are not tested (Foucquier and Guedj 2015; Tallarida 2006). The developers of APR-246 chose to use the 'Additive model' to evaluate synergies. According to this model, if drug A and B individually results in cell viabilities of 0.4 and 0.6, respectively, the additive model predicts the viability of 0.24 (0.4×0.6) for their combination (Jonsson et al. 1998). While this model may be applicable, it only requires two data points to predict the expected additive effect and appears to be too simplistic given that more than 300 mechanism-specific equations have been derived to predict the additive effect (Chou 2006, 2010). Importantly, the developers the APR-246 generally discarded the Chou-Talalay Method, a widely used method to calculate synergies, because the DRC of APR-246 was found to be too steep when compared with agents such as cisplatin and doxorubicin (Mohell et al. 2015). The Chou-Talalay Method based on the mass-action law has been called the 'the unified theory' because fundamental equations of biochemistry and biophysics, such as the Michaelis-Menten equation of enzyme kinetics, Henderson-Hasselbalch equation for estimating pH of a buffer system and Hill and Scatchard equations for describing ligand binding to the receptor, can be derived from this method (Chou 2006, 2010). Most studies in the field also have used the Additive model for calculating synergies, with exceptions such as Sobhani et al. 2015, Synnott et al. 2017 and Liu et al. 2015 who have employed the Chou-Talalay method. Evaluation of the pharmacological basis for choosing a model to

predict synergy remains outside of the expertise of the candidate. The Additive model may well be superior to the Chou-Talalay method. Legitimate synergistic interactions should be proven by multiple methods. Furthermore, such studies should be made available for researchers who search for them in scientific databases. It is also unclear whether such studies are conducted at all or remain unpublished due to the commercial nature of the drug companies.

6.5 Conclusions

The aim of this study was to investigate effects of mutant-p53 on the expression of lncRNAs using a small molecule known as APR-246, which had been reported to restore wt-p53 activities from mutant-p53 by stabilising its structure. APR-246 is currently undergoing phase Ib/II trials for recurrent HGSOC and an induction of p53-activities in the context of HGSOC has not been tested. Using RT-qPCR and global transcriptomic analysis, we conclude that APR-246 does not induce a robust wt-p53-response in the models tested, and, as a result, we could not use this system to identify a broad range of lncRNAs affected by mutant-p53. We observed that the IC_{50} of APR-246 in p53-null cells transfected with varied amounts of mutant-p53 expression vector increased in a dose-dependent manner, which is in sharp contrast to the hypothesis that APR-246 is specific to mutant-p53. Preliminary analysis suggests that APR-246 could act by increasing ROS levels.

Chapter 7

Final discussion and future directions

7.1 Final discussion

Ovarian cancer (OC) is the seventh most common form of cancer and eighth cause of death from cancer in women worldwide. Approximately 152,000 women succumb to OC annually (Ferlay et al. 2015). The overall aim of the research presented in this thesis was to address three challenges facing the clinical management of OC by applying the recently emerging field of noncoding RNAs. Noncoding RNAs are a widely transcribed species of RNA that does not code for proteins but can play a crucial role in normal physiology as well as disease progression. Specific aims of the thesis were as follows: (1) to test the utility of serum microRNAs, a class of small noncoding RNAs, in predicting the surgical outcome, (2) to investigate the role of long non-coding RNAs (lncRNAs) in promoting cisplatin resistance, and (3) to investigate the effects of mutant-p53 on lncRNAs and general gene expression by using a small compound known as APR-246 that has been published to function by restoration of wild-type p53 activity in mutant-p53 cells.

7.1.1 Importance of thorough quality control in serum microRNA profiling

A number of analytical and pre-analytical factors can affect accurate quantification of serum microRNAs (McDonald et al. 2011; Witwer 2015). Release of the microRNA contents of

red blood cells upon haemolysis can dramatically influence the profile of serum microRNAs (Kirschner et al. 2011, 2013; Pritchard et al. 2012). Unfortunately, haemolysis is common in routine diagnostic samples, potentially confounding the use of serum microRNA as robust biomarkers of disease (Hawkins 2010).

A significant contribution of this thesis to the field is to recommend a methodology to detect low levels of haemolysis in serum to identify, and potentially exclude, samples that are severely affected by haemolysis. In our publication in *Plos One*, we suggested a flowchart to assist researchers to choose appropriate methodologies to detect haemolysis in their studies (Shah, Soon, and Marsh 2016). Although the 'miR ratio' was found to be the most sensitive method to detect low levels of haemolysis, it may be impractical in reality due to time-consuming procedures and associated costs. We showed that serum samples exhibiting spectroscopic absorbance at 414 nm > 0.3, typically measured on a Nanodrop™ spectrophotometer, compared to water used as a 'blank' identified samples that were likely to be severely affected by haemolysis. This detection method based on spectroscopic absorbance is cost-effective and has low sample requirements (5-10 µl). This work has already been cited four times within a year of its publication in April, 2016 (Scopus). Furthermore, this research has been practice changing, as spectroscopic absorbance of serum samples is now being recorded by the Kolling Institute Tumour Bank to allow researchers the option of excluding potentially haemolysed samples in their serum microRNA studies.

7.1.2 Separating patients of HGSOC from healthy women using serum microRNAs

OC is termed the 'silent killer' due to vague symptoms such as constipation, diarrhoea, nausea and vomiting that are also manifested by aging, menopause, weight gain and other benign conditions of the gastrointestinal tract (Bankhead et al. 2008; Goff et al. 2000; Jayson et al. 2014). Serum protein CA-125 is the only biomarker routinely used for the diagnosis of OC. However, the level of CA-125 is known to be influenced by factors such as pregnancy, menstruation, race and presence/history of other cancers (Medeiros et al. 2009; Pauler et al. 2001; Verheijen et al. 1999).

Serum levels of the miR-200 family of microRNAs were found to be predictive of OC from a previous study conducted in our laboratory (Kan et al. 2012); however, the current study examined a much greater number of microRNAs. Before proceeding to the prediction of surgical outcome using serum microRNAs, a proof-of-principle analysis was directed to

test whether serum microRNAs can separate patients of HGSOC from healthy women using the identical platform as the current study. A total of 170 serum microRNAs were profiled, which seems a fraction of the currently known >3,500 microRNAs (Londin et al. 2015). However, a significant proportion of these microRNAs may not be detectable in serum or plasma whereas the 170 microRNAs used in the profiling were found to be present in the majority of serum samples in a study conducted by Exiqon, the platform used for serum microRNA profiling in this thesis (Blondal et al. 2013). miR-375 and miR-210 were found to be predictive of HGSOC in our study. Although serum levels of miR-375 and miR-210 were reported to be predictive of cancers of pancreas (Carlsen et al. 2013; Ho et al. 2010; Yingxia et al. 2015), prostate (Cheng et al. 2013; He et al. 2015; Kachakova et al. 2015; Selth et al. 2012; Wach et al. 2015), breast (Huo et al. 2016) and, gastric cancers (Zhang et al. 2012b), neither microRNA have been reported to predict HGSOC to our knowledge. miR-210 was found to be affected by haemolysis, suggesting that it may not be suitable for routine clinical use, whereas miR-375 remained unaffected. Despite its novelty, the predictive power of miR-375 alone to distinguish healthy women from those with ovarian cancer was inferior to that of CA-125 (AUC: 0.765 versus 0.929; accuracy: 0.756 versus 0.884). A combination of miR-375 and CA-125 increased the accuracy of CA-125 in separating patients of HGSOC from healthy women. The potential of measurement of both CA-125 and serum miR-375 to discriminate healthy women from those with HGSOC needs to be confirmed in a larger cohort.

A number of circulatory microRNAs in the literature have been reported for their predictive power to separate patients with OC from healthy women. To prioritise microRNAs that could improve the predictive power of CA-125, the candidate summarised currently known microRNAs predictive of OC in Table 3.8. Surprisingly, many studies failed to report the performance of the predictive power to separate patients with OC from healthy women even though samples from healthy women were used in the studies as controls. The predictive power of miR-375 was found to be comparable with a previous study from our laboratory (Kan et al. 2012) and others (Table 3.8). miR-200a, -b or -c have been reported for their predictive power from at least three independent studies (Kan et al. 2012; Selth et al. 2012; Taylor and Gercel-Taylor 2008), suggesting that they should be prioritised for validation in large cohorts. Although levels of miR-1290 in plasma and miR-343-5p in whole blood were found to have a higher AUC of ~0.85 compared to miR-375 identified from the current study as well as miR-200 family members from multiple studies, microRNAs, in general, were found to be inferior to CA-125. This indicates that microRNAs by themselves would probably be unable to replace CA-125 in routine practice, but they could improve

the predictive power of CA-125 when combined together. A panel of serum microRNAs might be valuable in identifying patients of OC from healthy women if they are shown to be resistant to the factors that are known to influence CA-125 levels. Since microRNAs themselves are affected by pre-analytical factors, it is currently unclear whether microRNAs could overcome the limitations of CA-125 without imposing a different set of limitations.

7.1.3 Prediction of surgical outcome using serum microRNAs

Pre-operative prediction of surgical outcome has the potential to customise timing of the surgery. Integration of tools to predict the surgical outcome was identified as one of the seven priorities likely to improve outcomes for women with advanced OC in the consensus of the most recent 'Ovarian Cancer Action' meeting held in 2015 (Bowtell et al. 2015). The current study is the first study, to our knowledge, to investigate the utility of serum microRNAs to predict surgical outcome. miR-34a-5p was found to be superior to CA-125 for the prediction of surgical outcome. In fact, miR-34a-5p was the only biomarker out of a total of 48 that remained significant at 5% FDR in the pooled dataset. This finding was confirmed by the machine learning algorithm DLDA, where miR-34a-5p was found to have a higher inclusion frequency than CA-125 in 100-times 4-fold cross validation. Additionally, miR-34a-5p was not affected by haemolysis. It remains intriguing why miR-34a-5p, which was found to be downregulated in late versus early stages of EOC (Eitan et al. 2009; Zhang et al. 2008) as well as in EOC compared to the normal ovarian surface epithelial cells (Corney et al. 2010; Schmid et al. 2016), is upregulated in serum of suboptimally cytoreduced patients. Should patient material have been available, it would have been interesting to assess the levels of miR-34a-5p in normal secretory epithelial cells of the fallopian tube given the likely site of origin of these tumours (discussed in subsection 1.1.2.1).

7.1.4 Investigating the role of lncRNAs in promoting cisplatin resistance

Investigation of the role of lncRNAs in promoting cisplatin resistance in OC was novel in the field when this project commenced in 2013. Five lncRNAs (SNHG1, SNHG6, Y RNA-

1*, Malat1 and UCA1) out of ninety were found to be differentially expressed in the cell line models of cisplatin resistance. Only Malat1 and UCA1 were reported to promote cisplatin resistance in multiple cancers (Fan et al. 2014; Lopez-Ayllon et al. 2015; Mimeault and Batra 2013; Pan et al. 2016; Schmidt et al. 2014; Wang et al. 2008); however, both had not been implicated in promoting drug resistance in OC. UCA1 was selected for further investigation due its role in promoting cisplatin resistance in bladder cancer as well as cell proliferation through the PI3K pathway (Yang et al. 2012), which had been extensively studied in our laboratory previously.

Coincidentally, UCA1 was one of the earliest lncRNAs reported, by a separate group, for its potential role in promoting drug resistance in the OC cell line SKOV-3 (Wang et al. 2015). We discovered that the sensitivity of OC cells to cisplatin remained unchanged upon siRNA-mediated knockdown of UCA1, which contradicted the findings of Wang et al. 2015. There were significant differences in methodologies which could have led to a different conclusion. Wang et al. 2015 overexpressed UCA1 in SKOV-3 cells, which is 'unlikely' to be representative of HGSOC according to Domcke et al. 2013, whereas we downregulated UCA1 in two cell line models, OVCAR-3 and OVCAR4, representative of HGSOC (Domcke et al. 2013) as well as the PEO1/PEO4 cell lines that were not tested by Domcke et al. 2013. Further experiments modulating UCA1 expression by siRNA-mediated gene silencing as well as forced overexpression in additional OC cell lines are needed to assess the potential role of UCA1 in promoting drug resistance in OC. Since lncRNAs exhibit a remarkable tissue-specific expression (Derrien et al. 2012), it is likely that the effects of UCA1 are restricted to bladder cancer. In addition, indirect evidence that UCA1 might be downstream of p53 should be validated in future studies, probably in bladder cancer because of the known functional role of UCA1 in this cancer.

7.1.5 Investigating the effects of mutant-p53 on lncRNAs by using the p53-activating drug APR-246

p53 is perhaps the most investigated of all transcription factors which is universally mutated in HGSOC. Mis-sense mutations are the most common type of mutations in *TP53* and are expressed at a higher level in cancer cells (Bieging and Attardi 2012; Muller, Vousden, and Norman 2011; Walerych, Lisek, and Del Sal 2015). Mutant-p53 can inhibit activities of wt-p53 as well as other members of the p53 protein family such as p63 and p73 by

*Y RNA-1 is technically a small noncoding RNA (length: 83-112 nucleotides), but it is included in this discussion for simplicity.

dominant-negative mechanisms (Goh, Coffill, and Lane 2010; Thukral et al. 1995). In addition, by binding to other transcription factors and proteins, some mutant-p53 can activate or prevent gene expression, depending on interacting partners and the nature of the mutations (Muller and Vousden 2013). Recently, wt-p53 has been found to influence expression of both small and noncoding RNAs. Since half of all p53-binding sites on the DNA were found to be outside protein coding regions, aberrant transcription of noncoding RNAs upon mutations could be a significant part of carcinogenesis promoted by mutant-p53 (Idogawa et al. 2014).

Experiments conducted as part of this thesis aimed to examine the effect of mutant-p53 on lncRNA transcription using a small molecule known as APR-246. APR-246 has been reported to activate wt-p53 functions from mutant-p53 by stabilising the protein structure, resulting in expression of typical p53-response genes such as *CDKN1A/p21* (Liu et al. 2015; Zandi et al. 2011), *GADD45α* (Liu et al. 2015), *Bax* (Bykov et al. 2005b; Izetti et al. 2014; Zandi et al. 2011), *BBC3/PUMA* (Bykov et al. 2005b; Liu et al. 2015) and *MDM2* (Izetti et al. 2014; Zandi et al. 2011) in a range of cancer cell lines harbouring mutant-p53, their xenografts, and, in selected cases, patient-derived xenografts transplanted in to immuno-incompetent mice. Moreover, APR-246 was found to synergise with cisplatin in OC cell lines as well as other cancers (Bykov et al. 2005a; Fransson et al. 2016; Izetti et al. 2014; Liu et al. 2015; Mohell et al. 2015). Importantly, APR-246 is currently being evaluated in a phase Ib/II clinical trial for the treatment of recurrent OC (NCT02098343 2014).

Despite the current clinical trial, there are only three reports (Fransson et al. 2016; Mohell et al. 2015; Yoshikawa et al. 2016), to the candidate's knowledge, on the use of APR-246 in OC, and none have tested activation of p53-response genes upon the drug treatment. Instead, it appears that activation of wt-p53 activities upon the drug treatment have been assumed in OC based on evidence from other cancers. Therefore, by studying APR-246 in OC, the candidate also aimed to investigate: (1) transcriptome-side effects of APR-246 in OC cell lines, and (2) possible mechanisms of synergy between APR-246 and cisplatin in OC cell lines.

Synergy between APR-246 and cisplatin in OVCAR-3 cells was reported by Mohell et al. 2015, and this study supports this finding. In addition, we also report synergy between these two compounds in Kuramochi cells, which is novel. Three of four gene sets from well-known sources (KEGG, Biocarta, PID and the Broad Institute's 'Hallmark' gene sets) did not show enrichment of the p53 pathway in our dataset. The four gene sets had only six members in common, indicating variability between resources as well as under the p53-response in experimental conditions used. Fischer 2017 compiled a list of 116 genes that

were activated by p53 in at least six genome-wide studies. These genes were also not found to be enriched following APR-246 treatment in OVCAR-3 and Kuramochi cells. miR-34a directly transcribed by p53 was also not found to be induced in both cells. Moreover, only PVT1 was induced following ARP-246 treatment in both cell lines out of seven lncRNAs (PANDA (Hung et al. 2011), Pint (Huarte et al. 2010), NORAD (Lee et al. 2016), TUG1 (Guttman et al. 2009; Khalil et al. 2009), LOC105371267/PR-LncRNA-1 (Sánchez et al. 2014), PVT1 (Barsotti et al. 2012) and LINP1 (Zhang et al. 2016c)) reported to be activated by wt-p53. Although only two OC cell lines were used, both models were found to be representative of HGSOC according to a study by Domcke et al. 2013. Experiments using additional OC cell lines are needed to confirm the effects of APR-246 on p53-response genes and lncRNAs.

Because APR-246 was proposed to act on mutant-p53, we hypothesised that the IC_{50} of the p53-null SKOV-3 cells transfected with varied amounts of the mammalian expression vector harbouring mutant-p53 R248Q would be inversely proportion to the amount of plasmids transfected. However, a dose-dependent increase in IC_{50} was observed, contradicting this hypothesis.

Results presented in this thesis consistently indicated that APR-246 could work independently of mutant-p53. In contrast, according to our bioinformatics analysis, APR-246 could function by inducing high levels of ROS. Modulation of ROS levels has been an attractive therapeutic option for treatment of cancer (Gorrini, Harris, and Mak 2013; Pelicano, Carney, and Huang 2004; Sosa et al. 2013). Glutathione (GSH) and thioredoxin are the key components in neutralising ROS. Cancer cells have re-wired metabolic pathways to sustain rapid growth. A shift towards aerobic glycolysis (the Warburg effect) for rapid production of energy often results in a high oxidative stress (Liberti and Locasale 2016). As a result, cancer cells are much more prone to an imbalance in ROS compared to healthy cells, which is exploited by the therapies targeting ROS (Gorrini, Harris, and Mak 2013). Critical genes responsible for *de novo* glutathione synthesis such as *SLC7A11*, *GCLC* and *GCLM* (Gorrini, Harris, and Mak 2013) were strongly induced by APR-246. These genes are a direct transcriptional target of NRF2, a ROS-sensitive transcription factor (Gorrini, Harris, and Mak 2013), suggesting induction of ROS upon APR-246 treatment, which is in agreement with a study by Yoshikawa et al. 2016.

7.2 Future directions

7.2.1 Biomarker potential of noncoding RNAs

The detection of microRNAs in as many as twelve biofluids despite the presence of potent RNases has been unexpected and potentially revolutionary when it comes to identifying new diagnostic and prognostic biomarkers (Weber et al. 2010). An ease of access and stability of circulating microRNAs make them appealing biomarkers (Cortez et al. 2011). We anticipate that wider implementation of stringent quality control protocols in clinical laboratories, such as monitoring levels of haemolysis in serum as discussed in Chapter 4, should ultimately lead to reliable quantification of serum microRNAs, and subsequently, promote their routine use as biomarkers. Recently, lncRNAs have been emerging as novel biomarkers. For example, levels of the lncRNA PCA3 in urine has been shown to be superior to the current PSA-based tests to detect early prostate cancer (Chandra Gupta and Nandan Tripathi 2017). Combined measurements of the lncRNAs CCAT1 and HOTAIR in serum have been suggested as an effective screening tool for colorectal cancer (Zhao et al. 2015). While increasing accessibility of technologies such as RNA-seq should greatly enhance the biomarker discovery process, much remains to be learnt about the presence of lncRNAs in a range of biofluids as well as appropriate quality control protocols. Nevertheless, the number of lncRNAs has been currently estimated to as high as 58,000 (Iyer et al. 2015), and investigation of the biomarker potential of lncRNAs remains a promising avenue of research.

7.2.2 Detection of OC using noncoding RNAs

A population-wide screening test to detect OC has remained elusive, partly because of the low incidence rate of OC, demanding a test with a sensitivity of >0.75 and a specificity of >0.996, criteria that are extremely difficult to meet (Clarke-Pearson 2009; Hennessy, Coleman, and Markman 2009). As discussed in Chapter 3, serum levels of miR-375 identified from this thesis could improve the accuracy of CA-125 in detecting OC, but a number of microRNAs will probably be required to meet the performance criteria required for population-wide screening. The miR-200 family of microRNAs have been found to detect OC from healthy women from at least three independent studies, identifying them as robust candidates to be tested in future studies in combination with CA-125. Emerging evidence shows that the serum protein HE4 could be superior to CA-125 in detecting OC (Chen et al. 2016; Ferrarow et al. 2013; Hu et al. 2016). Although HE4 is not routinely

used in clinical practice currently, a test known as ROMA, comprising CA-125 and HE4, is approved by the FDA to assess the risk of EOC in women with a pelvic mass (ROMA® 2011). It remains to be seen whether microRNAs can further improve the performance of ROMA or predict patient response to first-line chemotherapy. The biomarker potential of lncRNAs remains to be fully explored in future studies. Furthermore, future studies should investigate the role of lncRNAs in pathogenesis of HGSOC in the context of fallopian tube as its likely source.

7.2.3 Prediction of surgical outcome for HGSOC patients

Prediction of surgical outcome remains difficult to achieve despite a range of tools such as computed tomography (CT), laparoscopy, aberrant expression of certain genes in tumour tissue, measurement of serum proteins CA-125 and HE4, machine learning/artificial intelligence and obtaining a two-surgeon opinion on the resectability of ovarian tumours (The Anderson Algorithm) have been attempted. miR-34a-5p was found to be superior to CA-125 in predicting surgical outcome, and serum levels of CA-125, HE4 and miR-34a-5p should be tested in combination in future studies.

The challenge of accurately predicting surgical outcome could partly be attributed to variation in the skills and attitudes of surgeons, as well as policies of institutions regarding aggressive surgeries. Although the study on 'The Anderson Algorithm' is yet to be officially published, the initial results reported in a review by Nick et al. 2015 have been promising, with the rate of R0 increasing from 20% to 84% since implementation of the protocol. A 2-surgeon opinion may be difficult to achieve in smaller centres; however, if successful, the study is likely to indicate whether prediction of surgical outcome could simply be improved by implementing standard guidelines. 'The Anderson Algorithm' utilises laparoscopy in predicting resectability of the tumours, which is minimally invasive but may be time-consuming. A simple, accurate blood test to predict surgical outcome, by potentially combining levels of CA-125, HE4, miR-34a-5p and lncRNAs if they are investigated for this purpose in future studies, remains appealing.

7.2.4 Role of lncRNAs in promoting cisplatin resistance

The finding that our genome actively transcribes RNAs only became apparent by the application of technologies such as RNA-seq, and lack of RNA-seq data still remains a significant limiting factor to fully explore the biological roles of lncRNAs in disease. For example, TCGA-OV study used microarrays for quantifying expression of mRNAs and microRNAs,

which are biased towards the choice of hybridisation probes. A clever study in the field identified the microarray probes corresponding to lncRNAs from existing microarray experiments (Du et al. 2013). By applying ~10,000 're-purposed' lncRNAs reported by Du et al. 2013 to the TCGA-OV dataset, Liu et al. 2017 identified eight differentially expressed lncRNAs (ZFAS1, RP5-1061H20.5, LINC01514, TUG1, RP11-489O18.1, RP11-136I14.5, RP11-16E12.1 and CTD-2555A7.3) between cisplatin sensitive and resistant HGSOC. The role of most of these eight lncRNAs as well as four lncRNAs reported by the candidate (SNHG1, SNHG6, Y RNA-1 and Malat1) remains to be investigated in future studies. Furthermore, proteins involved in the key biological pathways regulated by these lncRNAs could represent potentially novel drug targets.

7.2.5 Investigating the effects of mutant-p53 on lncRNAs by using the p53-activating drug APR-246

Despite being widely reported as a p53-activating drug, APR-246 failed to induce a robust p53-response, based on our bioinformatic analyses, in two representative cell line models of HGSOC in this thesis. We also tested the specificity of APR-246 for mutant-p53 by transfecting p53-null SKOV-3 cells with varied amounts of an expression vector harbouring mutant-p53 R248Q, and observed a dose dependent increase in IC_{50} for this drug. The developers of APR-246 showed induction of p21 and PUMA at a protein level upon APR-246 treatment in the p53-null H1299 cells transfected with p53 mutants R175H or R273H (Bykov et al. 2005a; Bykov et al. 2002) whereas we focused on the *TP53* mutation R248Q endogenously harboured in the OVCAR-3 cells. APR-246 has been shown to stabilise the mutant-p53 by alkylating the cysteine residues independent of the mutation itself as long as the entire mRNA is translated (missense mutations) (Lambert et al. 2009), hence, choice of the actual missense mutation is, in theory, irrelevant. However, it is possible that APR-246 was unable to restore wt-p53 activities from certain mutant-p53 such as R248Q. Future experiments should test this by transfecting p53-null cell lines H1299 and SKOV-3 with mutant-p53 R248Q as well as R273H and R175H serving as positive controls due to their use by the developer of the drug.

There was some evidence suggesting that APR-246 could potentially kill cancer cells by inducing high levels of ROS. Future experiments should confirm this, potentially by attempting to rescue cells from APR-246-induced ROS by treating with NAC, an antioxidant/ROS scavenger (Yoshikawa et al. 2016), especially in the OC cell lines harbouring nonsense or frame-shift mutations of *TP53*. Platinum drugs such as cisplatin and carbo-

platin also result in a high level of ROS (Conklin 2004b). APR-246 has been found to inhibit thioredoxin reductase 1, an important enzyme for recycling thioredoxin to its normal state (Peng et al. 2013). Interestingly, auranofin, an inhibitor of thioredoxin, was able to induce apoptosis by increasing the release of cytochrome-c in cisplatin resistant OC cells (Marzano et al. 2007). Buthionine sulphoximine (BSO) inhibiting GCL, a rate limiting enzyme in GSH production, is currently in clinical use (Gorrini, Harris, and Mak 2013). Thus, actions of APR-246 may overlap with other ROS-modulating drugs. Future studies should clarify whether the observed synergy between APR-246 and cisplatin is due to induction of ROS at high levels by each drug individually. Furthermore, efficiencies of APR-246, BSO and auranofin should be tested using drugs individually or in combination with drugs such as cisplatin that could potentially synergise with ROS-modulating drugs. While multiple modes of actions of a drug could de clinically desired, based on evidence presented in this thesis and by Yoshikawa et al. 2016, the purpose of APR-246 as a reactivator of wt-p53 function from mutant-p53 should be questioned in OC.

We captured an early transcriptomic response to APR-246 and cisplatin alone as well as their synergistic combinations in two cell lines representative of OC. A lack of induction of p53-response genes in OVCAR-3 and Kuramochi cells upon APR-246 treatment was unexpected, which led to a detailed investigation of mechanisms of APR-246 in these cell lines. It would probably be difficult to identify lncRNAs affected by mutant-p53 in the absence of a clear p53-response as discussed above. Only lncRNA PVT1 out of five p53-responsive lncRNAs was found to be differentially expressed in both cell lines following APR-246 treatment from the RNA-seq experiment, but this should be confirmed by RT-qPCR. Approaches such as 'guilt-by-association' could be utilised to predict putative functions of differentially expressed lncRNAs based on their correlation with mRNAs (Guttman et al. 2009). Nevertheless, further analyses of our dataset should identify molecular pathways that work together to result in the synergy observed between the two compounds, which will be of tremendous impact for identifying potential side effects or mechanism of resistance to the dual drug treatment.

In the absence of a robust induction of the p53-response following APR-246 treatment, the original question of identifying lncRNAs affected by mutant-p53 could be answered by transfecting expression vectors harbouring wild-type or mutant-p53 in p53-null cell lines such as SKOV-3 and H1299, followed by RNA-seq. In addition, genome-editing tools such as Clustered regularly interspaced short palindromic repeats (CRISPR)/CRISPR associated protein 9 (Cas9) could be utilised to revert the endogenous missense *TP53* mutations in OC cell lines to wild-type *TP53*. Additionally, the same CRISPR/Cas9 approach could also

be used to test the specificity of APR-246 for mutant-p53 in additional OC cell lines. It is expected that lncRNAs downstream of mutant-p53 could be oncogenic, which should be tested for their role in promoting OC. Modulating levels of oncogenic lncRNAs by tools such as antisense oligonucleotides (ASO) could represent novel anti-cancer targets.

7.3 Concluding remarks

The potential of non-coding RNAs in the clinical management of women with ovarian cancer remains to be fully explored. As discussed in Chapter 3, we identified novel microRNA biomarkers miR-375 and miR-34a-5p that could separate patients of HGSOC from healthy women and predict their surgical outcome, respectively. In addition, both microRNAs were unaffected by haemolysis, which is common in diagnostic samples and can dramatically alter the serum microRNA profile. Chapter 4 discussed methodologies to detect low levels of haemolysis in serum, which should lead to discovery of robust microRNA biomarkers suitable for routine clinical use. This work is published in *Plos One* (Shah, Soon, and Marsh 2016). In Chapter 5, five lncRNAs were found to be associated with promoting cisplatin resistance. Although UCA1, one of the five lncRNAs identified, was found to promote cisplatin resistance in bladder cancer, this was not the case in cell line models of ovarian cancer. We aimed to discover potential oncogenic lncRNAs affected by mutant-p53 by using the drug APR-246 that has been reported to activate wt-p53 activities and is currently undergoing a clinical trial to treat recurrent OC. Evidence presented in Chapter 6 suggested that APR-246 could act independently of mutant-p53 in cell line models of ovarian cancer. The human genome is estimated to harbour more than double the number of non-coding RNAs than the protein-coding genes. A thorough understanding of their functions has a potential to revolutionise the diagnosis and treatment of many diseases that are currently difficult to manage or cure.

Appendix A

Supplementary Figures

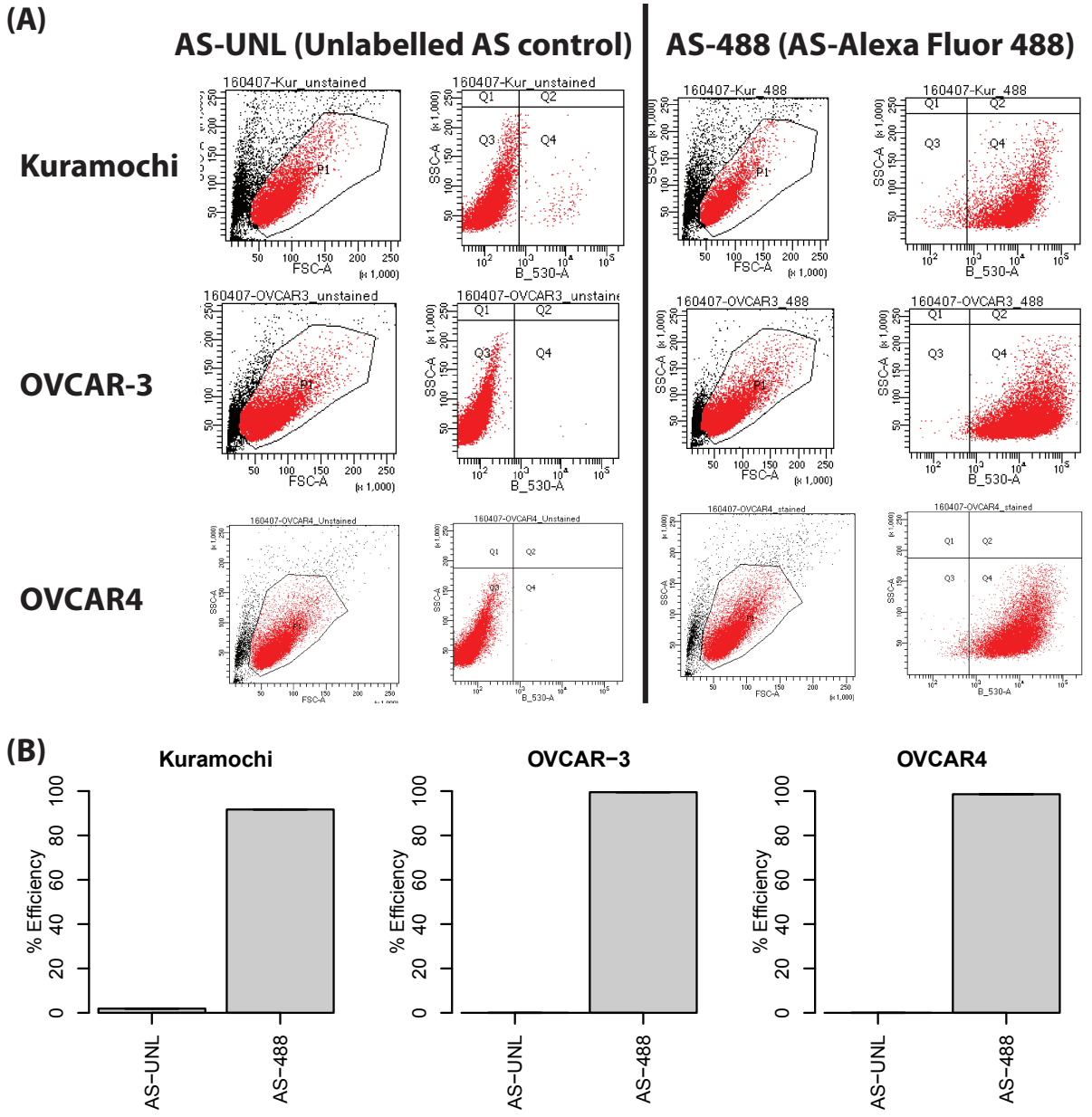

Figure A.1: Downregulation of UCA1 in Kuramochi, OVCAR-3 and OVCAR4 cells using HiPerFect reagent measured by flow cytometry

(A) Cells were transfected with 100 nmol of unlabelled AllStars Negative Control siRNA (AS-UNL) and AllStars Negative Control siRNA labelled with Alexa Fluor 488 (AS-488) using 12 µl HiPerFect reagent, and flow cytometry was performed 24 h post-transfection to test transfection efficiencies of the cells (N = 1). More than 80% of the cells were found to be positive for AS-488, reflecting high transfection efficiencies of these cells. **(B)** Quantification of transfection efficiency shown in (A).

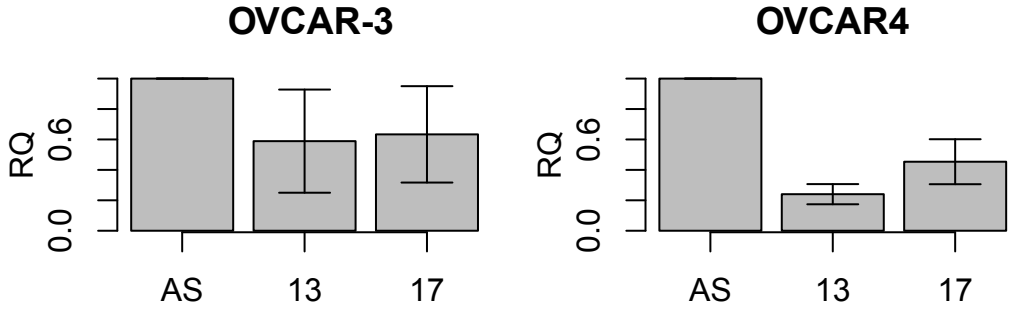

Figure A.2: Downregulation of UCA1 in OVCAR-3 and OVCAR4 cells using HiPerFect reagent and measured by TaqMan RT-qPCR

UCA1 siRNA #13 and #17 were transfected into OVCAR-3 and OVCAR4 cells, and their effect on reducing *UCA1* levels determined by TaqMan RT-qPCR 24 h post-transfection. Each siRNA resulted in an average knockdown efficiency of ~40-60% in both cells, which was found unsatisfactory for functional assays.

Appendix B

Supplementary Tables

Table B.1: Differentially expressed biomarkers in healthy versus HGSOC samples

¶ : unadjusted-*P* < 0.05.

	Discovery				Validation			Pooled		
Biomarker	***P* <0.05**	**Log FC**	***P***	**Adj-*P***	**Log FC**	***P***	**Adj-*P***	**Log FC**	***P***	**Adj-*P***
Log_2 CA-125	¶	5.49	1.8E-09	3.0E-07	5.11	2.0E-07	9.5E-06	5.30	4.2E-14	2.0E-12
150-5p	¶	-0.78	1.0E-03	3.4E-02	-1.45	1.8E-06	4.4E-05	-1.12	2.6E-06	6.2E-05
375	¶	-1.29	3.1E-04	1.8E-02	-1.95	5.6E-05	8.9E-04	-1.51	5.5E-05	8.6E-04
210	¶	0.73	1.5E-03	3.6E-02	0.62	1.6E-03	1.9E-02	0.65	1.5E-04	1.8E-03
181a-5p	¶	-0.65	4.7E-03	7.9E-02	-0.58	2.5E-02	2.0E-01	-0.60	2.6E-03	2.4E-02
106b-5p		-0.27	3.6E-01	7.5E-01	-0.34	7.8E-03	7.5E-02	-0.30	7.4E-03	5.8E-02
141-3p	¶	1.32	9.3E-04	3.4E-02	0.75	1.5E-01	4.7E-01	1.06	1.0E-02	7.0E-02
200c-3p	¶	2.33	3.6E-09	3.0E-07	0.86	1.2E-01	4.7E-01	1.01	1.3E-02	7.4E-02
551b-3p	¶	-0.68	5.2E-03	8.0E-02	-0.56	6.1E-02	4.2E-01	-0.57	3.5E-02	1.7E-01
629-5p	¶	0.58	1.4E-02	1.6E-01	0.24	2.6E-01	5.3E-01	0.36	3.6E-02	1.7E-01
142-3p	¶	-0.56	3.1E-02	2.6E-01	-0.51	1.5E-01	4.7E-01	-0.53	6.3E-02	2.7E-01
200a-3p	¶	1.11	2.1E-03	4.5E-02	0.41	3.8E-01	6.0E-01	0.57	1.2E-01	4.7E-01
103a-3p		-0.36	1.6E-01	6.4E-01	-0.28	2.1E-01	5.1E-01	-0.23	1.8E-01	5.7E-01
16-5p		0.23	4.4E-01	8.2E-01	0.00	9.9E-01	9.9E-01	0.10	1.6E-01	5.7E-01
605		-0.67	2.0E-01	6.8E-01	-0.62	8.2E-02	4.7E-01	-0.64	1.9E-01	5.7E-01
let-7i-3p		-0.22	4.6E-01	8.3E-01	-0.26	2.6E-01	5.3E-01	-0.32	1.8E-01	5.7E-01
222-3p	¶	0.40	4.5E-02	3.0E-01	0.12	5.5E-01	8.0E-01	0.25	2.1E-01	5.8E-01
122-5p		-0.34	3.2E-01	7.5E-01	-0.43	3.4E-01	6.0E-01	-0.40	2.9E-01	7.0E-01
19a-3p		0.11	6.8E-01	9.2E-01	0.01	9.2E-01	9.6E-01	0.11	2.8E-01	7.0E-01
361-3p		-0.36	5.9E-02	3.4E-01	-0.23	3.6E-01	6.0E-01	-0.27	3.0E-01	7.0E-01
144-3p		-0.24	5.4E-01	8.5E-01	-0.12	6.1E-01	8.2E-01	-0.22	3.6E-01	7.2E-01
25-3p		0.15	6.1E-01	8.9E-01	0.07	5.9E-01	8.2E-01	0.10	3.7E-01	7.2E-01
29c-3p		0.00	1.0E+00	1.0E+00	-0.28	1.0E-01	4.7E-01	-0.16	3.6E-01	7.2E-01

	Discovery				Validation			Pooled		
Biomarker	***P* <0.05**	**Log FC**	***P***	**Adj-*P***	**Log FC**	***P***	**Adj-*P***	**Log FC**	***P***	**Adj-*P***
99b-5p	¶	0.83	3.3E-03	6.3E-02	-0.20	6.1E-01	8.2E-01	0.29	3.5E-01	7.2E-01
UniSp2		-0.09	6.8E-01	9.2E-01	-0.45	1.6E-01	4.7E-01	-0.24	4.0E-01	7.6E-01
146a-5p		-0.02	9.4E-01	9.8E-01	-0.34	2.4E-01	5.3E-01	-0.18	4.5E-01	7.9E-01
22-3p		0.00	9.9E-01	1.0E+00	0.15	2.6E-01	5.3E-01	0.12	4.7E-01	7.9E-01
34a-5p		0.11	6.9E-01	9.2E-01	0.35	3.8E-01	6.0E-01	0.25	4.6E-01	7.9E-01
29a-5p		0.03	8.8E-01	9.8E-01	-0.25	3.9E-01	6.0E-01	-0.17	4.9E-01	8.0E-01
20a-5p		0.06	8.2E-01	9.5E-01	0.01	9.0E-01	9.6E-01	0.02	5.5E-01	8.0E-01
UniSp4		-0.04	8.2E-01	9.5E-01	-0.33	3.1E-01	5.9E-01	-0.18	5.3E-01	8.0E-01
UniSp5		-0.37	1.8E-01	6.5E-01	-0.37	3.5E-01	6.0E-01	-0.21	5.4E-01	8.0E-01
106a-5p		-0.01	9.6E-01	9.9E-01	0.02	8.0E-01	9.1E-01	-0.01	7.2E-01	8.7E-01
145-5p	¶	-0.63	8.4E-03	1.1E-01	-0.12	7.3E-01	8.5E-01	-0.12	7.5E-01	8.7E-01
15b-3p		0.02	9.4E-01	9.8E-01	0.19	1.1E-01	4.7E-01	0.03	6.8E-01	8.7E-01
20b-5p		0.25	3.4E-01	7.5E-01	0.04	8.4E-01	9.2E-01	0.05	7.4E-01	8.7E-01
30a-5p		-0.04	8.6E-01	9.7E-01	0.11	7.1E-01	8.5E-01	0.09	7.6E-01	8.7E-01
451a		0.10	7.8E-01	9.4E-01	-0.08	6.8E-01	8.5E-01	-0.04	7.6E-01	8.7E-01
505-3p		0.17	4.2E-01	8.1E-01	0.09	6.9E-01	8.5E-01	0.09	7.2E-01	8.7E-01
92b-3p	¶	0.57	1.2E-03	3.4E-02	0.06	8.2E-01	9.1E-01	0.12	6.2E-01	8.7E-01
let-7b-3p		0.15	3.8E-01	7.7E-01	-0.38	1.5E-01	4.7E-01	-0.09	6.9E-01	8.7E-01
UniSp6		0.13	5.1E-01	8.4E-01	-0.43	1.8E-01	4.7E-01	-0.12	8.2E-01	9.1E-01
23a-3p		-0.09	6.4E-01	9.2E-01	-0.24	2.1E-01	5.1E-01	-0.11	8.7E-01	9.5E-01
29b-2-5p	¶	0.39	3.3E-02	2.6E-01	-0.32	1.5E-01	4.7E-01	0.03	9.0E-01	9.6E-01
93-5p		0.02	9.3E-01	9.8E-01	0.00	9.9E-01	9.9E-01	0.00	9.2E-01	9.6E-01
101-3p		0.22	4.5E-01	8.2E-01	-0.16	4.1E-01	6.1E-01	0.00	9.9E-01	9.9E-01
cel-39-3p		0.46	1.8E-01	6.5E-01	-0.44	1.7E-01	4.7E-01	0.01	9.7E-01	9.9E-01
106b-3p		0.19	3.0E-01	7.5E-01						

	Discovery				Validation			Pooled		
Biomarker	***P* <0.05**	**Log FC**	***P***	**Adj-*P***	**Log FC**	***P***	**Adj-*P***	**Log FC**	***P***	**Adj-*P***
107		-0.11	7.1E-01	9.2E-01						
10b-5p	¶	0.53	3.4E-02	2.6E-01						
125a-5p		0.10	6.8E-01	9.2E-01						
125b-5p		0.24	2.7E-01	7.5E-01						
126-3p		-0.13	4.8E-01	8.3E-01						
127-3p	¶	-0.41	5.0E-02	3.0E-01						
130a-3p		0.17	5.0E-01	8.4E-01						
130b-3p		-0.01	9.6E-01	9.9E-01						
132-3p		-0.20	2.8E-01	7.5E-01						
133a		-0.44	7.2E-02	3.8E-01						
133b		-0.36	9.5E-02	4.9E-01						
136-5p	¶	-0.83	8.7E-03	1.1E-01						
139-5p		-0.25	3.1E-01	7.5E-01						
140-3p		0.37	2.1E-01	6.9E-01						
140-5p		0.03	9.0E-01	9.8E-01						
142-5p	¶	-0.93	1.3E-02	1.5E-01						
143-3p		0.14	5.9E-01	8.9E-01						
144-5p		0.00	9.9E-01	1.0E+00						
146b-5p		-0.14	4.9E-01	8.3E-01						
148a-3p		0.17	3.5E-01	7.5E-01						
148b-3p		0.05	8.2E-01	9.5E-01						
151a-3p		0.25	2.6E-01	7.5E-01						
151a-5p		-0.07	7.7E-01	9.4E-01						
152		-0.07	7.4E-01	9.3E-01						
154-5p		0.35	1.5E-01	6.2E-01						

	Discovery				Validation			Pooled		
Biomarker	***P* <0.05**	**Log FC**	***P***	**Adj-*P***	**Log FC**	***P***	**Adj-*P***	**Log FC**	***P***	**Adj-*P***
155-5p	¶	-0.40	4.0E-02	3.0E-01						
15a-5p		0.18	4.7E-01	8.3E-01						
15b-5p		0.10	6.6E-01	9.2E-01						
16-2-3p		0.17	6.0E-01	8.9E-01						
17-5p		-0.35	1.8E-01	6.5E-01						
185-5p	¶	0.60	3.4E-02	2.6E-01						
186-5p		0.23	3.2E-01	7.5E-01						
18a-3p		0.02	9.1E-01	9.8E-01						
18a-5p		-0.09	7.1E-01	9.2E-01						
18b-5p		-0.01	9.6E-01	9.9E-01						
191-5p		0.08	7.6E-01	9.4E-01						
192-5p		0.00	9.8E-01	1.0E+00						
193b-3p		0.08	7.9E-01	9.4E-01						
194-5p		0.16	4.5E-01	8.2E-01						
195-5p	¶	-0.60	2.0E-02	2.1E-01						
197-3p		-0.22	3.5E-01	7.5E-01						
199a-3p		-0.11	6.2E-01	9.0E-01						
199a-5p		-0.43	2.9E-01	7.5E-01						
19b-3p		0.28	3.5E-01	7.5E-01						
200b-3p					0.23	6.4E-01	8.3E-01			
204-5p		0.02	9.2E-01	9.8E-01						
205-5p		0.18	6.0E-01	8.9E-01						
20a-3p	¶	-0.41	2.3E-02	2.3E-01						
21-5p		0.28	1.2E-01	5.8E-01						
215		-0.09	6.6E-01	9.2E-01						

	Discovery				Validation			Pooled		
Biomarker	***P* <0.05**	**Log FC**	***P***	**Adj-*P***	**Log FC**	***P***	**Adj-*P***	**Log FC**	***P***	**Adj-*P***
22-5p		-0.20	4.8E-01	8.3E-01						
221-3p		0.10	7.1E-01	9.2E-01						
223-3p		-0.29	2.4E-01	7.2E-01						
223-5p		-0.02	9.2E-01	9.8E-01						
23b-3p		-0.06	7.7E-01	9.4E-01						
24-3p		0.04	8.3E-01	9.5E-01						
26a-5p		-0.24	2.9E-01	7.5E-01						
26b-5p		-0.35	1.8E-01	6.5E-01						
27a-3p		-0.12	5.3E-01	8.5E-01						
27b-3p		0.01	9.8E-01	1.0E+00						
28-3p		-0.16	3.9E-01	7.7E-01						
28-5p		-0.16	5.7E-01	8.7E-01						
296-5p		0.32	1.1E-01	5.2E-01						
29a-3p		-0.12	5.7E-01	8.7E-01						
29b-3p		-0.09	7.4E-01	9.3E-01						
301a-3p		-0.30	1.6E-01	6.4E-01						
30b-5p		-0.25	2.2E-01	7.0E-01						
30c-5p		-0.20	3.5E-01	7.5E-01						
30d-5p	¶	0.41	4.2E-02	3.0E-01						
30e-3p		-0.05	7.7E-01	9.4E-01						
30e-5p		0.08	7.0E-01	9.2E-01						
32-5p		-0.36	2.9E-01	7.5E-01						
320a	¶	0.58	2.7E-02	2.6E-01						
320b		0.45	6.3E-02	3.5E-01						
324-3p		-0.07	7.0E-01	9.2E-01						

	Discovery				Validation			Pooled		
Biomarker	***P* <0.05**	**Log FC**	***P***	**Adj-*P***	**Log FC**	***P***	**Adj-*P***	**Log FC**	***P***	**Adj-*P***
324-5p		-0.04	8.6E-01	9.7E-01						
326		-0.47	1.7E-01	6.5E-01						
328		-0.28	2.1E-01	6.9E-01						
331-3p		0.02	9.2E-01	9.8E-01						
335-5p		0.13	4.5E-01	8.2E-01						
338-3p		-0.26	3.3E-01	7.5E-01						
339-3p		-0.15	4.5E-01	8.2E-01						
33a-5p		-0.59	6.1E-02	3.4E-01						
342-3p		-0.28	1.1E-01	5.2E-01						
363-3p		0.20	5.4E-01	8.5E-01						
365a-3p		0.20	4.3E-01	8.2E-01						
374a-5p		-0.37	1.4E-01	6.2E-01						
374b-5p		-0.27	3.0E-01	7.5E-01						
378a-3p		0.28	1.3E-01	6.0E-01						
382-5p		0.14	5.1E-01	8.4E-01						
409-3p	¶	-0.46	4.7E-02	3.0E-01						
421		0.27	1.9E-01	6.7E-01						
423-3p		0.20	3.8E-01	7.7E-01						
423-5p		0.23	2.7E-01	7.5E-01						
424-5p		0.18	4.7E-01	8.3E-01						
425-3p		0.17	3.7E-01	7.6E-01						
425-5p		0.09	7.4E-01	9.3E-01						
484		0.29	2.6E-01	7.5E-01						
485-3p		-0.19	5.1E-01	8.4E-01						
486-5p		0.39	2.4E-01	7.2E-01						

	Discovery				Validation			Pooled		
Biomarker	***P* <0.05**	**Log FC**	***P***	**Adj-*P***	**Log FC**	***P***	**Adj-*P***	**Log FC**	***P***	**Adj-*P***
497-5p	¶	-0.55	4.9E-02	3.0E-01						
500a-5p		-0.25	3.4E-01	7.5E-01						
501-3p		-0.20	3.6E-01	7.5E-01						
502-3p		0.36	1.4E-01	6.2E-01						
532-3p		0.19	3.4E-01	7.5E-01						
532-5p		0.13	5.8E-01	8.7E-01						
574-3p		0.12	5.3E-01	8.5E-01						
590-5p		-0.22	3.4E-01	7.5E-01						
652-3p		-0.11	6.1E-01	8.9E-01						
660-5p		0.04	8.4E-01	9.7E-01						
766-3p		0.13	5.6E-01	8.7E-01						
885-5p		0.29	3.0E-01	7.5E-01						
92a-3p		0.32	2.5E-01	7.5E-01						
93-3p		-0.06	7.9E-01	9.4E-01						
99a-5p		0.09	7.2E-01	9.3E-01						
let-7a-5p		0.06	7.6E-01	9.4E-01						
let-7b-5p		0.02	9.2E-01	9.8E-01						
let-7c		-0.14	5.3E-01	8.5E-01						
let-7d-3p		-0.03	8.5E-01	9.7E-01						
let-7e-5p		0.34	2.1E-01	6.9E-01						
let-7f-5p		-0.04	8.7E-01	9.7E-01						
let-7g-5p		-0.33	1.5E-01	6.3E-01						
let-7i-5p		0.11	6.7E-01	9.2E-01						

Table B.2: Differentially expressed biomarkers in Optimally versus Suboptimally cytoreduced samples §: unadjusted-*P* < 0.05

	Discovery				Validation			Pooled		
Biomarker	***P* <0.05**	**Log FC**	***P***	**Adj-*P***	**Log FC**	***P***	**Adj-*P***	**Log FC**	***P***	**Adj-*P***
34a-5p	§	0.93	0.00	0.20	1.27	0.00	0.19	1.30	0.00	0.02
222-3p		0.43	0.08	0.76	0.60	0.01	0.24	0.70	0.00	0.04
Log_2 CA-125		1.89	0.06	0.76	2.36	0.04	0.32	2.12	0.01	0.15
141-3p	§	1.04	0.04	0.58	1.16	0.08	0.35	1.24	0.02	0.15
29a-5p		0.35	0.16	0.91	0.45	0.16	0.40	0.62	0.02	0.15
30a-5p		0.55	0.07	0.76	0.52	0.12	0.35	0.73	0.02	0.15
92b-3p		0.05	0.84	0.97	0.73	0.03	0.31	0.67	0.03	0.15
let-7b-3p	§	0.47	0.03	0.58	0.43	0.16	0.40	0.58	0.02	0.15
200a-3p		-0.06	0.90	0.97	0.73	0.20	0.42	0.98	0.03	0.16
200c-3p		0.23	0.61	0.96	1.41	0.05	0.34	1.07	0.04	0.19
29b-2-5p		0.37	0.10	0.77	0.30	0.26	0.43	0.48	0.04	0.19
UniSp4		0.29	0.25	0.93	0.64	0.10	0.35	0.65	0.06	0.23
122-5p	§	0.89	0.03	0.58	0.59	0.25	0.43	0.77	0.08	0.25
505-3p	§	0.51	0.05	0.61	0.28	0.35	0.48	0.56	0.08	0.25
99b-5p		0.35	0.29	0.93	0.62	0.18	0.41	0.65	0.07	0.25
UniSp2		0.32	0.30	0.93	0.62	0.11	0.35	0.61	0.08	0.25
375	§	0.81	0.04	0.61	0.43	0.39	0.52	0.68	0.11	0.30
210		0.17	0.52	0.94	0.12	0.65	0.73	0.33	0.12	0.31
150-5p		0.12	0.67	0.96	0.34	0.32	0.47	0.40	0.13	0.31
UniSp5		0.30	0.39	0.93	0.49	0.27	0.43	0.56	0.15	0.36
181a-5p		-0.09	0.75	0.96	0.27	0.41	0.54	0.34	0.17	0.38
146a-5p		0.07	0.79	0.96	0.24	0.52	0.62	0.32	0.27	0.57
UniSp6		0.34	0.19	0.91	0.79	0.06	0.34	0.64	0.28	0.57

	Discovery				Validation			Pooled		
Biomarker	***P* <0.05**	**Log FC**	***P***	**Adj-*P***	**Log FC**	***P***	**Adj-*P***	**Log FC**	***P***	**Adj-*P***
145-5p	§	-0.70	0.02	0.58	0.47	0.27	0.43	0.34	0.45	0.77
16-5p		-0.21	0.56	0.94	-0.08	0.63	0.72	0.07	0.43	0.77
25-3p		-0.25	0.45	0.93	0.02	0.90	0.92	0.10	0.46	0.77
29c-3p		-0.18	0.56	0.94	0.08	0.69	0.73	0.15	0.43	0.77
451a		-0.33	0.44	0.93	-0.32	0.20	0.42	-0.12	0.44	0.77
106a-5p		-0.24	0.44	0.93	-0.20	0.03	0.31	-0.01	0.83	0.95
106b-5p		-0.12	0.73	0.96	-0.37	0.02	0.24	-0.07	0.64	0.95
142-3p		0.17	0.57	0.94	-0.04	0.93	0.93	0.15	0.66	0.95
144-3p		-0.22	0.62	0.96	-0.47	0.11	0.35	-0.13	0.65	0.95
19a-3p		-0.44	0.17	0.91	-0.25	0.11	0.35	0.04	0.77	0.95
22-3p		-0.32	0.27	0.93	0.17	0.26	0.43	0.08	0.67	0.95
361-3p	§	-0.48	0.03	0.58	0.27	0.35	0.48	0.10	0.74	0.95
551b-3p	§	-0.63	0.01	0.58	0.20	0.56	0.66	0.08	0.80	0.95
605	§	-1.36	0.04	0.58	0.40	0.32	0.47	-0.14	0.81	0.95
629-5p	§	-0.59	0.03	0.58	0.21	0.44	0.55	-0.07	0.72	0.95
93-5p		-0.27	0.39	0.93	-0.12	0.28	0.43	0.01	0.74	0.95
cel-39-3p		-0.68	0.09	0.76	0.72	0.07	0.34	0.21	0.63	0.95
let-7i-3p	§	-0.73	0.02	0.58	0.32	0.17	0.41	0.07	0.81	0.95
103a-3p		-0.17	0.59	0.94	-0.13	0.68	0.73	0.04	0.85	0.95
20a-5p		-0.28	0.40	0.93	-0.17	0.15	0.40	0.00	0.91	0.95
20b-5p	§	-0.66	0.02	0.58	0.06	0.81	0.85	0.02	0.90	0.95
23a-3p		0.19	0.42	0.93	-0.30	0.23	0.43	0.10	0.90	0.95
15b-3p		-0.25	0.44	0.93	-0.17	0.28	0.43	0.01	0.96	0.98
101-3p		-0.13	0.71	0.96	-0.18	0.44	0.55	0.00	0.99	0.99
106b-3p		-0.06	0.79	0.96						

	Discovery				Validation			Pooled		
Biomarker	***P* <0.05**	**Log FC**	***P***	**Adj-*P***	**Log FC**	***P***	**Adj-*P***	**Log FC**	***P***	**Adj-*P***
107		-0.56	0.11	0.77						
10b-5p		0.44	0.17	0.91						
125a-5p		0.10	0.74	0.96						
125b-5p		0.39	0.18	0.91						
126-3p		0.20	0.41	0.93						
127-3p		0.14	0.53	0.94						
130a-3p		-0.03	0.92	0.97						
130b-3p		-0.20	0.44	0.93						
132-3p		0.06	0.81	0.97						
133a		0.11	0.73	0.96						
133b		0.03	0.92	0.97						
136-5p		-0.36	0.21	0.91						
139-5p		0.29	0.32	0.93						
140-3p		-0.47	0.18	0.91						
140-5p		-0.11	0.68	0.96						
142-5p		-0.33	0.45	0.93						
143-3p		0.21	0.53	0.94						
144-5p		0.06	0.83	0.97						
146b-5p		0.16	0.53	0.94						
148a-3p		-0.04	0.87	0.97						
148b-3p		-0.33	0.20	0.91						
151a-3p		0.00	1.00	1.00						
151a-5p		0.00	1.00	1.00						
152		0.06	0.81	0.97						
154-5p		0.03	0.92	0.97						

	Discovery				Validation			Pooled		
Biomarker	***P* <0.05**	**Log FC**	***P***	**Adj-*P***	**Log FC**	***P***	**Adj-*P***	**Log FC**	***P***	**Adj-*P***
155-5p		0.13	0.57	0.94						
15a-5p		-0.25	0.45	0.93						
15b-5p		-0.29	0.29	0.93						
16-2-3p		-0.60	0.11	0.77						
17-5p		-0.32	0.36	0.93						
185-5p		-0.23	0.48	0.94						
186-5p		-0.26	0.36	0.93						
18a-3p		0.29	0.19	0.91						
18a-5p		-0.20	0.48	0.94						
18b-5p		-0.08	0.78	0.96						
191-5p		0.06	0.85	0.97						
192-5p		0.02	0.93	0.97						
193b-3p		0.62	0.11	0.77						
194-5p		-0.08	0.77	0.96						
195-5p		0.53	0.09	0.76						
197-3p		0.04	0.88	0.97						
199a-3p		-0.05	0.86	0.97						
199a-5p		-0.38	0.41	0.93						
19b-3p		-0.29	0.40	0.93						
200b-3p					1.16	0.07	0.34			
204-5p		-0.19	0.50	0.94						
205-5p		0.82	0.08	0.76						
20a-3p		-0.07	0.73	0.96						
21-5p		0.31	0.19	0.91						
215		-0.08	0.74	0.96						

	Discovery				Validation			Pooled		
Biomarker	***P* <0.05**	**Log FC**	***P***	**Adj-*P***	**Log FC**	***P***	**Adj-*P***	**Log FC**	***P***	**Adj-*P***
22-5p		-0.12	0.73	0.96						
221-3p		0.09	0.78	0.96						
223-3p		-0.10	0.76	0.96						
223-5p		0.19	0.52	0.94						
23b-3p		0.02	0.93	0.97						
24-3p		0.14	0.54	0.94						
26a-5p		0.01	0.96	0.99						
26b-5p		0.16	0.63	0.96						
27a-3p		0.35	0.15	0.91						
27b-3p		0.05	0.86	0.97						
28-3p		-0.08	0.74	0.96						
28-5p		-0.23	0.46	0.93						
296-5p		0.11	0.64	0.96						
29a-3p		0.20	0.44	0.93						
29b-3p		-0.36	0.29	0.93						
301a-3p		-0.22	0.39	0.93						
30b-5p		-0.01	0.96	0.98						
30c-5p		-0.14	0.58	0.94						
30d-5p		-0.09	0.71	0.96						
30e-3p		0.11	0.64	0.96						
30e-5p		-0.14	0.58	0.94						
32-5p		-0.45	0.25	0.93						
320a		-0.18	0.57	0.94						
320b		-0.23	0.44	0.93						
324-3p		0.07	0.76	0.96						

	Discovery				Validation			Pooled		
Biomarker	***P* <0.05**	**Log FC**	***P***	**Adj-*P***	**Log FC**	***P***	**Adj-*P***	**Log FC**	***P***	**Adj-*P***
324-5p		0.07	0.79	0.96						
326		-0.36	0.41	0.93						
328		0.09	0.75	0.96						
331-3p		-0.16	0.49	0.94						
335-5p		-0.10	0.67	0.96						
338-3p		-0.08	0.82	0.97						
339-3p		-0.14	0.57	0.94						
33a-5p		-0.46	0.24	0.93						
342-3p		0.04	0.84	0.97						
363-3p		-0.31	0.43	0.93						
365a-3p		0.03	0.91	0.97						
374a-5p		-0.01	0.97	0.99						
374b-5p		-0.26	0.40	0.93						
378a-3p		-0.09	0.69	0.96						
382-5p		0.08	0.76	0.96						
409-3p		0.53	0.07	0.76						
421		0.02	0.94	0.98						
423-3p		-0.25	0.35	0.93						
423-5p		-0.38	0.12	0.81						
424-5p		0.27	0.41	0.93						
425-3p		0.30	0.22	0.92						
425-5p		-0.14	0.66	0.96						
484		-0.27	0.37	0.93						
485-3p		-0.33	0.38	0.93						
486-5p		-0.37	0.33	0.93						

	Discovery				Validation			Pooled		
Biomarker	***P* <0.05**	**Log FC**	***P***	**Adj-*P***	**Log FC**	***P***	**Adj-*P***	**Log FC**	***P***	**Adj-*P***
497-5p		0.40	0.26	0.93						
500a-5p		-0.06	0.86	0.97						
501-3p		-0.02	0.93	0.97						
502-3p		-0.11	0.69	0.96						
532-3p		0.25	0.35	0.93						
532-5p		-0.35	0.19	0.91						
574-3p		0.06	0.79	0.96						
590-5p		-0.22	0.45	0.93						
652-3p		-0.11	0.69	0.96						
660-5p		-0.01	0.98	0.99						
766-3p		0.06	0.84	0.97						
885-5p		0.41	0.19	0.91						
92a-3p		-0.24	0.46	0.93						
93-3p		-0.19	0.49	0.94						
99a-5p		0.39	0.22	0.92						
let-7a-5p		-0.06	0.82	0.97						
let-7b-5p		-0.33	0.26	0.93						
let-7c		-0.04	0.88	0.97						
let-7d-3p		0.14	0.51	0.94						
let-7e-5p		-0.43	0.20	0.91						
let-7f-5p		0.14	0.67	0.96						
let-7g-5p		-0.16	0.58	0.94						
let-7i-5p		-0.33	0.27	0.93						

Appendix C

The R script to process data from MTS assays

Automatic processing of data from MTS assays and calculation of synergy

Defining custom functions

Main interface: 'easy.mts()' function

This is the main function which is called from external file handling data to process. 'KEYS' instructs R to manage biological replicates. In most cases, KEYS is a combination of 'Treatment1' (three technical replicates) and 'Treatment5' (biological group).

```
rm(list = ls())
library(ggplot2)
```

```
## Warning: package 'ggplot2' was built under R version 3.2.5
```

```
library(plotrix)
```

```
## Warning: package 'plotrix' was built under R version 3.2.5
```

```
library(RColorBrewer)
library(drc)
```

```
## Warning: package 'drc' was built under R version 3.2.5
## Loading required package: MASS
## Warning: package 'MASS' was built under R version 3.2.5
##
## 'drc' has been loaded.
## Please cite R and 'drc' if used for a publication,
## for references type 'citation()' and 'citation('drc')'.
##
## Attaching package: 'drc'
## The following objects are masked from 'package:stats':
##
##     gaussian, getInitial
```

```
## --- Processing of MTS data, Script V5
easy.mts <- function(INFO, plotTechRep = FALSE, NORMBY = "vehicle", KEYS,...){
  ## the main interaction function
  final <- final.raw <- data.frame()
  plots <- list()
  INFO <- subset(INFO,!is.na(INFO$File_name))
  for(i in 1:nrow(INFO)){
    mts.list <- process_MTS(INFO, i, NORMBY, KEYS, ...)
    mts.results <- mts.list[[1]]

    mts.results <- transform(mts.results,
                             Treatment2 = as.numeric(Treatment2))
    mts.results <- mts.results[order(mts.results$Treatment2),]
```

```
    if(plotTechRep){
      require(drc)
      keys <- na.omit(unique(mts.list[[2]]$Keys))

      tech.ic50 <- sapply(1: length(keys), function(i){
        temp2 <- subset(mts.list[[2]], Keys ==  keys[i])
        if(length(unique(temp2$Treatment2)) <= 1){
          print (paste("not enough data for", keys[i],
                       paste(unique(temp2$Keys),unique(temp2$FileName)), sep =" : "))
        } else {
          fit <- drm(Percent_control ~ Treatment2,
                     fct = LL.4(names = c("Slope", "Lower Limit", "Upper Limit", "ED50")),
                     data = temp2)
          plot(fit, type = "all", xlab = unique(temp2$Treatment3),
               main = keys[i], sub = "(Technical replicates only)", cex.main = 0.8)
          ed50 <- coef(summary(fit))[4,1] # returns IC50/ED50
          legend("bottomleft", paste("IC50:", signif(ed50,3)),bty = "n")
          ED(fit, 50, interval = "delta", display = FALSE)
        }

      })
    }

    if (i == 1){
      final <- mts.results
      final.raw <- mts.list[[2]]
    }else{
      final <- rbind(final, mts.results)
      final.raw <- rbind(final.raw, mts.list[[2]])

    }

  }
  # Ensuring all data is in correct format.
  final <- transform(final, Treatment2 = as.numeric(Treatment2))
  return(list(processed_data = final, raw_data = final.raw))
}
```

Processing of each MTS plate by function 'process_MTS()'

This functions is called by 'easy.mts()' and reads an Excel file, substracts background absorbance and normalises cell viability to the vehicle control.

```
process_MTS <- function(infoDF, n, NORMBY, KEYS){
  require(xlsx)
  tempInfo <- infoDF[n,]
  columns <- 1
  plate <- as.numeric (unique(tempInfo$Plate))
  if(plate == 96){columns <- 12} else {
    stop(paste("Incorrect plate dimension in file:",
               infoDF[1, "File_name"], ". \n Only 96 well plates are supported"))
  }
```

```
seq.cols <- seq(1, columns, 1)
seq.rows <- seq(1, (plate/columns),1)
#----
#Reading and preparing data
#----

wrkbk <- loadWorkbook(as.character(tempInfo[1, "File_name"]))
wrksheets <- names(getSheets(wrkbk))

## Reading data

trt1 <- read.xlsx(file = as.character(tempInfo[1, "File_name"]),
                  sheetName = as.character(tempInfo[1,  "Treatment1_sheet"]),
                  row.names = TRUE)
trt1 <- wp2DF2.MTS(trt1[seq.rows, seq.cols],
                   colNames = c("Well", "Treatment1"),
                   origin = as.character(tempInfo[1, "File_name"]))

trt2 <- read.xlsx(file = as.character(tempInfo[1,  "File_name"]),
                  sheetName = as.character(tempInfo[1,  "Treatment2_sheet"]),
                  row.names = TRUE)
trt2 <- wp2DF2.MTS(trt2[seq.rows, seq.cols],
                   colNames = c("Well", "Treatment2"),
                   origin = as.character(tempInfo[1, "File_name"]))

if(is.na(match("Treatment3_sheet", colnames(tempInfo)))){
  trt3 <- wp2DF2.MTS(getEmptyFrame = TRUE,
                     colNames = c("Well", "Treatment3"),
                     origin = as.character(tempInfo[1, "File_name"]))
} else{

  trt3 <- read.xlsx(file = as.character(tempInfo[1,  "File_name"]),
                    sheetName = as.character(tempInfo[1,  "Treatment3_sheet"]),
                    row.names = TRUE,
                    origin = as.character(tempInfo[1, "File_name"]))
  trt3 <- wp2DF2.MTS(trt3[seq.rows, seq.cols],
                     colNames = c("Well", "Treatment3"),
                     origin = as.character(tempInfo[1, "File_name"]))
}

if(is.na(match("Treatment4_sheet", colnames(tempInfo)))){
  trt4 <- wp2DF2.MTS(getEmptyFrame = TRUE,
                     colNames = c("Well", "Treatment4"),
                     origin = as.character(tempInfo[1, "File_name"]))
} else{
  trt4 <- read.xlsx(file = as.character(tempInfo[1,  "File_name"]),
                    sheetName = as.character(tempInfo[1,  "Treatment4_sheet"]),
                    row.names = TRUE, origin = as.character(tempInfo[1, "File_name"]))
  trt4 <- wp2DF2.MTS(trt4[seq.rows, seq.cols],
                     colNames = c("Well", "Treatment4"),
                     origin = as.character(tempInfo[1, "File_name"]))
}
```

```
if(is.na(match("Treatment5_sheet", colnames(tempInfo)))){
  trt5 <- wp2DF2.MTS(getEmptyFrame = TRUE,
                     colNames = c("Well", "Treatment5"),
                     origin = as.character(tempInfo[1, "File_name"]))
} else{
  trt5 <- read.xlsx(file = as.character(tempInfo[1,  "File_name"]),
                    sheetName = as.character(tempInfo[1,  "Treatment5_sheet"]),
                    row.names = TRUE, origin = as.character(tempInfo[1, "File_name"]))
  trt5 <- wp2DF2.MTS(trt5[seq.rows, seq.cols],
                     colNames = c("Well", "Treatment5"),
                     origin = as.character(tempInfo[1, "File_name"]))
}

if(tempInfo[1, "Transform_Abs"] == "TRUE"){
  abs <- read.xlsx(file = as.character(tempInfo[1,  "File_name"]),
                   sheetName = as.character(tempInfo[1,  "Abs_sheet"]),
                   row.names = TRUE)
  abs <- wp2DF2.MTS(abs, colNames = c("Well", "Abs"))

}
else  {
  abs <- read.xlsx(file = as.character(tempInfo[1,  "File_name"]),
                   sheetName = as.character(tempInfo[1,  "Abs_sheet"]))

  abs <- abs[, c(3,6)]

}
colnames(abs) <- c("Well", "Abs")
abs <- transform(abs, Abs = as.numeric(Abs))

df <- Reduce(function(x,y) merge(x,y, all = FALSE),
             list(trt1, trt2, trt3, trt4, trt5,abs))
df <- subset(df, Treatment1 != "" | is.na(Treatment1)) # removing empty wells


#---
# All data read. Algorithm to remove background and normalise to the vehicle control.
#---

# Step 1: Remove background
blk <- mean(df[df$Treatment1 == tempInfo[1, "Blank_indicator"], "Abs"])
df[,"Background"] <- blk
df[,"Abs_corrected"] <- df[,"Abs"] - blk
df <- subset(df, Treatment1 != tempInfo[1, "Blank_indicator"])

#---
# Step 2: Defining Keys to handle biological groups etc
#---

if(length(KEYS) == 1){
  df[,"Keys"] <- df[,KEYS]
}
else{
```

```
    df[,"Keys"] <- apply( df[,KEYS ] , 1 , paste , collapse = ";" )
  }
  u.keys <- unique(df$Keys)

  for(i in 1:length(u.keys)){
    if (NORMBY == "vehicle"){
      control <-
        mean(df[df$Keys ==  u.keys[i] & df$Treatment2 == tempInfo[1, "Vehicle_control"],
                "Abs_corrected"])
      df[df$Keys ==  u.keys[i], "Abs_Vehicle_control"] <- control
      df[df$Keys ==  u.keys[i],"Percent_control"] <-
        (100*df[df$Keys == u.keys[i],"Abs_corrected"])/control
    } else{
      df[df$Keys ==  u.keys[i], "Abs_Vehicle_control"] <- NA
      df[df$Keys ==  u.keys[i],"Percent_control"] <-
        df[df$Keys ==  u.keys[i],"Abs_corrected"]
    }
  }
  ## Step 3: Average and SEM
  require(plotrix)
  df.abs<- aggregate(df$Abs_corrected,
                     by = list(df$Treatment1, df$Treatment2, df$Treatment3,
                               df$Treatment4, df$Treatment5), mean)
  colnames(df.abs) <- c("Treatment1", "Treatment2", "Treatment3",
                        "Treatment4","Treatment5" , "Abs_corrected")

  df.mean <- aggregate(df$Percent_control,
                       by = list(df$Treatment1, df$Treatment2, df$Treatment3,
                                 df$Treatment4, df$Treatment5), mean)
  colnames(df.mean) <- c("Treatment1", "Treatment2", "Treatment3",
                         "Treatment4","Treatment5" , "Percent_control")
  df.sem <- aggregate(df$Percent_control,
                      by = list(df$Treatment1, df$Treatment2, df$Treatment3,
                                df$Treatment4, df$Treatment5), std.error)
  colnames(df.sem) <- c("Treatment1", "Treatment2", "Treatment3",
                        "Treatment4","Treatment5" , "Tech_rep_sem")

  df.mean <- Reduce(function(x,y) merge(x,y, all =TRUE), list(df.mean, df.sem, df.abs))
  df.mean[,"FileName"] <- tempInfo[,"File_name"]
  if(length(KEYS) == 1){
    df.mean[,"Keys"] <- df.mean[,KEYS]
  }
  else{
    df.mean[,"Keys"] <- apply( df.mean[,KEYS ] , 1 , paste , collapse = ";" )
  }

  df.mean <- transform(df.mean, Treatment2 = as.numeric(as.character (Treatment2)))

  df[,"FileName"] <-tempInfo[,"File_name"]
  df <- transform(df, Treatment2 = as.numeric(as.character (Treatment2)))
  return(list(df.mean, df))
}
```

Calculating and plotting IC50

This performed using a four-parameter log-logistic model supplied by R pacakge 'drc'.

```
plot.ic50 <- calculate.ic50 <-
  function(myData, y="Percent_control", x = "Treatment2",
           cat = c("Treatment1", "Treatment3"), plot = FALSE, compact = TRUE,
           textX = 0.5, textY = 20 ,  ...){
    ## both name performs same because of compatibility with previous version

    myData[,"tempKeys"] <- paste(myData[,cat[1]], myData[,cat[2]], sep = ";")
    keys <- unique(myData$tempKeys)

    ic50 <- sapply(1: length(keys), function(i){

      temp <- subset(myData, tempKeys == keys[i])
      temp <- transform(temp, Treatment2 = as.numeric(as.character(Treatment2)))
      temp[,y] <- as.numeric(as.character(temp[,y]))
      temp <- subset(temp, Treatment2 >0)
      fit <- drm(temp[,y] ~ temp[,x],
                 fct = LL.4(names=c("Slope","Lower Limit","Upper Limit","ED50")))
      ed50 <- coef(summary(fit))[4,1] #ED50
      if(plot){plot(fit, main = paste(temp$Treatment1[1],
                                      temp$Treatment3[1], sep = ", "), ...)
        text(x=textX, y =textY, paste("IC50:", signif(ed50,3)))
      }
      ed50
    })
    myData2 <- data.frame(keys, ic50)
    myData2 <- merge(myData, myData2, by.x = c("tempKeys"), by.y=c("keys"))
    if(compact){
      return(subset(myData2, !(duplicated(tempKeys)), select = c(cat, "ic50")))

    }else{
      return(myData2)
    }
  }

ic50 <- function(merged,plotType = "all", xlab = NULL, ylab = NULL,
                 main = NULL, showIC50 = TRUE, ...){
  require(drc)
  bioGroups <- na.omit(unique(merged$BioGroup))

  biogroup.ic50 <- sapply(1: length(bioGroups), function(i){
    temp2 <- subset(merged, BioGroup ==  bioGroups[i])
    fit <- drm(Percent_control ~ Treatment2,
               fct = LL.4(names = c("Slope", "Lower Limit", "Upper Limit", "ED50")),
               data = temp2)
    plot(fit, type = plotType, main = bioGroups[i], ann = FALSE,  ...)

    if(is.null(xlab)){
      title(xlab = unique(temp2$Treatment3))
    } else{
      title(xlab = xlab)
```

```
    }
    if(is.null(ylab)){
      title(ylab = "% viability")
    } else{
      title(ylab = ylab)
    }
    if(is.null(main)){
      title(main = bioGroups[i])
    } else{
      title(main = main)
    }
    ed50 <- coef(summary(fit))[4,1] #ED50
    if(showIC50){
      legend("bottomleft", paste("IC50:", signif(ed50,3)),bty = "n")
    }
    ED(fit, 50, interval = "delta", display = FALSE)
  })
  colnames(biogroup.ic50) <- bioGroups
  rownames(biogroup.ic50) <- c("IC50", "SEM", "Lower", "Upper")
  t(biogroup.ic50)
}
```

Extracting experimental design of a large experiment.

In an experiment with several MTS plates, it could become difficult to determine number of biological replicates and their assignment to a biological/treatment group. The following function returns such information from an experiment.

```
generate.ExpDesign <- function(temp, KEYS){
  temp.expDesign <- temp

  if(length(KEYS) == 1){
    temp.expDesign[,"Keys"] <- temp.expDesign[,KEYS]
  }
  else{
    temp.expDesign[,"Keys"] <- apply( temp.expDesign[,KEYS ],
                                      1 , paste , collapse = ";" )
  }
  temp.expDesign <- subset(temp.expDesign, !duplicated(Keys),
                           select = c(1,3:5,10))
  cbind(temp.expDesign, BioGroup = "", isAccurate = "", Comments = "")
}
```

Conversion of a layout of 96 well-plate (8 x 12) to a data frame (96 x 1)

This functions makes it easy to work with layouts of an MTS file. Typically, it is easier to assign treatment groups and drug doses in an Excel file in 8 x 12 format (96 well-plates). The spectrophometer also displays absorbances in 8 x 12 format. In contrast, operations are easier when performed in a table or data frame. Following function convert information such as well A1 to corresponding numeric format of a data frame.

```
wp2DF2.MTS <- function (template, plate= 96, IsNA.empty = TRUE,
                        colNames = c("Well","Value"), getEmptyFrame = FALSE, origin=""){
```

```
  df <- data.frame()
  columns  <- NA
  if(plate == 384){columns=24} else {columns=12}

  if(getEmptyFrame)
  {
    for (i in seq(1, to = plate/columns, by =1)) # looping throuh rows
    {
      df [seq(columns * (i-1) + 1, columns * i),"Well"]  <- seq(columns * (i-1) + 1, columns * i)
      df [seq(columns * (i-1) + 1, columns * i),"Value"] <- ""
    }
  }
  else{
    ## checking if correct dimensions
    if(ncol(template) >= (columns + 1) | nrow(template) >= ((plate/columns)+1)){
      print(paste("INCORRECT DIMENTSION IN FILE in file", origin, sep = ":"))
      print(paste("dimension, R X C :",nrow(template) ,ncol(template), origin))

    }
    for (i in seq(1, to = plate/columns, by =1)) # looping throuh rows
    {
      temp.fill <- t(template[i,])
      not.empty <-   which(is.na(temp.fill) != TRUE)      #
      df [seq(columns * (i-1) + 1, columns * i),"Well"]  <-
        seq(columns * (i-1) + 1, columns * i)
      if (!IsNA.empty){
        df [seq(columns * (i-1) + 1, columns * i),"Sample Name"]  <-
          paste(LETTERS[i], seq(1:columns), sep="") #fills with A1 etc by default
        df [columns * (i-1) + not.empty ,"Sample Name"] <- temp.fill[not.empty] #works
      } else{
        df [seq(columns * (i-1) + 1, columns * i),"Detector"] <- ""
        df [columns * (i-1) + not.empty ,"Detector"] <- temp.fill[not.empty]
      }
    }
  }

  colnames(df) <- colNames
  df
}
```

Calculation of synergy using the Additive model

```
get4parameters <- function(merged, ...){
  bioGroups <- na.omit(unique(merged$BioGroup))
  biogroup.ic50 <- sapply(1: length(bioGroups), function(i){
    temp2 <- subset(merged, BioGroup ==  bioGroups[i])
    fit <- drm(Percent_control ~ Treatment2,
               fct = LL.4(names = c("Slope", "Lower Limit", "Upper Limit", "ED50")),
               data = temp2)
    a <- summary(fit)
    rse <- a$rseMat
    c(coef(a)[,1], a$rseMat)
```

```
  })

  #   # dev.off()
  colnames(biogroup.ic50) <- bioGroups
  rownames(biogroup.ic50) <- c("slope", "min", "max", "ic50", "rse", "df")
  biogroup.ic50 <- as.data.frame(t(biogroup.ic50))
  biogroup.ic50[,"BioGroup"] <- rownames(biogroup.ic50)
  merge(merged, biogroup.ic50)
}
estimate.response <- function(x, min, max, slope, ic50){
  min +((max - min)/(1+ (exp(slope * (log(x) - log(ic50))))))
}

additive.synergy <- function(merged, plotGraph = TRUE){
  results <- subset(merged, select = c("Keys", "BioGroup","Treatment1", "Treatment2",
                                       "Treatment3", "Treatment4", "Percent_control"))
  results[,"Percent_control"] <- results[,"Percent_control"]/100 #Converted to fractions
  results <- get4parameters(results)

  results[, "Type"] <- with(results,
                            ifelse((Treatment4 == "" & Treatment3 !="") |
                                     (Treatment3 == "" & Treatment4 !=""), "individual", "combination"))

  results[,"Cisp"] <- as.numeric(results[,"Treatment3"])
  results[,"APR"] <- as.numeric(results[,"Treatment4"])

  results[,"Frac_Cisp"] <- results$Treatment2 *(results$Cisp/(results$Cisp + results$APR))
  results[,"Frac_APR"] <- results$Treatment2 *(results$APR/(results$Cisp + results$APR))

  #checking if all fractikons all up to Treatment2. used fussy logic
  print("---Checking if drug fractions correspond to total dose---")
  print(paste("Is difference > 0.01? :",
              any(na.omit((results$Frac_APR + results$Frac_Cisp) - results$Treatment2) > 0.01)))

  ## -- expected values based on DRC
  drugs <- unique(results[results$Type == "individual", "BioGroup"])
  logic.string <- intersect(grep(toupper("drc"), toupper(results$BioGroup)),
                            grep(toupper("cisplatin"), toupper(results$BioGroup)))
  temp <- unique(results[logic.string, c("min", "max", "slope", "ic50")])
  results[,"Exp_cisp"] <- with(temp,
                               estimate.response(results$Frac_Cisp, min, max,slope,ic50))

  logic.string <- intersect(grep(toupper("drc"), toupper(results$BioGroup)),
                            grep(toupper("apr-246"), toupper(results$BioGroup)))
  temp <- unique(results[logic.string, c("min", "max", "slope", "ic50")])
  results[,"Exp_APR"] <- with(temp,
                              estimate.response(results$Frac_APR, min, max,slope,ic50))



  ###-- Additive model of synergy
  ## Ref: Jonsson et al. Eur J Clin Pharmacol (1998) 54: 509 -514.
  results[,"Expected_viability"] <- results[,"Exp_cisp"] * results[,"Exp_APR"]
```

```
  results[,"Ratio_obs_exp"] <- with(results, Percent_control/Expected_viability)

  results[,"Comb_effect"] <- with(results,
                                  ifelse(Ratio_obs_exp < 0.8, "Synergy",
                                         ifelse(Ratio_obs_exp > 1.2, "subadditive", "additive")))
  results <- results[order(results$Comb_effect, decreasing = TRUE),]
  if(plotGraph){
    plot(x = results$Expected_viability, y = results$Percent_control, pch = 1,
         main = unique(results$Treatment1),
         sub = "(Size of the points is inversely propotional to the SI)",
         cex.sub = 0.7,
         xlab = "Predicted viability", ylab="Observed viability",
         cex = 1/results$Ratio_obs_exp,
         col = ifelse(results$Comb_effect == "Synergy", "red",
                      ifelse (results$Comb_effect == "subadditive", "blue", "grey40")))
    legend("topleft", legend = c("Synergy","Additive", "Subadditive"), pch = 1,
           col = c("red", "grey40", "blue"))
  }
  return(results)
}
```

Miscellaneous functions for plotting graphs

```
custom.ic50 <- function(merged,plotType = "all", xlab = NULL, ylab = NULL,
                        main = NULL, showIC50 = TRUE, plot = TRUE, ...){
  require(drc)
  require(magicaxis)
  bioGroups <- na.omit(unique(merged$BioGroup))

  biogroup.ic50 <- sapply(1: length(bioGroups), function(i){
    temp2 <- subset(merged, BioGroup ==  bioGroups[i])
    fit <- drm(Percent_control ~ Treatment2,
               fct = LL.4(names = c("Slope", "Lower Limit", "Upper Limit", "ED50")),
               data = temp2)
    ed50 <- coef(summary(fit))[4,1] #ED50
    if(plot){
      plot(fit, type = plotType, main = bioGroups[i], ann = FALSE,
           axes = FALSE,
           bty = "n", ...)
      magaxis(tcl=-0.75, mgp = c(2,1,0))


      if(is.null(xlab)){
        title(xlab = unique(temp2$Treatment3))
      } else{
        title(xlab = xlab)
      }
      if(is.null(ylab)){
        title(ylab = "% viability")
      } else{
        title(ylab = ylab)
      }
```

```
      if(is.null(main)){
        title(main = bioGroups[i])
      } else{
        title(main = main)
      }

      if(showIC50){
        legend("topright", paste("IC50:", signif(ed50,3)),bty = "n")
      }
    }
    ED(fit, 50, interval = "delta", display = FALSE)
  })
  colnames(biogroup.ic50) <- bioGroups
  rownames(biogroup.ic50) <- c("IC50", "SEM", "Lower", "Upper")
  t(biogroup.ic50)
}

multiplot <- function(..., plotlist=NULL, file, cols=1, layout=NULL) {
  require(grid)

  plots <- c(list(...), plotlist)
  numPlots = length(plots)

  if (is.null(layout)) {
    layout <- matrix(seq(1, cols * ceiling(numPlots/cols)),
                     ncol = cols, nrow = ceiling(numPlots/cols))
  }

  if (numPlots==1) {
    print(plots[[1]])

  } else {
    # Set up the page
    grid.newpage()
    pushViewport(viewport(layout = grid.layout(nrow(layout), ncol(layout))))

    # Make each plot, in the correct location
    for (i in 1:numPlots) {
      # Get the i,j matrix positions of the regions that contain this subplot
      matchidx <- as.data.frame(which(layout == i, arr.ind = TRUE))

      print(plots[[i]], vp = viewport(layout.pos.row = matchidx$row,
                                      layout.pos.col = matchidx$col))
    }
  }
}
```

Running an experiment

Reading data

All appropriate runs were merged in to an Excel file '160130 all input'. These include 160111, 160121 and 160125. Each run was mentioned using ExpID column. Each run was normalised to vehicle (intra-plate normalisation).

```
KEYS <- c("Treatment1","Treatment5")
library(xlsx)
```

```
## Loading required package: rJava
```

```
## Loading required package: xlsxjars
```

```
### ----------------------------
### --- PREPROCESSING CODE ---
### ----------------------------
INFO <- read.xlsx("160130_all_inputs.xlsx", sheetName = "Sheet1")
INFO<- INFO[INFO$Exclude != "Y",]

# read all files in INFO aka 160130_all_inputs.xlsx
df <- Reduce(function(f,i){
  # print(paste (f, i))
  temp <- easy.mts(subset(INFO, ExpID == i), plotTechRep  = FALSE, KEYS= KEYS)[[1]]
  if(i == unique(INFO$ExpID)[1]){
    f <- temp
  } else{
    f <- rbind(f,temp)
  }
}, unique(INFO$ExpID), init = unique(INFO$ExpID)[1])

ExpDesign <- generate.ExpDesign(df, KEYS = KEYS)
ExpDesign[,"BioGroup"] <- ExpDesign$Treatment5

### removing conditions with n = 1
temp <- table(ExpDesign$BioGroup)
temp <- temp[which(temp >1)]
ExpDesign <- subset(ExpDesign, ExpDesign$BioGroup %in% names(temp))

merged <- merge(df, ExpDesign[, c("Keys", "BioGroup", "isAccurate")], all = FALSE)
merged <- transform(merged, Treatment2 = as.numeric(as.character(Treatment2)))
merged <- droplevels(subset(merged, Treatment2 > 0))
merged <- transform(merged, Treatment2 = as.numeric (Treatment2))

### ----------------------------
### --- End of PREPROCESSING CODE ---
### ----------------------------
```

IC50s according to biological groups

Experimental design was generated using a function in MTS5 R file. Treatment5 was assigned at BioGroups.

```
ic50 <- try(custom.ic50(merged, xlab = "Total dose (uM)", plot = F))
```

```
## Loading required package: magicaxis
## Warning: package 'magicaxis' was built under R version 3.2.5
## Loading required package: sm
## Warning: package 'sm' was built under R version 3.2.5
## Package 'sm', version 2.2-5.4: type help(sm) for summary information
##
## Attaching package: 'sm'
## The following object is masked from 'package:MASS':
##
##     muscle
## Loading required package: mapproj
## Warning: package 'mapproj' was built under R version 3.2.5
## Loading required package: maps
## Warning: package 'maps' was built under R version 3.2.5
## Loading required package: celestial
## Warning: package 'celestial' was built under R version 3.2.5
## Loading required package: RANN
## Warning: package 'RANN' was built under R version 3.2.5
```

```
ic50 <- ic50[order(ic50[,"IC50"], decreasing = TRUE),]
library(gplots)
```

```
## Warning: package 'gplots' was built under R version 3.2.5
##
## Attaching package: 'gplots'
## The following object is masked from 'package:plotrix':
##
##     plotCI
## The following object is masked from 'package:stats':
##
##     lowess
```

```
par(mar= c(3,16,2,2), mgp = c(2,1,0), mfrow = c(1,1))
barplot2(ic50[,1], plot.ci = TRUE, ci.l = ic50[,"Lower"],
         ci.u = ic50[,"Upper"],
         las = 2, cex.names = 0.7, xlab = "IC50 (uM)",
         main ="IC50 of all conditions", horiz = TRUE)
```

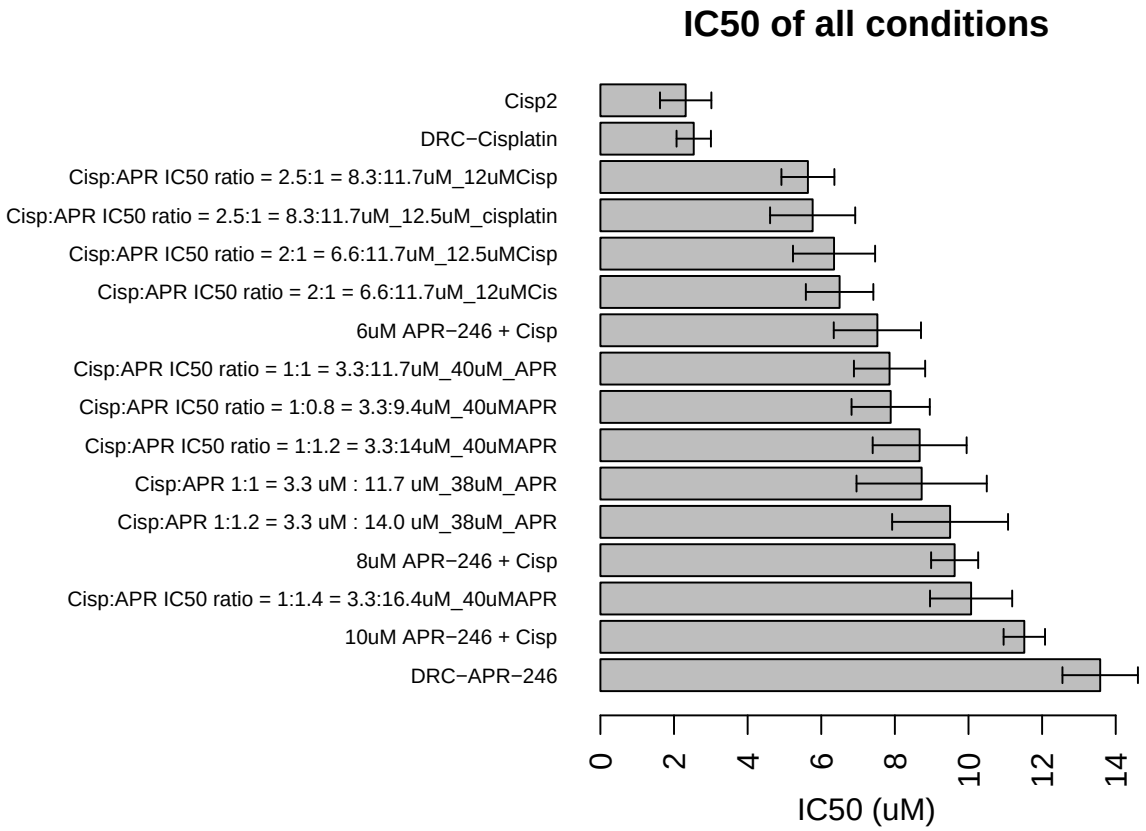

Synergy

Additive model was implimented in R. First, expected effect (death) was estimated using DRC of both drugs and exptected additive effect was calculated, which was compared to the observed effect. Ratio of observed/predicted indicates type of drug interaction. If ratio is < 0.8, it's synergy and > 1.2 indicates subaddtivity. Ratio between these values are considered additive because of error in measurements.

160103 and 160108 were exclused as it only has DRCs. This gives n = 3 for IC50 ratio dilutions and fixed APR-246 + varied cisplatin.

Overview of synergies

Following code identifies synergistic combinations by calculating SI and SEM at each drug combination.

```
temp <- unique(merged$Treatment1)
par(mar=c(5.1,4.1,4.1,2.1))
synergy.df <- Reduce(function(f,i){
  # print(i)
  tempdf <- subset(merged, Treatment1 == i)
  temp2 <- additive.synergy(tempdf, plotGraph = F)
  if(i == temp[1]){
    f <- temp2
  } else{
    f <- rbind(f,temp2)
```

```
  }
}, temp, init = temp[1])
```

```
## [1] "---Checking if drug fractions correspond to total dose---"
## [1] "Is difference > 0.01? : FALSE"
## [1] "---Checking if drug fractions correspond to total dose---"
## [1] "Is difference > 0.01? : FALSE"
## [1] "---Checking if drug fractions correspond to total dose---"
## [1] "Is difference > 0.01? : FALSE"
```

```
syn.mean <- aggregate(synergy.df$Ratio_obs_exp,
                      by = list(synergy.df$BioGroup,
                                synergy.df$Treatment3,synergy.df$Treatment4),
                      mean)
colnames(syn.mean) <- c("BioGroup", "Treatment3","Treatment4", "mean_ratio")
syn.sem <- aggregate(synergy.df$Ratio_obs_exp,
                     by = list(synergy.df$BioGroup,
                               synergy.df$Treatment3,synergy.df$Treatment4),
                     std.error)
syn.sem <- syn.sem[order(syn.sem$x, decreasing = TRUE),]
colnames(syn.sem) <- c("BioGroup", "Treatment3","Treatment4", "sem_ratio")
syn.summary <- merge(syn.mean, syn.sem)
syn.summary <- transform(syn.summary, Treatment3 = as.numeric(Treatment3),
                         Treatment4 = as.numeric(Treatment4))
master.syn.df <- syn.summary

plot(x= syn.summary$Treatment4, syn.summary$Treatment3,
     cex = 1/syn.summary$mean_ratio,
     xlab ="APR-246 (uM)", ylab = "Cisplatin (uM)",
     main = "Synergy at different concentrations - All data",
     sub = "Dotted line represent IC50 of each drug; size of bubbles represent strength of synergy")
abline(h = ic50["DRC-Cisplatin","IC50"], lty = 2)
abline(v = ic50["DRC-APR-246","IC50"], lty = 2)
```

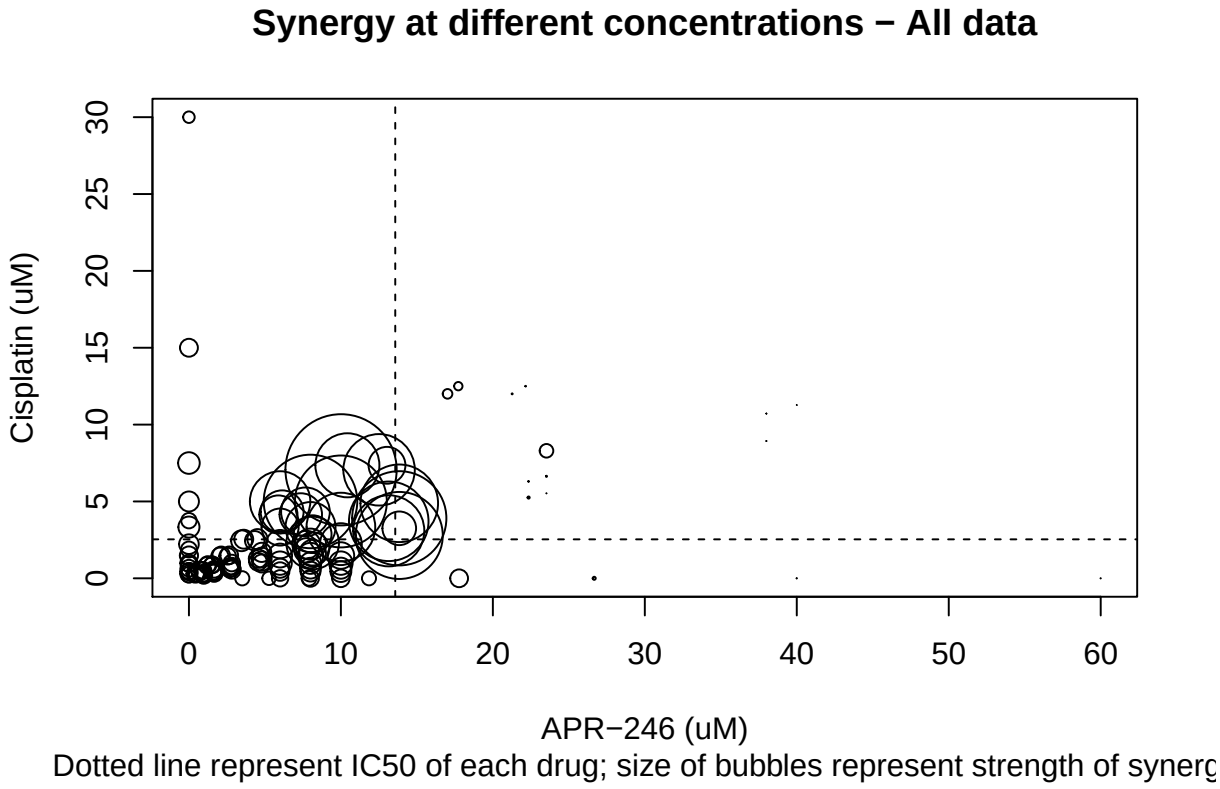

Filtered data

All points with synergy ratio < 0 (some points have negative values) and those with >1 ratio were excluded. This allows to focus on synergistic interactions, ie SI ratio < 0.8.

```
syn.summary <- subset(syn.summary, mean_ratio >0 & mean_ratio <1)
syn.summary <- syn.summary[order(syn.summary$sem_ratio),]
syn.summary$Col <- brewer.pal(9, "Set1")[as.numeric(cut(syn.summary$sem_ratio,breaks = 9))]
syn.summary <- syn.summary[order(syn.summary$sem_ratio, decreasing = FALSE),]
layout(matrix(c(1,2), 2,1), widths = c(1,1), heights = c(3,1))
par(mar = c(3, 3, 2,1), mgp = c(2,1,0))
range(syn.summary$sem_ratio)
```

```
## [1] 0.01692255 0.25010933
```

```
a <- seq(range(syn.summary$sem_ratio)[1],
         range(syn.summary$sem_ratio)[2], length.out = 9)
plot(x= syn.summary$Treatment4, syn.summary$Treatment3,
     cex = 1/syn.summary$mean_ratio, pch = 16,
     xlab = bquote("APR-246 ("*mu*"M)"),
     ylab = bquote("Cisplatin ("*mu*"M)"),
     main = "Synergies at different concentrations - filtered data",
     sub = "Dotted line represent IC50 of each drug; size of bubbles represent strength of synergy",
     col = alpha(syn.summary$Col, 0.6))

abline(h = ic50["DRC-Cisplatin","IC50"], lty = 2, col = "grey50")
abline(v = ic50["DRC-APR-246","IC50"], lty = 2,col = "grey50")
par(mar = c(1,1,1,1))
```

```
plot(1:2,1:2, type = "n", bty = "n", axes = FALSE, xlab = "", ylab = "")

legend("top", pch = 16, col = alpha(brewer.pal(9, "Set1"),0.6), cex = 1,
       legend = round(seq(range(syn.summary$sem_ratio)[1],
                          range(syn.summary$sem_ratio)[2], length.out = 9),2),
       ncol = 9, title = "Colour codes represent SEM")
```

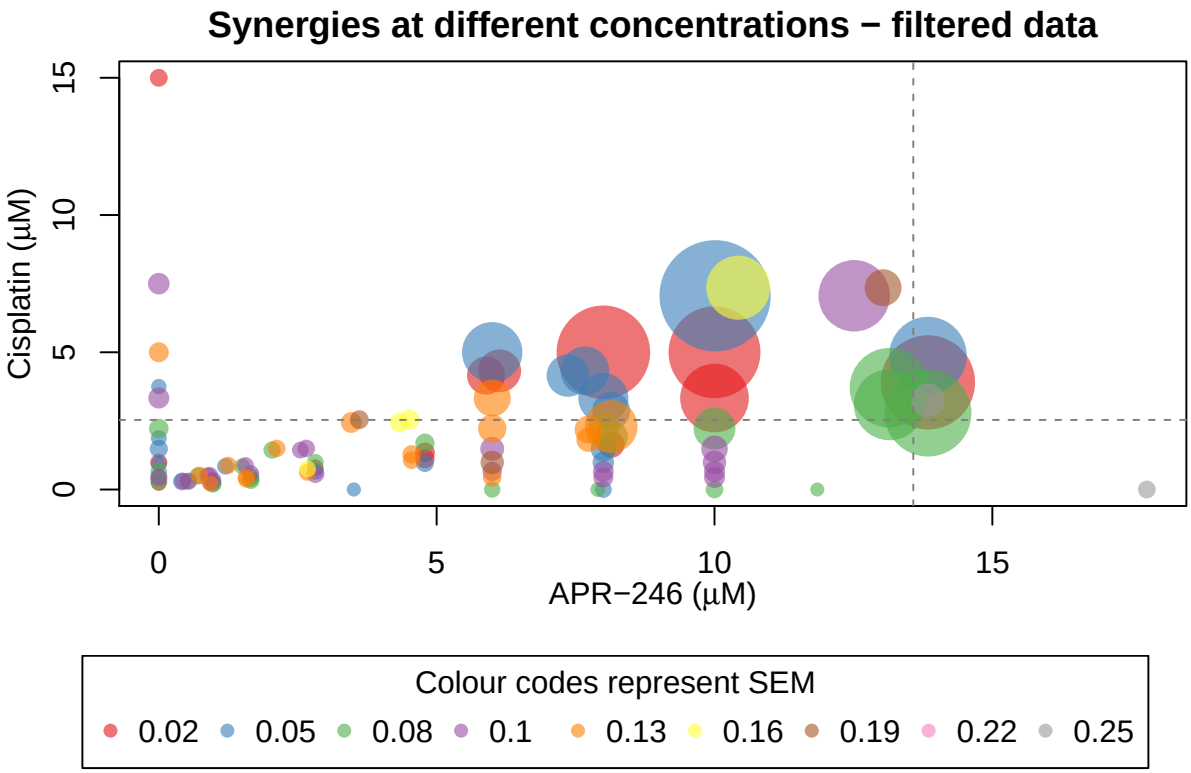

Appendix D

Publications

RESEARCH ARTICLE

Comparison of Methodologies to Detect Low Levels of Hemolysis in Serum for Accurate Assessment of Serum microRNAs

Jaynish S. Shah[1], Patsy S. Soon[2,3,4], Deborah J. Marsh[1]*

1 Hormones and Cancer Group, Kolling Institute of Medical Research, Royal North Shore Hospital, University of Sydney, St. Leonards, New South Wales, Australia, **2** South Western Sydney Clinical School, University of New South Wales, Kensington, New South Wales, Australia, **3** Department of Surgery, Bankstown Hospital, Bankstown, New South Wales, Australia, **4** Medical Oncology Group, Ingham Institute for Applied Medical Research, Liverpool Hospital, Liverpool, New South Wales, Australia

* deborah.marsh@sydney.edu.au

Abstract

microRNAs have emerged as powerful regulators of many biological processes, and their expression in many cancer tissues has been shown to correlate with clinical parameters such as cancer type and prognosis. Present in a variety of biological fluids, microRNAs have been described as a 'gold mine' of potential noninvasive biomarkers. Release of microRNA content of blood cells upon hemolysis dramatically alters the microRNA profile in blood, potentially affecting levels of a significant number of proposed biomarker microRNAs and, consequently, accuracy of serum or plasma-based tests. Several methods to detect low levels of hemolysis have been proposed; however, a direct comparison assessing their sensitivities is currently lacking. In this study, we evaluated the sensitivities of four methods to detect hemolysis in serum (listed in the order of sensitivity): measurement of hemoglobin using a Coulter® AcT diff™ Analyzer, visual inspection, the absorbance of hemoglobin measured by spectrophotometry at 414 nm and the ratio of red blood cell-enriched miR-451a to the reference microRNA miR-23a-3p. The miR ratio detected hemolysis down to approximately 0.001%, whereas the Coulter® AcT diff™ Analyzer was unable to detect hemolysis lower than 1%. The spectrophotometric method could detect down to 0.004% hemolysis, and correlated with the miR ratio. Analysis of hemolysis in a cohort of 86 serum samples from cancer patients and healthy controls showed that 31 of 86 (36%) were predicted by the miR ratio to be hemolyzed, whereas only 8 of these samples (9%) showed visible pink discoloration. Using receiver operator characteristic (ROC) analyses, we identified absorbance cutoffs of 0.072 and 0.3 that could identify samples with low and high levels of hemolysis, respectively. Overall, this study will assist researchers in the selection of appropriate methodologies to test for hemolysis in serum samples prior to quantifying expression of microRNAs.

OPEN ACCESS

Citation: Shah JS, Soon PS, Marsh DJ (2016) Comparison of Methodologies to Detect Low Levels of Hemolysis in Serum for Accurate Assessment of Serum microRNAs. PLoS ONE 11(4): e0153200. doi:10.1371/journal.pone.0153200

Editor: Damir Janigro, Cleveland Clinic, UNITED STATES

Received: December 15, 2015

Accepted: March 24, 2016

Published: April 7, 2016

Data Availability Statement: All relevant data are within the paper and its Supporting Information files.

Funding: This study was supported by Ovarian Cancer Research Foundation (Australia) and the University of Sydney Cancer Research Fund [DJM] (http://www.ocrf.com.au/); Australian Postgraduate Award and Northern Clinical School Top-Up Scholarship [JSS]; Australian Research Council (ARC) (ARC Future Fellowship [FT100100489]) and National Health and Medical Research Council (NHMRC) (NHMRC Senior Research Fellowship [APP1004799]) [DJM]. (http://www.arc.gov.au) & (https://www.nhmrc.gov.au). The funders had no role

in study design, data collection and analysis, decision to publish, or preparation of the manuscript.

Competing Interests: The authors have declared that no competing interests exist.

Introduction

A class of small non-coding RNAs known as microRNA plays a central role in almost all known biological processes. microRNAs are approximately 17–22 nucleotides in length and when bound to the 3' UTR of target mRNAs, repress gene expression by degradation of target mRNA or suppressing translation [1–3]. The human genome is estimated to encode more than 1,000 microRNAs, which collectively regulate more than half of all protein coding genes [1–4]. Therefore, it is not surprising that aberrant microRNA expression is linked to development and progression of many diseases including cancer [1–3, 5, 6]. Furthermore, microRNA signatures of cancer tissues are associated with cancer types and subtypes as well as staging, progression, prognosis and response to treatments [3, 7–9].

Recently, microRNAs were identified in a range of body fluids including urine, serum, plasma, tears and saliva, highlighting them as potential 'gold mines' of noninvasive disease biomarkers [5, 6, 10–14]. Serum microRNAs can withstand extreme conditions such as extended storage, multiple freeze-thaw cycles, high and low pH and even boiling [6, 15, 16]. The encapsulation of microRNA into vesicles (exosomes, microvesicles and high-density lipoproteins), chemical modifications or association with protein complexes such as Ago2, an essential protein for RNA interference, are all currently thought to provide protection against potent endogenous ribonucleases present in the blood [5, 6, 14, 17–20].

The source of microRNAs, collection protocol, extraction and detection methods, as well as inter-individual variables such as age, diet, race and even altitude have been shown to influence the ability to robustly determine microRNA levels. These and other pre-analytical and analytical factors must be addressed in the development of reliable and reproducible microRNA-based tests for clinical settings [15, 16, 21]. In addition, microRNA content released from blood cells upon hemolysis can dramatically alter the expression of certain microRNA, and may lead to false discovery of disease-associated biomarkers [22–24]. One study identified over half of the proposed microRNA biomarkers of solid cancers have been identified at high levels in one or more types of blood cells [25]. Further, up to 65% of detectable microRNAs in plasma have been shown to be affected by hemolysis [23]. While a number of studies have suggested that miR-16 is suitable as a reference microRNA for normalization of samples [26, 27], it is significantly altered by hemolysis, raising some concern for its routine use as a reference microRNA in serum or plasma studies [15, 23].

Currently, there is a lack of consensus on methods to detect low levels of hemolysis in serum that has the potential to affect the accuracy of microRNA-based tests. Reports have revealed that serum microRNA content is already altered due to hemolysis before samples manifest pink discoloration that is visible to the naked eye [23, 24]. In search of methods to detect low levels of hemolysis, Blondal *et al.* (2013) suggested that the ratio of red blood cell-enriched miR-451a to miR-23a, the latter microRNA being unaffected by hemolysis, can be used as a surrogate indicator of hemolysis [22]. miR-451a:miR-23a ratios of <5, 5–7 and >7 are, respectively, indicative of samples at low, moderate or severe risk of hemolysis [22]. The spectrophotometric absorbance of hemoglobin has also been suggested as a measure of hemolysis [22, 24]. A direct comparison of these methods has not been previously reported, nor have their sensitivities to detect low levels of hemolysis in serum been determined.

In this study, we evaluated the sensitivities of four separate methods to detect hemolysis in serum from healthy volunteers and women with ovarian cancer: (1) Coulter® AcT diff™ Analyzer measurement of hemoglobin, (2) visual inspection, (3) spectrophotometric measurement of absorbance of hemoglobin at 414 nm [22–24], and (4) the ratio of miR-451a to miR-23a [22].

Materials and Methods

Blood collection, processing and storage

Written consent was obtained and blood collected from 56 women with high-grade serous ovarian carcinoma (HGSOC; 64.1 ± 3.4 years) and 30 healthy females age matched within 5 years (61.0 ± 4.7 years) under a protocol approved by the Northern Sydney Local Health District Human Research Ethics Committee (Protocol #0310-209B). For women undergoing surgical resection of their tumor, blood was collected from the peripherally inserted central catheter (PICC line) prior to the induction of anesthesia. Blood from healthy volunteers was collected using a 21 gauge needle. In both cases, samples were transferred or collected into a 9 ml BD Vacutainer serum tube (BD #455092, North Ryde, NSW, Australia). Blood was allowed to clot for 15–30 minutes at 4°C and centrifuged at 3000 rpm for 15 minutes at 4°C. Serum was carefully withdrawn without disturbing the buffy coat and immediately stored at -80°C in 500 μl aliquots as part of the Kolling Institute Gynecological Tumor Bank. Samples were rapidly thawed in a 37°C water bath as required.

Hemolysis dilution series

Whole blood, 0.5 ml collected from a healthy volunteer, was allowed to clot in an eppendorf tube, and sonicated until the sample was completely fluid and bright red, indicative of a high degree of hemolysis. Serum was isolated from the blood of a healthy volunteer as per the healthy volunteers' protocol described above. This sample, collected under optimal conditions, was classified as unhemolyzed for the purpose of this study. A hemolysis dilution series comprising 100%, 20%, 4%, 1%, 0.25%, 0.062%, 0.016%, 0.004%, 0.001% hemolyzed and unhaemolysed samples (v/v) was prepared by serial dilution of the 100% hemolyzed sample with unhemolyzed serum.

Assessment of hemolysis

Hemolysis in serum samples was measured using 4 methods. The first method measured hemoglobin concentration using the Coulter® AcT diff™ Analyzer and the Tainer Reagent Kit (Beckman Coulter Inc # 8547135, Lane Cove, NSW, Australia). Three technical replicates were performed for each sample. The second method to assess hemolysis was simple visual inspection of serum samples for pink discoloration indicative of free hemoglobin against a white background. Visual discoloration of each sample was scored from 0 (unhemolyzed serum) to 5 (100% hemolyzed serum). The third method was measurement of the absorbance of hemoglobin at 414 nm using a NanoDrop™ 1000 spectrophotometer (Thermo Scientific, Scoresby, Victoria, Australia), averaging two technical replicates per sample. Lastly, the fourth method used determined the ratio of miR-451a to miR-23a-3p (delta Cq (miR-23a-3p—miR-451a)) referred to hereon as the "miR ratio"), with real-time reverse transcription (RT)-PCR using a 7900HT Fast Real-Time PCR System (Life Technologies, Scoresby, Victoria, Australia). Three RT reactions were performed for each sample followed by one PCR per RT.

RNA extraction and real-time RT-PCR

RNA was extracted from 200 μl serum using the miRCURY RNA isolation kit for Biofluids (Exiqon #300112, Vedbaek, Denmark) according to the manufacturer's instructions. One μg MS2 bacteriophage carrier RNA (Roche #10165948001, Castle Hill, NSW, Australia) was added during the lysis step. RNA was eluted in 25 μl nuclease-free water twice (final volume 50 μl) and stored at -80°C. RT was performed using 2 μl RNA template per 10 μl RT reaction using the Universal cDNA Synthesis kit (Exiqon #203301). Three independent RT reactions

were performed per sample, and one PCR conducted for each. The real-time RT-PCR master mix contained 100-fold diluted cDNA, 1X ExiLENT SYBR Green master mix (Exiqon #203420) and 1X ROX reference dye (Life Technologies #12223–012). Ten μl of the master mix was transferred to each well of a Serum/Plasma Focus microRNA PCR panel (Exiqon #203843) or Pick-&-Mix microRNA PCR panel (Exiqon #203802) containing locked nucleic acid (LNA) primers using the epMotion 5070 liquid handling system (Eppendorf, North Ryde, NSW, Australia). Real-time RT-PCR was performed on a 7900HT Fast Real-Time PCR System (Life Technologies). PCR conditions were as follows: 95°C for 10 minutes; followed by 40 amplification cycles of 95°C for 10 seconds and 60°C for 1 minute, followed by melting curve analysis.

Statistical analyses

Real-time RT-PCR data was exported and analyzed in GenEx software V6 (Exiqon #207016) and adjusted for plate-to-plate PCR variability using the spike-in miR UniSP3. Further analyses were performed in the statistical language R using 'ggplot2', 'ROCR', 'verification', 'car' and 'plotrix' packages. An average of the technical replicates was calculated for each sample. A *P-value* of <0.05 using the student's t-test assuming equal variance or Mann–Whitney *U* test was considered as significant. Results are presented as mean ± 2 × S.E.M. Error bars in all Figs represent S.E.M.

Results

Sensitivities of four methods to detect hemolysis

Four methods for the detection of hemolysis were compared using the hemolysis dilution series as described. The Coulter® AcT diff™ Analyzer measurement of hemoglobin could detect down to 1% hemolysis, while the 0.25% hemolyzed and the unhemolyzed sample remained indistinguishable (Fig 1B). By visual inspection alone, the pink discoloration of free-hemoglobin could be detected down to 0.25% hemolysis (Fig 1A and 1C; S1 File). In contrast, the spectrophotometric method could detect down to 0.004% hemolysis (Fig 1D). The calculated miR ratio could detect down to 0.001% hemolysis, the lowest point tested, making it the most sensitive method (Fig 1E). The Coulter® AcT diff™ method was excluded from further analyses due to its low sensitivity. Therefore, in order of decreasing sensitivity, the methods used can be ranked as miR ratio > spectrophotometry > visual inspection > Coulter® AcT diff™ Analyzer.

Next, we determined the hemolysis levels of 86 samples (56 women with ovarian cancer and 30 age-matched, healthy females) using visual inspection, spectrophotometric absorbance and the miR ratio (S2 File). Using the miR ratio as the 'gold standard', 16% (14/86), 48% (41/86) and 36% (31/86) of the samples were found to have low (miR ratio <5), moderate (miR ratio between 5 and 7) or severe (miR ratio >7) hemolysis, respectively, according to the criteria defined by Blondal *et al.* (2013), highlighting hemolysis as potentially a problematical factor, even when serum samples are collected under optimal conditions (Fig 2A). The miR ratio of the unhemolyzed sample used to construct the dilution series was 4.59 ± 0.10. In contrast, the miR ratio for the 0.25% hemolyzed sample, the limit of visual inspection, was 7.67 ± 0.14. Furthermore, 100% of the samples with pink discoloration (8/8) had a miR ratio >7, suggesting that any samples with visible pink discoloration were already severely affected by hemolysis (Fig 2A).

Identification of severely hemolyzed samples using visual inspection and the absorbance of hemoglobin

Since the majority of the severely hemolyzed samples based on the miR ratio (74%; 23/31) were visually undetectable, we investigated whether the absorbance of hemoglobin could be utilized

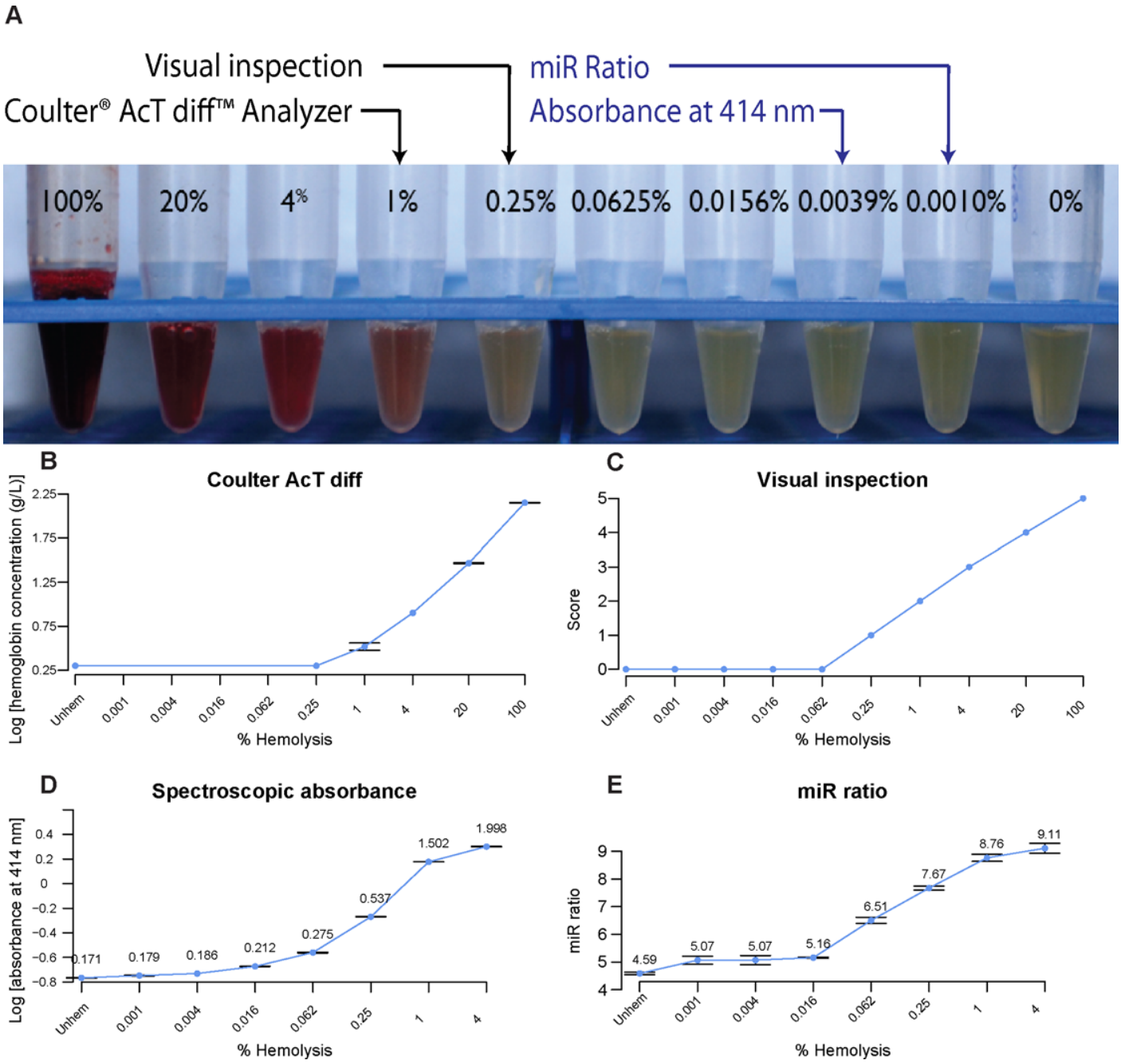

Fig 1. Sensitivities of four methods to detect hemolysis. (A) A hemolysis series was prepared by diluting 100% hemolyzed sample with unhemolyzed serum (0%), and the sensitivity of each method determined by its ability to detect hemolysis (indicated by arrows). **(B—E)** Detection of hemolysis using four methods. For visual inspection, samples were scored from 0 (unhemolyzed sample) to 5 (100% hemolysis). Averages of technical replicates are shown where appropriate. 'Unhem' denotes unhemolyzed serum. Absorbance measures (D) and miR ratios (E) are noted on the graphs.

doi:10.1371/journal.pone.0153200.g001

to detect additional severely hemolyzed samples, i.e miR ratio >7. The samples with pink discoloration had both higher absorbance (0.46 ± 0.11) and miR ratios (8.29 ± 0.51; Fig 2B).

No significant differences were observed between the absorbance of low and moderate hemolyzed samples as classified by the miR ratio ($P = 0.13$; Fig 3A); however, low and

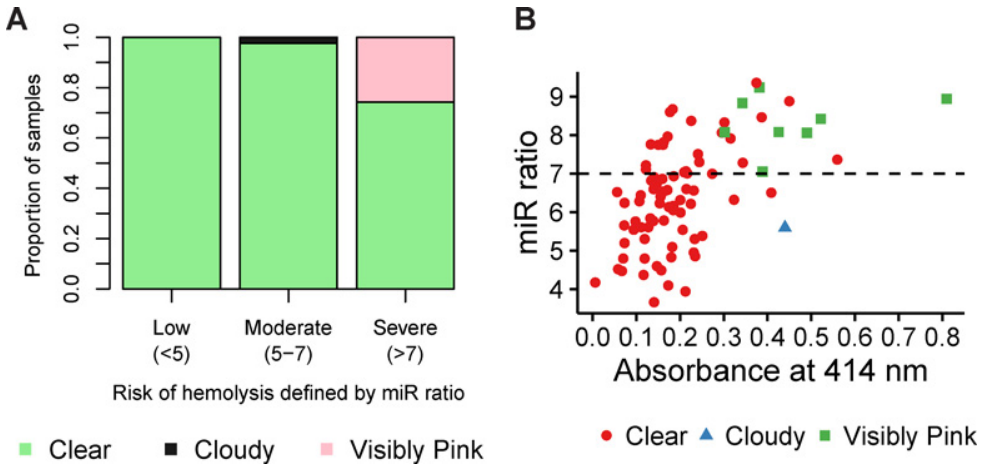

Fig 2. Comparison of methodologies for determining hemolysis in serum samples. Serum samples (N = 86) categorized by low (miR ratio <5; N = 14), moderate (miR ratio 5–7; N = 41) and severe (miR ratio >7; N = 31) hemolysis. Results of visual inspection are recorded for each category as the proportion of samples that are clear, cloudy or visibly pink. **(B)** Absorbance at 414 nm and the miR ratio of the cohort (N = 86). The dotted line represents the threshold above which samples are considered to be severely hemolysed according to the miR ratio (>7). Samples are color-coded according to their visual appearance (clear, cloudy or visibly pink).

doi:10.1371/journal.pone.0153200.g002

moderately hemolyzed samples were significantly different from the severely hemolyzed samples ($P < 0.001$ & < 0.0001, respectively). In other words, the miR ratio could further quantify hemolysis in the samples that were indistinguishable by absorbance. Severely hemolyzed samples (miR ratio >7) had 1.85-fold higher absorbance than low and moderately hemolyzed samples combined together (miR ratio <7; $P < 0.0001$; Fig 3B), indicating that the absorbance of hemoglobin could have predictive value in discriminating severely hemolyzed (miR ratio >7) samples. The receiver operator characteristic (ROC) curve separated severely hemolyzed samples from the rest with an area under curve (AUC) of 0.8038 ($P < 0.0001$; Fig 3C). The cut-off absorbance of 0.3 identified 48.4% (15/31) of hemolyzed samples, of which 8 were visually undetectable. The accuracy of prediction using this cut-off ($\frac{True\ Positive+True\ Negative}{Positive+Negtive}$) was 0.779.

We tested whether a similar analysis could identify an absorbance cut-off below which a sample is likely to have low levels of hemolysis (miR ratio <5; Fig 3D). Despite similar median values between the two groups (miR ratio <5 and >5), the cut-off absorbance of 0.072 could identify samples with a low risk of hemolysis with AUC of 0.7173 (Fig 3E). In general, absorbance-based tests to predict hemolysis suffered from low sensitivity, but offered high specificity and moderate positive and negative predictive values (Table 1).

Impact of hemolysis on hemolysis-sensitive microRNAs

Since the microRNAs affected by hemolysis originate predominantly from the rupture of red blood cells (RBC), the extent to which a specific microRNA is altered may depend on its abundance in RBC. Using RBC-derived miR-16-5p and miR-15b-3p surrogates for hemolysis-sensitive high and low abundant microRNAs based on Cq values in the cohort as a whole (Fig 4), we calculated differences in their levels across the 3 categories defined by the miR ratio, especially for miR-15b-3p as most microRNAs in serum are likely to present at moderate or low levels. The levels of miR-16-5p and miR-15b-3p increased as the miR ratio increased (Fig 4A and 4B). miR-16-5p and miR-15b-3p were found to be altered by 5.9-fold ($P < 0.0001$) and 4.5-fold ($P < 0.0001$), respectively, in the samples at severe risk of hemolysis (miR ratio >7) compared to

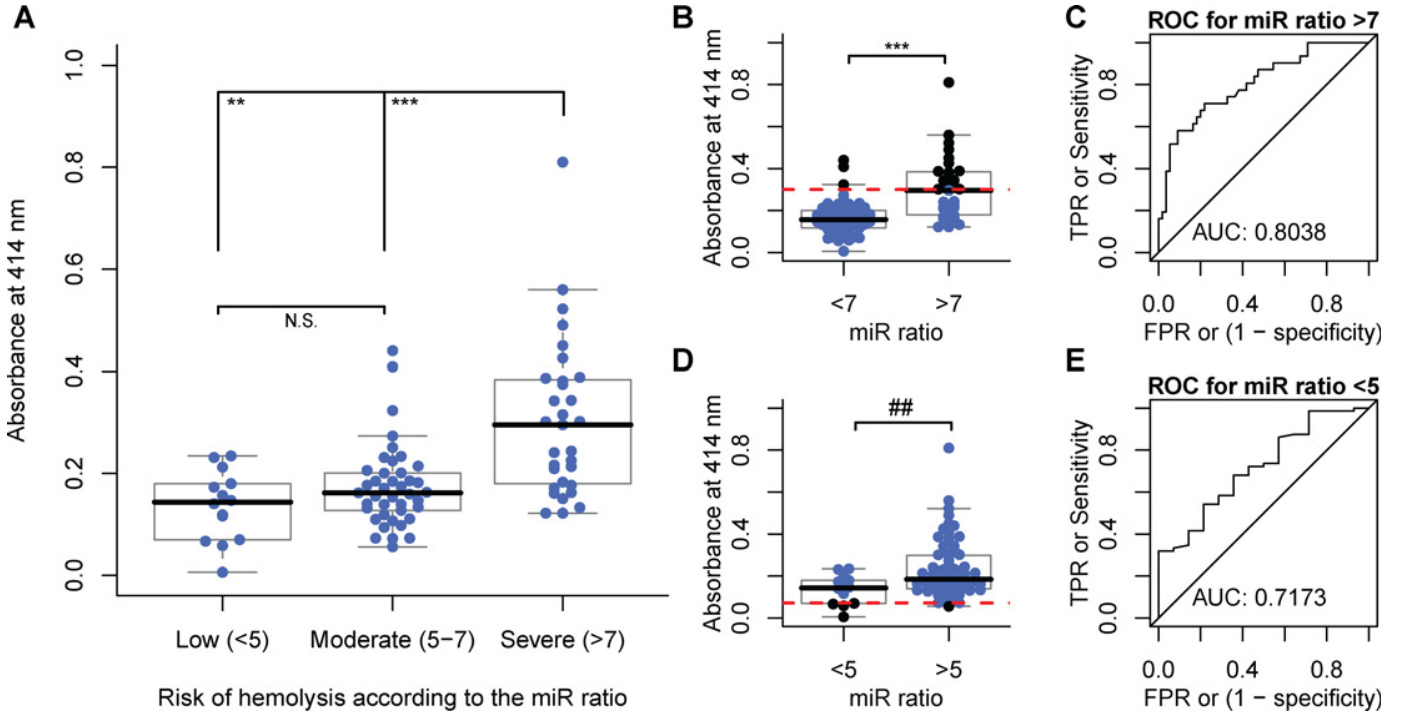

Fig 3. Identification of samples with low or severe hemolysis by spectrophotometric absorbance. (A) Cohort (N = 86) is grouped by low (miR ratio <5; N = 14), moderate (miR ratio 5–7; N = 41) and severe (miR ratio >7; N = 31) predicted risk of hemolysis, and absorbance at 414 nm was compared between groups. No significant differences in absorbance of samples were observed between the low and moderate groups; however, both were significantly different to the severe hemolysis group. **(B-C)** Absorbance of samples with miR ratio >7 was 1.85-fold higher than those with miR ratio <7. ROC analysis suggested that absorbance could predict severely hemolyzed samples (miR ratio >7). The cut-off for absorbance of 0.3 identified by ROC is shown as a dotted red line. **(D-E)** ROC analysis revealed a cut-off for absorbance of 0.072 (depicted as a dotted red line) below which samples would be predicted to have low levels of hemolysis (miR ratio <5). ** $P < 0.001$, *** $P < 0.0001$ and ## Mann-Whitney U test $P < 0.001$. 'TPR' and 'FPR' refer to true and false positive rates, respectively.

doi:10.1371/journal.pone.0153200.g003

those at low risk (miR ratio <5). Both microRNAs were also found to be elevated by approximately two-fold between miR ratio categories <5 compared to 5–7, as well as 5–7 compared to >7. Thus, both high and low abundant microRNAs susceptible to hemolysis are significantly

Table 1. Assessment of performance of the spectrophotometric absorbance of hemoglobin at 414 nm for predicting the miR ratio.

	Low risk (miR ratio <5)		Severe risk (miR ratio >7)	
	All samples (N = 86)	Clear samples* (N = 77)	All samples (N = 86)	Clear samples* (N = 77)
Cut-off absorbance	0.072	0.072	0.300	0.300
AUC	0.717	0.733	0.804	0.756
Accuracy	0.849	0.831	0.779	0.779
Sensitivity	0.250	0.250	0.484	0.333
Specificity	0.986	0.984	0.946	0.981
PPV	0.800	0.800	0.833	0.889
NPV	0.852	0.833	0.765	0.765

Absorbance measurements of samples were split into two groups for each comparison: (I) prediction of low risk of hemolysis (miR ratio <5): <5 versus >5, and (II) prediction of high risk of hemolysis (miR ratio >7): >7 versus <7. ROC analysis was performed for each comparison, and the cut-off absorbance that maximized the accuracy of prediction was selected. Sensitivity, specificity, PPV and NPV were calculated based on the chosen cut-off.

PPV: positive predictive values

NPV negative predictive values

*refers to samples that did not have a pink discoloration or were cloudy.

doi:10.1371/journal.pone.0153200.t001

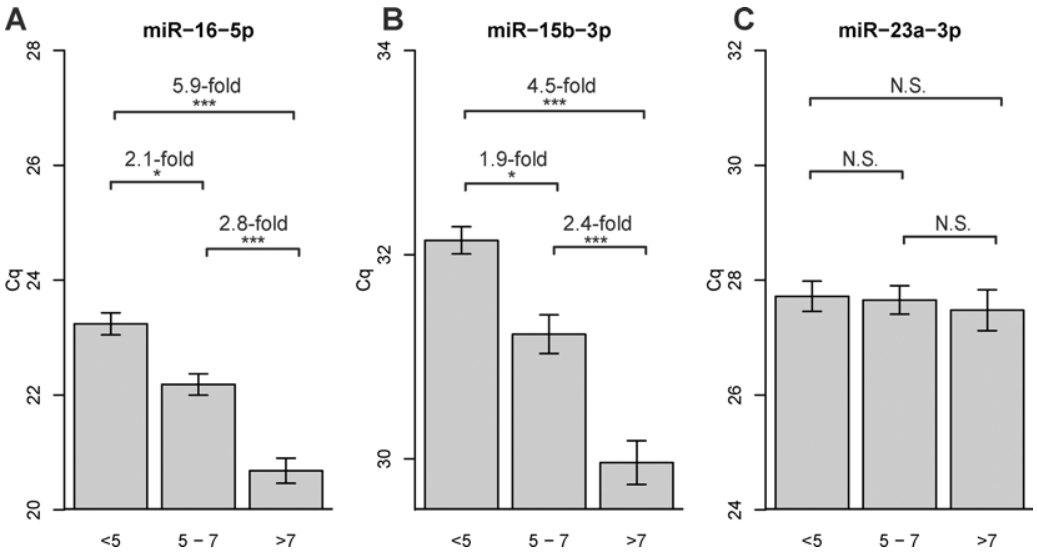

Fig 4. Hemolysis-sensitive high and low abundant microRNAs are significantly altered between categories defined by the miR ratio. (A) Levels of hemolysis-sensitive highly abundant serum microRNA miR–16–5p was found to be significantly altered across low, moderate and severely hemolyzed serum samples defined by miR ratios **(B)** Levels of a hemolysis-sensitive low abundant microRNA miR–15b–3p were also different across all miR ratio categories. **(C)** miR–23a–3p was present at a similar level amongst three categories, supporting its use as a reference microRNA in determining the miR ratio. * P <0.05, ** P < 0.001 and *** P < 0.0001.

doi:10.1371/journal.pone.0153200.g004

altered amongst 3 categories defined by the miR ratio. miR-23a-3p was present at a similar level in each of the 3 categories as expected (Fig 4C).

Discussion

Serum microRNAs are attractive non-invasive biomarkers because of their disease-specific expression and stability in a wide range of conditions. However, a series of pre-analytical and analytical variables must be considered in the development of robust and reliable microRNA-based tests [1, 2, 5–7, 9, 15, 16, 21]. The effect of release of the microRNA content of blood cells upon hemolysis dramatically alters the level of specific serum microRNAs. Recent studies have shown that 58% (46/79) of proposed microRNA biomarkers [25] for solid cancers were highly expressed in one or more blood cell types, and up to 65% of detectable microRNAs in plasma were affected by hemolysis [23]. Hemolysis in clinical samples is common. Reports have suggested that approximately 43% of clinical samples are hemolyzed as determined by free hemoglobin >0.5 g/L, whereas visual detection indicated by the presence of a pink discoloration is seen in less than 6% of samples [28, 29]. Therefore, quantifying hemolysis is an essential step for any procedure measuring circulatory microRNAs for diagnostic purposes or biomarker discovery. A number of methods to measure hemolysis in serum have been described; however, a direct comparison assessing their sensitivities has not been reported.

In our study of serum, using a 4-fold dilution series, visual inspection could only detect down to 0.25% hemolysis (v/v). This is comparable to the detection limit of 0.125% (v/v) identified by Kirschner *et al.* (2011) using a 2-fold dilution series of plasma [24]. We and others have shown that visual inspection, i.e. identification of visible pink, as a measure of hemolysis is insufficient as levels of hemolysis-sensitive microRNA such as miR-451a are already compromised prior to visual detection [22, 24].

The ratio of miR-451a to miR-23a-3p was found to be the most sensitive method that could detect down to 0.001% hemolysis in serum. We quantified hemolysis levels of 86 samples using

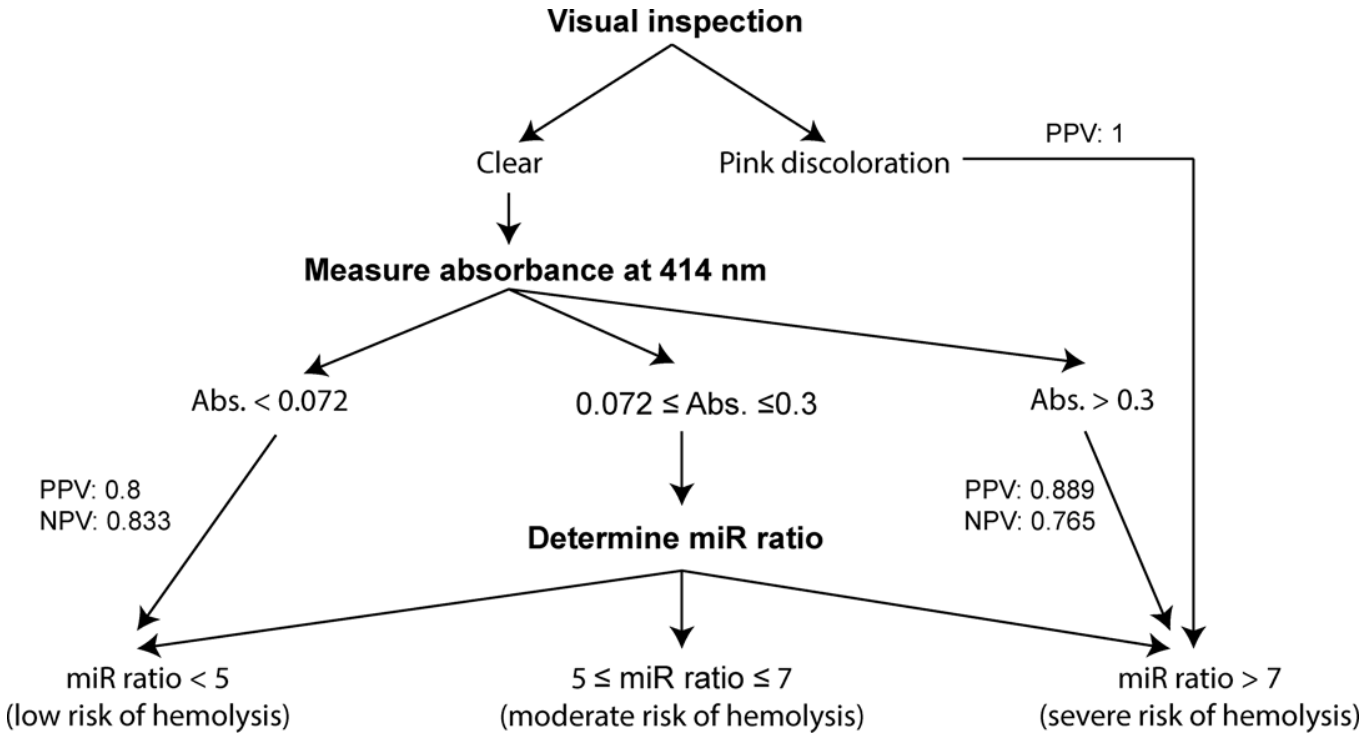

Fig 5. Assessment of hemolysis in serum samples. All serum samples exhibiting pink discoloration were found to be strongly affected by hemolysis for microRNA profiling according to the miR ratio. After exclusion of the visibly hemolyzed samples, samples with absorbance at 414 nm of >0.3 are also likely to be have miR ratio >7, predicting severe hemolysis. In contrast, samples with an absorbance at 414 nm of <0.072 are predicted to have a miR ratio <5. Samples meeting these criteria may be excluded from miR ratio for the purpose of determining hemolysis; however, the miR ratio should be determined for samples with absorbance between 0.072 and 0.3. PPV and NPV refer to positive and negative predictive values after removal of visibly hemolyzed or cloudy samples, respectively.

doi:10.1371/journal.pone.0153200.g005

the miR ratio, and discovered that hemolysis-sensitive microRNAs miR-15b-3p and miR-16-5p were significantly affected in the categories of hemolysis (low, moderate and severe) defined by Blondal *et al.* (2013) [22]. In particular, the levels of low abundant, hemolysis-sensitive miR-15b-3p were approximately 4.5-fold higher in the samples with low (miR ratio <5) versus severe (miR ratio >7) risk of hemolysis. The differences were greater for the more abundant miR-16-5p between the same groups (5.9-fold).

While the miR ratio was the most sensitive method to detect low levels of hemolysis, it may not be suitable for all large-scale screening for hemolysis due to additional cost and a relatively large requirement for starting material (200 μl serum). The absorbance of hemoglobin at 414 nm, on the other hand, is a suitable alternative as it overcomes these restrictions and was found to be more sensitive than visual inspection in our dataset. We tested whether absorbance could identify samples that are at a severe risk of hemolysis (miR ratio >7) but remained undetectable by visual inspection. ROC analysis revealed that absorbance at 414 nm >0.3 (water as blank) identified severely hemolyzed samples with accuracy, PPV and NPV of approximately 80% (Fig 5). Over half (8/15) of the samples were visually undetectable. Similarly, Kirschner *et al.* (2013) suggested use of absorbance at 414 nm >0.2 (unhemolyzed plasma as blank) to identify hemolysis in plasma as it reduced variability in miR-451 levels [23]. The different choices of blanks and serum versus plasma may have led to the differences observed. Interestingly, some samples in our study had lower absorbance than the unhemolyzed serum used in the dilution series; therefore, water seemed to be an appropriate choice of blank. Similarly,

based on our data, samples with absorbance less than 0.072 are likely to be at low risk of hemolysis (miR ratio <5).

Given that a substantial number of circulatory microRNAs are known to be affected by hemolysis, the miR ratio is recommended as the final quality control step unless clearly indicated in the literature that the microRNA of interest is not affected by hemolysis, for example miR-122 [15, 30, 31]. If a promising microRNA is found to be sensitive to hemolysis, clinical interpretation of the test should evaluate the extent to which it is modified by the underlying condition or disease as well as hemolysis. Since hemolysis is common in clinical samples, this comparison will also help identify levels of hemolysis that are acceptable in the samples without significantly affecting the performance of a given test. Failure to meet quality standards would jeopardize accuracy of measurement in the context of a disease specific relationship of any microRNA known to be affected by hemolysis. Measuring absorbance of hemoglobin at 414 nm can identify samples that are likely to be at either a low or severe risk of hemolysis, reducing the total number of samples that would require testing by miR ratio to determine hemolysis. Despite high specificity, we have shown that the absorbance-based method is inaccurate for predicting hemolysis between absorbance readings at 414 nm of 0.3 and 0.072, and suggest that the miR ratio should be used to test for hemolysis in samples that fall within this range. Further, bilirubin is known to interfere with the absorbance of hemoglobin, rendering this method inaccurate in conditions such as jaundice where serum bilirubin levels are elevated [32].

Conclusion

The pivotal role of hemolysis as a quality control measure in any serum microRNA profiling cannot be underestimated. The ratio of miR-451a to miR-23a-3p proposed by Blondal *et al.* (2013) was found to be the most sensitive method to detect low levels of hemolysis, and should be routinely employed. High and low abundant microRNAs sensitive to hemolysis are significantly altered in the three categories of hemolysis (low, moderate and severe) defined by Blondal *et al.* (2013). Visual inspection to detect hemolysis is insufficient as microRNA in serum samples that do not display a visible pink discoloration can still show effects of hemolysis, as shown by a miR ratio >7. Measuring hemoglobin's absorbance at 414 nm can identify samples that are likely to be at a low or high risk of hemolysis, therefore reducing the total number of samples that should be further analysed for hemolysis using the miR ratio test.

Supporting Information

S1 File. Sensitivities of four methods to detect hemolysis. This table shows levels of hemolysis measured by Coulter® AcT diff™ Analyzer, visual inspection, absorbance at 414 nm and the miR ratio in the hemolysis dilution series. The values represent averages of technical replicates.
(XLSX)

S2 File. Hemolysis levels in the cohort. This table shows hemolysis levels in 86 serum samples measured by visual inspection, absorbance at 414 nm and the miR ratio. In addition, levels of hsa-miR-16-5p and hsa-miR-15b-3p are also displayed. The values represent averages of technical replicates.
(XLSX)

Acknowledgments

This work was supported by a grant from the Ovarian Cancer Research Foundation (Australia) and the University of Sydney Cancer Research Fund. JSS was supported by an Australian

Postgraduate Award and Northern Clinical School Top-Up Scholarship. DJM was supported by the Australian Research Council (ARC) (ARC Future Fellowship [FT100100489]) and National Health and Medical Research Council (NHMRC) (NHMRC Senior Research Fellowship [APP1004799]). The Kolling Institute Gynecological Tumour Bank,Dr. Gregory Gard and Dr Sue Valmadre are thanked for supply of serum samples.

Author Contributions

Conceived and designed the experiments: JSS PSS DJM. Performed the experiments: JSS. Analyzed the data: JSS DJM. Contributed reagents/materials/analysis tools: JSS DJM. Wrote the paper: JSS PSS DJM.

References

1. Lin S, Gregory RI. MicroRNA biogenesis pathways in cancer. Nature Reviews Cancer. 2015; 15 (6):321–33. doi: 10.1038/nrc3932 PMID: 25998712
2. Schickel R, Boyerinas B, Park S, Peter M. MicroRNAs: key players in the immune system, differentiation, tumorigenesis and cell death. Oncogene. 2008; 27(45):5959–74. doi: 10.1038/onc.2008.274 PMID: 18836476
3. Volinia S, Calin GA, Liu C-G, Ambs S, Cimmino A, Petrocca F, et al. A microRNA expression signature of human solid tumors defines cancer gene targets. Proceedings of the National academy of Sciences of the United States of America. 2006; 103(7):2257–61. PMID: 16461460
4. Selbach M, Schwanhäusser B, Thierfelder N, Fang Z, Khanin R, Rajewsky N. Widespread changes in protein synthesis induced by microRNAs. Nature. 2008; 455(7209):58–63. doi: 10.1038/nature07228 PMID: 18668040
5. Cortez MA, Bueso-Ramos C, Ferdin J, Lopez-Berestein G, Sood AK, Calin GA. MicroRNAs in body fluids—the mix of hormones and biomarkers. Nature reviews Clinical oncology. 2011; 8(8):467–77. doi: 10.1038/nrclinonc.2011.76 PMID: 21647195
6. Cortez MA, Calin GA. MicroRNA identification in plasma and serum: A new tool to diagnose and monitor diseases. Expert Opinion on Biological Therapy. 2009; 9(6):703–11. doi: 10.1517/14712590902932889 PMID: 19426115
7. Lu J, Getz G, Miska EA, Alvarez-Saavedra E, Lamb J, Peck D, et al. MicroRNA expression profiles classify human cancers. Nature. 2005; 435(7043):834–8. doi: 10.1038/nature03702 PMID: 15944708
8. Iorio M, Visone R, Di Leva G, Donati V, Petrocca F, Casalini P, et al. MicroRNA signatures in human ovarian cancer. Cancer research. 2007; 67(18):8699–707. PMID: 17875710
9. Calin GA, Croce CM. MicroRNA signatures in human cancers. Nature Reviews Cancer. 2006; 6 (11):857–66. doi: 10.1038/nrc1997 PMID: 17060945
10. Mitchell PS, Parkin RK, Kroh EM, Fritz BR, Wyman SK, Pogosova-Agadjanyan EL, et al. Circulating microRNAs as stable blood-based markers for cancer detection. Proceedings of the National Academy of Sciences. 2008; 105(30):10513–8.
11. Taylor DD, Gercel-Taylor C. MicroRNA signatures of tumor-derived exosomes as diagnostic biomarkers of ovarian cancer. Gynecologic Oncology. 2008; 110(1):13–21. doi: 10.1016/j.ygyno.2008.04.033 PMID: 18589210
12. Resnick KE, Alder H, Hagan JP, Richardson DL, Croce CM, Cohn DE. The detection of differentially expressed microRNAs from the serum of ovarian cancer patients using a novel real-time PCR platform. Gynecologic Oncology. 2009; 112(1):55–9. doi: 10.1016/j.ygyno.2008.08.036 PMID: 18954897
13. Weber JA, Baxter DH, Zhang S, Huang DY, Huang K, Lee M, et al. The MicroRNA Spectrum in 12 Body Fluids. Clinical Chemistry. 2010; 56(11):1733–41. doi: 10.1373/clinchem.2010.147405 PMID: 20847327
14. Wang J, Zhang K-Y, Liu S-M, Sen S. Tumor-Associated Circulating MicroRNAs as Biomarkers of Cancer. Molecules. 2014; 19(2). doi: 10.3390/molecules19021912
15. McDonald JS, Milosevic D, Reddi HV, Grebe SK, Algeciras-Schimnich A. Analysis of circulating microRNA: preanalytical and analytical challenges. Clinical chemistry. 2011; 57(6):833–40. doi: 10.1373/clinchem.2010.157198 PMID: 21487102
16. Becker N, Lockwood CM. Pre-analytical variables in miRNA analysis. Clinical Biochemistry. 2013; 46 (10–11):861–8. doi: 10.1016/j.clinbiochem.2013.02.015 PMID: 23466658

17. Kosaka N, Iguchi H, Ochiya T. Circulating microRNA in body fluid: a new potential biomarker for cancer diagnosis and prognosis. Cancer science. 2010; 101(10):2087–92. doi: 10.1111/j.1349-7006.2010.01650.x PMID: 20624164

18. Arroyo JD, Chevillet JR, Kroh EM, Ruf IK, Pritchard CC, Gibson DF, et al. Argonaute2 complexes carry a population of circulating microRNAs independent of vesicles in human plasma. Proceedings of the National Academy of Sciences. 2011; 108(12):5003–8.

19. Turchinovich A, Weiz L, Langheinz A, Burwinkel B. Characterization of extracellular circulating microRNA. Nucleic acids research. 2011:gkr254.

20. Vickers KC, Palmisano BT, Shoucri BM, Shamburek RD, Remaley AT. MicroRNAs are transported in plasma and delivered to recipient cells by high-density lipoproteins. Nature cell biology. 2011; 13(4):423–33. doi: 10.1038/ncb2210 PMID: 21423178

21. Witwer KW. Circulating MicroRNA biomarker studies: pitfalls and potential solutions. Clinical chemistry. 2015; 61(1):56–63. doi: 10.1373/clinchem.2014.221341 PMID: 25391989

22. Blondal T, Nielsen SJ, Baker A, Andreasen D, Mouritzen P, Teilum MW, et al. Assessing sample and miRNA profile quality in serum and plasma or other biofluids. Methods. 2013; 59(1):S1–S6. doi: 10.1016/j.ymeth.2012.09.015 PMID: 23036329

23. Kirschner MB, Edelman JJB, Kao SC-H, Vallely MP, Van Zandwijk N, Reid G. Hemolysis and its impact on cell-free microRNA biomarkers. Frontiers in Genetics. 2013; 4. doi: 10.3389/fgene.2013.00094

24. Kirschner MB, Kao SC, Edelman JJ, Armstrong NJ, Vallely MP, van Zandwijk N, et al. Haemolysis during sample preparation alters microRNA content of plasma. PloS one. 2011; 6(9):e24145. doi: 10.1371/journal.pone.0024145 PMID: 21909417

25. Pritchard CC, Kroh E, Wood B, Arroyo JD, Dougherty KJ, Miyaji MM, et al. Blood cell origin of circulating microRNAs: a cautionary note for cancer biomarker studies. Cancer prevention research (Philadelphia, Pa). 2012; 5(3):492–7. doi: 10.1158/1940-6207.CAPR-11-0370 PMID: PMC4186243.

26. Chang KH, Mestdagh P, Vandesompele J, Kerin MJ, Miller N. MicroRNA expression profiling to identify and validate reference genes for relative quantification in colorectal cancer. BMC cancer. 2010; 10(1):173.

27. Davoren PA, McNeill RE, Lowery AJ, Kerin MJ, Miller N. Identification of suitable endogenous control genes for microRNA gene expression analysis in human breast cancer. BMC molecular biology. 2008; 9(1):76.

28. Lippi G, Salvagno GL, Favaloro EJ, Guidi GC. Survey on the prevalence of hemolytic specimens in an academic hospital according to collection facility: opportunities for quality improvement. Clinical Chemistry and Laboratory Medicine. 2009; 47(5):616–8. doi: 10.1515/CCLM.2009.132 PMID: 19317651

29. Hawkins RC. Phlebotomy site haemolysis rates vary inversely with workload. Clinical Chemistry and Laboratory Medicine. 2010; 48(7):1049–51. doi: 10.1515/CCLM.2010.224 PMID: 20441475

30. Qiu Z, Dai Y. Roadmap of miR-122-related clinical application from bench to bedside. Expert opinion on investigational drugs. 2014; 23(3):347–55. doi: 10.1517/13543784.2014.867327 PMID: 24354366

31. Ding X, Ding J, Ning J, Yi F, Chen J, Zhao D, et al. Circulating microRNA-122 as a potential biomarker for liver injury. Molecular medicine reports. 2012; 5(6):1428–32. doi: 10.3892/mmr.2012.838 PMID: 22427142

32. Noe DA, Weedn V, Bell WR. Direct spectrophotometry of serum hemoglobin: an Allen correction compared with a three-wavelength polychromatic analysis. Clinical chemistry. 1984; 30(5):627–30. PMID: 6713623

frontiers in
ONCOLOGY

REVIEW ARTICLE
published: 12 June 2014
doi: 10.3389/fonc.2014.00144

Histones and their modifications in ovarian cancer – drivers of disease and therapeutic targets

Deborah J. Marsh*, Jaynish S. Shah and Alexander J. Cole

Hormones and Cancer Group, Kolling Institute of Medical Research, Royal North Shore Hospital, The University of Sydney, Sydney, NSW, Australia

Edited by:
Ivan Garcia-Bassets, University of California San Diego, USA

Reviewed by:
Dineo Khabele, Vanderbilt University, USA
Alex Vaquero, The Bellvitge Institute for Biomedical Research (IDIBELL), Spain

****Correspondence:***
Deborah J. Marsh, Functional Genomics Laboratory, Hormones and Cancer Group, Kolling Institute of Medical Research, Royal North Shore Hospital, St Leonards, Sydney, NSW 2065, Australia
e-mail: deborah.marsh@sydney.edu.au

Epithelial ovarian cancer has the highest mortality of the gynecological malignancies. High grade serous epithelial ovarian cancer (SEOC) is the most common subtype, with the majority of women presenting with advanced disease where 5-year survival is around 25%. Platinum-based chemotherapy in combination with paclitaxel remains the most effective treatment despite platinum therapies being introduced almost 40 years ago. Advances in molecular medicine are underpinning new strategies for the treatment of cancer. Major advances have been made by international initiatives to sequence cancer genomes. For SEOC, with the exception of *TP53* that is mutated in virtually 100% of these tumors, there is no other gene mutated at high frequency. There is extensive copy number variation, as well as changes in methylation patterns that will influence gene expression. To date, the role of histones and their post-translational modifications in ovarian cancer is a relatively understudied field. Post-translational histone modifications play major roles in gene expression as they direct the configuration of chromatin and so access by transcription factors. Histone modifications include methylation, acetylation, and monoubiquitination, with involvement of enzymes including histone methyltransferases, histone acetyltransferases/deacetylases, and ubiquitin ligases/deubiquitinases, respectively. Complexes such as the Polycomb repressive complex also play roles in the control of histone modifications and more recently roles for long non-coding RNA and microRNAs are emerging. Epigenomic-based therapies targeting histone modifications are being developed and offer new approaches for the treatment of ovarian cancer. Here, we discuss histone modifications and their aberrant regulation in malignancy and specifically in ovarian cancer. We review current and upcoming histone-based therapies that have the potential to inform and improve treatment strategies for women with ovarian cancer.

Keywords: histone, ovarian cancer, splicing, lncRNA, polycomb repressive complex, histone deacetylase inhibitors, deubiquitinases, histone methyltransferases

INTRODUCTION

Epithelial ovarian cancer has the highest mortality of all of the gynecological malignancies, with high grade serous epithelial ovarian cancer (SEOC) the most common subtype. Due to general or non-descript symptoms of early stage disease, the majority of women initially present with advanced malignancy (Stage III or IV) where 5-year survival can be as low as 25% (1, 2). Standard of care is surgical debulking followed by combinations of platin-based drugs such as carboplatin with paclitaxel [reviewed in Ref. (3)]. Cisplatin was first approved by the Food and Drug Administration (FDA) for the treatment of ovarian cancer in 1978 (4), while paclitaxel was approved in 1992 (5). Some evidence exists to support the success of neoadjuvant chemotherapy in women who present with advanced, unresectable primary ovarian cancer, followed by interval debulking; however, data also exist suggesting there is little or no benefit to this approach (6, 7). Most women respond to standard of care chemotherapeutic drugs initially; but the majority relapse within 2 years, ultimately developing broad chemoresistance (8, 9).

Additional factors complicating the success of current treatment strategies for SEOC is lack of a clear understanding of the true site and cells of origin of this malignancy, with evidence mounting that SEOC may in fact arise in the secretory fimbrial cells of the fallopian tube (10, 11). Molecular heterogeneity of ovarian cancer also poses challenges, with distinct molecular subtypes based on gene expression identified within identical histopathological groupings such as SEOC (12). Knowledge of post-translational histone modifications associated with cancer, including ovarian cancer, is emerging. This review discusses histones and their post-translational modifications (PTMs) as key regulators of gene expression and DNA repair with relevance for the treatment of ovarian cancer.

GENETICS AND GENOMICS OF SEOC, INFORMING NEW THERAPIES

While advances in genetics have not fully addressed the challenges of treating ovarian cancer, elucidation of the mutational SEOC landscape is informing the development of therapies targeting DNA damage signaling pathways. Extensive international efforts channeled into sequencing a large cohort of sporadic SEOC through The Cancer Genome Atlas (TCGA) project has been revealing. With the exception of *TP53* that is mutated in

almost 100% of these cancers, there is a relatively low frequency of mutations (approximately 2–6%) in genes including *BRCA1*, *BRCA2*, *CSMD3*, *NF1*, *CDK12*, *FAT3*, *GABRA6*, and *RB1*, that might otherwise have been more directive for therapeutic targeting (13). Determining the role of multiple gene mutations in relation to the activation of cancer-associated signaling pathways for individual tumors will however be of value for guiding targeted therapies. The development of strategies to target mutant p53 proteins will clearly have major relevance to SEOC (14). Furthermore, large cohort studies of primary SEOC and SEOC cell line models have revealed extensive copy number variations that would function as a major driver of aberrant gene expression (13, 15).

Creating great excitement in this field is the introduction of a new class of drugs known as [poly (ADP-ribose) polymerase, PARP] inhibitors, including drugs such as Olaparib® (AZD2281, AstraZeneca), Rucaparib® (AG 014699, Clovis), and Veliparib® (ABT-888, Abbot) (16, 17). PARP1 is important in the cellular response to DNA damage, binding to single and double-strand breaks where it mediates recruitment of factors activated in the DNA damage response such as the serine/threonine protein kinase Ataxia telangiectasia mutated (ATM) (18). In cells lacking functional homologous recombination pathways, e.g., with mutation, silencing, or other functional dysregulation of proteins involved in DNA repair such as BRCA1 and BRCA2, PARP1 inhibition leads to persistent double-strand breaks and cell death. This is particularly relevant to SEOC where aberrations in DNA damage pathways are well recognized as major driver of these tumors. The frequency of germline *BRCA1* and *BRCA2* mutation in familial ovarian cancer is around 17% (19, 20). While encouraging, not all women with SEOC respond to PARP1 inhibition, and some that do will develop resistance. Key molecular drivers of PARP1 sensitivity and resistance are beginning to be elucidated (21–23) and trials of PARP1 inhibitors have shown promise (24). It is interesting to speculate that manipulation of factors involved in chromatin accessibility may have the potential to increase the success of PARP1 inhibitors that are undoubtedly an exciting new therapeutic option for SEOC.

EPIGENOMICS AND SEOC, UNLOCKING NEW OPPORTUNITIES FOR THERAPY

Aberrant DNA methylation and microRNA (miRNA) expression have also been identified in SEOC (25, 26). DNA methylation refers to the addition of a methyl group to the cytosine-5 position of a CpG dinucleotide that is controlled by DNA methyltransferases. There are well described cases of gene regulation in ovarian cancer relying on hyper- or hypomethylation, including down-regulation of both *BRCA1* and the *PTEN* tumor suppressors by promoter hypermethylation (27, 28). Of note, the cell surface marker CD133 that is part of a panel used to define ovarian cancer-initiating cells has been shown to be regulated by both histone modification and promoter methylation (29). Other cancer-associated genes with increased expression in ovarian cancer due to promoter hypomethylation include *TUBB3* and *HOXA10* (30, 31). Epigenetic silencing of genes has been linked to the development of platin-based resistance in ovarian cancer, including DNA hypermethylation at CpG sites of *MLH1*, *ARMCX2*, *COL1A1*, *MDK*, and *MEST* gene promoters (26, 32). Treatment of cisplatin resistant human ovarian cancer cell line xenografts with the demethylating agent 5-aza-2′-deoxycytidine resensitized tumors to platin-based therapy, likely through re-expression of MLH1 associated with a decrease in *MLH1* promoter hypermethylation (33). While unlikely to be efficacious as monotherapy, the value of demethylating agents for the treatment of ovarian cancer may be in combinatorial treatments with more conventionally used DNA damaging agents such as the platin-drugs or other epigenomic-based therapies. Interactions between histone modifications and DNA methylation that together influence gene expression have been reported (34). A number of reviews addressing the topic of DNA methylation in ovarian cancer, including discussion of clinical trials of demethylating agents, are available (25, 35, 36).

Elucidation of the role of post-translational histone modifications and parallel development of therapeutic strategies targeting them is gaining momentum in many tumor streams; however, this area of epigenomics is to date relatively understudied in ovarian cancer, although examples of this form of gene regulation are emerging. Targeting histone modifications has the potential to be of particular relevance to the treatment of SEOC given that these strategies embrace a whole genome approach, and so have the potential to overcome issues created by focusing on infrequently mutated genes. Furthermore, many histone modifications have been implicated in the DNA damage response given their fine control of chromatin configuration that determines access by transcription factors and DNA repair proteins (37). SEOC is undoubtedly a tumor driven by aberrant DNA damage signaling, therefore the potential exists to improve the way this pathway is targeted with current therapies by a greater understanding of the chromatin landscape. It has recently been stated that we stand at the "*tipping point*" for epigenetic based therapies for the treatment of cancer (38). The strategies being developed have large potential for the treatment of ovarian cancer.

MODIFYING CORE HISTONES

POST-TRANSLATIONAL HISTONE MODIFICATIONS

Histones are small basic proteins of around 14 kDa that contain a high percentage of positively charged amino acids (39). They are the most abundant proteins bound to DNA in eukaryotic cells and predominantly function to regulate gene expression and DNA packaging around nucleosomes, the functional units of chromatin. Nucleosomes are comprised of a histone octamer with two copies each of the core histone proteins H2A, H2B, H3, and H4 wrapped around by approximately 147 bp of DNA (39). Within this structure, H3:H4 exists as a tetramer and there are two H2A:H2B dimers (40). The histone linker H1 binds nucleosomes together thereby participating in a higher order compaction of chromatin (41). NH_2-terminal histone tails protrude from the core octamer structure, with residues located in these tails subject to a large number of dynamic and reversible PTMs that include, but are not limited to, methylation, acetylation, phosphorylation, ubiquitination, and SUMOylation (42).

Post-translational modifications of core histone proteins regulate gene transcription, replication, and DNA repair processes by influencing chromatin configuration and providing important platforms or docking sites for the recruitment of proteins and enzyme complexes such as methyltransferases and acetylases required for chromatin modeling. New terminology has recently

entered this field describing chromatin "writers" that lay down histone modifications, chromatin "erasers" that remove them, and chromatin "readers" that are involved in interpretation of signals that may influence subsequent changes (40). Histone H3 lysine 4 di- and tri-methylation (H3K4me2 and H3K4me3), as well as histone H3 lysine 79 methylation (H3K79me), histone H3 lysine 36 (H3K36me), histone acetylation and monoubiquitination of histone H2B at lysine 120 (H2Bub1) have been linked to "open" chromatin and active transcription. Other modifications, including methylation of histone H3 lysine 9 (H3K9me), histone H3 lysine 27 (H3K27me), and histone H4 lysine 20 (H4K20me) are associated with "closed" chromatin and transcriptional repression (42, 43). Suppression of H3K27me3 in cell lines overexpressing the dominant negative mutant H3-K27R led to re-expression of the RASSF1 tumor suppressor and resensitization of ovarian cancer cells to cisplatin, likely due to a more relaxed and open chromatin configuration (44). Methylation is controlled in a reversible fashion by methyltransferases and demethyltransferases, often associating in complexes, whilst monoubiquitination is dynamically controlled by ubiquitin ligases such as the RING finger proteins RNF20 and RNF40 (45, 46) and deubiquitinases (DUBs), again often in complex structures.

Histone acetylation is generally associated with an open chromatin structure that facilitates transcription, controlled in a dynamic fashion by histone acetyltransferases (HATs) and histone deacetyltransferases (HDACs) (47). Acetylation acts to neutralize the positive charge of lysine residues located on histone tails, resulting in disruption of nucleosomal structure and promoting unfolding of local DNA making it more accessible by transcription machinery. HDACs remove acetyl residues and consequently are associated with gene repression. In many cancers including ovarian, aberrant HDAC pathways are believed to promote cancer growth and metastasis (48–50). Histone tail residues can provide platforms for multiple enzyme writers, such as lysine 120 of histone H2B that in addition to being monoubiquitinated, can also be acetylated (H2BK120ac). It is thought in this case that H2BK120ac precedes H2Bub1 in a temporal fashion, suggesting that it may be an early mark of poised or active chromatin functioning as a dual switch to keep nucleosomes "hot" for rounds of induction and transcriptional elongation (51).

Histone deacetyltransferases that are aberrantly expressed in cancer include sirtuins of which there are seven family members. Sirtuins are mammalian homologs of the yeast silent information regulator (Sir2), that as well as functioning as HDACs can act as deacetylases for non-histone proteins such as p53 (52). SIRT1 is a nicotinamide adenine dinucleotide (NAD^+) – dependent lysine deacetylase and a class III HDAC. SIRT1 expression was reported to be higher in malignant EOC compared to benign, and expression was seen more commonly in SEOC relative to mucinous tumors (53). This same study reported higher levels of SIRT1 in a subset of malignant SEOC that correlated with increased overall survival. Of note, BRCA1-associated breast cancers have been reported to have lower levels of SIRT1 relative to BRCA1 wild-type (54). To date, levels of SIRT1 in BRCA1-associated EOCs have not been assessed. SIRT1 is also associated with acquired drug resistance, influencing the tumor microenvironment, functioning in DNA repair and promoting cancer stem cell survival (55). For all these reasons, SIRT1 is being considered as a possible target to overcome drug resistance seen in many malignancies and may have relevance to future treatment strategies for SEOC.

There is emerging evidence to support the theory that subpopulations of cells exist in SEOC that are of a stem cell-like nature, demonstrate resistance to chemotherapy and are responsible for the development of chemoresistance in women with ovarian cancer (56–58). This is supported by a recent study demonstrating that the bivalent chromatin mark seen in embryonic stem cells and required for silencing of developmental genes, H3K27me3/H3K4me3, is found in SEOC at the transcription start sites of silenced genes (59). H3K27 methylation is written by the methyltransferase Enhancer of Zeste Homolog 2 (EZH2) that forms the catalytic unit of Polycomb repressive complex 2 (PRC2). EZH2 is overexpressed in SEOC, as well as in cancer-associated stromal cells (60). H3K27me has also been associated with chemoresistance in ovarian cancer (59). Histone PTMs play a major role in maintenance of an undifferentiated stem cell phenotype (61, 62).

Studies of histone PTMs in primary tumors support discoveries in cancer cell line models of complex histone modifications and furthermore, have been shown to correlate with tumor stage and prognosis. Loss of global H3K27me3 has been shown in ovarian, as well as breast and pancreatic cancers, correlating with shorter overall survival (63). Loss of global levels of H2Bub1 has been reported in advanced breast tumors, as well as colon, lung, parathyroid, and ovarian cancers (64–67).

CROSS-TALK BETWEEN HISTONE MODIFICATIONS

Histone cross-talk is defined as the influence that one or more post-translationally modified histones have on the writing, erasing, and reading of other histone PTMs. The language of histones is both complex and wide spread, influencing processes involved in development, stem cell differentiation, transcription, replication, and DNA repair with a major role in the regulation of gene expression (68, 69). Examples of histone cross-talk include the recruitment of the methyltransferase complex COMPASS (complex of proteins associated with Set1) by H2Bub1 that is involved in the methylation of lysine 4 on histone H3 (70–73) (**Figure 1**). This cross-talk also has implications for DNA damage signaling as methylated H3K4 recruits the DNA damage-associated chromatin remodeling factor SNF2H leading to recruitment of DNA repair proteins RAD51 and BRCA1 (74, 75). The DOT1L methyltransferase has been shown to methylate H3K79 after its expression was first stimulated by increased H2Bub1 (76). Complex patterns of cross-talk and their influence on gene expression and cellular processes are only just beginning to be elucidated. This will be an area of considerable focus in the future given the importance of understanding how therapies targeting one histone modification may in fact be influencing another.

DIFFERENTIAL HISTONE SPLICING

The study of histone splice variants in ovarian cancer is still in its infancy, with few studies published to date, although evidence suggests roles in tumor progression (77). Slight structural changes to the core histone octamer as the result of incorporation of

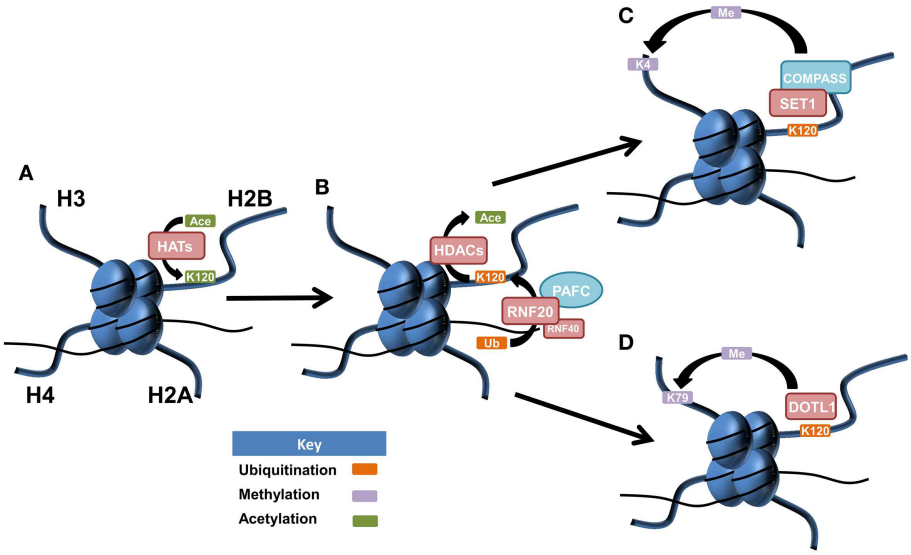

FIGURE 1 | Postulated patterns of histone cross-talk in malignancy. **(A)** Lysine 120 of histone H2B is acetylated by histone acetyltransferases (HATs), acting as a precursor for histone H2B monoubiquitination at the same amino acid residue. **(B)** Lysine 120 of histone H2B becomes deacetylated *via* histone deacetylases (HDACs), allowing for the E3 ubiquitin ligase complex of RNF20/RN40, in association with the PAF1 transcriptional regulatory complex (PAFC) to facilitate monoubiquitination of lysine 120 (H2Bub1). **(C)** SET1 is recruited to the site of H2Bub1 where it interacts with COMPASS (complex of proteins associated with Set1) to facilitate the active mark of methylated histone 3 at lysine 4 (H3K4me). **(D)** H2Bub1 can recruit and activate the DOT1L methyltransferase, responsible for the active chromatin mark of methylated histone H3 at lysine 79 (H3K79me).

differentially spliced histones can alter the overall structure of the nucleosome, changing the way in which DNA wraps around it and influencing nucleosome dynamics (78). These non-canonical variants can influence the function of chromatin domains and lead to differences in nucleosome stability causing aberrant transcription and DNA repair (79). Roles for histone splicing are just beginning to be elucidated in ovarian cancer. A link between alternative histone splicing of a group of H2A-type histone variants, referred to as macroH2As (macroH2A1.1, macroH2A1.2, and macroH2A2), and proliferation has been reported in a number of cancers, including ovarian (80). The RNA binding protein QKI (Quaking) was shown to regulate alternative pre-mRNA splicing of macroH2A1. Interestingly, macroH2A1.1-mediated suppression of proliferation occurs, at least in part, through the reduction of PARP1 protein levels. Given the interest in PARP1 inhibition for therapy, this area requires further attention.

Another histone variant identified to be down-regulated in ovarian cancer is histone variant H2A.Z, loss of which resulted in tumor progression (81). H2A.Z is a conserved variant of histone H2A, and has recently been shown to regulate a variety of targets including the glucocorticoid receptor (82), estrogen receptor (83), and p53 (84). The ovarian cancer cell lines A2780 and OVCAR3 were shown to have lost H2A.Z from regulatory regions of the urokinase receptor (u-PAR) leading to activation of this receptor and suggesting a mechanism for upregulation of u-PAR that is seen in a number of different malignancies (81, 85, 86). Furthermore, expression of linker histone H1 splice variants has been shown to discriminate ovarian adenocarcinomas from adenomas, suggesting their value as potential epigenetic biomarkers of ovarian cancer (87).

ROLE OF NON-CODING RNAs IN THE REGULATION OF HISTONES

The surprising finding that at least 80% of the human genome is transcribed has boosted an interest in understanding the role of non-coding RNAs (lncRNAs) in biological processes and diseases. The number of protein coding genes has remained relatively stable at approximately 21,000 during the last decade; however, the number of lncRNAs has grown to 9000 small lncRNAs (<200 nt) and 10,000–32,000 long lncRNAs (>200 nt) (88).

The role of miRNAs, a subset of small lncRNAs, in regulation of post-transcriptional gene silencing has been well established; however, our understanding of their effects on biological networks is still far from complete (88). Global deregulation of miRNAs has been implicated in ovarian cancer, and miRNAs have been found to target DICER, a key enzyme in miRNA processing, in breast cancer (13, 89–92). Of note, DICER levels do not appear to be altered in ovarian cancer (91). DNA methyltransferases such as DNMT1 and DNMT3B, histone deacetylases such as HDAC2 and HDAC4, and HATs such as KAT2B and KAT6A themselves are predicted to be targeted by dysregulated miRNAs in ovarian cancer (miR-100, 140, 145, 21, 26a, and 93) according to miRTarBase, a database of experimentally validated miRNA targets, influencing the epigenome (93).

HOTAIR, EZH2, AND THE POLYCOMB REPRESSIVE COMPLEX

Non-coding RNAs are versatile, with roles ranging from chromatin structure modification, X chromosome inactivation, scaffold function, miRNA decoys, nuclear import and export, RNA splicing, and the regulation of gene expression (94–96). Recently, approximately 20% of long intergenic lincRNAs, a subset of lncRNAs,

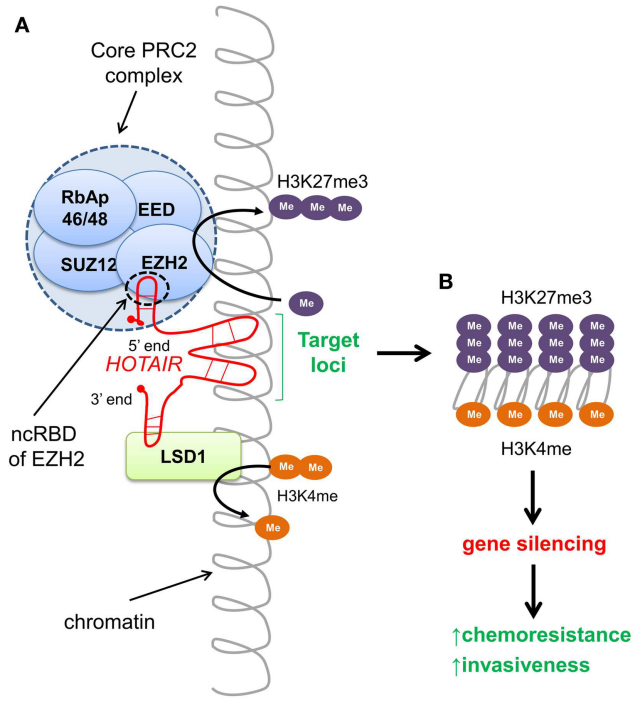

FIGURE 2 | *HOTAIR*-directed epigenetic reprograming of the cancer genome. **(A)** The long intergenic non-coding (linc) RNA *HOTAIR* recognizes specific DNA sequences and targets chromatin-modifying complexes PRC2 and LSD1 to silence gene loci. The 5′ end of *HOTAIR* tethers the PRC2 complex to the target by binding to the non-coding RNA binding domain (ncRBD) of the HMTase EZH2, catalyzing tri-methylation of H3K27. The 3′ end of *HOTAIR* facilitates demethylation of H3K4me2 by the lysine-specific demethylase LSD1. Both H3K27me3 and lack of methylation at H3K4 are repressive chromatin marks associated with gene silencing. **(B)** Expression of *HOTAIR* results in silencing of >40-kb region spanning *HOXD8–11* of the *HOXD* locus. Aberrant *HOTAIR* expression in multiple cancers has been shown to promote invasiveness.

have been found to be associated with PRC2 that functions as a chromatin-modifying complex (97). *HOTAIR* (*HOX* transcript antisense intergenic RNA), an approximately 2.1 kb lincRNA transcribed from the *HOXC* locus, is known to alter chromatin configuration and promote cancer. In healthy cells, *HOTAIR* functions to epigenetically silence approximately 40 kb spanning *HOXD8–HOXD11* of the *HOXD* region on chromosome 2 (98, 99). By working as a scaffold, *HOTAIR* tethers and directs the PRC2 containing the H3K27 methylase EZH2, and the lysine-specific demethylase 1 (LSD1) to silence targets by catalyzing H3K27me3 and demethylating H3K4me2, depicted in **Figure 2** (100).

Over-expression of *HOTAIR* promotes metastasis of breast, pancreatic, endometrial, colorectal, and other cancers (99, 101–104). Conversely, silencing of *HOTAIR* impaired migration and invasion of EOC cells *in vitro*, as well as inhibited tumor spread in a mouse model of intraperitoneal metastasis, likely *via* metalloproteinases (MMP3 and matrix metalloproteinase-9, MMP9) and epithelial-to-mesenchymal pathways (105). *HOTAIR* levels were reported to be elevated in ovarian cancer relative to normal ovary, and its expression was inversely correlated with the degree of differentiation (101, 105). Elevated levels of *HOTAIR* correlated with worse overall and disease free survival in women with EOC and were also correlated with the presence of lymph node metastasis (105). Furthermore, *HOTAIR* is expressed at a fivefold higher level in cisplatin resistant A2780cisR cells compared to parental A2780 cells, and its down-regulation restored cisplatin sensitivity (106). Levels of *HOTAIR* have been reported to be fourfold higher in colon and breast cancer stem cell-like cells ($CD133^+/CD44^+$) compared to non-stem cell-like cells ($CD133^-/CD44^-$), and its down-regulation reduced the number and size of colonies assessed by anchorage-independent growth (107). *HOTAIR* was also shown to induce epithelial-to-mesenchymal transition (EMT) following TGF-β1 treatment in colon and breast cancer cell lines (107).

Polycomb-group (PcG) proteins are involved in maintaining the repression of genes in specific cells and subsequent cells originating from them. These proteins are essential in lineage commitment where they and their antagonists, Trithorax proteins, selectively express and repress a subset of *HOX* genes required to specify a particular cell type. Tumor suppressors including $p16^{Ink4a}$, $p19^{Arf}$, and $p15^{Ink4b}$ are epigenetically silenced due to abrogation of PcG proteins in cancer (108). Most PcG proteins form multimeric complexes of either Polycomb repressive complex 1 (PRC1) or 2 (PRC2). Mammalian PRC2 complex comprises four core PcG proteins: EED, SUZ12, EZH1/2, and RbAp46/48, with many other proteins interacting with this core complex. EZH1 and EZH2 are histone methyltransferases (HMTases) and form part of the PRC2 complex that initiates gene silencing. As HMTases, gene silencing is enabled as both EZH1 and EZH2 contain SET domains required to catalyze di- or tri-methylation of H3K27 (H3K27me2 and H3K27me3) and repress chromatin. The PRC1 complex binds to chromatin bearing the H3K27me3 mark. PRC1 is composed of ubiquitin ligases RING1A and RING1B together with BMI1, MEL18 (PCGF2), and NSPC1 (PCGF1), with RING proteins functioning to monoubiquitinate histone H2A at lysine 119 (H2AK119ub1) (108). Both PRC1 and PRC2 are required to maintain gene suppression, and remain associated with condensed chromatin, even in the absence of the initial trigger. Although PRC1 usually follows the activity of PRC2, there are some reports where PRC2 silenced genes do not contain the PRC1-mediated H2AK119ub1 mark (108).

The components of PRC2 are upregulated in many malignancies such as melanoma, lymphoma, and breast cancers. High expression of EZH2 is seen in ovarian cancer, correlating with advanced stage and is a predictor of poor survival (109). Furthermore, higher levels of EZH2 have been seen in a subpopulation of ovarian cancer cells with stem cell-like properties at relapse following platinum-based chemotherapy. Down-regulation of EZH2 in these stem cell-like populations in ovarian cancer cell models reduced anchorage-independent growth and tumor growth *in vivo* (110). Furthermore, down-regulation of EZH2 was shown to resensitize cisplatin resistant ovarian cancer cells to cisplatin and decrease H3K27me3 levels (111). In line with this discovery, down-regulation of EZH2 leads to re-expression of $p21^{waf1/cip1}$, subsequently promoting apoptosis (112).

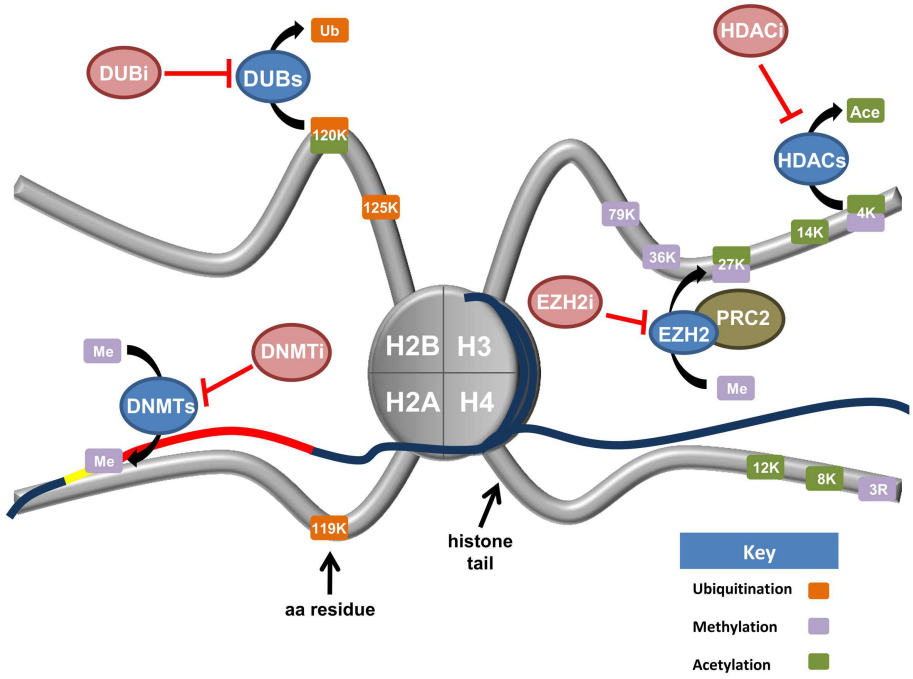

FIGURE 3 | Current and upcoming therapies for the targeting of epigenetic modifiers in ovarian cancer. Tumor suppressor genes are commonly silenced in ovarian cancer through epigenetic writers and erasers (blue ovals). These proteins regulate a variety of modifications including DNA methylation (DNMTs), histone methylation (EZH2), the removal of both histone acetylation (HDACs), and histone monoubiquitination (DUBs). Various inhibiting agents (red ovals) have been designed to stop the action of these enzymes. DNA methyltransferases (DNMTs) silence tumor suppressor genes (red line) by hypermethylation of CpG islands in gene promoters (yellow line). Consequently, DNMT inhibitors (DNMTi) are currently being trialed in ovarian cancer cell models with value in the reactivation of a tumor suppressive phenotype. Deubiquitinating enzymes (DUBs) function to cleave ubiquitin from their target proteins. Recent research has demonstrated H2Bub1 is lost in ovarian cancer, implicating H2Bub1-specific DUBs. H2Bub1-associated DUB inhibitors (DUBi) may be viable treatments for ovarian cancer. The histone methyltransferase EZH2 is a member of the Polycomb repressive complex 2 (PRC2). EZH2 functions to tri-methylate lysine 27 of histone H3 (H3K27), a repressive chromatin mark. Consequently, EZH2-inhibitors (EZH2i) are currently being trialed to remove this repressive mark. Histone deacetylase (HDACs) remove acetyl groups from specific histone residues. HDAC inhibitors (HDACi) prevent this enzymatic function, facilitating gene transcription.

The PRC2 complex proteins rely on association with molecules that have DNA-binding abilities such as the lncRNAs *HOTAIR* and *Xist* or the transcription factor JARID2 to direct it to its target (108). A number of repressed or deleted miRNAs associated with ovarian cancer, including miR-199a, miR-214, and miR-26a (89, 90), are also predicted (miRTarBase)[1] and/or reported to directly target EZH2 suggesting a possible mechanism of its overexpression (113, 114). Interestingly, the tumor suppressor BRCA1 negatively modulates PRC2 by interacting with EZH2 due to overlap in the BRCA1-binding region and *HOTAIR* binding domain of EZH2 (115). *HOTAIR* reprograms luminal breast cancer cells into an aggressive, basal-like state in the absence of functionally wild-type BRCA1 (115). Although the dominant mechanism of PRC2 function is *via* the H3K27me3 repressive mark on target loci, multiple epigenetic mechanisms could also be involved in PRC2-mediated gene silencing since EZH2 and EED are reported to interact with DNMTs and HDACs (25). Unlike EZH1, which is present in both dividing and differentiated cells, EZH2 expression is specific to actively dividing cells (108), making it an attractive therapeutic target for cancer.

[1]http://mirtarbase.mbc.nctu.edu.tw/

RISE OF EPIGENETIC THERAPIES TARGETING HISTONE MODIFICATIONS

Knowledge of epigenetic modifications and the enzymes that regulate them underpin new options for the treatment of ovarian cancer. Drugs specifically targeting DNA methylation will not be discussed but we recommend a recent review addressing this topic (116). In this section, we will examine the rapidly expanding field of drugs targeting histone modifications and the enzymatic machinery driving these changes with the view of application for the treatment of ovarian cancer. **Figure 3** depicts histone modifying enzymes currently being targeted or in pre-clinical models for ovarian cancer.

HISTONE DEACETYLASE INHIBITORS

Histone deacetyltransferase inhibitors have been demonstrated to decrease cancer cell growth, induce apoptosis and promote cell differentiation (117). Currently, there exists a wide variety of compounds that can function as HDAC inhibitors including; organic hydroxamic acids, short-chain fatty acids, benzamides, cyclic tetrapeptides, and sulfonamides (118). Many different type of agents derived from these fundamental families are currently going through clinical trials. Of the current HDAC inhibitors, three

have been tested in ovarian cancer; suberoylanilide hydroxamic acid (SAHA), valproic acid (VPA), and Romidepsin, either as standalone treatments or in conjunction with DNA damaging agents such as cisplatin. Although this section will focus on FDA approved HDAC inhibitors, other HDAC inhibitors have also recently shown for the potential treatment of ovarian cancer. The HDAC inhibitor M344, which is specific for HDAC6 and to a lesser extent HDAC1, has been shown to promote growth inhibition, cell cycle arrest, and apoptosis, as well as inhibit BRCA1 expression in ovarian cancer cell lines (119, 120). The HDAC inhibitor Trichostatin A (TSA), which specifically inhibits class I and II mammalian HDAC families, has been shown to increase p73 expression and promote Bax-dependent apoptosis in cisplatin resistant ovarian cancer cells (121).

SAHA (Vorinostat®)

Suberoylanilide hydroxamic acid has showed promising results in a number of *in vitro* models of ovarian cancer. Early research demonstrated that SAHA was capable of promoting cell cycle arrest, apoptosis, and caspase 3 activation, as well as decrease cell viability in ovarian cancer cell lines and isolated primary cancer cells (122–124). More recent studies have demonstrated that SAHA works effectively in conjunction with paclitaxel in ovarian cancer cell lines (125), while a SAHA–decitabine combination inhibited ovarian cancer cell growth in both *in vitro* and in xenograft models, in addition to increasing the expression of imprinted tumor suppressor genes, increasing apoptosis, cell cycle arrest, and autophagy (126). Further work has shown SAHA to be effective in combination with cisplatin in platinum resistant ovarian cancer cells (127, 128); however, the mechanism of this effectiveness is still poorly defined. Research has linked SAHA treatment to growth arrest, apoptosis and differentiation in a wide range of cancers. The antiproliferative effect of SAHA has been suggested to be a result of the accumulation of acetylated proteins, including; BCL6, p53, Hsp90, and the core histones (129). Currently, Vorinostat has been through phase I and II clinical trials for ovarian cancer. Phase II trials in women with recurrent platinum-refractory ovarian cancers showed little benefit when this drug was used as a single agent, although the drug was well tolerated (130). Vorinostat was FDA approved in 2006 for the treatment of Cutaneous T-cell lymphoma (CTCL).

Valproic acid (Valproate®)

Another HDAC inhibitor showing promise is the short-chain fatty acid drug VPA. Valproate has the advantage of already being a well establish FDA approved drug, used clinically as an anticonvulsant. VPA acts to directly inhibit HDAC activity; however, the specific details of how it exerts its effects are still unclear. Early research demonstrated that VPA promoted cell cycle arrest and apoptosis in ovarian cancer cell lines (122). VPA was also demonstrated to sensitize ovarian cancer cell lines to cisplatin treatment and to resensitize cisplatin resistant cells to treatment (131). More recent research showed that VPA was effective at treating a mouse subcutaneous xenograft model of ovarian cancer, as well as ovarian cancer cell lines (132). This same study demonstrated that VPA treatment resulted in an increase in E-cadherin expression, while decreasing MMP9 and vascular endothelial growth factor (VEGF). Similar to SAHA, VPA has been shown to act as an effective treatment against ovarian cancer cells by itself and in combination with other drugs. Combination treatments of ovarian cancer cell line models with VPA and the Aurora Kinase inhibitor VE465 showed increased apoptosis compared to VE465 alone (133). Monti and colleagues offer an extensive review of VPA mechanisms (134).

Romidepsin (FK228, Istodax®)

Romidepsin is a class I HDAC inhibitor, which received FDA approval in 2009 for the treatment of CTCL. In a biological system Romidepsin functions as a pro-drug whereby its reduction results in the release of a thiol, which blocks the activity of Zn-dependent histone deacetylase through its interactions with the zinc atom present in the deacetylase's binding domain (135). A study has demonstrated that Romidepsin inhibited cell viability and induced apoptosis in ovarian cancer cell lines (136). More recent work by the same group demonstrated that Romidepsin worked effectively in combination with cisplatin increasing cell apoptosis in *in vitro* and *in vivo* models (137). Romidepsin is currently in phase 2 trials for ovarian cancer[2] (NCT00085527).

DEUBIQUITINASES – TARGETING MONOUBIQUITINATED HISTONE H2B (H2BUB1)

Ubiquitin is traditionally thought of in the context of polyubiquitination that leads to protein degradation *via* the ubiquitin–proteasome system; however, monoubiquitination of histones H2A and H2B are clear instances of alternative roles for ubiquitin in transcription and DNA repair (45, 46, 138). DUBs are proteases that cleave ubiquitin from target proteins, including core histone proteins, and are recognized as important regulators of the ubiquitin–proteasome system. Given that DUBs occur upstream of the proteasome, they have the potential to show greater specificity and less toxicity compared to FDA approved proteasome inhibitors such as Velcade® (bortezomib) or Kyprolis® (carfilzomib). For these reasons, extensive efforts are currently being focused on DUBs as drug targets (139, 140). Currently, no specific DUB inhibitor has entered clinical trials; however, DUB inhibitors have shown promise in pre-clinical models, including P0591, an inhibitor of USP7, that has amongst its substrates H2Bub1 and the p53 regulator HDM2 (141). In studies of multiple myeloma, P5091 was demonstrated to induce apoptosis in both bortezomib refractory multiple myeloma cells and animal tumor models (141). Further, there is considerable interest in the H2Bub1-targeting DUB USP22 given its membership of an 11-gene panel termed the "*Death-from-Cancer*" signature that predicts rapid disease recurrence, distal metastasis, and poor response to therapy (142).

HISTONE METHYLTRANSFERASES – TARGETING EZH2

Like DNMTs, HMTases such as EZH2 can be targeted for therapy. 3-Deazaneplanocin A (DZNep) was the first indirect inhibitor of EZH2, leading to decreased global levels of H3K27me3 and restoration of expression of genes involved in growth inhibition or apoptosis (143). It was subsequently discovered that DZNep also inhibited other HMTases (60, 143, 144). Specific inhibitors of

[2]http://clinicaltrials.gov/ct2/crawl/42

EZH2 have since been developed including GSK126, EPZ005687, and EI1 (60, 145–147). Recently, a peptide-based inhibitor, SAH-EZH2, was developed to target the PRC2 by disrupting EZH2/EED interactions (148).

Results of preliminary studies of EZH2-inhibitors in combination with other drugs have been encouraging. DZNep was shown to enhance the anti-proliferative effects of Gemcitabine in pancreatic cancer cells (149). The combination of both DNA demethylating agents (5-aza-2′-deoxycytidine) and DZNep targeting histone methylation has shown promise in cell line models of leukemia (150). A report on the use of DZNep treatment of the ovarian cancer cell line A2780 showed reduction in proliferation, an increase in apoptosis, inhibition of migration, and upregulation of E-cadherin expression (151). It remains to be seen whether these therapeutic strategies may be of value for the treatment of ovarian cancer.

CONCLUDING REMARKS

Targeting of histone modifications and the enzymes regulating them in the ovarian cancer epigenome represents, to date essentially an unmet opportunity. With further focus on this field, it is probable that within the next decade new drugs targeting HDACs, HTMases, and DUBs will emerge as the next generation of cancer therapeutics. Whether these drugs will be most efficacious as single agents, or in combinatorial approaches with more traditional DNA damage-based chemotherapeutics, or with other perhaps yet to be developed molecular based targeted drugs remains to be determined. It is clear that complex networks of histone cross-talk will need to be understood and markers of histone dysregulation will need to be identified to ensure that patients receive maximal benefit from these therapies (152). In summary, the field of epigenomic-based histone therapies promises to offer a new generation of cancer therapeutics giving fresh hope for the treatment of women with ovarian cancer.

AUTHOR CONTRIBUTIONS

Deborah J. Marsh., Jaynish S. Shah, and Alexander J. Cole conceived, wrote, and critically revised this manuscript.

ACKNOWLEDGMENTS

This work was supported by the Australian Research Council (ARC) [ARC Future Fellowship (FT100100489) to Deborah J. Marsh], Cancer Institute NSW [Career Development Fellowship (10/CDF/2-11) to Deborah J. Marsh], National Health and Medical Research Council (NHMRC) [NHMRC Senior Research Fellowship (APP1004799) to Deborah J. Marsh], [Cancer Council NSW (RG 13-10) to Deborah J. Marsh], Australian Postgraduate Award (to Jaynish S. Shah and Alexander J. Cole), Northern Clinical School Top-Up Scholarship (to Jaynish S. Shah and Alexander J. Cole), and Northern Translational Cancer Research Unit Scholar Award (to Jaynish S. Shah and Alexander J. Cole).

REFERENCES

1. Visintin I, Feng Z, Longton G, Ward DC, Alvero AB, Lai Y, et al. Diagnostic markers for early detection of ovarian cancer. *Clin Cancer Res* (2008) **14**:1065–72. doi:10.1158/1078-0432.CCR-07-1569
2. Jemal A, Siegel R, Xu J, Ward E. Cancer statistics, 2010. *CA Cancer J Clin* (2010) **60**:277–300. doi:10.3322/caac.20073
3. Jordan S, Steer C, Defazio A, Quinn M, Obermair A, Friedlander M, et al. Patterns of chemotherapy treatment for women with invasive epithelial ovarian cancer – a population-based study. *Gynecol Oncol* (2013) **129**:310–7. doi:10.1016/j.ygyno.2013.02.007
4. Monneret C. Platinum anticancer drugs. From serendipity to rational design. *Ann Pharm Fr* (2011) **69**:286–95. doi:10.1016/j.pharma.2011.10.001
5. Wani MC, Horwitz SB. Nature as a remarkable chemist: a personal story of the discovery and development of Taxol. *Anticancer Drugs* (2014) **25**:482–7. doi:10.1097/CAD.0000000000000063
6. Tangjitgamol S, Manusirivithaya S, Laopaiboon M, Lumbiganon P, Bryant A. Interval debulking surgery for advanced epithelial ovarian cancer. *Cochrane Database Syst Rev* (2013) **4**:CD006014. doi:10.1002/14651858.CD006014.pub6
7. da Costa Miranda V, De Souza Fede AB, Dos Anjos CH, Da Silva JR, Sanchez FB, Da Silva, et al. Neoadjuvant chemotherapy with six cycles of carboplatin and paclitaxel in advanced ovarian cancer patients unsuitable for primary surgery: safety and effectiveness. *Gynecol Oncol* (2014) **132**:287–91. doi:10.1016/j.ygyno.2013.12.002
8. Sabbatini P. Consolidation therapy in ovarian cancer: a clinical update. *Int J Gynecol Cancer* (2009) **19**(Suppl 2):S35–9. doi:10.1111/IGC.0b013e3181c14007
9. Vaughan S, Coward JI, Bast RC Jr, Berchuck A, Berek JS, Brenton JD, et al. Rethinking ovarian cancer: recommendations for improving outcomes. *Nat Rev Cancer* (2011) **11**:719–25. doi:10.1038/nrc3144
10. Levanon K, Crum C, Drapkin R. New insights into the pathogenesis of serous ovarian cancer and its clinical impact. *J Clin Oncol* (2008) **26**:5284–93. doi:10.1200/JCO.2008.18.1107
11. Perets R, Wyant GA, Muto KW, Bijron JG, Poole BB, Chin KT, et al. Transformation of the fallopian tube secretory epithelium leads to high-grade serous ovarian cancer in Brca;Tp53;Pten models. *Cancer Cell* (2013) **24**:751–65. doi:10.1016/j.ccr.2013.10.013
12. Tothill RW, Tinker AV, George J, Brown R, Fox SB, Lade S, et al. Novel molecular subtypes of serous and endometrioid ovarian cancer linked to clinical outcome. *Clin Cancer Res* (2008) **14**:5198–208. doi:10.1158/1078-0432.CCR-08-0196
13. Cancer Genome Atlas Research Network. Integrated genomic analyses of ovarian carcinoma. *Nature* (2011) **474**:609–15. doi:10.1038/nature10166
14. Kobayashi N, Abedini M, Sakuragi N, Tsang BK. PRIMA-1 increases cisplatin sensitivity in chemoresistant ovarian cancer cells with p53 mutation: a requirement for Akt down-regulation. *J Ovarian Res* (2013) **6**:7. doi:10.1186/1757-2215-6-7
15. Domcke S, Sinha R, Levine DA, Sander C, Schultz N. Evaluating cell lines as tumour models by comparison of genomic profiles. *Nat Commun* (2013) **4**:2126. doi:10.1038/ncomms3126
16. Chionh F, Mitchell G, Lindeman GJ, Friedlander M, Scott CL. The role of poly adenosine diphosphate ribose polymerase inhibitors in breast and ovarian cancer: current status and future directions. *Asia Pac J Clin Oncol* (2011) **7**:197–211. doi:10.1111/j.1743-7563.2011.01430.x
17. Itamochi H, Kigawa J. Clinical trials and future potential of targeted therapy for ovarian cancer. *Int J Clin Oncol* (2012) **17**:430–40. doi:10.1007/s10147-012-0459-8
18. Ciccia A, Elledge SJ. The DNA damage response: making it safe to play with knives. *Mol Cell* (2010) **40**:179–204. doi:10.1016/j.molcel.2010.09.019
19. Alsop K, Fereday S, Meldrum C, Defazio A, Emmanuel C, George J, et al. BRCA mutation frequency and patterns of treatment response in BRCA mutation-positive women with ovarian cancer: a report from the Australian Ovarian Cancer Study Group. *J Clin Oncol* (2012) **30**:2654–63. doi:10.1200/JCO.2011.39.8545
20. O'Sullivan CC, Moon DH, Kohn EC, Lee JM. Beyond breast and ovarian cancers: PARP inhibitors for BRCA mutation-associated and BRCA-like solid tumors. *Front Oncol* (2014) **4**:42. doi:10.3389/fonc.2014.00042
21. Nowsheen S, Cooper T, Bonner JA, Lobuglio AF, Yang ES. HER2 overexpression renders human breast cancers sensitive to PARP inhibition independently of any defect in homologous recombination DNA repair. *Cancer Res* (2012) **72**:4796–806. doi:10.1158/0008-5472.CAN-12-1287
22. Barber LJ, Sandhu S, Chen L, Campbell J, Kozarewa I, Fenwick K, et al. Secondary mutations in BRCA2 associated with clinical resistance to a PARP inhibitor. *J Pathol* (2013) **229**:422–9. doi:10.1002/path.4140
23. Fojo T, Bates S. Mechanisms of resistance to PARP inhibitors – three and counting. *Cancer Discov* (2013) **3**:20–3. doi:10.1158/2159-8290.CD-12-0514

Appendix D. Publications

24. Wang Z, Wang F, Tang T, Guo C. The role of PARP1 in the DNA damage response and its application in tumor therapy. *Front Med* (2012) **6**:156–64. doi:10.1007/s11684-012-0197-3
25. Kwon MJ, Shin YK. Epigenetic regulation of cancer-associated genes in ovarian cancer. *Int J Mol Sci* (2011) **12**:983–1008. doi:10.3390/ijms12020983
26. Zeller C, Dai W, Steele NL, Siddiq A, Walley AJ, Wilhelm-Benartzi CS, et al. Candidate DNA methylation drivers of acquired cisplatin resistance in ovarian cancer identified by methylome and expression profiling. *Oncogene* (2012) **31**:4567–76. doi:10.1038/onc.2011.611
27. Baldwin RL, Nemeth E, Tran H, Shvartsman H, Cass I, Narod S, et al. BRCA1 promoter region hypermethylation in ovarian carcinoma: a population-based study. *Cancer Res* (2000) **60**:5329–33.
28. Schondorf T, Ebert MP, Hoffmann J, Becker M, Moser N, Pur S, et al. Hypermethylation of the PTEN gene in ovarian cancer cell lines. *Cancer Lett* (2004) **207**:215–20. doi:10.1016/j.canlet.2003.10.028
29. Baba T, Convery PA, Matsumura N, Whitaker RS, Kondoh E, Perry T, et al. Epigenetic regulation of CD133 and tumorigenicity of CD133+ ovarian cancer cells. *Oncogene* (2009) **28**:209–18. doi:10.1038/onc.2008.374
30. Izutsu N, Maesawa C, Shibazaki M, Oikawa H, Shoji T, Sugiyama T, et al. Epigenetic modification is involved in aberrant expression of class III beta-tubulin, TUBB3, in ovarian cancer cells. *Int J Oncol* (2008) **32**:1227–35.
31. Cheng W, Jiang Y, Liu C, Shen O, Tang W, Wang X. Identification of aberrant promoter hypomethylation of HOXA10 in ovarian cancer. *J Cancer Res Clin Oncol* (2010) **136**:1221–7. doi:10.1007/s00432-010-0772-4
32. Gifford G, Paul J, Vasey PA, Kaye SB, Brown R. The acquisition of hMLH1 methylation in plasma DNA after chemotherapy predicts poor survival for ovarian cancer patients. *Clin Cancer Res* (2004) **10**:4420–6. doi:10.1158/1078-0432.CCR-03-0732
33. Plumb JA, Strathdee G, Sludden J, Kaye SB, Brown R. Reversal of drug resistance in human tumor xenografts by 2'-deoxy-5-azacytidine-induced demethylation of the hMLH1 gene promoter. *Cancer Res* (2000) **60**:6039–44.
34. Fuks F. DNA methylation and histone modifications: teaming up to silence genes. *Curr Opin Genet Dev* (2005) **15**:490–5. doi:10.1016/j.gde.2005.08.002
35. Balch C, Fang F, Matei DE, Huang TH, Nephew KP. Minireview: epigenetic changes in ovarian cancer. *Endocrinology* (2009) **150**:4003–11. doi:10.1210/en.2009-0404
36. Asadollahi R, Hyde CA, Zhong XY. Epigenetics of ovarian cancer: from the lab to the clinic. *Gynecol Oncol* (2010) **118**:81–7. doi:10.1016/j.ygyno.2010.03.015
37. Hendzel MJ, Greenberg RA. Conversations between chromatin modifications and DNA double strand break repair: a commentary. *Mutat Res* (2013) **750**:1–4. doi:10.1016/j.mrfmmm.2013.08.003
38. Jones PA. At the tipping point for epigenetic therapies in cancer. *J Clin Invest* (2014) **124**:14–6. doi:10.1172/JCI74145
39. Luger K, Mader AW, Richmond RK, Sargent DF, Richmond TJ. Crystal structure of the nucleosome core particle at 2.8 A resolution. *Nature* (1997) **389**:251–60. doi:10.1038/38444
40. Dawson MA, Kouzarides T, Huntly BJ. Targeting epigenetic readers in cancer. *N Engl J Med* (2012) **367**:647–57. doi:10.1056/NEJMra1112635
41. Th'ng JP, Sung R, Ye M, Hendzel MJ. H1 family histones in the nucleus. Control of binding and localization by the C-terminal domain. *J Biol Chem* (2005) **280**:27809–14. doi:10.1074/jbc.M501627200
42. Dawson MA, Kouzarides T. Cancer epigenetics: from mechanism to therapy. *Cell* (2012) **150**:12–27. doi:10.1016/j.cell.2012.06.013
43. Barski A, Cuddapah S, Cui K, Roh TY, Schones DE, Wang Z, et al. High-resolution profiling of histone methylations in the human genome. *Cell* (2007) **129**:823–37. doi:10.1016/j.cell.2007.05.009
44. Abbosh PH, Montgomery JS, Starkey JA, Novotny M, Zuhowski EG, Egorin MJ, et al. Dominant-negative histone H3 lysine 27 mutant derepresses silenced tumor suppressor genes and reverses the drug-resistant phenotype in cancer cells. *Cancer Res* (2006) **66**:5582–91. doi:10.1158/0008-5472.CAN-05-3575
45. Johnsen SA. The enigmatic role of H2Bub1 in cancer. *FEBS Lett* (2012) **586**:1592–601. doi:10.1016/j.febslet.2012.04.002
46. Fuchs G, Oren M. Writing and reading H2B monoubiquitylation. *Biochim Biophys Acta* (2014). doi:10.1016/j.bbagrm.2014.01.002
47. Zhang K, Dent SY. Histone modifying enzymes and cancer: going beyond histones. *J Cell Biochem* (2005) **96**:1137–48. doi:10.1002/jcb.20615
48. Verdin E, Dequiedt F, Kasler HG. Class II histone deacetylases: versatile regulators. *Trends Genet* (2003) **19**:286–93. doi:10.1016/S0168-9525(03)00073-8
49. Ropero S, Esteller M. The role of histone deacetylases (HDACs) in human cancer. *Mol Oncol* (2007) **1**:19–25. doi:10.1016/j.molonc.2007.01.001
50. Hayashi A, Horiuchi A, Kikuchi N, Hayashi T, Fuseya C, Suzuki A, et al. Type-specific roles of histone deacetylase (HDAC) overexpression in ovarian carcinoma: HDAC1 enhances cell proliferation and HDAC3 stimulates cell migration with downregulation of E-cadherin. *Int J Cancer* (2010) **127**:1332–46. doi:10.1002/ijc.25151
51. Gatta R, Dolfini D, Zambelli F, Imbriano C, Pavesi G, Mantovani R. An acetylation-mono-ubiquitination switch on lysine 120 of H2B. *Epigenetics* (2011) **6**:630–7. doi:10.4161/epi.6.5.15623
52. Yuan H, Su L, Chen WY. The emerging and diverse roles of sirtuins in cancer: a clinical perspective. *Onco Targets Ther* (2013) **6**:1399–416. doi:10.2147/ott.s37750
53. Jang KY, Kim KS, Hwang SH, Kwon KS, Kim KR, Park HS, et al. Expression and prognostic significance of SIRT1 in ovarian epithelial tumours. *Pathology* (2009) **41**:366–71. doi:10.1080/00313020902884451
54. Wang RH, Zheng Y, Kim HS, Xu X, Cao L, Luhasen T, et al. Interplay among BRCA1, SIRT1, and survivin during BRCA1-associated tumorigenesis. *Mol Cell* (2008) **32**:11–20. doi:10.1016/j.molcel.2008.09.011
55. Wang Z, Chen W. Emerging roles of SIRT1 in cancer drug resistance. *Genes Cancer* (2013) **4**:82–90. doi:10.1177/1947601912473826
56. Steffensen KD, Alvero AB, Yang Y, Waldstrom M, Hui P, Holmberg JC, et al. Prevalence of epithelial ovarian cancer stem cells correlates with recurrence in early-stage ovarian cancer. *J Oncol* (2011) **2011**:620523. doi:10.1155/2011/620523
57. McAuliffe SM, Morgan SL, Wyant GA, Tran LT, Muto KW, Chen YS, et al. Targeting Notch, a key pathway for ovarian cancer stem cells, sensitizes tumors to platinum therapy. *Proc Natl Acad Sci U S A* (2012) **109**:E2939–48. doi:10.1073/pnas.1206400109
58. Ahmed N, Abubaker K, Findlay J, Quinn M. Cancerous ovarian stem cells: obscure targets for therapy but relevant to chemoresistance. *J Cell Biochem* (2013) **114**:21–34. doi:10.1002/jcb.24317
59. Chapman-Rothe N, Curry E, Zeller C, Liber D, Stronach E, Gabra H, et al. Chromatin H3K27me3/H3K4me3 histone marks define gene sets in high-grade serous ovarian cancer that distinguish malignant, tumour-sustaining and chemo-resistant ovarian tumour cells. *Oncogene* (2013) **32**:4586–92. doi:10.1038/onc.2012.477
60. Li H, Zhang R. Role of EZH2 in epithelial ovarian cancer: from biological insights to therapeutic target. *Front Oncol* (2013) **3**:47. doi:10.3389/fonc.2013.00047
61. Bibikova M, Laurent LC, Ren B, Loring JF, Fan JB. Unraveling epigenetic regulation in embryonic stem cells. *Cell Stem Cell* (2008) **2**:123–34. doi:10.1016/j.stem.2008.01.005
62. Orkin SH, Hochedlinger K. Chromatin connections to pluripotency and cellular reprogramming. *Cell* (2011) **145**:835–50. doi:10.1016/j.cell.2011.05.019
63. Wei Y, Xia W, Zhang Z, Liu J, Wang H, Adsay NV, et al. Loss of trimethylation at lysine 27 of histone H3 is a predictor of poor outcome in breast, ovarian, and pancreatic cancers. *Mol Carcinog* (2008) **47**:701–6. doi:10.1002/mc.20413
64. Prenzel T, Begus-Nahrmann Y, Kramer F, Hennion M, Hsu C, Gorsler T, et al. Estrogen-dependent gene transcription in human breast cancer cells relies upon proteasome-dependent monoubiquitination of histone H2B. *Cancer Res* (2011) **71**:5739–53. doi:10.1158/0008-5472.CAN-11-1896
65. Hahn MA, Dickson KA, Jackson S, Clarkson A, Gill AJ, Marsh DJ. The tumor suppressor CDC73 interacts with the ring finger proteins RNF20 and RNF40 and is required for the maintenance of histone 2B monoubiquitination. *Hum Mol Genet* (2012) **21**:559–68. doi:10.1093/hmg/ddr490
66. Urasaki Y, Heath L, Xu CW. Coupling of glucose deprivation with impaired histone H2B monoubiquitination in tumors. *PLoS One* (2012) **7**:e36775. doi:10.1371/journal.pone.0036775
67. Marsh DJ, Defazio A, Clarkson A, Kennedy C, Australian Ovarian Cancer Study G, Gard GG, et al. Loss of histone H2B monoubiquitination in ovarian cancer – new therapeutic targeting opportunities based on chromatin relaxation. *AACR Advances in Ovarian Cancer Research: From Concepts to Clinic*. Miami, FL: American Association for Cancer Research (2013).
68. Izzo A, Schneider R. Chatting histone modifications in mammals. *Brief Funct Genomics* (2010) **9**:429–43. doi:10.1093/bfgp/elq024

Appendix D. Publications

69. Lee JS, Smith E, Shilatifard A. The language of histone crosstalk. *Cell* (2010) **142**:682–5. doi:10.1016/j.cell.2010.08.011
70. Wood A, Schneider J, Shilatifard A. Cross-talking histones: implications for the regulation of gene expression and DNA repair. *Biochem Cell Biol* (2005) **83**:460–7. doi:10.1139/o05-116
71. Kim J, Guermah M, Mcginty RK, Lee JS, Tang Z, Milne TA, et al. RAD6-Mediated transcription-coupled H2B ubiquitylation directly stimulates H3K4 methylation in human cells. *Cell* (2009) **137**:459–71. doi:10.1016/j.cell.2009.02.027
72. Smith E, Shilatifard A. The chromatin signaling pathway: diverse mechanisms of recruitment of histone-modifying enzymes and varied biological outcomes. *Mol Cell* (2010) **40**:689–701. doi:10.1016/j.molcel.2010.11.031
73. Shilatifard A. The COMPASS family of histone H3K4 methylases: mechanisms of regulation in development and disease pathogenesis. *Annu Rev Biochem* (2012) **81**:65–95. doi:10.1146/annurev-biochem-051710-134100
74. Kouskouti A, Talianidis I. Histone modifications defining active genes persist after transcriptional and mitotic inactivation. *EMBO J* (2005) **24**:347–57. doi:10.1038/sj.emboj.7600516
75. Nakamura K, Kato A, Kobayashi J, Yanagihara H, Sakamoto S, Oliveira DV, et al. Regulation of homologous recombination by RNF20-dependent H2B ubiquitination. *Mol Cell* (2011) **41**:515–28. doi:10.1016/j.molcel.2011.02.002
76. Min J, Feng Q, Li Z, Zhang Y, Xu RM. Structure of the catalytic domain of human DOT1L, a non-SET domain nucleosomal histone methyltransferase. *Cell* (2003) **112**:711–23. doi:10.1016/S0092-8674(03)00114-4
77. Vardabasso C, Hasson D, Ratnakumar K, Chung CY, Duarte LF, Bernstein E. Histone variants: emerging players in cancer biology. *Cell Mol Life Sci* (2014) **71**:379–404. doi:10.1007/s00018-013-1343-z
78. Zlatanova J, Bishop TC, Victor JM, Jackson V, Van Holde K. The nucleosome family: dynamic and growing. *Structure* (2009) **17**:160–71. doi:10.1016/j.str.2008.12.016
79. Talbert PB, Henikoff S. Histone variants – ancient wrap artists of the epigenome. *Nat Rev Mol Cell Biol* (2010) **11**:264–75. doi:10.1038/nrm2861
80. Novikov L, Park JW, Chen H, Klerman H, Jalloh AS, Gamble MJ. QKI-mediated alternative splicing of the histone variant MacroH2A1 regulates cancer cell proliferation. *Mol Cell Biol* (2011) **31**:4244–55. doi:10.1128/MCB.05244-11
81. Chauhan S, Boyd DD. Regulation of u-PAR gene expression by H2A.Z is modulated by the MEK-ERK/AP-1 pathway. *Nucleic Acids Res* (2012) **40**:600–13. doi:10.1093/nar/gkr725
82. John S, Sabo PJ, Johnson TA, Sung MH, Biddie SC, Lightman SL, et al. Interaction of the glucocorticoid receptor with the chromatin landscape. *Mol Cell* (2008) **29**:611–24. doi:10.1016/j.molcel.2008.02.010
83. Gevry N, Hardy S, Jacques PE, Laflamme L, Svotelis A, Robert F, et al. Histone H2A.Z is essential for estrogen receptor signaling. *Genes Dev* (2009) **23**:1522–33. doi:10.1101/gad.1787109
84. Gevry N, Chan HM, Laflamme L, Livingston DM, Gaudreau L. p21 Transcription is regulated by differential localization of histone H2A.Z. *Genes Dev* (2007) **21**:1869–81. doi:10.1101/gad.1545707
85. Cantero D, Friess H, Deflorin J, Zimmermann A, Brundler MA, Riesle E, et al. Enhanced expression of urokinase plasminogen activator and its receptor in pancreatic carcinoma. *Br J Cancer* (1997) **75**:388–95. doi:10.1038/bjc.1997.63
86. Morita S, Sato A, Hayakawa H, Ihara H, Urano T, Takada Y, et al. Cancer cells overexpress mRNA of urokinase-type plasminogen activator, its receptor and inhibitors in human non-small-cell lung cancer tissue: analysis by Northern blotting and in situ hybridization. *Int J Cancer* (1998) **78**:286–92. doi:10.1002/(SICI)1097-0215(19981029)78:3<286::AID-IJC4>3.0.CO;2-R
87. Medrzycki M, Zhang Y, Mcdonald JF, Fan Y. Profiling of linker histone variants in ovarian cancer. *Front Biosci (Landmark Ed)* (2012) **17**:396–406. doi:10.2741/3934
88. Tay Y, Rinn J, Pandolfi PP. The multilayered complexity of ceRNA crosstalk and competition. *Nature* (2014) **505**:344–52. doi:10.1038/nature12986
89. Iorio MV, Visone R, Di Leva G, Donati V, Petrocca F, Casalini P, et al. MicroRNA signatures in human ovarian cancer. *Cancer Res* (2007) **67**:8699–707. doi:10.1158/0008-5472.CAN-07-1936
90. Nam EJ, Yoon H, Kim SW, Kim H, Kim YT, Kim JH, et al. MicroRNA expression profiles in serous ovarian carcinoma. *Clin Cancer Res* (2008) **14**:2690–5. doi:10.1158/1078-0432.CCR-07-1731
91. Zhang L, Volinia S, Bonome T, Calin GA, Greshock J, Yang N, et al. Genomic and epigenetic alterations deregulate microRNA expression in human epithelial ovarian cancer. *Proc Natl Acad Sci U S A* (2008) **105**:7004–9. doi:10.1073/pnas.0801615105
92. Martello G, Rosato A, Ferrari F, Manfrin A, Cordenonsi M, Dupont S, et al. A microRNA targeting dicer for metastasis control. *Cell* (2010) **141**:1195–207. doi:10.1016/j.cell.2010.05.017
93. Hsu SD, Tseng YT, Shrestha S, Lin YL, Khaleel A, Chou CH, et al. miRTarBase update 2014: an information resource for experimentally validated miRNA-target interactions. *Nucleic Acids Res* (2014) **42**:D78–85. doi:10.1093/nar/gkt1266
94. Mercer TR, Dinger ME, Mattick JS. Long non-coding RNAs: insights into functions. *Nat Rev Genet* (2009) **10**:155–9. doi:10.1038/nrg2521
95. Gutschner T, Diederichs S. The hallmarks of cancer: a long non-coding RNA point of view. *RNA Biol* (2012) **9**:703–19. doi:10.4161/rna.20481
96. Spizzo R, Almeida MI, Colombatti A, Calin GA. Long non-coding RNAs and cancer: a new frontier of translational research? *Oncogene* (2012) **31**:4577–87. doi:10.1038/onc.2011.621
97. Khalil AM, Guttman M, Huarte M, Garber M, Raj A, Rivea Morales D, et al. Many human large intergenic noncoding RNAs associate with chromatin-modifying complexes and affect gene expression. *Proc Natl Acad Sci U S A* (2009) **106**:11667–72. doi:10.1073/pnas.0904715106
98. Rinn JL, Kertesz M, Wang JK, Squazzo SL, Xu X, Brugmann SA, et al. Functional demarcation of active and silent chromatin domains in human HOX loci by noncoding RNAs. *Cell* (2007) **129**:1311–23. doi:10.1016/j.cell.2007.05.022
99. Gupta RA, Shah N, Wang KC, Kim J, Horlings HM, Wong DJ, et al. Long non-coding RNA HOTAIR reprograms chromatin state to promote cancer metastasis. *Nature* (2010) **464**:1071–6. doi:10.1038/nature08975
100. Tsai MC, Manor O, Wan Y, Mosammaparast N, Wang JK, Lan F, et al. Long noncoding RNA as modular scaffold of histone modification complexes. *Science* (2010) **329**:689–93. doi:10.1126/science.1192002
101. Kogo R, Shimamura T, Mimori K, Kawahara K, Imoto S, Sudo T, et al. Long noncoding RNA HOTAIR regulates polycomb-dependent chromatin modification and is associated with poor prognosis in colorectal cancers. *Cancer Res* (2011) **71**:6320–6. doi:10.1158/0008-5472.CAN-11-1021
102. Kim K, Jutooru I, Chadalapaka G, Johnson G, Frank J, Burghardt R, et al. HOTAIR is a negative prognostic factor and exhibits pro-oncogenic activity in pancreatic cancer. *Oncogene* (2013) **32**:1616–25. doi:10.1038/onc.2012.193
103. Lv XB, Lian GY, Wang HR, Song E, Yao H, Wang MH. Long noncoding RNA HOTAIR is a prognostic marker for esophageal squamous cell carcinoma progression and survival. *PLoS One* (2013) **8**:e63516. doi:10.1371/journal.pone.0063516
104. He X, Bao W, Li X, Chen Z, Che Q, Wang H, et al. The long non-coding RNA HOTAIR is upregulated in endometrial carcinoma and correlates with poor prognosis. *Int J Mol Med* (2014) **33**:325–32. doi:10.3892/ijmm.2013.1570
105. Qiu JJ, Lin YY, Ye LC, Ding JX, Feng WW, Jin HY, et al. Overexpression of long non-coding RNA HOTAIR predicts poor patient prognosis and promotes tumor metastasis in epithelial ovarian cancer. *Gynecol Oncol* (2014). doi:10.1016/j.ygyno.2014.03.556
106. Ozes AR, Miller D, Guio C, Bhattrai A, Liu Y, Nephew KP. The transcriptional regulation of the long non-coding RNA HOTAIR in ovarian cancer. *Proceedings of the 104th Annual Meeting of the American Association for Cancer Research.* Washington, DC (2013).
107. Padua Alves C, Fonseca AS, Muys BR, de Barros E Lima Bueno R, Burger MC, De Souza JE, et al. Brief report: the lincRNA Hotair is required for epithelial-to-mesenchymal transition and stemness maintenance of cancer cell lines. *Stem Cells* (2013) **31**:2827–32. doi:10.1002/stem.1547
108. Margueron R, Reinberg D. The polycomb complex PRC2 and its mark in life. *Nature* (2011) **469**:343–9. doi:10.1038/nature09784
109. Rao ZY, Cai MY, Yang GF, He LR, Mai SJ, Hua WF, et al. EZH2 supports ovarian carcinoma cell invasion and/or metastasis via regulation of TGF-beta1 and is a predictor of outcome in ovarian carcinoma patients. *Carcinogenesis* (2010) **31**:1576–83. doi:10.1093/carcin/bgq150
110. Rizzo S, Hersey JM, Mellor P, Dai W, Santos-Silva A, Liber D, et al. Ovarian cancer stem cell-like side populations are enriched following chemotherapy and overexpress EZH2. *Mol Cancer Ther* (2011) **10**:325–35. doi:10.1158/1535-7163.MCT-10-0788
111. Hu S, Yu L, Li Z, Shen Y, Wang J, Cai J, et al. Overexpression of EZH2 contributes to acquired cisplatin resistance in ovarian cancer cells in vitro and in vivo. *Cancer Biol Ther* (2010) **10**:788–95. doi:10.4161/cbt.10.8.12913

Appendix D. Publications

112. Seward S, Semaan A, Qazi AM, Gruzdyn OV, Chamala S, Bryant CC, et al. EZH2 blockade by RNA interference inhibits growth of ovarian cancer by facilitating re-expression of p21(waf1/cip1) and by inhibiting mutant p53. *Cancer Lett* (2013) **336**:53–60. doi:10.1016/j.canlet.2013.04.012
113. Wong CF, Tellam RL. MicroRNA-26a targets the histone methyltransferase enhancer of Zeste homolog 2 during myogenesis. *J Biol Chem* (2008) **283**:9836–43. doi:10.1074/jbc.M709614200
114. Juan AH, Kumar RM, Marx JG, Young RA, Sartorelli V. Mir-214-dependent regulation of the polycomb protein Ezh2 in skeletal muscle and embryonic stem cells. *Mol Cell* (2009) **36**:61–74. doi:10.1016/j.molcel.2009.08.008
115. Wang L, Zeng X, Chen S, Ding L, Zhong J, Zhao JC, et al. BRCA1 is a negative modulator of the PRC2 complex. *EMBO J* (2013) **32**:1584–97. doi:10.1038/emboj.2013.95
116. Murphy SK. Targeting the epigenome in ovarian cancer. *Future Oncol* (2012) **8**:151–64. doi:10.2217/fon.11.152
117. Zhou Q, Melkoumian ZK, Lucktong A, Moniwa M, Davie JR, Strobl JS. Rapid induction of histone hyperacetylation and cellular differentiation in human breast tumor cell lines following degradation of histone deacetylase-1. *J Biol Chem* (2000) **275**:35256–63. doi:10.1074/jbc.M003106200
118. Takai N, Narahara H. Histone deacetylase inhibitor therapy in epithelial ovarian cancer. *J Oncol* (2010) **2010**:458431. doi:10.1155/2010/458431
119. Takai N, Ueda T, Nishida M, Nasu K, Narahara H. M344 is a novel synthesized histone deacetylase inhibitor that induces growth inhibition, cell cycle arrest, and apoptosis in human endometrial cancer and ovarian cancer cells. *Gynecol Oncol* (2006) **101**:108–13. doi:10.1016/j.ygyno.2005.09.044
120. Weberpals JI, O'Brien AM, Niknejad N, Garbuio KD, Clark-Knowles KV, Dimitroulakos J. The effect of the histone deacetylase inhibitor M344 on BRCA1 expression in breast and ovarian cancer cells. *Cancer Cell Int* (2011) **11**:29. doi:10.1186/1475-2867-11-29
121. Muscolini M, Cianfrocca R, Sajeva A, Mozzetti S, Ferrandina G, Costanzo A, et al. Trichostatin A up-regulates p73 and induces Bax-dependent apoptosis in cisplatin-resistant ovarian cancer cells. *Mol Cancer Ther* (2008) **7**:1410–9. doi:10.1158/1535-7163.MCT-08-0299
122. Takai N, Kawamata N, Gui D, Said JW, Miyakawa I, Koeffler HP. Human ovarian carcinoma cells: histone deacetylase inhibitors exhibit antiproliferative activity and potently induce apoptosis. *Cancer* (2004) **101**:2760–70. doi:10.1002/cncr.20709
123. Sonnemann J, Gange J, Pilz S, Stotzer C, Ohlinger R, Belau A, et al. Comparative evaluation of the treatment efficacy of suberoylanilide hydroxamic acid (SAHA) and paclitaxel in ovarian cancer cell lines and primary ovarian cancer cells from patients. *BMC Cancer* (2006) **6**:183. doi:10.1186/1471-2407-6-183
124. Cooper AL, Greenberg VL, Lancaster PS, Van Nagell JR Jr, Zimmer SG, Modesitt SC. In vitro and in vivo histone deacetylase inhibitor therapy with suberoylanilide hydroxamic acid (SAHA) and paclitaxel in ovarian cancer. *Gynecol Oncol* (2007) **104**:596–601. doi:10.1016/j.ygyno.2006.09.011
125. Dietrich CS III, Greenberg VL, Desimone CP, Modesitt SC, Van Nagell JR, Craven R, et al. Suberoylanilide hydroxamic acid (SAHA) potentiates paclitaxel-induced apoptosis in ovarian cancer cell lines. *Gynecol Oncol* (2010) **116**:126–30. doi:10.1016/j.ygyno.2009.09.039
126. Chen MY, Liao WS, Lu Z, Bornmann WG, Hennessey V, Washington MN, et al. Decitabine and suberoylanilide hydroxamic acid (SAHA) inhibit growth of ovarian cancer cell lines and xenografts while inducing expression of imprinted tumor suppressor genes, apoptosis, G2/M arrest, and autophagy. *Cancer* (2011) **117**:4424–38. doi:10.1002/cncr.26073
127. Ong PS, Wang XQ, Lin HS, Chan SY, Ho PC. Synergistic effects of suberoylanilide hydroxamic acid combined with cisplatin causing cell cycle arrest independent apoptosis in platinum-resistant ovarian cancer cells. *Int J Oncol* (2012) **40**:1705–13. doi:10.3892/ijo.2012.1354
128. Chen S, Zhao Y, Gou WF, Zhao S, Takano Y, Zheng HC. The anti-tumor effects and molecular mechanisms of suberoylanilide hydroxamic acid (SAHA) on the aggressive phenotypes of ovarian carcinoma cells. *PLoS One* (2013) **8**:e79781. doi:10.1371/journal.pone.0079781
129. Richon VM. Cancer biology: mechanism of antitumour action of vorinostat (suberoylanilide hydroxamic acid), a novel histone deacetylase inhibitor. *Br J Cancer* (2006) **95**:S2–6. doi:10.1038/sj.bjc.6603463
130. Modesitt SC, Sill M, Hoffman JS, Bender DP. A phase II study of vorinostat in the treatment of persistent or recurrent epithelial ovarian or primary peritoneal carcinoma: a Gynecologic Oncology Group study. *Gynecol Oncol* (2008) **109**:182–6. doi:10.1016/j.ygyno.2008.01.009
131. Lin CT, Lai HC, Lee HY, Lin WH, Chang CC, Chu TY, et al. Valproic acid resensitizes cisplatin-resistant ovarian cancer cells. *Cancer Sci* (2008) **99**:1218–26. doi:10.1111/j.1349-7006.2008.00793.x
132. Shan Z, Feng-Nian R, Jie G, Ting Z. Effects of valproic acid on proliferation, apoptosis, angiogenesis and metastasis of ovarian cancer in vitro and in vivo. *Asian Pac J Cancer Prev* (2012) **13**:3977–82. doi:10.7314/APJCP.2012.13.8.3977
133. Li Y, Liu T, Ivan C, Huang J, Shen DY, Kavanagh JJ, et al. Enhanced cytotoxic effects of combined valproic acid and the aurora kinase inhibitor VE465 on gynecologic cancer cells. *Front Oncol* (2013) **3**:58. doi:10.3389/fonc.2013.00058
134. Monti B, Polazzi E, Contestabile A. Biochemical, molecular and epigenetic mechanisms of valproic acid neuroprotection. *Curr Mol Pharmacol* (2009) **2**:95–109. doi:10.2174/1874-470210902010095
135. Ueda H, Nakajima H, Hori Y, Fujita T, Nishimura M, Goto T, et al. FR901228, a novel antitumor bicyclic depsipeptide produced by *Chromobacterium violaceum* no. 968. I. Taxonomy, fermentation, isolation, physico-chemical and biological properties, and antitumor activity. *J Antibiot (Tokyo)* (1994) **47**:301–10. doi:10.7164/antibiotics.47.301
136. Wilson AJ, Cheng YQ, Khabele D. Thailandepsins are new small molecule class I HDAC inhibitors with potent cytotoxic activity in ovarian cancer cells: a preclinical study of epigenetic ovarian cancer therapy. *J Ovarian Res* (2012) **5**:12. doi:10.1186/1757-2215-5-12
137. Wilson AJ, Lalani AS, Wass E, Saskowski J, Khabele D. Romidepsin (FK228) combined with cisplatin stimulates DNA damage-induced cell death in ovarian cancer. *Gynecol Oncol* (2012) **127**:579–86. doi:10.1016/j.ygyno.2012.09.016
138. Braun S, Madhani HD. Shaping the landscape: mechanistic consequences of ubiquitin modification of chromatin. *EMBO Rep* (2012) **13**:619–30. doi:10.1038/embor.2012.78
139. Colland F. The therapeutic potential of deubiquitinating enzyme inhibitors. *Biochem Soc Trans* (2010) **38**:137–43. doi:10.1042/BST0380137
140. Nicholson B, Suresh Kumar KG. The multifaceted roles of USP7: new therapeutic opportunities. *Cell Biochem Biophys* (2011) **60**:61–8. doi:10.1007/s12013-011-9185-5
141. Chauhan D, Tian Z, Nicholson B, Kumar KG, Zhou B, Carrasco R, et al. A small molecule inhibitor of ubiquitin-specific protease-7 induces apoptosis in multiple myeloma cells and overcomes bortezomib resistance. *Cancer Cell* (2012) **22**:345–58. doi:10.1016/j.ccr.2012.08.007
142. Glinsky GV, Berezovska O, Glinskii AB. Microarray analysis identifies a death-from-cancer signature predicting therapy failure in patients with multiple types of cancer. *J Clin Invest* (2005) **115**:1503–21. doi:10.1172/JCI23412
143. Tan J, Yang X, Zhuang L, Jiang X, Chen W, Lee PL, et al. Pharmacologic disruption of polycomb-repressive complex 2-mediated gene repression selectively induces apoptosis in cancer cells. *Genes Dev* (2007) **21**:1050–63. doi:10.1101/gad.1524107
144. Miranda TB, Cortez CC, Yoo CB, Liang G, Abe M, Kelly TK, et al. DZNep is a global histone methylation inhibitor that reactivates developmental genes not silenced by DNA methylation. *Mol Cancer Ther* (2009) **8**:1579–88. doi:10.1158/1535-7163.MCT-09-0013
145. Knutson SK, Wigle TJ, Warholic NM, Sneeringer CJ, Allain CJ, Klaus CR, et al. A selective inhibitor of EZH2 blocks H3K27 methylation and kills mutant lymphoma cells. *Nat Chem Biol* (2012) **8**:890–6. doi:10.1038/nchembio.1084
146. McCabe MT, Ott HM, Ganji G, Korenchuk S, Thompson C, Van Aller GS, et al. EZH2 inhibition as a therapeutic strategy for lymphoma with EZH2-activating mutations. *Nature* (2012) **492**:108–12. doi:10.1038/nature11606
147. Qi W, Chan H, Teng L, Li L, Chuai S, Zhang R, et al. Selective inhibition of Ezh2 by a small molecule inhibitor blocks tumor cells proliferation. *Proc Natl Acad Sci U S A* (2012) **109**:21360–5. doi:10.1073/pnas.1210371110
148. Kim W, Bird GH, Neff T, Guo G, Kerenyi MA, Walensky LD, et al. Targeted disruption of the EZH2-EED complex inhibits EZH2-dependent cancer. *Nat Chem Biol* (2013) **9**:643–50. doi:10.1038/nchembio.1331
149. Avan A, Crea F, Paolicchi E, Funel N, Galvani E, Marquez VE, et al. Molecular mechanisms involved in the synergistic interaction of the EZH2 inhibitor 3-deazaneplanocin A with gemcitabine in pancreatic cancer cells. *Mol Cancer Ther* (2012) **11**:1735–46. doi:10.1158/1535-7163.MCT-12-0037
150. Momparler RL, Idaghdour Y, Marquez VE, Momparler LF. Synergistic antileukemic action of a combination of inhibitors of DNA methylation and histone methylation. *Leuk Res* (2012) **36**:1049–54. doi:10.1016/j.leukres.2012.03.001

151. Shen L, Cui J, Pang YX, Ma YH, Liu PS. 3-Deazaneplanocin A is a promising therapeutic agent for ovarian cancer cells. *Asian Pac J Cancer Prev* (2013) **14**:2915–8. doi:10.7314/APJCP.2013.14.5.2915
152. Treppendahl MB, Kristensen LS, Gronbaek K. Predicting response to epigenetic therapy. *J Clin Invest* (2014) **124**:47–55. doi:10.1172/JCI69737

Conflict of Interest Statement: The authors declare that the research was conducted in the absence of any commercial or financial relationships that could be construed as a potential conflict of interest.

Received: 19 April 2014; accepted: 27 May 2014; published online: 12 June 2014.

*Citation: Marsh DJ, Shah JS and Cole AJ (2014) Histones and their modifications in ovarian cancer – drivers of disease and therapeutic targets. Front. Oncol. **4**:144. doi: 10.3389/fonc.2014.00144*

This article was submitted to Women's Cancer, a section of the journal Frontiers in Oncology.

Appendix D. Publications

Bibliography

Abdallah, R. et al. (2015). Prediction of optimal cytoreductive surgery of serous ovarian cancer with gene expression data. In: *International Journal of Gynecological Cancer* 25.6, pp. 1000–1009.

Adams, B. D., C. Parsons, and F. J. Slack (2016). The tumor-suppressive and potential therapeutic functions of miR-34a in epithelial carcinomas. In: *Expert Opinion on Therapeutic Targets* 20.6, pp. 737–753.

Agarwal, Roshan and Stan B Kaye (2003). Ovarian cancer: strategies for overcoming resistance to chemotherapy. In: *Nature Reviews Cancer* 3.7, pp. 502–516.

AIHW (2017). Australian Institute of Health and Welfare: Gynaecological cancers in Australia — an overview. In: URL: http://www.aihw.gov.au/WorkArea/DownloadAsset.aspx?id=10737422901.

Akane, Atsushi et al. (1994). Identification of the heme compound copurified with deoxyribonucleic acid (DNA) from bloodstains, a major inhibitor of polymerase chain reaction (PCR) amplification. In: *Journal of Forensic Science* 39.2, pp. 362–372.

Akrami, Rozita et al. (2013). Comprehensive analysis of long non-coding RNAs in ovarian cancer reveals global patterns and targeted DNA amplification. In: *PloS one* 8.11, e80306.

Al-Soud, Waleed Abu, Leif J Jönsson, and Peter Rådström (2000). Identification and characterization of immunoglobulin G in blood as a major inhibitor of diagnostic PCR. In: *Journal of Clinical Microbiology* 38.1, pp. 345–350.

Al-Soud, Waleed Abu and Peter Rådström (2001). Purification and characterization of PCR-inhibitory components in blood cells. In: *Journal of clinical microbiology* 39.2, pp. 485–493.

Alsop, Kathryn et al. (2012). BRCA mutation frequency and patterns of treatment response in BRCA mutation–positive women with ovarian cancer: a report from the Australian Ovarian Cancer Study Group. In: *Journal of Clinical Oncology* 30.21, pp. 2654–2663.

Amaral, Paulo P et al. (2010). lncRNAdb: a reference database for long noncoding RNAs. In: *Nucleic acids research* 39.suppl_1, pp. D146–D151.

Anderson, Douglas M et al. (2015). A micropeptide encoded by a putative long noncoding RNA regulates muscle performance. In: *Cell* 160.4, pp. 595–606.

Andre, Fabrice et al. (2002). Malignant effusions and immunogenic tumour-derived exosomes. In: *The Lancet* 360.9329, pp. 295–305.

Angioli, Roberto et al. (2013). Can the preoperative HE4 level predict optimal cytoreduction in patients with advanced ovarian carcinoma? In: *Gynecologic oncology* 128, pp. 579–583.

Anglesio, MS et al. (2013). Cancer-associated somatic DICER1 hotspot mutations cause defective miRNA processing and reverse-strand expression bias to predominantly mature 3p strands through loss of 5p strand cleavage. In: *The Journal of pathology* 229.3, pp. 400–409.

Arits, AHMM et al. (2008). Preoperative serum CA125 levels do not predict suboptimal cytoreductive surgery in epithelial ovarian cancer. In: *International Journal of Gynecological Cancer* 18.4, pp. 621–628.

Arroyo, Jason D et al. (2011). Argonaute2 complexes carry a population of circulating microRNAs independent of vesicles in human plasma. In: *Proceedings of the National Academy of Sciences* 108.12, pp. 5003–5008. ISSN: 0027-8424.

Aushev, Vasily N et al. (2013). Comparisons of microRNA patterns in plasma before and after tumor removal reveal new biomarkers of lung squamous cell carcinoma. In: *PloS one* 8.10, e78649.

Axtell, Allison E et al. (2007). Multi-institutional reciprocal validation study of computed tomography predictors of suboptimal primary cytoreduction in patients with advanced ovarian cancer. In: *Journal of clinical oncology* 25.4, pp. 384–389.

Ayaz, L. et al. (2014). Circulating microRNA expression profiles in ovarian cancer. In: *Journal of Obstetrics and Gynaecology* 34.7, pp. 620–624.

Bamford, Sally et al. (2004). The COSMIC (Catalogue of Somatic Mutations in Cancer) database and website. In: *British journal of cancer* 91.2, pp. 355–358.

Banerjee, Susana and Stanley B Kaye (2013). New Strategies in the Treatment of Ovarian Cancer: Current Clinical Perspectives and Future Potential. In: *Clinical Cancer Research* 19.5, pp. 961–968.

Bankhead, C.R. et al. (2008). Identifying symptoms of ovarian cancer: A qualitative and quantitative study. In: *BJOG: An International Journal of Obstetrics and Gynaecology* 115.8, pp. 1008–1014.

Barlow, TS et al. (2006). The utility of presurgical CA125 to predict optimal tumor cytoreduction of epithelial ovarian cancer. In: *International Journal of Gynecological Cancer* 16.2, pp. 496–500.

Barry, G. (2014). Integrating the roles of long and small non-coding RNA in brain function and disease. In: *Molecular Psychiatry* 19.4, pp. 410–416.

Barsotti, Anthony M et al. (2012). p53-Dependent induction of PVT1 and miR-1204. In: *Journal of Biological Chemistry* 287.4, pp. 2509–2519.

Bassuk, S.S. and J.E. Manson (2015). Oral contraceptives and menopausal hormone therapy: Relative and attributable risks of cardiovascular disease, cancer, and other health outcomes. In: *Annals of Epidemiology* 25.3, pp. 193–200.

Bast Jr., R.C. et al. (1981). Reactivity of a monoclonal antibody with human ovarian carcinoma. In: *Journal of Clinical Investigation* 68.5, pp. 1331–1337.

Becker, N. and C. M. Lockwood (2013). Pre-analytical variables in miRNA analysis. In: *Clinical Biochemistry* 46.10-11, pp. 861–868.

Bell, D et al. (2011). Integrated genomic analyses of ovarian carcinoma. In: *Nature* 474.7353, pp. 609–615. ISSN: 0028-0836.

Berchuck, Andrew et al. (2004). Prediction of optimal versus suboptimal cytoreduction of advanced-stage serous ovarian cancer with the use of microarrays. In: *American journal of obstetrics and gynecology* 190.4, pp. 910–923.

Berenbaum, MC (1977). Synergy, additivism and antagonism in immunosuppression. A critical review. In: *Clinical and experimental immunology* 28.1, p. 1.

Berg-Bakker, Cornelia AM van den et al. (1993). Establishment and characterization of 7 ovarian carcinoma cell lines and one granulosa tumor cell line: growth features and cytogenetics. In: *International journal of cancer* 53.4, pp. 613–620.

Bian, E.-B. et al. (2016). Epigenetic modification of miR-141 regulates SKA2 by an endogenous 'sponge' HOTAIR in glioma. In: *Oncotarget* 7.21. cited By 4, pp. 30610–30625.

Bieging, Kathryn T and Laura D Attardi (2012). Deconstructing p53 transcriptional networks in tumor suppression. In: *Trends in cell biology* 22.2, pp. 97–106.

Bieging, Kathryn T, Stephano Spano Mello, and Laura D Attardi (2014). Unravelling mechanisms of p53-mediated tumour suppression. In: *Nature Reviews Cancer* 14.5, pp. 359–370.

Blondal, Thorarinn et al. (2013). Assessing sample and miRNA profile quality in serum and plasma or other biofluids. In: *Methods* 59.1, S1–S6. ISSN: 1046-2023.

Boeckler, Frank M et al. (2008). Targeted rescue of a destabilized mutant of p53 by an in silico screened drug. In: *Proceedings of the National Academy of Sciences* 105.30, pp. 10360–10365.

Bohrens, Brent C et al. (1987). Characterization of ac/s-Diamrninedichloroplatinum (II)-resistant Human Ovarian Cancer Cell Line and Its Use in Evaluation of Platinum Analogues1. In: *CANCER RESEARCH* 47, p. 418.

Bonome, Tomas et al. (2008). A gene signature predicting for survival in suboptimally debulked patients with ovarian cancer. In: *Cancer research* 68.13, pp. 5478–5486.

Boon, R. A. et al. (2013). MicroRNA-34a regulates cardiac ageing and function. In: *Nature* 495.7439, pp. 107–110.

Borley, J. et al. (2015). Radiological predictors of cytoreductive outcomes in patients with advanced ovarian cancer. In: *BJOG: An International Journal of Obstetrics and Gynaecology* 122.6, pp. 843–849.

Bougeard, Gaëlle et al. (2008). Molecular basis of the Li–Fraumeni syndrome: an update from the French LFS families. In: *Journal of medical genetics* 45.8, pp. 535–538.

Bowtell, David D et al. (2015). Rethinking ovarian cancer II: reducing mortality from high-grade serous ovarian cancer. In: *Nature Reviews Cancer* 15.11, pp. 668–679. ISSN: 1474-175X.

Bowtell, David DL (2010). The genesis and evolution of high-grade serous ovarian cancer. In: *Nature Reviews Cancer* 10.11, pp. 803–808.

Braicu, E.I. et al. (2014). HE4 expression in plasma correlates with surgical outcome and overall survival in patients with first ovarian cancer relapse. In: *Annals of Surgical Oncology* 21.3, pp. 955–962.

Brannan, Camilynn I et al. (1990). The product of the H19 gene may function as an RNA. In: *Molecular and cellular biology* 10.1, pp. 28–36.

Bristow, Robert E (2006). Predicting "unresectable" ovarian cancer: taking aim at a moving target. In: *Gynecologic oncology* 100.3, pp. 449–450.

Bristow, Robert E et al. (2000). A model for predicting surgical outcome in patients with advanced ovarian carcinoma using computed tomography. In: *Cancer* 89.7, pp. 1532–1540.

Bristow, Robert E et al. (2002). Survival effect of maximal cytoreductive surgery for advanced ovarian carcinoma during the platinum era: a meta-analysis. In: *Journal of Clinical Oncology* 20.5, pp. 1248–1259.

Bristow, Robert E et al. (2007). Delaying the primary surgical effort for advanced ovarian cancer: a systematic review of neoadjuvant chemotherapy and interval cytoreduction. In: *Gynecologic oncology* 104.2, pp. 480–490.

Burg, ME Van der, FB Lammes, and J Verweij (1992). CA 125 in ovarian cancer. In: *The Netherlands journal of medicine* 40.1-2, pp. 36–51.

— (1993). The role of CA 125 and conventional examinations in diagnosing progressive carcinoma of the ovary. In: *Surgery, gynecology & obstetrics* 176.4, pp. 310–314.

Burnham, Kenneth P and David R Anderson (2004). Multimodel inference understanding AIC and BIC in model selection. In: *Sociological methods & research* 33.2, pp. 261–304.

Bykov, V. J. N. et al. (2005a). PRIMA-1MET synergizes with cisplatin to induce tumor cell apoptosis. In: *Oncogene* 24.21, pp. 3484–3491.

Bykov, V. J. N. et al. (2016). Targeting of mutant P53 and the cellular redox balance by APR-246 as a strategy for efficient cancer therapy. In: *Frontiers in Oncology* 6.FEB.

Bykov, Vladimir JN et al. (2002). Restoration of the tumor suppressor function to mutant p53 by a low-molecular-weight compound. In: *Nature medicine* 8.3, pp. 282–288.

Bykov, Vladimir JN et al. (2005b). PRIMA-1MET synergizes with cisplatin to induce tumor cell apoptosis. In: *Oncogene* 24.21, pp. 3484–3491. ISSN: 0950-9232.

Bykov, Vladimir JN et al. (2005c). Reactivation of mutant p53 and induction of apoptosis in human tumor cells by maleimide analogs. In: *Journal of Biological Chemistry* 280.34, pp. 30384–30391.

Cabanski, Christopher R et al. (2015). Pan-cancer transcriptome analysis reveals long noncoding RNAs with conserved function. In: *RNA biology* 12.6, pp. 628–642.

Cai, Xuezhong and Bryan R Cullen (2007). The imprinted H19 noncoding RNA is a primary microRNA precursor. In: *Rna* 13.3, pp. 313–316.

Calin, George A. and Carlo M. Croce (2006). MicroRNA signatures in human cancers. In: *Nature Reviews Cancer* 6.11, pp. 857–866. ISSN: 1474-175X.

Calin, George Adrian et al. (2002). Frequent deletions and down-regulation of micro-RNA genes miR15 and miR16 at 13q14 in chronic lymphocytic leukemia. In: *Proceedings of the National Academy of Sciences* 99.24, pp. 15524–15529.

Cannistra, S. A. (2004). Cancer of the ovary. In: *New England Journal of Medicine* 351.24, pp. 2519–2529+2565. ISSN: 00284793 (ISSN).

Carlsen, Anting Liu et al. (2013). Cell-free plasma microRNA in pancreatic ductal adenocarcinoma and disease controls. In: *Pancreas* 42.7, pp. 1107–1113. ISSN: 0885-3177.

Casanova, Miguel et al. (2013). Heterochromatin reorganization during early mouse development requires a single-stranded noncoding transcript. In: *Cell reports* 4.6, pp. 1156–1167.

Chakravarty, Dimple et al. (2014). The oestrogen receptor alpha-regulated lncRNA NEAT1 is a critical modulator of prostate cancer. In: *Nature communications* 5.

Chandra Gupta, Subash and Yashoda Nandan Tripathi (2017). Potential of long non-coding RNAs in cancer patients: From biomarkers to therapeutic targets. In: *International journal of cancer* 140.9, pp. 1955–1967.

Chang, L. et al. (2016). Upregulation of SNHG6 regulates ZEB1 expression by competitively binding miR-101-3p and interacting with UPF1 in hepatocellular carcinoma. In: *Cancer Letters* 383.2, pp. 183–194.

Chang, Suk-Joon et al. (2013). Survival impact of complete cytoreduction to no gross residual disease for advanced-stage ovarian cancer: a meta-analysis. In: *Gynecologic oncology* 130.3, pp. 493–498.

Chen, Hui et al. (2014). Cisplatin and paclitaxel target significant long noncoding RNAs in laryngeal squamous cell carcinoma. In: *Medical Oncology* 31.11, p. 246. ISSN: 1559-131X.

Chen, Vivien W et al. (2003). Pathology and classification of ovarian tumors. In: *Cancer* 97.S10, pp. 2631–2642.

Chen, Y. et al. (2016). Serum human epididymis protein 4 vs. carbohydrate antigen 125 and their combination for endometrial cancer diagnosis: A meta-Analysis. In: *European Review for Medical and Pharmacological Sciences* 20.10, pp. 1974–1985.

Chendrimada, Thimmaiah P et al. (2005). TRBP recruits the Dicer complex to Ago2 for microRNA processing and gene silencing. In: *Nature* 436.7051, pp. 740–744.

Cheng, Hanyin et al. (2011). Circulating plasma MiR-141 is a novel biomarker for metastatic colon cancer and predicts poor prognosis. In: *PloS one* 6.3, e17745.

Cheng, Heather H et al. (2013). Circulating microRNA profiling identifies a subset of metastatic prostate cancer patients with evidence of cancer-associated hypoxia. In: *PloS one* 8.7, e69239. ISSN: 1932-6203.

Cheng, Zhongping et al. (2015). A long noncoding RNA AB073614 promotes tumorigenesis and predicts poor prognosis in ovarian cancer. In: *Oncotarget* 6.28, p. 25381.

Chi, Dennis S et al. (2009). A contemporary analysis of the ability of preoperative serum CA-125 to predict primary cytoreductive outcome in patients with advanced ovarian, tubal and peritoneal carcinoma. In: *Gynecologic oncology* 112.1, pp. 6–10.

Cho, Shih-Feng et al. (2014). MALAT1 long non-coding RNA is overexpressed in multiple myeloma and may serve as a marker to predict disease progression. In: *BMC cancer* 14.1, p. 809.

Choi, Yongwook et al. (2012). Predicting the functional effect of amino acid substitutions and indels. In: *PloS one* 7.10, e46688.

Chorley, Brian N et al. (2012). Identification of novel NRF2-regulated genes by ChIP-Seq: influence on retinoid X receptor alpha. In: *Nucleic acids research*, gks409.

Chou, Ting-Chao (2006). Theoretical basis, experimental design, and computerized simulation of synergism and antagonism in drug combination studies. In: *Pharmacological reviews* 58.3, pp. 621–681.

Chou, Ting-Chao (2010). Drug combination studies and their synergy quantification using the Chou-Talalay method. In: *Cancer research* 70.2, pp. 440–446.
Christov, Christo P et al. (2006). Functional requirement of noncoding Y RNAs for human chromosomal DNA replication. In: *Molecular and cellular biology* 26.18, pp. 6993–7004.
Christov, C.P., E. Trivier, and T. Krude (2008). Noncoding human Y RNAs are overexpressed in tumours and required for cell proliferation. In: *British Journal of Cancer* 98.5, pp. 981–988.
Chudecka-Głaz, A.M. (2015). ROMA, an algorithm for ovarian cancer. In: *Clinica Chimica Acta* 440, pp. 143–151.
Chung, Y.-W. et al. (2013). Detection of microRNA as novel biomarkers of epithelial ovarian cancer from the serum of ovarian cancer patient. In: *International Journal of Gynecological Cancer* 23.4, pp. 673–679.
Clarke-Pearson, Daniel (2009). Screening for ovarian cancer. In: *The New England journal of medicine* 361.2, pp. 170–177.
Clemson, Christine M et al. (2009). An architectural role for a nuclear noncoding RNA: NEAT1 RNA is essential for the structure of paraspeckles. In: *Molecular cell* 33.6, pp. 717–726.
Cole, Kristina A et al. (2008). A functional screen identifies miR-34a as a candidate neuroblastoma tumor suppressor gene. In: *Molecular Cancer Research* 6.5, pp. 735–742.
Coleman, Robert L., Pedro T. Ramirez, and David M. Gershenson (2017). *Comprehensive Gynecology*. Ed. by Rogerio A. Lobo et al. 7th ed. Elsevier. Chap. Neoplastic Diseases of the Ovary, pp. 733–788.
Coleman, Robert L et al. (2013). Latest research and treatment of advanced-stage epithelial ovarian cancer. In: *Nature reviews Clinical oncology* 10.4, pp. 211–224.
Colgan, Terence J et al. (2001). Occult carcinoma in prophylactic oophorectomy specimens: prevalence and association with BRCA germline mutation status. In: *The American journal of surgical pathology* 25.10, pp. 1283–1289.
Conklin, Kenneth A (2004a). Chemotherapy-associated oxidative stress: impact on chemotherapeutic effectiveness. In: *Integrative cancer therapies* 3.4, pp. 294–300.
— (2004b). Chemotherapy-associated oxidative stress: impact on chemotherapeutic effectiveness. In: *Integrative cancer therapies* 3.4, pp. 294–300.
Cooke, Susanna L et al. (2010). Genomic analysis of genetic heterogeneity and evolution in high-grade serous ovarian carcinoma. In: *Oncogene* 29.35, pp. 4905–4913.
Corney, David C et al. (2010). Frequent downregulation of miR-34 family in human ovarian cancers. In: *Clinical Cancer Research* 16.4, pp. 1119–1128. ISSN: 1078-0432.
Cortez, Maria Angelica and George Adrian Calin (2009). MicroRNA identification in plasma and serum: a new tool to diagnose and monitor diseases. In: 9, pp. 703–711.
Cortez, Maria Angelica et al. (2011). MicroRNAs in body fluids—the mix of hormones and biomarkers. In: *Nature reviews Clinical oncology* 8.8, pp. 467–477. ISSN: 1759-4774.
Creighton, Chad J et al. (2012). Integrated analyses of microRNAs demonstrate their widespread influence on gene expression in high-grade serous ovarian carcinoma. In: *PloS one* 7.3, e34546. ISSN: 1932-6203.
Crispens, M. (2012). Endometrial and ovarian cancer in lynch syndrome. In: *Clinics in Colon and Rectal Surgery* 25.2, pp. 97–102.

Crum, Christopher P et al. (2013). Through the glass darkly: intraepithelial neoplasia, top-down differentiation, and the road to ovarian cancer. In: *The Journal of pathology* 231.4, pp. 402–412.

Davidovich, Chen et al. (2013). Promiscuous RNA binding by Polycomb repressive complex 2. In: *Nature structural & molecular biology* 20.11, pp. 1250–1257.

Davies, J.R. et al. (2007). MUC16 is produced in tracheal surface epithelium and submucosal glands and is present in secretions from normal human airway and cultured bronchial epithelial cells. In: *International Journal of Biochemistry and Cell Biology* 39.10, pp. 1943–1954.

Davison, A. C. and D. V. Hinkley (1997). *Bootstrap Methods and Their Applications*. Cambridge, United Kingdom: Cambridge University Press. ISBN: 0-521-57391-2.

Deben, C. et al. (2016). APR-246 (PRIMA-1MET) strongly synergizes with AZD2281 (olaparib) induced PARP inhibition to induce apoptosis in non-small cell lung cancer cell lines. In: *Cancer Letters* 375.2, pp. 313–322.

Demma, Mark et al. (2010). SCH529074, a small molecule activator of mutant p53, which binds p53 DNA binding domain (DBD), restores growth-suppressive function to mutant p53 and interrupts HDM2-mediated ubiquitination of wild type p53. In: *Journal of Biological Chemistry* 285.14, pp. 10198–10212.

Denli, Ahmet M et al. (2004). Processing of primary microRNAs by the Microprocessor complex. In: *Nature* 432.7014, pp. 231–235.

Derrien, Thomas et al. (2012). The GENCODE v7 catalog of human long noncoding RNAs: analysis of their gene structure, evolution, and expression. In: *Genome research* 22.9, pp. 1775–1789. ISSN: 1088-9051.

Desgrosellier, Jay S and David A Cheresh (2010). Integrins in cancer: biological implications and therapeutic opportunities. In: *Nature Reviews Cancer* 10.1, pp. 9–22.

Dhamija, S. and S. Diederichs (2016). From junk to master regulators of invasion: LncRNA functions in migration, EMT and metastasis. In: *International Journal of Cancer* 139.2, pp. 269–280.

Diaz-Padilla, I. et al. (2012). Prognostic and predictive value of CA-125 in the primary treatment of epithelial ovarian cancer: Potentials and pitfalls. In: *Clinical and Translational Oncology* 14.1, pp. 15–20.

Ding, Xianfeng et al. (2012). Circulating microRNA-122 as a potential biomarker for liver injury. In: *Molecular medicine reports* 5.6, pp. 1428–1432. ISSN: 1791-2997.

Domcke, Silvia et al. (2013). Evaluating cell lines as tumour models by comparison of genomic profiles. In: *Nature communications* 4, p. 2126. ISSN: 2041-1723.

Dong, Yongqiang et al. (2015). MALAT1 promotes the proliferation and metastasis of osteosarcoma cells by activating the PI3K/Akt pathway. In: *Tumor Biology* 36.3, pp. 1477–1486.

Dowdy, Sean C et al. (2004). The utility of computed tomography scans in predicting suboptimal cytoreductive surgery in women with advanced ovarian carcinoma. In: *Cancer* 101.2, pp. 346–352.

Doyle, Brendan et al. (2010). p53 mutation and loss have different effects on tumourigenesis in a novel mouse model of pleomorphic rhabdomyosarcoma. In: *The Journal of pathology* 222.2, pp. 129–137.

Du, Zhou et al. (2013). Integrative genomic analyses reveal clinically relevant long noncoding RNAs in human cancer. In: *Nature structural & molecular biology* 20.7, pp. 908–913.

du Bois, Andreas et al. (2009). Role of surgical outcome as prognostic factor in advanced epithelial ovarian cancer: A combined exploratory analysis of 3 prospectively randomized phase 3 multicenter trials. In: *Cancer* 115.6, pp. 1234–1244.

Eisenhauer, Eric L et al. (2008). The effect of maximal surgical cytoreduction on sensitivity to platinum-taxane chemotherapy and subsequent survival in patients with advanced ovarian cancer. In: *Gynecologic oncology* 108.2, pp. 276–281.

Eitan, Ram et al. (2009). Tumor microRNA expression patterns associated with resistance to platinum based chemotherapy and survival in ovarian cancer patients. In: *Gynecologic oncology* 114.2, pp. 253–259.

ENCODE (2012). An integrated encyclopedia of DNA elements in the human genome. In: *Nature* 489.7414, pp. 57–74. ISSN: 0028-0836.

Engel, C. et al. (2012). Risks of less common cancers in proven mutation carriers with lynch syndrome. In: *Journal of Clinical Oncology* 30.35, pp. 4409–4415.

Enshaei, A., C. N. Robson, and R. J. Edmondson (2015). Artificial Intelligence Systems as Prognostic and Predictive Tools in Ovarian Cancer. In: *Annals of Surgical Oncology* 22.12, pp. 3970–3975.

Eo, W. et al. (2016). Preoperative lymphocyte-monocyte ratio is a predictor of suboptimal cytoreduction in stage III-IV epithelial ovarian cancer. In: *Journal of Cancer* 7.13, pp. 1772–1779.

Esteller, Manel (2011). Non-coding RNAs in human disease. In: *Nature Reviews Genetics* 12.12, pp. 861–874.

Fabian, Marc R and Nahum Sonenberg (2012). The mechanics of miRNA-mediated gene silencing: a look under the hood of miRISC. In: *Nature structural & molecular biology* 19.6, pp. 586–593.

Fader, Amanda Nickles and Peter G Rose (2007). Role of surgery in ovarian carcinoma. In: *Journal of clinical oncology* 25.20, pp. 2873–2883.

Fagotti, A. et al. (2005). Role of laparoscopy to assess the chance of optimal cytoreductive surgery in advanced ovarian cancer: A pilot study. In: *Gynecologic Oncology* 96.3, pp. 729–735.

Fagotti, A. et al. (2006). A laparoscopy-based score to predict surgical outcome in patients with advanced ovarian carcinoma: A pilot study. In: *Annals of Surgical Oncology* 13.8, pp. 1156–1161.

Fagotti, A. et al. (2008). Prospective validation of a laparoscopic predictive model for optimal cytoreduction in advanced ovarian carcinoma. In: *American Journal of Obstetrics and Gynecology* 199.6, 642.e1–642.e6.

Fagotti, A. et al. (2014). Introduction of staging laparoscopy in the management of advanced epithelial ovarian, tubal and peritoneal cancer: Impact on prognosis in a single institution experience. In: *Obstetrical and Gynecological Survey* 69.3, pp. 144–146.

Fan, Y. et al. (2014). Long non-coding RNA UCA1 increases chemoresistance of bladder cancer cells by regulating Wnt signaling. In: *FEBS Journal* 281.7, pp. 1750–1758.

Farazi, Thalia A et al. (2011). MicroRNA sequence and expression analysis in breast tumors by deep sequencing. In: *Cancer research* 71.13, pp. 4443–4453.

Fata, Jimmie E et al. (2012). Nongenomic mechanisms of PTEN regulation. In: *International journal of cell biology* 2012.

FDA (2016). *Rucaparib*. URL: https://www.fda.gov/Drugs/InformationOnDrugs/ApprovedDrugs/ucm533891.htm.

— (2017). *Niraparib*. URL: https://www.accessdata.fda.gov/drugsatfda_docs/nda/2017/208447_zejula_toc.cfm.

Feeley, KM and M Wells (2001). Precursor lesions of ovarian epithelial malignancy. In: *Histopathology* 38.2, pp. 87–95.

Fejes-Toth, Katalin et al. (2009). Post-transcriptional processing generates a diversity of 5′-modified long and short RNAs. In: *Nature* 457.7232, pp. 1028–1032.

Felder, M. et al. (2014). MUC16 (CA125): Tumor biomarker to cancer therapy, a work in progress. In: *Molecular Cancer* 13.1.

Feng, Zhaohui et al. (2011). Tumor suppressor p53 meets microRNAs. In: *Journal of molecular cell biology* 3.1, pp. 44–50.

Ferlay, J. et al. (2015). Cancer incidence and mortality worldwide: Sources, methods and major patterns in GLOBOCAN 2012. In: *International Journal of Cancer* 136.5, E359–E386.

Ferrarow, S. et al. (2013). Serum human epididymis protein 4 vs carbohydrate antigen 125 for ovarian cancer diagnosis: A systematic review. In: *Journal of Clinical Pathology* 66.4, pp. 273–281.

Finch, Amy et al. (2006). Clinical and pathologic findings of prophylactic salpingo-oophorectomies in 159 BRCA1 and BRCA2 carriers. In: *Gynecologic oncology* 100.1, pp. 58–64.

Fischer, M (2017). Census and evaluation of p53 target genes. In: *Oncogene*.

Foster, Barbara A et al. (1999). Pharmacological rescue of mutant p53 conformation and function. In: *Science* 286.5449, pp. 2507–2510.

Foucquier, Julie and Mickael Guedj (2015). Analysis of drug combinations: current methodological landscape. In: *Pharmacology research & perspectives* 3.3.

Fransson, et al. (2016). Strong synergy with APR-246 and DNA-damaging drugs in primary cancer cells from patients with TP53 mutant High-Grade Serous ovarian cancer. In: *Journal of Ovarian Research* 9.1.

Freed-Pastor, William A et al. (2012). Mutant p53 disrupts mammary tissue architecture via the mevalonate pathway. In: *Cell* 148.1, pp. 244–258.

Friedman, Robin C et al. (2009). Most mammalian mRNAs are conserved targets of microRNAs. In: *Genome research* 19.1, pp. 92–105.

Galindo, Máximo Ibo et al. (2007). Peptides encoded by short ORFs control development and define a new eukaryotic gene family. In: *PLoS Biol* 5.5, e106.

Gao, Y.-C. and J. Wu (2015). MicroRNA-200c and microRNA-141 as potential diagnostic and prognostic biomarkers for ovarian cancer. In: *Tumor Biology* 36.6, pp. 4843–4850.

Gao, Yuan et al. (2015). LncRNA-HOST2 regulates cell biological behaviors in epithelial ovarian cancer through a mechanism involving microRNA let-7b. In: *Human molecular genetics* 24.3, pp. 841–852.

Garcia, Amandine I et al. (2011). The rs2910164: G> C SNP in the MIR146A gene is not associated with breast cancer risk in BRCA1 and BRCA2 mutation carriers. In: *Human mutation* 32.9, pp. 1004–1007.

Gatsiou, A. et al. (2012). MicroRNAs in platelet biogenesis and function: Implications in vascular homeostasis and inflammation. In: *Current Vascular Pharmacology* 10.5, pp. 524–531.

Gemer, O et al. (2005). A multicenter study of CA 125 level as a predictor of non-optimal primary cytoreduction of advanced epithelial ovarian cancer. In: *European Journal of Surgical Oncology (EJSO)* 31.9, pp. 1006–1010.

Giaccone, G et al. (1992). Neuromedin B is present in lung cancer cell lines. In: *Cancer research* 52.9 Supplement, 2732s–2736s.

Gloss, Brian et al. (2014). ZNF300P1 Encodes a lincRNA that regulates cell polarity and is epigenetically silenced in type II epithelial ovarian cancer. In: *Molecular cancer* 13.1, p. 3.

Goff, B.A. et al. (2000). Ovarian carcinoma diagnosis: Results of a national ovarian cancer survey. In: *Cancer* 89.10, pp. 2068–2075.

Goh, A. M., C. R. Coffill, and D. P. Lane (2010). The role of mutant p53 in human cancer. In: *Journal of Pathology* 223.2, pp. 116–126.

Gorai, Itsuo et al. (1995). Establishment and characterization of two human ovarian clear cell adenocarcinoma lines from metastatic lesions with different properties. In: *Gynecologic oncology* 57.1, pp. 33–46.

Gorrini, Chiara, Isaac S Harris, and Tak W Mak (2013). Modulation of oxidative stress as an anticancer strategy. In: *Nature reviews Drug discovery* 12.12, pp. 931–947.

Grabovsky, Yury and Ronald J Tallarida (2004). Isobolographic analysis for combinations of a full and partial agonist: curved isoboles. In: *Journal of Pharmacology and Experimental Therapeutics* 310.3, pp. 981–986.

Gregory, Richard I et al. (2004). The Microprocessor complex mediates the genesis of microRNAs. In: *Nature* 432.7014, pp. 235–240.

Grellety, T. et al. (2015). PRIMA-1MET induces death in soft-tissue sarcomas cell independent of p53. In: *BMC Cancer* 15.1.

Grenache, D.G. et al. (2015). Clinical performance of two multi-marker blood tests for predicting malignancy in women with an adnexal mass. In: *Clinica Chimica Acta* 438, pp. 358–363.

Griffiths, C Thomas (1975). Surgical resection of tumor bulk in the primary treatment of ovarian carcinoma. In: *National Cancer Institute Monograph* 42, pp. 101–104.

Guan, Yinghui et al. (2007). Amplification of PVT1 contributes to the pathophysiology of ovarian and breast cancer. In: *Clinical cancer research* 13.19, pp. 5745–5755.

Guo, F. et al. (2013). Serum microRNA-92 expression in patients with ovarian epithelial carcinoma. In: *Journal of International Medical Research* 41.5, pp. 1456–1461.

Gupta, Rajnish A et al. (2010). Long non-coding RNA HOTAIR reprograms chromatin state to promote cancer metastasis. In: *Nature* 464.7291, pp. 1071–1076.

Gutschner, Tony, Monika Hämmerle, and Sven Diederichs (2013). MALAT1 — a paradigm for long noncoding RNA function in cancer. In: *Journal of Molecular Medicine* 91.7, pp. 791–801. ISSN: 1432-1440.

Guttman, Mitchell and John L Rinn (2012). Modular regulatory principles of large non-coding RNAs. In: *Nature* 482.7385, pp. 339–346.
Guttman, Mitchell et al. (2009). Chromatin signature reveals over a thousand highly conserved large non-coding RNAs in mammals. In: *Nature* 458.7235, pp. 223–227.
Guttman, Mitchell et al. (2011). lincRNAs act in the circuitry controlling pluripotency and differentiation. In: *Nature* 477.7364, pp. 295–300.
Ha, Minju and V Narry Kim (2014). Regulation of microRNA biogenesis. In: *Nature reviews Molecular cell biology* 15.8, pp. 509–524.
Hall, A.E., C. Turnbull, and T. Dalmay (2013). Y RNAs: Recent developments. In: *Biomolecular Concepts* 4.2, pp. 103–110.
Hamajima, N. et al. (2012). Menarche, menopause, and breast cancer risk: Individual participant meta-analysis, including 118 964 women with breast cancer from 117 epidemiological studies. In: *The Lancet Oncology* 13.11, pp. 1141–1151.
Hamilton, Thomas C, Robert C Young, and Robert F Ozols (1984). Experimental model systems of ovarian cancer: applications to the design and evaluation of new treatment approaches. In: *Semin Oncol* 11.3, pp. 285–298.
Hamilton, Thomas C et al. (1983). Characterization of a human ovarian carcinoma cell line (NIH: OVCAR-3) with androgen and estrogen receptors. In: *Cancer research* 43.11, pp. 5379–5389.
Han, Jiang, Daniel Kim, and Kevin V Morris (2007). Promoter-associated RNA is required for RNA-directed transcriptional gene silencing in human cells. In: *Proceedings of the National Academy of Sciences* 104.30, pp. 12422–12427.
Han, Jinju et al. (2004). The Drosha-DGCR8 complex in primary microRNA processing. In: *Genes & development* 18.24, pp. 3016–3027.
Hansen, Thomas B, Jørgen Kjems, and Christian K Damgaard (2013). Circular RNA and miR-7 in cancer. In: *Cancer research* 73.18, pp. 5609–5612.
Hansen, Thomas B et al. (2011). miRNA-dependent gene silencing involving Ago2-mediated cleavage of a circular antisense RNA. In: *The EMBO journal* 30.21, pp. 4414–4422.
Hansen, Thomas B et al. (2013). Natural RNA circles function as efficient microRNA sponges. In: *Nature* 495.7441, pp. 384–388.
Hattrup, C.L. and S.J. Gendler (2008). Structure and function of the cell surface (tethered) mucins. In: *Annual Review of Physiology* 70, pp. 431–457.
Hausler, S.F.M. et al. (2010). Whole blood-derived miRNA profiles as potential new tools for ovarian cancer screening. In: *British Journal of Cancer* 103.5, pp. 693–700.
Hawkins, Robert C (2010). Phlebotomy site haemolysis rates vary inversely with workload. In: *Clinical Chemistry and Laboratory Medicine* 48.7, pp. 1049–1051. ISSN: 1437-4331.
Hayes, J., P. P. Peruzzi, and S. Lawler (2014). MicroRNAs in cancer: Biomarkers, functions and therapy. In: *Trends in Molecular Medicine* 20.8, pp. 460–469.
He, Lin et al. (2005). A microRNA polycistron as a potential human oncogene. In: *Nature* 435.7043, pp. 828–833.
He, Lin et al. (2007). A microRNA component of the p53 tumour suppressor network. In: *Nature* 447.7148, pp. 1130–1134.

He, Xiaoying et al. (2014). The long non-coding RNA HOTAIR is upregulated in endometrial carcinoma and correlates with poor prognosis. In: *Int J Mol Med* 33.2, pp. 325–32.

He, Y. et al. (2015). Current state of circulating microRNAs as cancer biomarkers. In: *Clinical Chemistry* 61.9, pp. 1138–1155.

Heneghan, Helen M et al. (2010). Circulating microRNAs as novel minimally invasive biomarkers for breast cancer. In: *Annals of surgery* 251.3, pp. 499–505.

Hennessy, Bryan, Robert Coleman, and Maurie Markman (2009). Ovarian cancer. In: *Lancet* 374.9698, pp. 1371–1382.

Heravi-Moussavi, Alireza et al. (2012). Recurrent somatic DICER1 mutations in nonepithelial ovarian cancers. In: *New England Journal of Medicine* 366.3, pp. 234–242.

Hermeking, Heiko (2012). MicroRNAs in the p53 network: micromanagement of tumour suppression. In: *Nature Reviews Cancer* 12.9, pp. 613–626. ISSN: 1474-175X.

Herzog, Thomas J and Bhavana Pothuri (2006). Ovarian cancer: a focus on management of recurrent disease. In: *Nature clinical practice Oncology* 3.11, pp. 604–611.

Hesse, Marlen and Christoph Arenz (2014). MicroRNA maturation and human disease. In: *miRNA Maturation: Methods and Protocols*, pp. 11–25.

Hills, CA et al. (1989). Biological properties of ten human ovarian carcinoma cell lines: calibration in vitro against four platinum complexes. In: *British journal of cancer* 59.4, p. 527.

Ho, A. S. et al. (2010). Circulating miR-210 as a novel hypoxia marker in pancreatic cancer. In: *Translational Oncology* 3.2, pp. 109–113.

Horowitz, Neil S et al. (2015). Does aggressive surgery improve outcomes? Interaction between preoperative disease burden and complex surgery in patients with advanced-stage ovarian cancer: an analysis of GOG 182. In: *Journal of Clinical Oncology* 33.8, pp. 937–943.

Hu, L. et al. (2016). Comparison of Serum Human Epididymis Protein 4 and Carbohydrate Antigen 125 as Markers in Endometrial Cancer: A Meta-Analysis. In: *International Journal of Gynecological Cancer* 26.2, pp. 331–340.

Hu, Wenwei et al. (2010a). Negative regulation of tumor suppressor p53 by microRNA miR-504. In: *Molecular cell* 38.5, pp. 689–699.

Hu, Xiaowen et al. (2014). A functional genomic approach identifies FAL1 as an oncogenic long noncoding RNA that associates with BMI1 and represses p21 expression in cancer. In: *Cancer cell* 26.3, pp. 344–357.

Hu, Zhibin et al. (2010b). Serum MicroRNA signatures identified in a genome-wide serum MicroRNA expression profiling predict survival of non–small-cell lung cancer. In: *Journal of Clinical Oncology* 28.10, pp. 1721–1726.

Huang, Kuan-Chun et al. (2002a). Relationship of XIST Expression and Responses of Ovarian Cancer to Chemotherapy 1 This work was partly supported by NIH Grants CA70216 and GM 59920 (to SW. N.). 1. In: *Molecular cancer therapeutics* 1.10, pp. 769–776.

— (2002b). Relationship of XIST Expression and Responses of Ovarian Cancer to Chemotherapy 1 This work was partly supported by NIH Grants CA70216 and GM 59920 (to SW. N.). 1. In: *Molecular cancer therapeutics* 1.10, pp. 769–776. ISSN: 1535-7163.

Huarte, M. et al. (2010). A large intergenic noncoding RNA induced by p53 mediates global gene repression in the p53 response. In: *Cell* 142.3. cited By 859, pp. 409–419.
Hung, Tiffany et al. (2011). Extensive and coordinated transcription of noncoding RNAs within cell-cycle promoters. In: *Nature genetics* 43.7, pp. 621–629.
Hunn, J. and G.C. Rodriguez (2012). Ovarian cancer: Etiology, risk factors, and epidemiology. In: *Clinical Obstetrics and Gynecology* 55.1, pp. 3–23.
Huo, D. et al. (2016). Identification of a circulating MicroRNA signature to distinguish recurrence in breast cancer patients. In: *Oncotarget* 7.34, pp. 55231–55248.
Ibeanu, Okechukwu A and Robert E Bristow (2010). Predicting the outcome of cytoreductive surgery for advanced ovarian cancer: a review. In: *International Journal of Gynecological Cancer* 20.10, S1–S11. ISSN: 1048-891X.
Idogawa, M. et al. (2014). Identification and analysis of large intergenic non-coding RNAs regulated by p53 family members through a genome-wide analysis of p53-binding sites. In: *Human Molecular Genetics* 23.11, pp. 2847–2857.
Ingolia, Nicholas T, Liana F Lareau, and Jonathan S Weissman (2011). Ribosome profiling of mouse embryonic stem cells reveals the complexity and dynamics of mammalian proteomes. In: *Cell* 147.4, pp. 789–802.
Iorio, Marilena V et al. (2007). MicroRNA signatures in human ovarian cancer. In: *Cancer Research* 67.18, pp. 8699–8707.
Ipsaro, Jonathan J and Leemor Joshua-Tor (2015). From guide to target: molecular insights into eukaryotic RNA-interference machinery. In: *Nature structural & molecular biology* 22.1, pp. 20–28.
Irwin, MS and WG Kaelin (2001). Role of the newer p53 family proteins in malignancy. In: *Apoptosis* 6.1-2, pp. 17–29.
Iterson, Maarten van, Herman HHBM van Haagen, and Jelle J Goeman (2012). Resolving confusion of tongues in statistics and machine learning: A primer for biologists and bioinformaticians. In: *Proteomics* 12.4-5, pp. 543–549.
Iwamoto, H. et al. (2014). Serum miR-210 as a potential biomarker of early clear cell renal cell carcinoma. In: *International Journal of Oncology* 44.1, pp. 53–58.
Iyer, M. K. et al. (2015). The landscape of long noncoding RNAs in the human transcriptome. In: *Nature Genetics* 47.3, pp. 199–208.
Izetti, P. et al. (2014). PRIMA-1, a mutant p53 reactivator, induces apoptosis and enhances chemotherapeutic cytotoxicity in pancreatic cancer cell lines. In: *Investigational New Drugs* 32.5, pp. 783–794.
Jacobs, I.J. et al. (2016). Ovarian cancer screening and mortality in the UK Collaborative Trial of Ovarian Cancer Screening (UKCTOCS): A randomised controlled trial. In: *The Lancet* 387.10022, pp. 945–956.
Jayson, G.C. et al. (2014). Ovarian cancer. In: *The Lancet* 384.9951, pp. 1376–1388.
Jed Wing, Max Kuhn. Contributions from et al. (2016). *caret: Classification and Regression Training*.
Ji, Ping et al. (2003). MALAT-1, a novel noncoding RNA, and thymosin beta 4 predict metastasis and survival in early-stage non-small cell lung cancer. In: *Oncogene* 22.39, p. 8031.

Jiao, Feng et al. (2014). Elevated expression level of long noncoding RNA MALAT-1 facilitates cell growth, migration and invasion in pancreatic cancer. In: *Oncology reports* 32.6, pp. 2485–2492.

Johnson, Charles D et al. (2007). The let-7 microRNA represses cell proliferation pathways in human cells. In: *Cancer research* 67.16, pp. 7713–7722.

Jonas, Stefanie and Elisa Izaurralde (2015). Towards a molecular understanding of microRNA-mediated gene silencing. In: *Nature Reviews Genetics* 16.7, pp. 421–433.

Jones, Siân et al. (2010). Frequent mutations of chromatin remodeling gene ARID1A in ovarian clear cell carcinoma. In: *Science* 330.6001, pp. 228–231.

Jonsson, Elin et al. (1998). Synergistic interactions of combinations of topotecan with standard drugs in primary cultures of human tumor cells from patients. In: *European journal of clinical pharmacology* 54.7, pp. 509–514.

Kachakova, D. et al. (2015). Combinations of serum prostate-specific antigen and plasma expression levels of let-7c, miR-30c, miR-141, and miR-375 as potential better diagnostic biomarkers for prostate cancer. In: *DNA and Cell Biology* 34.3, pp. 189–200.

Kan, Casina WS et al. (2012). Elevated levels of circulating microRNA-200 family members correlate with serous epithelial ovarian cancer. In: *BMC cancer* 12.1, p. 627.

Kapranov, Philipp et al. (2007). RNA maps reveal new RNA classes and a possible function for pervasive transcription. In: *Science* 316.5830, pp. 1484–1488.

Kapranov, Philipp et al. (2010). New class of gene-termini-associated human RNAs suggests a novel RNA copying mechanism. In: *Nature* 466.7306, pp. 642–646.

Karlan, B.Y. et al. (1988). Plasminogen activator secretion by established lines of human ovarian carcinoma cells in vitro. In: *Gynecologic Oncology* 31.1, pp. 103–112.

Kasinski, Andrea L and Frank J Slack (2012). miRNA-34 prevents cancer initiation and progression in a therapeutically resistant K-ras and p53-induced mouse model of lung adenocarcinoma. In: *Cancer research* 72.21, pp. 5576–5587.

Katayama, S et al. (2005). Antisense transcription in the mammalian transcriptome. In: *Science* 309.5740, pp. 1564–1566.

Kawaji, Hideya and Yoshihide Hayashizaki (2008). Exploration of small RNAs. In: *PLoS Genet* 4.1, e22.

Kawano, Masanori et al. (2015). microRNA-93 promotes cell proliferation via targeting of PTEN in Osteosarcoma cells. In: *Journal of Experimental & Clinical Cancer Research* 34.1, p. 76.

Kehoe, S. et al. (2015). Primary chemotherapy versus primary surgery for newly diagnosed advanced ovarian cancer (CHORUS): An open-label, randomised, controlled, non-inferiority trialc. In: *The Lancet* 386.9990, pp. 249–257.

Khalil, Ahmad et al. (2009). Many human large intergenic noncoding RNAs associate with chromatin-modifying complexes and affect gene expression. In: *Proceedings of the National Academy of Sciences of the United States of America* 106.28, pp. 11667–11672.

Khoury, Marie P and Jean-Christophe Bourdon (2010). The isoforms of the p53 protein. In: *Cold Spring Harbor perspectives in biology* 2.3, a000927.

Kim, K et al. (2012). HOTAIR is a negative prognostic factor and exhibits pro-oncogenic activity in pancreatic cancer. In: *Oncogene*.

Kim, Young-Kook and V Narry Kim (2007). Processing of intronic microRNAs. In: *The EMBO journal* 26.3, pp. 775–783.
Kindelberger, David W et al. (2007). Intraepithelial carcinoma of the fimbria and pelvic serous carcinoma: evidence for a causal relationship. In: *The American journal of surgical pathology* 31.2, pp. 161–169.
Kino, Tomoshige et al. (2010). Noncoding RNA Gas5 is a growth arrest and starvation-associated repressor of the glucocorticoid receptor. In: *Science signaling* 3.107, ra8.
Kirschner, Michaela B et al. (2011). Haemolysis during sample preparation alters microRNA content of plasma. In: *PloS one* 6.9, e24145. ISSN: 1932-6203.
Kirschner, Michaela B et al. (2013). Hemolysis and its impact on cell-free microRNA biomarkers. In: *Frontiers in Genetics* 4. ISSN: 1664-8021.
Kogo, Ryunosuke et al. (2011). Long noncoding RNA HOTAIR regulates polycomb-dependent chromatin modification and is associated with poor prognosis in colorectal cancers. In: *Cancer research* 71.20, pp. 6320–6326.
Komatsu, Shuhei et al. (2013). Prognostic impact of circulating miR-21 in the plasma of patients with gastric carcinoma. In: *Anticancer research* 33.1, pp. 271–276.
Kosaka, Nobuyoshi, Haruhisa Iguchi, and Takahiro Ochiya (2010). Circulating microRNA in body fluid: a new potential biomarker for cancer diagnosis and prognosis. In: *Cancer science* 101.10, pp. 2087–2092. ISSN: 1349-7006.
Kravchenko, JE et al. (2008). Small-molecule RETRA suppresses mutant p53-bearing cancer cells through a p73-dependent salvage pathway. In: *Proceedings of the National Academy of Sciences* 105.17, pp. 6302–6307.
Kroeger, P.T. and R. Drapkin (2017). Pathogenesis and heterogeneity of ovarian cancer. In: *Current Opinion in Obstetrics and Gynecology* 29.1. cited By 0, pp. 26–34.
Kuha, Jouni (2004). AIC and BIC: Comparisons of Assumptions and Performance. In: *Sociological methods & research* 33.2, pp. 188–229.
Kumar, Madhu S et al. (2009). Dicer1 functions as a haploinsufficient tumor suppressor. In: *Genes & development* 23.23, pp. 2700–2704.
Kurman, Robert J and Ie-Ming Shih (2011). Molecular pathogenesis and extraovarian origin of epithelial ovarian cancer — shifting the paradigm. In: *Human pathology* 42.7, pp. 918–931.
Lalwani, Neeraj et al. (2011). Histologic, molecular, and cytogenetic features of ovarian cancers: implications for diagnosis and treatment. In: *Radiographics* 31.3, pp. 625–646.
Lambert, J. M. R. et al. (2010). Mutant p53 reactivation by PRIMA-1 MET induces multiple signaling pathways converging on apoptosis. In: *Oncogene* 29.9, pp. 1329–1338.
Lambert, Jeremy MR et al. (2009). PRIMA-1 reactivates mutant p53 by covalent binding to the core domain. In: *Cancer cell* 15.5, pp. 376–388. ISSN: 1535-6108.
Lane, David P (1992). Cancer. p53, guardian of the genome. In: *Nature* 358, pp. 15–16.
Lang, Gene A et al. (2004). Gain of function of a p53 hot spot mutation in a mouse model of Li-Fraumeni syndrome. In: *Cell* 119.6, pp. 861–872.
Langdon, Simon P et al. (1988). Characterization and properties of nine human ovarian adenocarcinoma cell lines. In: *Cancer research* 48.21, pp. 6166–6172.
Le, Minh TN et al. (2009). MicroRNA-125b is a novel negative regulator of p53. In: *Genes & development* 23.7, pp. 862–876.

Lee, Sungyul et al. (2016). Noncoding RNA NORAD regulates genomic stability by sequestering PUMILIO proteins. In: *Cell* 164.1, pp. 69–80.

Lee, Y et al. (2007). A candidate precursor to serous carcinoma that originates in the distal fallopian tube. In: *The Journal of pathology* 211.1, pp. 26–35.

Lee, Yoontae et al. (2003). The nuclear RNase III Drosha initiates microRNA processing. In: *Nature* 425.6956, pp. 415–419.

Lee, Yoontae et al. (2004). MicroRNA genes are transcribed by RNA polymerase II. In: *The EMBO journal* 23.20, pp. 4051–4060.

Li, Andrew John (2012). *New biomarkers for ovarian cancer: OVA1 and ROMA in diagnosis*. URL: http://contemporaryobgyn.modernmedicine.com/contemporary-obgyn/news/modernmedicine/modern-medicine-feature-articles/new-biomarkers-ovarian-cance?page=full.

Li, Daochuan et al. (2011). Aberrant Expression of miR-638 Contributes to Benzo (a) pyrene–induced Human Cell Transformation. In: *Toxicological Sciences*, kfr299.

Li, Dun, Natalia D Marchenko, and Ute M Moll (2011). SAHA shows preferential cytotoxicity in mutant p53 cancer cells by destabilizing mutant p53 through inhibition of the HDAC6-Hsp90 chaperone axis. In: *Cell Death & Differentiation* 18.12, pp. 1904–1913.

Li, Jing et al. (2016). Overexpression of long non-coding RNA HOTAIR leads to chemoresistance by activating the Wnt/β-catenin pathway in human ovarian cancer. In: *Tumor Biology* 37.2, pp. 2057–2065.

Li, X. L. et al. (2015). PRIMA-1met (APR-246) inhibits growth of colorectal cancer cells with different p53 status through distinct mechanisms. In: *Oncotarget* 6.34, pp. 36689–36699.

Liberti, Maria V and Jason W Locasale (2016). The Warburg effect: how does it benefit cancer cells? In: *Trends in biochemical sciences* 41.3, pp. 211–218.

Lin, Haifan (2007). piRNAs in the germ line. In: *science* 316.5823, pp. 397–397.

Lin, Michael F, Irwin Jungreis, and Manolis Kellis (2011). PhyloCSF: a comparative genomics method to distinguish protein coding and non-coding regions. In: *Bioinformatics* 27.13, pp. i275–i282.

Lin, Shuibin and Richard I Gregory (2015). MicroRNA biogenesis pathways in cancer. In: *Nature Reviews Cancer* 15.6, pp. 321–333. ISSN: 1474-175X.

Lindsey, JK and Bradley Jones (1998). Choosing among generalized linear models applied to medical data. In: *Statistics in medicine* 17.1, pp. 59–68.

Lippi, Giuseppe et al. (2009). Survey on the prevalence of hemolytic specimens in an academic hospital according to collection facility: opportunities for quality improvement. In: *Clinical Chemistry and Laboratory Medicine* 47.5, pp. 616–618. ISSN: 1437-4331.

Liu, Can et al. (2011a). The microRNA miR-34a inhibits prostate cancer stem cells and metastasis by directly repressing CD44. In: *Nature medicine* 17.2, pp. 211–215.

Liu, D. S. H. et al. (2015). APR-246 potently inhibits tumour growth and overcomes chemoresistance in preclinical models of oesophageal adenocarcinoma. In: *Gut* 64.10, pp. 1506–1516.

Liu, Rong et al. (2017). Long noncoding RNA expression signature to predict platinum-based chemotherapeutic sensitivity of ovarian cancer patients. In: *Scientific Reports* 7.1, p. 18.

Liu, Rui et al. (2011b). A five-microRNA signature identified from genome-wide serum microRNA expression profiling serves as a fingerprint for gastric cancer diagnosis. In: *European journal of cancer* 47.5, pp. 784–791.

Liu, Shi-Ping et al. (2013a). Identification of differentially expressed long non-coding RNAs in human ovarian cancer cells with different metastatic potentials. In: *Cancer biology & medicine* 10.3, pp. 138–141.

Liu, X.-H. et al. (2014). Lnc RNA HOTAIR functions as a competing endogenous RNA to regulate HER2 expression by sponging miR-331-3p in gastric cancer. In: *Molecular Cancer* 13.1. cited By 209.

Liu, Xiangrui et al. (2013b). Small molecule induced reactivation of mutant p53 in cancer cells. In: *Nucleic acids research* 41.12, pp. 6034–6044.

Livak, Kenneth J and Thomas D Schmittgen (2001). Analysis of relative gene expression data using real-time quantitative PCR and the 2- $\Delta\Delta$CT method. In: *methods* 25.4, pp. 402–408.

Loewe, S (1953). The problem of synergism and antagonism of combined drugs. In: *Arzneimittel-Forschung* 3.6, p. 285.

Londin, Eric et al. (2015). Analysis of 13 cell types reveals evidence for the expression of numerous novel primate-and tissue-specific microRNAs. In: *Proceedings of the National Academy of Sciences* 112.10, E1106–E1115.

Lopez-Ayllon, B.D. et al. (2015). Cancer stem cells and cisplatin-resistant cells isolated from non-small-lung cancer cell lines constitute related cell populations. In: *Cancer Medicine* 3.5, pp. 1099–1111.

Louro, Rodrigo, Anna S Smirnova, and Sergio Verjovski-Almeida (2009). Long intronic noncoding RNA transcription: expression noise or expression choice? In: *Genomics* 93.4, pp. 291–298.

Lovis, P. et al. (2008). Alterations in MicroRNA expression contribute to fatty Acid-Induced pancreatic β-Cell dysfunction. In: *Diabetes* 57.10, pp. 2728–2736.

Lu, Jun et al. (2005). MicroRNA expression profiles classify human cancers. In: *nature* 435.7043, pp. 834–838.

Lujambio, Amaia and Scott W Lowe (2012). The microcosmos of cancer. In: *Nature* 482.7385, pp. 347–355.

Lv, Xiao-Bin et al. (2013). Long noncoding RNA HOTAIR is a prognostic marker for esophageal squamous cell carcinoma progression and survival. In: *PloS one* 8.5, e63516.

Mackintosh, M.L. et al. (2014). CT scan does not predict optimal debulking in stage III-IV epithelial ovarian cancer: A multicentre validation study. In: *Journal of Obstetrics and Gynaecology* 34.5, pp. 424–428.

Madhavan, Dharanija et al. (2012). Circulating miRNAs as surrogate markers for circulating tumor cells and prognostic markers in metastatic breast cancer. In: *Clinical Cancer Research* 18.21, pp. 5972–5982.

Mahn, Robert et al. (2011). Circulating microRNAs (miRNA) in serum of patients with prostate cancer. In: *Urology* 77.5, 1265–e9.

Marsh, Deborah J, Jaynish S Shah, and Alexander J Cole (2014). Histones and their modifications in ovarian cancer–drivers of disease and therapeutic targets. In: *Frontiers in oncology* 4.

Martianov, Igor et al. (2007). Repression of the human dihydrofolate reductase gene by a non-coding interfering transcript. In: *Nature* 445.7128, pp. 666–670.
Martín-Cameàn, M. et al. (2016). The role of surgery in advanced epithelial ovarian cancer. In: *ecancermedicalscience* 10.
Martynova, Elena et al. (2012). Gain-of-function p53 mutants have widespread genomic locations partially overlapping with p63. In: *Oncotarget* 3.2, pp. 132–143.
Marzano, Christine et al. (2007). Inhibition of thioredoxin reductase by auranofin induces apoptosis in cisplatin-resistant human ovarian cancer cells. In: *Free Radical Biology and Medicine* 42.6, pp. 872–881.
Matouk, Imad J et al. (2014). Oncofetal H19 RNA promotes tumor metastasis. In: *Biochimica et Biophysica Acta (BBA)-Molecular Cell Research* 1843.7, pp. 1414–1426.
Mattick, John S and John L Rinn (2015). Discovery and annotation of long noncoding RNAs. In: *Nature Structural and Molecular Biology* 22.1, pp. 5–8.
Matulonis, U.A. et al. (2016). Ovarian cancer. In: *Nature Reviews Disease Primers* 2, pp. 1–22.
McAlexander, Melissa, Maggie Phillips, and Kenneth Witwer (2013). Comparison of Methods for miRNA Extraction from Plasma and Quantitative Recovery of RNA from Cerebrospinal Fluid. In: *Frontiers in Genetics* 4, p. 83. ISSN: 1664-8021.
McDonald, Jennifer S et al. (2011). Analysis of circulating microRNA: preanalytical and analytical challenges. In: *Clinical chemistry* 57.6, pp. 833–840. ISSN: 0009-9147.
McWhinney, Sarah R, Richard M Goldberg, and Howard L McLeod (2009). Platinum neurotoxicity pharmacogenetics. In: *Molecular cancer therapeutics* 8.1, pp. 10–16.
Medeiros, Fabiola et al. (2006). The tubal fimbria is a preferred site for early adenocarcinoma in women with familial ovarian cancer syndrome. In: *The American journal of surgical pathology* 30.2, pp. 230–236.
Medeiros, L.R. et al. (2009). Accuracy of CA 125 in the diagnosis of ovarian tumors: A quantitative systematic review. In: *European Journal of Obstetrics Gynecology and Reproductive Biology* 142.2, pp. 99–105.
Melino, Gerry, Vincenzo De Laurenzi, and Karen H Vousden (2002). p73: Friend or foe in tumorigenesis. In: *Nature Reviews Cancer* 2.8, pp. 605–615.
Memarzadeh, S et al. (2003). CA125 levels are a weak predictor of optimal cytoreductive surgery in patients with advanced epithelial ovarian cancer. In: *International Journal of Gynecological Cancer* 13.2, pp. 120–124.
Meng, Fanyin et al. (2007). MicroRNA-21 regulates expression of the PTEN tumor suppressor gene in human hepatocellular cancer. In: *Gastroenterology* 133.2, pp. 647–658.
Menon, Usha et al. (2005). Prospective study using the risk of ovarian cancer algorithm to screen for ovarian cancer. In: *Journal of Clinical Oncology* 23.31, pp. 7919–7926.
Mercer, Tim R, Marcel E Dinger, and John S Mattick (2009). Long non-coding RNAs: insights into functions. In: *Nature Reviews Genetics* 10.3, pp. 155–159. ISSN: 1471-0056.
Mercer, Tim R and John S Mattick (2013). Structure and function of long noncoding RNAs in epigenetic regulation. In: *Nature structural & molecular biology* 20.3, pp. 300–307. ISSN: 1545-9993.
Mercer, Tim R et al. (2011). Expression of distinct RNAs from 3 untranslated regions. In: *Nucleic acids research* 39.6, pp. 2393–2403.

Meryet-Figuière, Matthieu et al. (2016). An overview of long non-coding RNAs in ovarian cancers. In: *Oncotarget* 7.28, p. 44719.

Meyer, David et al. (2015). *e1071: Misc Functions of the Department of Statistics, Probability Theory Group (Formerly: E1071), TU Wien*.

Miles, Gregory D et al. (2012). Identifying microRNA/mRNA dysregulations in ovarian cancer. In: *BMC research notes* 5.1, p. 164.

Mimeault, Murielle and Surinder K Batra (2013). Hypoxia-inducing factors as master regulators of stemness properties and altered metabolism of cancer-and metastasis-initiating cells. In: *Journal of cellular and molecular medicine* 17.1, pp. 30–54.

Mitchell, Patrick S et al. (2008). Circulating microRNAs as stable blood-based markers for cancer detection. In: *Proceedings of the National Academy of Sciences* 105.30, pp. 10513–10518. ISSN: 0027-8424.

Mitsudomi, T et al. (1992). p53 gene mutations in non-small-cell lung cancer cell lines and their correlation with the presence of ras mutations and clinical features. In: *Oncogene* 7.1, pp. 171–180.

Mohell, N et al. (2015). APR-246 overcomes resistance to cisplatin and doxorubicin in ovarian cancer cells. In: *Cell death & disease* 6.6, e1794.

Moorman, P.G. et al. (2013). Oral contraceptives and risk of ovarian cancer and breast cancer among high-risk women: A systematic review and meta-analysis. In: *Journal of Clinical Oncology* 31.33, pp. 4188–4198.

Morice, Philippe et al. (2003). Results of interval debulking surgery compared with primary debulking surgery in advanced stage ovarian cancer. In: *Journal of the American College of Surgeons* 197.6, pp. 955–963.

Morton, Jennifer P et al. (2010). Mutant p53 drives metastasis and overcomes growth arrest/senescence in pancreatic cancer. In: *Proceedings of the National Academy of Sciences* 107.1, pp. 246–251.

Moskwa, Patryk et al. (2011). miR-182-mediated downregulation of BRCA1 impacts DNA repair and sensitivity to PARP inhibitors. In: *Molecular cell* 41.2, pp. 210–220.

Motoyama, T (1982). Quantitative analysis on in vitro drug sensitivity of cultured human ovarian cancer cell lines (author's transl). In: *Nihon Sanka Fujinka Gakkai Zasshi* 34.3, pp. 308–314.

Mould, Tim (2012). An overview of current diagnosis and treatment in ovarian cancer. In: *International Journal of Gynecological Cancer* 22, S2–S4.

Muller, Patricia AJ and Karen H Vousden (2013). p53 mutations in cancer. In: *Nature cell biology* 15.1, pp. 2–8.

— (2014). Mutant p53 in cancer: new functions and therapeutic opportunities. In: *Cancer cell* 25.3, pp. 304–317.

Muller, Patricia AJ, Karen H Vousden, and Jim C Norman (2011). p53 and its mutants in tumor cell migration and invasion. In: *The Journal of cell biology* 192.2, pp. 209–218.

NCCN (2017). *National Comprehensive Cancer Network (NCCN) Guidelines: Epithelial Ovarian Cancer (including Fallopian Tube Cancer and Primary Peritoneal Cancer) Version 1.2017*.

NCT01461850 (2013). URL: `https://clinicaltrials.gov/ct2/show/NCT01461850?term=NCT01461850&rank=1`.

NCT02098343 (2014). *p53 Suppressor Activation in Recurrent High Grade Serous Ovarian Cancer, a Phase Ib/II Study of Systemic Carboplatin Combination Chemotherapy With or Without APR-246*. URL: https://clinicaltrials.gov/ct2/show/NCT02098343?term=APR-246+ovarian+cancer&rank=1.

Ng, Enders KO et al. (2009). Differential expression of microRNAs in plasma of colorectal cancer patients: a potential marker for colorectal cancer screening. In: *Gut*.

Nguyen, Han Christine Ngoc et al. (2013). Expression differences of circulating microRNAs in metastatic castration resistant prostate cancer and low-risk, localized prostate cancer. In: *The Prostate* 73.4, pp. 346–354.

Nick, Alpa M et al. (2015). A framework for a personalized surgical approach to ovarian cancer. In: *Nature reviews Clinical oncology* 12.4, pp. 239–245. ISSN: 1759-4774.

Noe, Dennis A, Victor Weedn, and William R Bell (1984). Direct spectrophotometry of serum hemoglobin: an Allen correction compared with a three-wavelength polychromatic analysis. In: *Clinical chemistry* 30.5, pp. 627–630. ISSN: 0009-9147.

Norquist, Barbara M et al. (2010). The molecular pathogenesis of hereditary ovarian carcinoma. In: *Cancer* 116.22, pp. 5261–5271.

Ocana, A et al. (2012). How valid are claims for synergy in published clinical studies? In: *Annals of oncology* 23.8, pp. 2161–2166.

Okazaki, Yea et al. (2002). Analysis of the mouse transcriptome based on functional annotation of 60,770 full-length cDNAs. In: *Nature* 420.6915, pp. 563–573.

Olive, Kenneth P et al. (2004). Mutant p53 gain of function in two mouse models of Li-Fraumeni syndrome. In: *Cell* 119.6, pp. 847–860.

Ono, S. et al. (2015). A direct plasma assay of circulating microRNA-210 of hypoxia can identify early systemic metastasis recurrence in melanoma patients. In: *Oncotarget* 6.9, pp. 7053–7064.

Oren, Moshe and Varda Rotter (2010). Mutant p53 gain-of-function in cancer. In: *Cold Spring Harbor perspectives in biology* 2.2, a001107.

Ozes, Ali R. et al. (2013). *The transcriptional regulation of the long non-coding RNA HOTAIR in ovarian cancer.* Conference Paper.

Pan, J. et al. (2016). Long non-coding RNA UCA1 promotes cisplatin/gemcitabine resistance through CREB modulating miR-196a-5p in bladder cancer cells. In: *Cancer Letters* 382.1, pp. 64–76.

Pang, Er-Jun et al. (2015). Overexpression of long non-coding RNA MALAT1 is correlated with clinical progression and unfavorable prognosis in pancreatic cancer. In: *Tumor Biology* 36.4, pp. 2403–2407.

Parmar, MKea et al. (2003). Paclitaxel plus platinum-based chemotherapy versus conventional platinum-based chemotherapy in women with relapsed ovarian cancer: the ICON4/AGO-OVAR-2.2 trial. In: *The Lancet* 361.9375, p. 2099.

Patil, Veena S, Rui Zhou, and Tariq M Rana (2014). Gene regulation by non-coding RNAs. In: *Critical reviews in biochemistry and molecular biology* 49.1, pp. 16–32.

Pauler, D.K. et al. (2001). Factors influencing serum ca125ii levels in healthy postmenopausal women. In: *Cancer Epidemiology Biomarkers and Prevention* 10.5, pp. 489–493.

Pelicano, Helene, Dennis Carney, and Peng Huang (2004). ROS stress in cancer cells and therapeutic implications. In: *Drug Resistance Updates* 7.2, pp. 97–110.

Peng, X. et al. (2013). APR-246/PRIMA-1MET inhibits thioredoxin reductase 1 and converts the enzyme to a dedicated NADPH oxidase. In: *Cell Death and Disease* 4.10.

Penna, Elisa, Francesca Orso, and Daniela Taverna (2015). miR-214 as a key hub that controls cancer networks: small player, multiple functions. In: *Journal of Investigative Dermatology* 135.4, pp. 960–969.

Perets, Ruth et al. (2013). Transformation of the fallopian tube secretory epithelium leads to high-grade serous ovarian cancer in Brca; Tp53; Pten models. In: *Cancer cell* 24.6, pp. 751–765.

Pfisterer, Jacobus et al. (2006). Gemcitabine plus carboplatin compared with carboplatin in patients with platinum-sensitive recurrent ovarian cancer: an intergroup trial of the AGO-OVAR, the NCIC CTG, and the EORTC GCG. In: *Journal of Clinical Oncology* 24.29, pp. 4699–4707.

Phizicky, Eric M and Anita K Hopper (2010). tRNA biology charges to the front. In: *Genes & development* 24.17, pp. 1832–1860.

Piek, Jurgen MJ et al. (2001). Dysplastic changes in prophylactically removed Fallopian tubes of women predisposed to developing ovarian cancer. In: *The Journal of pathology* 195.4, pp. 451–456.

Piek, Jurgen MJ et al. (2003). BRCA1/2-related ovarian cancers are of tubal origin: a hypothesis. In: *Gynecologic oncology* 90.2, p. 491.

Pignata, S. et al. (2011). Follow-up with CA125 after primary therapy of advanced ovarian cancer: In favor of continuing to prescribe CA125 during follow-up. In: *Annals of Oncology* 22.SUPPL.8, pp. 40–44.

Poliseno, Laura, Adele Haimovic, Paul J Christos, et al. (2011). Deletion of PTENP1 pseudogene in human melanoma. In: *The Journal of investigative dermatology* 131.12, p. 2497.

Poliseno, Laura et al. (2010). A coding-independent function of gene and pseudogene mRNAs regulates tumour biology. In: *Nature* 465.7301, pp. 1033–1038.

Ponjavic, Jasmina, Chris P Ponting, and Gerton Lunter (2007). Functionality or transcriptional noise? Evidence for selection within long noncoding RNAs. In: *Genome research* 17.5, pp. 556–565.

Poveda, Andres M et al. (2015). Bevacizumab combined with weekly paclitaxel, pegylated liposomal doxorubicin, or topotecan in platinum-resistant recurrent ovarian cancer: analysis by chemotherapy cohort of the randomized phase III AURELIA trial. In: *Journal of Clinical Oncology* 33.32, pp. 3836–3838.

Pramanik, Dipankar et al. (2011). Restitution of tumor suppressor microRNAs using a systemic nanovector inhibits pancreatic cancer growth in mice. In: *Molecular cancer therapeutics* 10.8, pp. 1470–1480.

Prensner, John R et al. (2013). The long noncoding RNA SChLAP1 promotes aggressive prostate cancer and antagonizes the SWI/SNF complex. In: *Nature genetics* 45.11, pp. 1392–1398.

Pritchard, Colin C et al. (2012). Blood cell origin of circulating microRNAs: a cautionary note for cancer biomarker studies. In: *Cancer prevention research* 5.3, pp. 492–497. ISSN: 1940-6207.

Probst, Aline V et al. (2010). A strand-specific burst in transcription of pericentric satellites is required for chromocenter formation and early mouse development. In: *Developmental cell* 19.4, pp. 625–638.

Pujade-Lauraine, Eric et al. (2010). Pegylated liposomal doxorubicin and carboplatin compared with paclitaxel and carboplatin for patients with platinum-sensitive ovarian cancer in late relapse. In: *Journal of Clinical Oncology* 28.20, pp. 3323–3329.

Pujade-Lauraine, Eric et al. (2014). Bevacizumab combined with chemotherapy for platinum-resistant recurrent ovarian cancer: the AURELIA open-label randomized phase III trial. In: *Journal of clinical oncology* 32.13, pp. 1302–1308.

Qin, B., H. Yang, and B. Xiao (2012). Role of microRNAs in endothelial inflammation and senescence. In: *Molecular Biology Reports* 39.4, pp. 4509–4518.

Qiu, Jun-jun et al. (2014). Overexpression of long non-coding RNA HOTAIR predicts poor patient prognosis and promotes tumor metastasis in epithelial ovarian cancer. In: *Gynecologic oncology* 134.1, pp. 121–128.

Qiu, Jun-Jun et al. (2015a). Long non-coding RNA ANRIL predicts poor prognosis and promotes invasion/metastasis in serous ovarian cancer. In: *International journal of oncology* 46.6, pp. 2497–2505.

Qiu, Jun-jun et al. (2015b). The long non-coding RNA HOTAIR promotes the proliferation of serous ovarian cancer cells through the regulation of cell cycle arrest and apoptosis. In: *Experimental cell research* 333.2, pp. 238–248.

Qiu, Zhihua and Yimin Dai (2014). Roadmap of miR-122-related clinical application from bench to bedside. In: *Expert opinion on investigational drugs* 23.3, pp. 347–355.

R Core Team (2016). *R: A Language and Environment for Statistical Computing*. R Foundation for Statistical Computing. Vienna, Austria.

Rabik, Cara A and M Eileen Dolan (2007). Molecular mechanisms of resistance and toxicity associated with platinating agents. In: *Cancer treatment reviews* 33.1, pp. 9–23.

Rai, A.J. et al. (2002). Proteomic approaches to tumor marker discovery: Identification of biomarkers for ovarian cancer. In: *Archives of Pathology and Laboratory Medicine* 126.12, pp. 1518–1526.

Raja, FA, N Chopra, and JA Ledermann (2012). Optimal first-line treatment in ovarian cancer. In: *Annals of Oncology* 23.suppl 10, pp. x118–x127.

Ramey, John A. (2016). *sparsediscrim: Sparse and Regularized Discriminant Analysis*.

Rebbeck, Timothy R, Margaret Spitz, and Xifeng Wu (2004). Assessing the function of genetic variants in candidate gene association studies. In: *Nature Reviews Genetics* 5.8, pp. 589–597.

Resnick, Kimberly E et al. (2009). The detection of differentially expressed microRNAs from the serum of ovarian cancer patients using a novel real-time PCR platform. In: *Gynecologic oncology* 112.1, pp. 55–59.

Richards, Edward J et al. (2015). A functional variant in HOXA11-AS, a novel long non-coding RNA, inhibits the oncogenic phenotype of epithelial ovarian cancer. In: *Oncotarget* 6.33, p. 34745.

Rinn, John L et al. (2007). Functional demarcation of active and silent chromatin domains in human HOX loci by noncoding RNAs. In: *Cell* 129.7, pp. 1311–1323.
Ritchie, Matthew E et al. (2015). limma powers differential expression analyses for RNA-sequencing and microarray studies. In: *Nucleic acids research*, gkv007.
Ritz, C. et al. (2015). Dose-Response Analysis Using R. In: *PLOS ONE* 10.e0146021 (12).
Rkaeus, N. et al. (2010). PRIMA-1 MET /APR-246 targets mutant forms of p53 family members p63 and p73. In: *Oncogene* 29.49, pp. 6442–6451.
Robin, Xavier et al. (2011). pROC: an open-source package for R and S+ to analyze and compare ROC curves. In: *BMC bioinformatics* 12.1, p. 1. ISSN: 1471-2105.
Robinson, Mark D, Davis J McCarthy, and Gordon K Smyth (2010). edgeR: a Bioconductor package for differential expression analysis of digital gene expression data. In: *Bioinformatics* 26.1, pp. 139–140.
Rodriguez, Antony et al. (2004). Identification of mammalian microRNA host genes and transcription units. In: *Genome research* 14.10a, pp. 1902–1910.
Rodriguez, Olga Catalina et al. (2012). Dietary downregulation of mutant p53 levels via glucose restriction: mechanisms and implications for tumor therapy. In: *Cell cycle* 11.23, pp. 4436–4446.
Rokavec, M. et al. (2014). The p53/miR-34 axis in development and disease. In: *Journal of Molecular Cell Biology* 6.3, pp. 214–230.
Romanidis, Konstantinos et al. (2014). The role of cytoreductive surgery in advanced ovarian cancer: the general surgeon's perspective. In: *Management* 7.9, p. 12.
ROMA®, LabCorp (2011). *Ovarian Malignancy Risk (ROMA®) Test #140045*.
Romero, Ignacio and Robert Bast (2012). Minireview: human ovarian cancer: biology, current management, and paths to personalizing therapy. In: *Endocrinology* 153.4, pp. 1593–1602.
Rong, Dawei et al. (2017). Novel insights into circular RNAs in clinical application of carcinomas. In: *OncoTargets and therapy* 10, p. 2183.
Rossi, Angela Cristina et al. (2004). A retrospective study of preoperative CA 125 levels in 82 patients with ovarian cancer. In: *Archives of gynecology and obstetrics* 269.4, pp. 263–265.
Rottiers, V. and A. M. Näär (2012). MicroRNAs in metabolism and metabolic disorders. In: *Nature Reviews Molecular Cell Biology* 13.4, pp. 239–251.
Ruiz-Orera, Jorge et al. (2014). Long non-coding RNAs as a source of new peptides. In: *Elife* 3, e03523.
Rupaimoole, Rajesha and Frank J Slack (2017). MicroRNA therapeutics: towards a new era for the management of cancer and other diseases. In: *Nature Reviews Drug Discovery* 16.3, pp. 203–222.
Rustin, Gordon JS et al. (2004). Use of CA-125 in clinical trial evaluation of new therapeutic drugs for ovarian cancer. In: *Clinical cancer research* 10.11, pp. 3919–3926.
Rustin, Gordon JS et al. (2010). Early versus delayed treatment of relapsed ovarian cancer (MRC OV05/EORTC 55955): a randomised trial. In: *The Lancet* 376.9747, pp. 1155–1163.
Saha, M. N. et al. (2013). PRIMA-1Met/APR-246 displays high antitumor activity in multiple myeloma by induction of p73 and noxa. In: *Molecular Cancer Therapeutics* 12.11, pp. 2331–2341.

Sahu, D. et al. (2016). Co-expression analysis identifies long noncoding RNA SNHG1 as a novel predictor for event-free survival in neuroblastoma. In: *Oncotarget* 7.36, pp. 58022–58037.

Salmena, Leonardo et al. (2011). A *ceRNA* Hypothesis: The Rosetta Stone of a Hidden RNA Language? In: *Cell* 146.3, pp. 353–358.

Sampson, Valerie B et al. (2007). MicroRNA let-7a down-regulates MYC and reverts MYC-induced growth in Burkitt lymphoma cells. In: *Cancer research* 67.20, pp. 9762–9770.

Samuel, Priya et al. (2016). miRNAs and ovarian cancer: a miRiad of mechanisms to induce cisplatin drug resistance. In: *Expert review of anticancer therapy* 16.1, pp. 57–70.

Sánchez, Yolanda et al. (2014). Genome-wide analysis of the human p53 transcriptional network unveils a lncRNA tumour suppressor signature. In: *Nature communications* 5.

Sand, Michael et al. (2016). Circular RNA expression in cutaneous squamous cell carcinoma. In: *Journal of dermatological science* 83.3, pp. 210–218.

Schickel, R et al. (2008). MicroRNAs: key players in the immune system, differentiation, tumorigenesis and cell death. In: *Oncogene* 27.45, pp. 5959–5974. ISSN: 0950-9232.

Schmid, Gabriel et al. (2016). Expression and promotor hypermethylation of miR-34a in the various histological subtypes of ovarian cancer. In: *BMC cancer* 16.1, p. 102.

Schmidt, Lars Henning et al. (2011). The long noncoding MALAT-1 RNA indicates a poor prognosis in non-small cell lung cancer and induces migration and tumor growth. In: *Journal of thoracic oncology* 6.12, pp. 1984–1992.

Schmidt, L.H. et al. (2014). Prognostic impact of Bcl-2 depends on tumor histology and expression of MALAT-1 lncRNA in non-small-cell lung cancer. In: *Journal of Thoracic Oncology* 9.9, pp. 1294–1304.

Schmitt, Adam M et al. (2016). An inducible long noncoding RNA amplifies DNA damage signaling. In: *Nature Genetics*.

Schwartz, Peter E et al. (1999). Neoadjuvant chemotherapy for advanced ovarian cancer: long-term survival. In: *Gynecologic oncology* 72.1, pp. 93–99.

Seila, Amy C et al. (2008). Divergent transcription from active promoters. In: *science* 322.5909, pp. 1849–1851.

Selth, LA et al. (2013). Circulating microRNAs predict biochemical recurrence in prostate cancer patients. In: *British journal of cancer* 109.3, pp. 641–650.

Selth, Luke A et al. (2012). Discovery of circulating microRNAs associated with human prostate cancer using a mouse model of disease. In: *International Journal of Cancer* 131.3, pp. 652–661. ISSN: 1097-0215.

Shah, Jaynish S, Patsy S Soon, and Deborah J Marsh (2016). Comparison of Methodologies to Detect Low Levels of Hemolysis in Serum for Accurate Assessment of Serum microRNAs. In: *PloS one* 11.4, e0153200. ISSN: 1932-6203.

Shapira, I. et al. (2014). Circulating biomarkers for detection of ovarian cancer and predicting cancer outcomes. In: *British Journal of Cancer* 110.4, pp. 976–983.

Sharma, Vivek et al. (2015). A BRCA1-interacting lncRNA regulates homologous recombination. In: *EMBO reports*, e201540437.

Shen, Jie et al. (2008). A functional polymorphism in the miR-146a gene and age of familial breast/ovarian cancer diagnosis. In: *Carcinogenesis* 29.10, pp. 1963–1966.

Shen, Jinfeng et al. (2013). APR-246/PRIMA-1MET rescues epidermal differentiation in skin keratinocytes derived from EEC syndrome patients with p63 mutations. In: *Proceedings of the National Academy of Sciences* 110.6, pp. 2157–2162.

Shen, Jing et al. (2012). Dysregulation of circulating microRNAs and prediction of aggressive prostate cancer. In: *The Prostate* 72.13, pp. 1469–1477.

Shen, Liqin et al. (2015). Long noncoding RNA MALAT1 promotes brain metastasis by inducing epithelial-mesenchymal transition in lung cancer. In: *Journal of neuro-oncology* 121.1, pp. 101–108.

Shen, Y. and L. Li (2016). Serum HE4 superior to CA125 in predicting poorer surgical outcome of epithelial ovarian cancer. In: *Tumor Biology* 37.11, pp. 14765–14772.

Sheng, Xiujie et al. (2014). Promoter hypermethylation influences the suppressive role of maternally expressed 3, a long non-coding RNA, in the development of epithelial ovarian cancer. In: *Oncology reports* 32.1, pp. 277–285.

Sherman-Baust, Cheryl A et al. (2014). A genetically engineered ovarian cancer mouse model based on fallopian tube transformation mimics human high-grade serous carcinoma development. In: *The Journal of pathology* 233.3, pp. 228–237.

Shih, Ie-Ming and Robert J Kurman (2004). Ovarian tumorigenesis: a proposed model based on morphological and molecular genetic analysis. In: *The American journal of pathology* 164.5, pp. 1511–1518.

Sibthorpe, Clare (2017). Advanced ovarian cancer treatment placed on the PBS, a move praised by doctors and patients. In: *Canberra Times*. URL: http://www.canberratimes.com.au/act-news/advanced-ovarian-cancer-treatment-placed-on-the-pbs-a-move-praised-by-doctors-and-patients-20170131-gu26us.html.

Silva, Jessica M et al. (2011). LSINCT5 is over expressed in breast and ovarian cancer and affects cellular proliferation. In: *RNA biology* 8.3, pp. 496–505.

Sim, S. and S.L. Wolin (2011). Emerging roles for the Ro 60-kDa autoantigen in noncoding RNA metabolism. In: *Wiley Interdisciplinary Reviews: RNA* 2.5, pp. 686–699.

Singh, Anurag and Jeffrey Settleman (2010). EMT, cancer stem cells and drug resistance: an emerging axis of evil in the war on cancer. In: *Oncogene* 29.34, pp. 4741–4751.

Singh, Siddharth and Preet Paul Singh (2013). Statin a day keeps cancer at bay. In: *World J Clin Oncol* 4.2, pp. 43–46.

Skates, Steven J, Donna K Pauler, and Ian J Jacobs (2001). Screening based on the risk of cancer calculation from Bayesian hierarchical changepoint and mixture models of longitudinal markers. In: *Journal of the American Statistical Association* 96.454, pp. 429–439.

Skates, Steven J et al. (1995). Toward an optimal algorithm for ovarian cancer screening with longitudinal tumor markers. In: *Cancer* 76.S10, pp. 2004–2010.

Smyth, Gordon K (2004). Linear models and empirical Bayes methods for assessing differential expression in microarray experiment. In: *Statistical Applications in Genetics and Molecular Biology* 3.1.

Sobhani, Mona et al. (2015). PRIMA-1Met induces apoptosis in Waldenström's Macroglobulinemia cells independent of p53. In: *Cancer biology & therapy* 16.5, pp. 799–806.

Soerjomataram, I. et al. (2012). Global burden of cancer in 2008: A systematic analysis of disability-adjusted life-years in 12 world regions. In: *The Lancet* 380.9856, pp. 1840–1850.

Sosa, Venus et al. (2013). Oxidative stress and cancer: an overview. In: *Ageing research reviews* 12.1, pp. 376–390.

Spizzo, R. et al. (2012). Long non-coding RNAs and cancer: a new frontier of translational research[quest]. In: *Oncogene* 31.43, pp. 4577–4587. ISSN: 0950-9232.

Stefani, Giovanni and Frank J Slack (2008). Small non-coding RNAs in animal development. In: *Nature reviews Molecular cell biology* 9.3, pp. 219–230.

Stepanov, Grigory A et al. (2015). Regulatory role of small nucleolar RNAs in human diseases. In: *BioMed research international* 2015.

Strano, S. et al. (2007a). Mutant p53: An oncogenic transcription factor. In: *Oncogene* 26.15, pp. 2212–2219.

Strano, S. et al. (2007b). Mutant p53 proteins: Between loss and gain of function. In: *Head and Neck* 29.5, pp. 488–496.

Strbenac, Dario et al. (2015). ClassifyR: an R package for performance assessment of classification with applications to transcriptomics. In: *Bioinformatics* 31.11, pp. 1851–1853.

Stults, Dawn M et al. (2008). Genomic architecture and inheritance of human ribosomal RNA gene clusters. In: *Genome research* 18.1, pp. 13–18.

Su, D.-N. et al. (2016). HOTAIR, a long non-coding RNA driver of malignancy whose expression is activated by FOXC1, negatively regulates miRNA-1 in hepatocellular carcinoma. In: *Oncology Letters* 12.5. cited By 1, pp. 4061–4067.

Subramanian, Aravind et al. (2005). Gene set enrichment analysis: a knowledge-based approach for interpreting genome-wide expression profiles. In: *Proceedings of the National Academy of Sciences* 102.43, pp. 15545–15550.

Swarbrick, Alexander et al. (2010). miR-380-5p represses p53 to control cellular survival and is associated with poor outcome in MYCN-amplified neuroblastoma. In: *Nat Med* 16.10, pp. 1134–1140. ISSN: 1078-8956.

Symonds, Matthew RE and Adnan Moussalli (2011). A brief guide to model selection, multimodel inference and model averaging in behavioural ecology using Akaike's information criterion. In: *Behavioral Ecology and Sociobiology* 65.1, pp. 13–21.

Synnott, NC et al. (2017). Mutant p53: a novel target for the treatment of patients with triple-negative breast cancer? In: *International Journal of Cancer* 140.1, pp. 234–246.

Taft, Ryan J et al. (2009). Tiny RNAs associated with transcription start sites in animals. In: *Nature genetics* 41.5, pp. 572–578.

Taft, Ryan J et al. (2010). Nuclear-localized tiny RNAs are associated with transcription initiation and splice sites in metazoans. In: *Nature structural & molecular biology* 17.8, pp. 1030–1034.

Tallarida, Ronald J (2001). Drug synergism: its detection and applications. In: *Journal of Pharmacology and Experimental Therapeutics* 298.3, pp. 865–872.

— (2006). An overview of drug combination analysis with isobolograms. In: *Journal of Pharmacology and Experimental Therapeutics* 319.1, pp. 1–7.

Tang, Z. et al. (2015). Usefulness of human epididymis protein 4 in predicting cytoreductive surgical outcomes for advanced ovarian tubal and peritoneal carcinoma. In: *Chinese Journal of Cancer Research* 27.3, pp. 309–317.

Tanos, Vasilios et al. (1999). Expression of the imprinted H19 oncofetal RNA in epithelial ovarian cancer. In: *European Journal of Obstetrics & Gynecology and Reproductive Biology* 85.1, pp. 7–11.

Taylor, Douglas D and Cicek Gercel-Taylor (2008). MicroRNA signatures of tumor-derived exosomes as diagnostic biomarkers of ovarian cancer. In: *Gynecologic oncology* 110.1, pp. 13–21.

Teschendorff, Andrew E et al. (2015). HOTAIR and its surrogate DNA methylation signature indicate carboplatin resistance in ovarian cancer. In: *Genome medicine* 7.1, p. 108.

Tessoulin, B. et al. (2014). PRIMA-1^{Met} induces myeloma cell death independent of p53 by impairing the GSH/ROS balance. In: *Blood* 124.10, pp. 1626–1636.

Thukral, Sushil K et al. (1995). Discrimination of DNA binding sites by mutant p53 proteins. In: *Molecular and cellular biology* 15.9, pp. 5196–5202.

Tothill, Richard W et al. (2008). Novel molecular subtypes of serous and endometrioid ovarian cancer linked to clinical outcome. In: *Clinical cancer research* 14.16, pp. 5198–5208.

Trimbos, J Baptist et al. (2003). Impact of adjuvant chemotherapy and surgical staging in early-stage ovarian carcinoma: European Organisation for Research and Treatment of Cancer–Adjuvant ChemoTherapy In Ovarian Neoplasm trial. In: *Journal of the National Cancer Institute* 95.2, pp. 113–125.

Tripathi, Vidisha et al. (2010). The nuclear-retained noncoding RNA MALAT1 regulates alternative splicing by modulating SR splicing factor phosphorylation. In: *Molecular cell* 39.6, pp. 925–938.

Tsai, Miao-Chih et al. (2010). Long noncoding RNA as modular scaffold of histone modification complexes. In: *Science* 329.5992, pp. 689–693.

Tsujiura, M et al. (2010). Circulating microRNAs in plasma of patients with gastric cancers. In: *British journal of cancer* 102.7, pp. 1174–1179.

Tucker, Susan L et al. (2014). Molecular biomarkers of residual disease after surgical debulking of high-grade serous ovarian cancer. In: *Clinical Cancer Research* 20.12, pp. 3280–3288.

Turchinovich, Andrey et al. (2011). Characterization of extracellular circulating microRNA. In: *Nucleic acids research*, gkr254. ISSN: 0305-1048.

Ueland, Frederick R et al. (2011). Effectiveness of a multivariate index assay in the preoperative assessment of ovarian tumors. In: *Obstetrics & Gynecology* 117.6, pp. 1289–1297.

Ulitsky, Igor and David P Bartel (2013). lincRNAs: genomics, evolution, and mechanisms. In: *Cell* 154.1, pp. 26–46.

Valadkhan, Saba (2005). snRNAs as the catalysts of pre-mRNA splicing. In: *Current opinion in chemical biology* 9.6, pp. 603–608.

Vance, Keith W et al. (2014). The long non-coding RNA Paupar regulates the expression of both local and distal genes. In: *The EMBO journal*, e201386225.

Vaughan, Sebastian et al. (2011). Rethinking ovarian cancer: recommendations for improving outcomes. In: *Nature Reviews Cancer* 11.10, pp. 719–725.

Venables, W. N. and B. D. Ripley (2002). *Modern Applied Statistics with S*. Fourth. New York, United States of America: Springer. ISBN: 0-387-95457-0.

Vergote, Ignace et al. (2010). Neoadjuvant chemotherapy or primary surgery in stage IIIC or IV ovarian cancer. In: *New England Journal of Medicine* 363.10, pp. 943–953.

Verhagen, A.P.M. and G.J.M. Pruijn (2011). Are the Ro RNP-associated Y RNAs concealing microRNAs? Y RNA-derived miRNAs may be involved in autoimmunity. In: *BioEssays* 33.9, pp. 674–682.

Verheijen, RHM et al. (1999). CA 125: fundamental and clinical aspects. In: *Seminars in cancer biology* 9.2, pp. 117–124.

Verheijen, R.H.M. et al. (2012). Cancer antigen 125: Lost to follow-up? A European Society of Gynaecological Oncology consensus statement. In: *International Journal of Gynecological Cancer* 22.1, pp. 170–174.

Vermillion (2009). *OVA1 Test*.

Volinia, Stefano et al. (2012). Breast cancer signatures for invasiveness and prognosis defined by deep sequencing of microRNA. In: *Proceedings of the National Academy of Sciences* 109.8, pp. 3024–3029.

Vorgias, George et al. (2009). Can the preoperative Ca-125 level predict optimal cytoreduction in patients with advanced ovarian carcinoma? A single institution cohort study. In: *Gynecologic oncology* 112.1, pp. 11–15.

Vousden, Karen H and David P Lane (2007). p53 in health and disease. In: *Nature reviews Molecular cell biology* 8.4, pp. 275–283.

Vousden, Karen H and Carol Prives (2009). Blinded by the light: the growing complexity of p53. In: *Cell* 137.3, pp. 413–431.

Wach, S. et al. (2015). The combined serum levels of miR-375 and urokinase plasminogen activator receptor are suggested as diagnostic and prognostic biomarkers in prostate cancer. In: *International Journal of Cancer* 137.6, pp. 1406–1416.

Wale, Nikil (2011). Machine learning in drug discovery and development. In: *Drug Development Research* 72.1, pp. 112–119. ISSN: 1098-2299.

Walerych, Dawid, Kamil Lisek, and Giannino Del Sal (2015). Mutant p53: one, no one, and one hundred thousand. In: *Frontiers in oncology* 5, p. 289.

Wang, F. et al. (2015). Involvement of SRPK1 in cisplatin resistance related to long noncoding RNA UCA1 in human ovarian cancer cells. In: *Neoplasma* 62.3, pp. 432–438.

Wang, Fan et al. (2008). UCA1, a non-protein-coding RNA up-regulated in bladder carcinoma and embryo, influencing cell growth and promoting invasion. In: *FEBS letters* 582.13, pp. 1919–1927. ISSN: 0014-5793.

Wang, J. et al. (2014). Tumor-Associated circulating micrornas as biomarkers of cancer. In: *Molecules* 19.2, pp. 1912–1938.

Wang, J. et al. (2016a). Knockdown of long noncoding RNA urothelial cancer-associated 1 enhances cisplatin chemosensitivity in tongue squamous cell carcinoma cells. In: *Pharmazie* 71.10, pp. 598–602.

Wang, Jiayi et al. (2010). CREB up-regulates long non-coding RNA, HULC expression through interaction with microRNA-372 in liver cancer. In: *Nucleic acids research* 38.16, pp. 5366–5383.

Wang, W. et al. (2016b). Circulating miR-210 as a diagnostic and prognostic biomarker for colorectal cancer. In: *European Journal of Cancer Care*.

Wang, Xiao-Song et al. (2006). Rapid identification of UCA1 as a very sensitive and specific unique marker for human bladder carcinoma. In: *Clinical cancer research* 12.16, pp. 4851–4858.

Wang, Y. et al. (2012). Long non-coding RNA UCA1a(CUDR) promotes proliferation and tumorigenesis of bladder cancer. In: *International Journal of Oncology* 41.1, pp. 276–284.

Weber, Jessica A. et al. (2010). The MicroRNA Spectrum in 12 Body Fluids. In: *Clinical Chemistry* 56.11, pp. 1733–1741. ISSN: 0009-9147.

Wei, Jun Stephen et al. (2008). The MYCN oncogene is a direct target of miR-34a. In: *Oncogene* 27.39, pp. 5204–5213.

Wei, Yao and Ben Niu (2015). Role of MALAT1 as a prognostic factor for survival in various cancers: a systematic review of the literature with meta-analysis. In: *Disease markers* 2015.

Weinberg, Richard L et al. (2004). Regulation of DNA binding of p53 by its C-terminal domain. In: *Journal of molecular biology* 342.3, pp. 801–811.

Weisz, L., M. Oren, and V. Rotter (2007). Transcription regulation by mutant p53. In: *Oncogene* 26.15, pp. 2202–2211.

Welch, C, Y Chen, and RL Stallings (2007). MicroRNA-34a functions as a potential tumor suppressor by inducing apoptosis in neuroblastoma cells. In: *Oncogene* 26.34, pp. 5017–5022.

Wentzensen, N. et al. (2016). Ovarian cancer risk factors by histologic subtype: An analysis from the Ovarian Cancer Cohort Consortium. In: *Journal of Clinical Oncology* 34.24, pp. 2888–2898.

Wiegand, Kimberly C et al. (2010). ARID1A mutations in endometriosis-associated ovarian carcinomas. In: *New England Journal of Medicine* 363.16, pp. 1532–1543.

Wiggins, Jason F et al. (2010). Development of a lung cancer therapeutic based on the tumor suppressor microRNA-34. In: *Cancer research* 70.14, pp. 5923–5930.

Williams, Gwyn T and Farzin Farzaneh (2012). Are snoRNAs and snoRNA host genes new players in cancer? In: *Nature reviews cancer* 12.2, pp. 84–88.

Winter, Julia et al. (2009). Many roads to maturity: microRNA biogenesis pathways and their regulation. In: *Nature cell biology* 11.3, pp. 228–234.

Winter, William E et al. (2008). Tumor residual after surgical cytoreduction in prediction of clinical outcome in stage IV epithelial ovarian cancer: a Gynecologic Oncology Group Study. In: *Journal of Clinical Oncology* 26.1, pp. 83–89.

Witwer, Kenneth W (2015). Circulating MicroRNA biomarker studies: pitfalls and potential solutions. In: *Clinical chemistry* 61.1, pp. 56–63. ISSN: 0009-9147.

Wu, L. et al. (2012). Diagnostic value of serum human epididymis protein 4 (HE4) in ovarian carcinoma: A systematic review and meta-analysis. In: *International Journal of Gynecological Cancer* 22.7, pp. 1106–1112.

Wu, Rong et al. (2013a). Type I to type II ovarian carcinoma progression: mutant Trp53 or Pik3ca confers a more aggressive tumor phenotype in a mouse model of ovarian cancer. In: *The American journal of pathology* 182.4, pp. 1391–1399.

Wu, W. et al. (2013b). Ets-2 Regulates Cell Apoptosis via the Akt Pathway, through the Regulation of Urothelial Cancer Associated 1, a Long Non-Coding RNA, in Bladder Cancer Cells. In: *PLoS ONE* 8.9.

Xian, Wa et al. (2010). The Li–Fraumeni syndrome (LFS): a model for the initiation of p53 signatures in the distal fallopian tube. In: *The Journal of pathology* 220.1, pp. 17–23.

Xiang, Jie and Ji Wu (2010). Feud or friend? The role of the miR-17-92 cluster in tumorigenesis. In: *Current genomics* 11.2, pp. 129–135.

Xu, F. and J. Zhang (2017). Long non-coding RNA HOTAIR functions as miRNA sponge to promote the epithelial to mesenchymal transition in esophageal cancer. In: *Biomedicine and Pharmacotherapy* 90. cited By 0, pp. 888–896.

Xu, Y.-Z. et al. (2013). Identification of serum microRNA-21 as a biomarker for early detection and prognosis in human epithelial ovarian cancer. In: *Asian Pacific Journal of Cancer Prevention* 14.2, pp. 1057–1060.

Xue, M., X. Li, and W. Chen (2013). Bioinformatics analysis and identification of transcriptional regulation of human UCA1 gene. In: *Nan fang yi ke da xue xue bao = Journal of Southern Medical University* 33.11, pp. 1596–1599.

Xue, Mei, Wei Chen, and Xu Li (2016). Urothelial cancer associated 1: a long noncoding RNA with a crucial role in cancer. In: *Journal of cancer research and clinical oncology* 142.7, pp. 1407–1419.

Yan, Wensheng et al. (2013). Histone deacetylase inhibitors suppress mutant p53 transcription via histone deacetylase 8. In: *Oncogene* 32.5, pp. 599–609.

Yang, C. et al. (2012). Long non-coding RNA UCA1 regulated cell cycle distribution via CREB through PI3-K dependent pathway in bladder carcinoma cells. In: *Gene* 496.1, pp. 8–16.

Yang, Liuqing et al. (2011). ncRNA-and Pc2 methylation-dependent gene relocation between nuclear structures mediates gene activation programs. In: *Cell* 147.4, pp. 773–788.

Yang, Z., T. Cappello, and L. Wang (2015). Emerging role of microRNAs in lipid metabolism. In: *Acta Pharmaceutica Sinica B* 5.2, pp. 145–150.

Yang, Z. et al. (2013). Diagnosis and preoperative predictive value of serum HE4 concentrations for optimal debulking in epithelial ovarian cancer. In: *Oncology Letters* 6.1, pp. 28–34.

Yi, Rui et al. (2003). Exportin-5 mediates the nuclear export of pre-microRNAs and short hairpin RNAs. In: *Genes & development* 17.24, pp. 3011–3016.

Yingxia, H. et al. (2015). Early diagnostic value of plasma miR-155, miR-196a, miR-21 and miR-210 in patients with pancreatic cancer. In: *Tumor* 35.10, pp. 1135–1143.

Yong, Fung Lin, Chee Wei Law, and Chee Woon Wang (2013). Potentiality of a triple microRNA classifier: miR-193a-3p, miR-23a and miR-338-5p for early detection of colorectal cancer. In: *BMC cancer* 13.1, p. 280.

Yoshikawa, N. et al. (2016). PRIMA-1MET induces apoptosis through accumulation of intracellular reactive oxygen species irrespective of p53 status and chemo-sensitivity in epithelial ovarian cancer cells. In: *Oncology Reports* 35.5, pp. 2543–2552.

You, J. et al. (2014). Noncoding RNA small nucleolar RNA host gene 1 promote cell proliferation in nonsmall cell lung cancer. In: *Indian Journal of Cancer* 51.7, e99–e102.

Yu, F. et al. (2017). HOTAIR Epigenetically Modulates PTEN Expression via MicroRNA-29b: A Novel Mechanism in Regulation of Liver Fibrosis. In: *Molecular Therapy* 25.1. cited By 0, pp. 205–217.

Yu, Gan et al. (2014a). Pseudogene PTENP1 functions as a competing endogenous RNA to suppress clear-cell renal cell carcinoma progression. In: *Molecular cancer therapeutics* 13.12, pp. 3086–3097.

Yu, H. et al. (2014b). Decreased circulating miR-375: A potential biomarker for patients with non-small-cell lung cancer. In: *Gene* 534.1, pp. 60–65.

Yu, Sung-Liang et al. (2008). MicroRNA signature predicts survival and relapse in lung cancer. In: *Cancer cell* 13.1, pp. 48–57.

Yu, Xin et al. (2012). Allele-specific p53 mutant reactivation. In: *Cancer cell* 21.5, pp. 614–625.

Zache, N. et al. (2008a). PRIMA-1MET inhibits growth of mouse tumors carrying mutant p53. In: *Cellular Oncology* 30.5, pp. 411–418.

Zache, Nicole et al. (2008b). Mutant p53 targeting by the low molecular weight compound STIMA-1. In: *Molecular oncology* 2.1, pp. 70–80.

Zandi, R. et al. (2011). PRIMA-1Met/APR-246 induces apoptosis and tumor growth delay in small cell lung cancer expressing mutant p53. In: *Clinical Cancer Research* 17.9, pp. 2830–2841.

Zanutto, Susanna et al. (2014). Circulating miR-378 in plasma: a reliable, haemolysis-independent biomarker for colorectal cancer. In: *British journal of cancer* 110.4, pp. 1001–1007.

Zapardiel, Ignacio et al. (2011). Diaphragmatic surgery during primary cytoreduction for advanced ovarian cancer: peritoneal stripping versus diaphragmatic resection. In: *International Journal of Gynecological Cancer* 21.9, pp. 1698–1703.

Záveský, L. et al. (2015). Evaluation of Cell-Free Urine microRNAs Expression for the Use in Diagnosis of Ovarian and Endometrial Cancers. A Pilot Study. In: *Pathology and Oncology Research* 21.4, pp. 1027–1035.

Zerdoumi, Yasmine et al. (2013). Drastic effect of germline TP53 missense mutations in Li–Fraumeni patients. In: *Human mutation* 34.3, pp. 453–461.

Zhang, A.T. et al. (2011a). Dynamic interaction of Y RNAs with chromatin and initiation proteins during human DNA replication. In: *Journal of Cell Science* 124.12, pp. 2058–2069.

Zhang, Bao Gui et al. (2012a). microRNA-21 promotes tumor proliferation and invasion in gastric cancer by targeting PTEN. In: *Oncology reports* 27.4, pp. 1019–1026.

Zhang, Chunzhi et al. (2011b). MicroRNA-221 and-222 regulate radiation sensitivity by targeting the PTEN pathway. In: *International Journal of Radiation Oncology* Biology* Physics* 80.1, pp. 240–248.

Zhang, H. et al. (2016a). Expression of long non-coding RNA (LncRNA) small nucleolar rna host gene 1 (SNHG1) exacerbates hepatocellular carcinoma through suppressing miR-195. In: *Medical Science Monitor* 22, pp. 4820–4829.

Zhang, Hai-min et al. (2015). Upregulation of long non-coding RNA MALAT1 correlates with tumor progression and poor prognosis in clear cell renal cell carcinoma. In: *Tumor Biology* 36.4, pp. 2947–2955.

Zhang, Lin et al. (2008). Genomic and epigenetic alterations deregulate microRNA expression in human epithelial ovarian cancer. In: *Proceedings of the National Academy of Sciences* 105.19, pp. 7004–7009.

Zhang, M. et al. (2016b). Long noncoding RNA SNHG1 predicts a poor prognosis and promotes hepatocellular carcinoma tumorigenesis. In: *Biomedicine and Pharmacotherapy* 80, pp. 73–79.

Zhang, W. H. et al. (2012b). The identification of miR-375 as a potential biomarker in distal gastric adenocarcinoma. In: *Oncology Research* 20.4, pp. 139–147.

Zhang, Youyou et al. (2016c). Long noncoding RNA LINP1 regulates repair of DNA double-strand breaks in triple-negative breast cancer. In: *Nature structural & molecular biology*.

Zhang, Z. et al. (2004). Three biomarkers identified from serum proteomic analysis for the detection of early stage ovarian cancer. In: *Cancer Research* 64.16, pp. 5882–5890.

Zhao, Weimin et al. (2015). Combined identification of long non-coding RNA CCAT1 and HOTAIR in serum as an effective screening for colorectal carcinoma. In: *International journal of clinical and experimental pathology* 8.11, p. 14131.

Zhao, Zhen-Jun and Jun Shen (2016). Circular RNA participates in the carcinogenesis and the malignant behavior of cancer. In: *RNA biology*, pp. 1–8.

Zheng, H. et al. (2013). Plasma miRNAs as diagnostic and prognostic biomarkers for ovarian cancer. In: *PLoS ONE* 8.11.

Zhou, Meng et al. (2015). Prioritizing candidate disease-related long non-coding RNAs by walking on the heterogeneous lncRNA and disease network. In: *Molecular BioSystems* 11.3, pp. 760–769.

Zhou, Yunli et al. (2007). Activation of p53 by MEG3 non-coding RNA. In: *Journal of Biological Chemistry* 282.34, pp. 24731–24742.

Zhu, Jia Yun et al. (2009). Identification of novel Epstein-Barr virus microRNA genes from nasopharyngeal carcinomas. In: *Journal of virology* 83.7, pp. 3333–3341.

Zilfou, Jack T. and Scott W. Lowe (2009). Tumor Suppressive Functions of p53. In: *Cold Spring Harbor Perspectives in Biology* 1.5.

Zou, A, R Liu, and X Wu (2016). Long non-coding RNA MALAT1 is up-regulated in ovarian cancer tissue and promotes SK-OV-3 cell proliferation and invasion. In: *Neoplasma* 6.